

**THE ROLE OF SOLVENTS IN MEDIATING THE REACTIONS
OF PHOTOPRODUCED COORDINATIVELY
UNSATURATED METAL FRAGMENTS**

by

Margaret Mary Walsh B.Sc.

A Thesis Submitted for the Degree

of

Doctor of Philosophy

Supervised by Dr. Conor Long

Dublin City University

December 1993

Declaration

I hereby certify that this material, which I now submit for assessment on the programme of study leading to the award of Ph. D. is entirely my own work and has not been taken from the work of others save and to the extent that such work has been cited and acknowledged within the text of my own work.

Signed: Margaret Walsh

Date: 10-1-'94

Margaret Walsh

To my family

Acknowledgements

The following are a number of people I would like to thank for making my past three years so enjoyable at D.C.U.

I would firstly like to acknowledge and thank my supervisor, Dr. Conor Long for his advice, encouragement and patience over the last three years.

Thanks also to the technical staff, both past and present for being so helpful in my hours of need.

Special thanks is extended to my fellow postgrads in AG07, and in particular to the C.L.R.G., both past and present, Graham, Barry, Gerry, Irene, Celia, Mick, Mary, Ciara and Siobhan for all their help, advice and entertainment throughout my lab days. Thanks also to all the other postgrads and academic staff for their help and friendship during my time at D.C.U.

A very special word of thanks goes to my sporting buddies, in particular, Catherine, Eithne, Miriam, Ann, Mary Mac and the D.C.U ladies soccer team for all the hours of entertainment both on and off the pitch. Long live Ladies Soccer.

I'm most grateful to all the inhabitants of 20 Botanic Rd., past and present, namely Alison, Sheila, Eithne, Mary, Fiona and Yvonne for putting up with me and for making my years in Dublin so enjoyable.

Very special thanks is extended to all my friends and relatives in Tipperary and elsewhere for all their help and advice, and in particular to two of my great friends, Sile and Angela. Keep up the writing.

Finally and most importantly I would like to thank my parents and family - Dad, Mam, James, Eileen and John for all their help and support throughout my life. A special thanks to James for proof-reading this thesis for me.

To all I've mentioned and to those I've probably forgotten , all I can say is
THANKS.

Table of Contents

Contents		Page
Title page		i
Declaration		ii
Dedication		iii
Acknowledgements		iv
Table of contents		v
Abstract		xi
Chapter 1	Introduction	1
1.1	Introduction	2
1.2	Bonding in metal carbonyl complexes	5
1.2.1	Bonding in $M(CO)_5(L)$ complexes	8
1.3	Photochemical loss of carbon monoxide	9
1.4	Low temperature matrix isolation	11
1.5	Flash photolysis	14
1.6	Structure, reactivity and photochemistry of $Cr(CO)_5$	16
1.7	Kinetics and mechanisms of substitution reactions of $M(CO)_6$ and $M(CO)_5(L)$ complexes, (L = solvent or ligand)	25
1.8	References	37
Chapter 2	An investigation into the effect of solvent on the reaction of $Cr(CO)_5(solvent)$ with CO	43
2.1	Introduction	44
2.2	Electronic spectrum of $Cr(CO)_6$	45

2.3	Flash photolysis of $\text{Cr}(\text{CO})_6$ in CO saturated aliphatic and cyclic hydrocarbon solvents	46
2.4	The effect of the power of the laser on the primary photoproduct	47
2.5	UV/visible difference spectrum for formation of $\text{Cr}(\text{CO})_5(\text{solvent})$	48
2.6	The rate of reaction of $\text{Cr}(\text{CO})_5(\text{solvent})$ with CO	52
2.7	Activation parameter studies for the reaction of $\text{Cr}(\text{CO})_5(\text{solvent})$ with CO	56
2.8	Quantum yields for the photosubstitution of $\text{Cr}(\text{CO})_6$ by pyridine	63
2.9	Conclusion	68
2.10	References	70
Chapter 3	The effect of ligand substituents on the displacement of solvent from $\text{Cr}(\text{CO})_5(\text{solvent})$ by donor ligands	73
3.1	Introduction	74
3.1.1	CNDO calculations for 2,2'-bipyridine	76
3.1.2	Electronic spectrum of $\text{Cr}(\text{CO})_5(\text{L})$ (L = pyridine or substituted pyridine)	82
3.2	Laser flash photolysis of $\text{Cr}(\text{CO})_6$ in the presence of excess ligand L, in cyclohexane (L = pyridine or substituted pyridine)	84
3.2.1	Flash photolysis of $\text{Cr}(\text{CO})_6$ in the presence of excess ligand L	85
3.2.2	The effect of the power of the laser on the primary photoproduct	87

3.2.3	UV/visible difference spectrum of $\text{Cr}(\text{CO})_5(\text{L})$	88
3.2.4	The rate of reaction of $\text{Cr}(\text{CO})_5(\text{S})$ with different ligand (L) concentrations	89
3.2.4.1	The effect of ligand basicity on the rate of reaction of $\text{Cr}(\text{CO})_5(\text{cyclohexane})$ with L	94
3.2.5	Activation parameter studies for the reaction of $\text{Cr}(\text{CO})_5(\text{cyclohexane})$ with L	96
3.3	Laser flash photolysis of $\text{Cr}(\text{CO})_6$ in the presence of excess ligand L, in toluene (L = pyridine or substituted pyridine)	101
3.3.1	Electronic spectrum of $\text{Cr}(\text{CO})_5(\text{L})$	102
3.3.2	Flash photolysis of $\text{Cr}(\text{CO})_6$ in the presence of excess ligand L	103
3.3.3	The effect of the power of the laser on the primary photoproduct	106
3.3.4	UV/visible difference spectrum of $\text{Cr}(\text{CO})_5(\text{L})$	107
3.3.5	The rate of reaction of $\text{Cr}(\text{CO})_5(\text{S})$ with different ligand (L) concentrations	108
3.3.5.1	The effect of ligand basicity on the rate of reaction of $\text{Cr}(\text{CO})_5(\text{toluene})$ with L	112
3.3.6	Activation parameter studies for the reaction of $\text{Cr}(\text{CO})_5(\text{toluene})$ with L	114
3.4	Conclusion	118
3.5	An investigation of the rate of reaction of $\text{Cr}(\text{CO})_6$ with L, in THF or ethanol using the stopped-flow technique, L = pyridine or substituted pyridine	119
3.5.1	UV/visible spectrum for the formation of $\text{Cr}(\text{CO})_5(\text{L})$	120

3.5.2	The rate of reaction of $\text{Cr}(\text{CO})_5(\text{S})$ with different ligand (L) concentrations	123
3.5.3	Activation parameter studies for the reaction of $\text{Cr}(\text{CO})_5(\text{S})$ with L	136
3.6	Conclusion	142
3.7	References	144
Chapter 4	Laser flash photolysis of $\text{ArCr}(\text{CO})_2(\text{L})$, (L = CO, pyridine, 4-acetylpyridine; Ar = $\eta^6\text{-C}_6\text{H}_6$) complexes in the presence of pyridine or 4-acetylpyridine	148
4.1	Photochemistry of $\text{ArCr}(\text{CO})_3$	149
4.1.1	Photochemistry of $\text{ArCr}(\text{CO})_2(\text{L})$ complexes	155
4.2	UV/visible electronic spectrum of $\text{ArCr}(\text{CO})_3$	157
4.3	Laser flash photolysis of $\text{ArCr}(\text{CO})_3$ in the presence of L, (L = py, 4-Acpy), in cyclohexane	158
4.3.1	The reactions of photogenerated $\text{ArCr}(\text{CO})_2(\text{S})$ with L	162
4.3.2	The rate of reaction of $\text{ArCr}(\text{CO})_2(\text{S})$ with L	165
4.3.3	Activation parameter studies for the formation of $\text{ArCr}(\text{CO})_2(\text{L})$	169
4.4	Laser flash photolysis of $(\eta^6\text{-C}_6\text{H}_6)\text{Cr}(\text{CO})_2(\text{pyridine})$	175
4.4.1	UV/visible electronic spectrum of $(\eta^6\text{-C}_6\text{H}_6)\text{Cr}(\text{CO})_2(\text{py})$	176
4.4.2	Flash photolysis of $\text{ArCr}(\text{CO})_2(\text{py})$ in cyclohexane	178
4.4.2.1	Flash photolysis of $\text{ArCr}(\text{CO})_2(\text{py})$ in argon saturated cyclohexane solution containing pyridine	180
4.4.2.2	Flash photolysis of $\text{ArCr}(\text{CO})_2(\text{py})$ in CO saturated cyclohexane solution containing pyridine	184
4.4.3	Activation parameter studies for $\text{ArCr}(\text{CO})_2(\text{py})$ system	188

4.5	Laser flash photolysis of $(\eta^6\text{-C}_6\text{H}_6)\text{Cr}(\text{CO})_2(4\text{-acetylpyridine})$	195
4.5.1	UV/visible electronic spectrum of $(\eta^6\text{-C}_6\text{H}_6)\text{Cr}(\text{CO})_2(4\text{-acetylpyridine})$	195
4.5.2	Flash photolysis of $\text{ArCr}(\text{CO})_2(4\text{-Acpy})$ in cyclohexane	198
4.5.2.1	Flash photolysis of $\text{ArCr}(\text{CO})_2(4\text{-Acpy})$ in argon saturated cyclohexane solution containing 4-acetylpyridine	199
4.5.2.2	Flash photolysis of $\text{ArCr}(\text{CO})_2(4\text{-Acpy})$ in CO saturated cyclohexane solution containing 4-acetylpyridine	203
4.5.3	Activation parameter studies for $\text{ArCr}(\text{CO})_2(4\text{-Acpy})$ system	206
4.6	Conclusion	213
4.7	References	215
Chapter 5	Experimental	219
5.1	Photolysis of metal carbonyl complexes	220
5.1.1	Photolysis apparatus	221
5.1.2	Materials	222
5.1.3	Equipment	222
5.1.4	Syntheses of $\text{Cr}(\text{CO})_5(\text{L})$ and $(\eta^6\text{-C}_6\text{H}_6)\text{Cr}(\text{CO})_2(\text{L})$ complexes, L = py or 4-Acpy	223
5.1.4.1	Preparation of $\text{Cr}(\text{CO})_5(\text{py})$	223
5.1.4.2	Preparation of $(\eta^6\text{-C}_6\text{H}_6)\text{Cr}(\text{CO})_3$	223
5.1.4.3	Preparation of $(\eta^6\text{-C}_6\text{H}_6)\text{Cr}(\text{CO})_2(\text{py})$	224
5.1.4.4	Preparation of $(\eta^6\text{-C}_6\text{H}_6)\text{Cr}(\text{CO})_2(4\text{-Acpy})$	225
5.2	Laser flash photolysis	225

5.2.1	Laser flash photolysis system with UV/visible monitoring	226
5.2.2	Sample preparation for laser flash photolysis	231
5.2.2.1	Preparation of $\text{Cr}(\text{CO})_6$ in various solvents	231
5.2.2.2	Preparation of $\text{Cr}(\text{CO})_6$ in the presence of excess ligand L (L = pyridine or substituted pyridine)	232
5.2.2.3	Preparation of $(\eta^6\text{-C}_6\text{H}_6)\text{Cr}(\text{CO})_2(\text{L})$, (L = py, 4-Acpy) complexes	232
5.3	Stopped-Flow technique	232
5.3.1	Stopped-Flow apparatus	233
5.3.2	Sample preparation	235
5.3.2.1	Preparation of $\text{Cr}(\text{CO})_6$ with a range of ligand concentrations	235
5.3.2.2	Preparation of solutions for activation studies	235
5.3.3	Determination of kinetic parameters	236
5.4	Determination of activation parameters	237
5.5	Determination of solubility of CO in alkane solvents	239
5.6	Determination of quantum yields for $\text{Cr}(\text{CO})_6$ in alkane solvents	239
5.7	Determination of extinction coefficients	240
5.8	References	241
Appendix A	Data for the determination of activation parameters	A1
Appendix B	Data for the determination of second-order rate constants	B1
Appendix C	Data for the determination of extinction coefficients	C1

**THE ROLE OF SOLVENTS IN MEDIATING THE REACTIONS
OF PHOTOPRODUCED COORDINATIVELY
UNSATURATED METAL FRAGMENTS**

Margaret Mary Walsh

Abstract

It is now understood that coordinatively unsaturated metal fragments bind rapidly to a solvent molecule. The role of this solvent-metal interaction in mediating reactions is investigated in this study. Chapter 1 serves as a general introduction and review of the structure, reactivity and photochemistry of these coordinatively unsaturated species and the techniques employed in order to investigate these species. The second chapter deals with the formation of solvent substituted pentacarbonyl species by flash photolysis of $\text{Cr}(\text{CO})_6$ in various alkane solvents. The nature of the solvent interaction with the $\text{Cr}(\text{CO})_5$ fragment was investigated by monitoring the displacement of the various alkane solvents by CO. The rate of reaction of the solvated species with CO was found to depend on the alkane solvent. The enthalpies of activation for all the reactions were very similar ($\Delta H^\ddagger = 20 \pm 4 \text{ kJmol}^{-1}$), while the entropy of activation values for the aliphatic alkanes increased with increasing length of the hydrocarbon chain ($\Delta S^\ddagger = -60$ and $-39 \text{ Jmol}^{-1}\text{K}^{-1}$ for pentane and heptane respectively). In chapter 3 the rate of reaction of $\text{Cr}(\text{CO})_5(\text{S})$, (S = cyclohexane, toluene, THF or ethanol) with various substituted-pyridine nucleophiles is investigated using laser flash photolysis and stopped-flow techniques. Differences in the rates of reaction were attributed to the steric and electronic effects of the substituents on the nucleophiles rather than the basicity of the nucleophiles. The rates of reaction were also influenced by the nature of the solvent-metal interaction. The activation parameters associated with these reactions were also measured. In the fourth chapter the photochemistry of $(\eta^6\text{-C}_6\text{H}_6)\text{Cr}(\text{CO})_3$ is investigated. The solvated dicarbonyl complex is produced upon laser flash photolysis of $(\eta^6\text{-C}_6\text{H}_6)\text{Cr}(\text{CO})_3$ and the rate of reaction of this complex with pyridine or 4-acetylpyridine is investigated. In addition, $(\eta^6\text{-C}_6\text{H}_6)\text{Cr}(\text{CO})_2(\text{L})$ (L = pyridine, 4-acetylpyridine) complexes are synthesised and the photochemistry of these complexes in the presence of excess ligand are also investigated. Irradiation of $(\eta^6\text{-C}_6\text{H}_6)\text{Cr}(\text{CO})_2(\text{pyridine})$ resulted in regeneration of the pyridine complex, while two isomeric complexes in which bonding was *via* the oxygen atom and the nitrogen atom were obtained for the 4-acetylpyridine complex. The O-linked isomer was short-lived. The final chapter deals with all the experimental techniques encountered in the course of this work.

CHAPTER 1

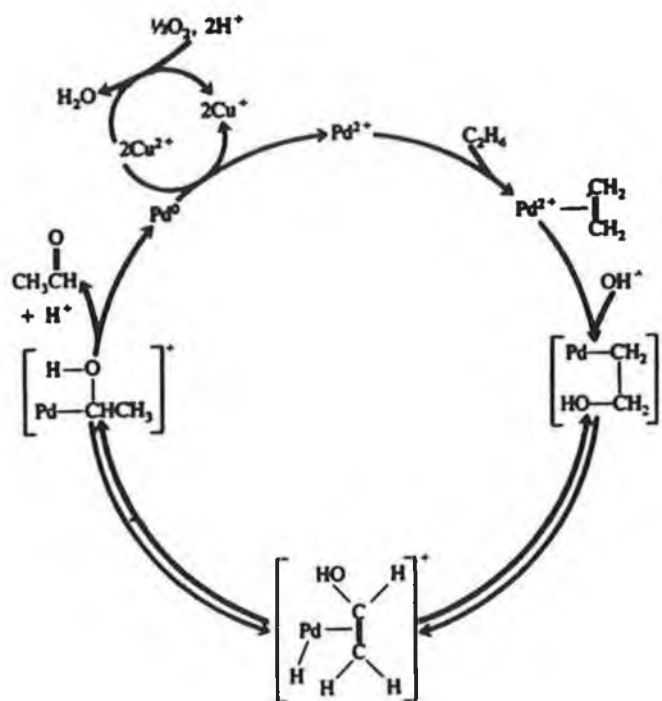
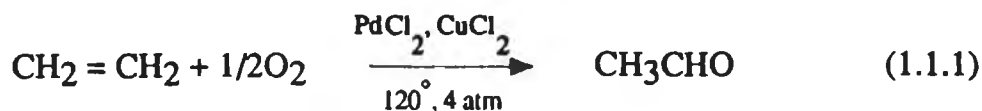
INTRODUCTION

1.1 Introduction

Much of the impetus for the development of organometallic chemistry over the latter half of this century has arisen from the ability of transition metals to catalyse various kinds of organic transformations. Initially the major source of most chemical compounds was coal and coal tar but more recently petroleum and natural gas industries have become the major source of the organic molecules required in industrial synthesis. Cracking of natural gas yields olefins, methane and synthesis gas ($\text{CO} + \text{H}_2$) all of which are principal building blocks for more industrially important compounds which include alcohols, aldehydes, acids and polymers. Over the last forty years or so, transition metals or complexes of these metals have been utilised as catalysts in the conversion of many raw materials to commercially important products. A catalyst acts by producing an alternative low energy pathway, which speeds up the reaction without losing its chemical identity. The use of heterogeneous catalysts in industrial processes is more extensive than that of homogeneous catalysts primarily because the former can easily be removed from the reaction medium. However, the use of homogeneous catalysts in some processes have become almost exclusive [1]. The basis of homogeneous catalysis as it is known today stems from the research pioneered by Fischer, Wilkinson, Zielger and Natta for which they were awarded Nobel prizes. Zielger and Natta were awarded the Nobel prize in 1963 for the development of the Zielger-Natta catalyst ($\text{TiCl}_3/\text{Et}_2\text{AlCl}$) essential in the production of millions of tons of polyethylene and polypropylene from alkenes.

Other renowned soluble transition metal catalysts are those involved in the "Wacker" process, the "oxo" process and the Wilkinson catalysts. The "Wacker" process results in the formation of aldehydes (especially

acetaldehyde) upon the oxidation of olefins by O₂ in the presence of an aqueous HCl solution of PdCl₂/CuCl₂ (Scheme 1.1.1).



Scheme 1.1.1

Another process of immense commercial use, involving a rhodium based catalyst [Rh(CO)₂I₂]⁻, is the carbonylation of methanol to produce acetic acid under low pressures of carbon monoxide (30 - 40 atm) (equation 1.1.2) [2].



Developments are still being carried out up to the present day in the search for new and more highly active and selective catalysts which will save energy and

materials. The major virtue of homogeneous catalysis that has led to its widespread adoption by industry is selectivity, the ability to produce pure products in high yield. This is of utmost importance in the preparation of pharmaceuticals and polymer intermediates which must be extremely pure. One such pharmaceutical product, L - dopa, used in the treatment of Parkinson's disease, is produced by the hydrogenation of a substituted cinnamic acid using a rhodium catalyst. The selectivity of homogeneous catalysis is demonstrated in this process as only one optical isomer is produced from an optically inactive precursor.

Certain metal carbonyl complexes are known to act as homogeneous catalysts. Among these are $\text{Ni}(\text{CO})_4$ which is used in the hydrocarboxylation of olefins [3] and photoactivated $\text{Fe}(\text{CO})_5$ and $\text{Fe}_3(\text{CO})_{12}$ whose uses are found in olefin isomerisation, hydrogenation and hydrosilylation reactions at low temperatures. The exact mechanisms of many of the catalytic reactions remain unknown, but as the processes involve coordination of a substrate to the metal, the initial steps involved must be the generation of a vacant site at the metal centre. In metal carbonyl complexes the principal process, involving the displacement of a carbonyl group by a nucleophilic ligand can occur either thermally or photochemically. The efficiency at which the latter process occurs is reflected in the quantum yield values. Initial studies reported a value of approximately 1 [4], but more recent studies have revealed a quantum yield value of 0.67 for such processes.

To enable further development and synthesis of homogeneous catalytic processes, a knowledge of the structure and reactivity of the coordinatively unsaturated intermediate must be gained. A number of techniques have been employed to aid in the elucidation of the identity, structure and reaction kinetics of these intermediates. Low temperature matrix isolation and flash photolysis

have been most successful in this regard. In order to obtain a greater understanding of these processes, kinetic studies of ligand substitution reactions of $\text{Cr}(\text{CO})_6$ were undertaken as the basis of this study.

1.2 Bonding in metal carbonyl complexes

The reactivity of metal carbonyl complexes cannot be explained without understanding the nature of the metal carbonyl bond. The energy level diagram depicting the interaction between the ligands and the metal σ -bonding orbitals in an octahedral $\text{M}(\text{CO})_6$ complex is shown in Figure 1.2.1.

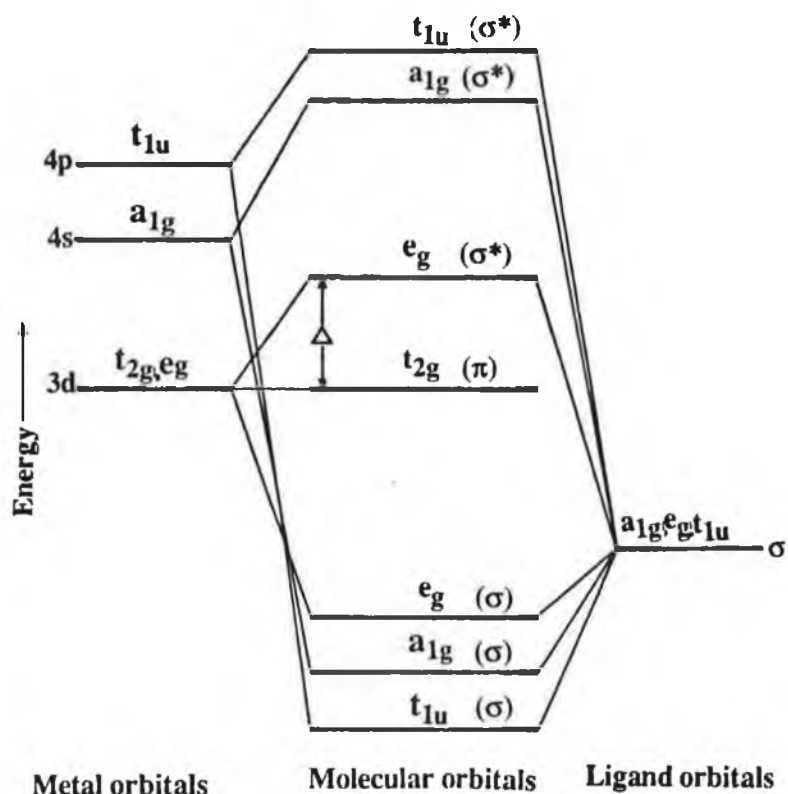


Figure 1.2.1 Energy level diagram for $\text{M}(\text{CO})_6$ complexes, with no π -bonding.

Interaction only occurs between orbitals of similar energy and symmetry. The carbonyl sp hybrid orbital is of the correct symmetry for overlap with the s , p , d_{z^2} and $d_{x^2-y^2}$ orbitals of the metal. Each such overlap results in the formation of a bonding molecular orbital (MO) which is of lower energy and a corresponding antibonding MO of higher energy. Three of the metal d orbitals have zero overlap with the ligand orbitals and therefore remain as non-bonding MO's. The net result of the interaction between the metal and the ligands is a lowering in the energy of the system, since the electrons enter the M-CO σ bonding orbitals. As these molecular orbitals possess more metal rather than ligand character, the interaction results in a greater electron density at the metal centre. However, this instability of the molecule is counteracted by the availability of empty low lying π^* antibonding orbitals on the CO ligands which are of the correct symmetry to interact with the t_{2g} orbitals of the metal. Each t_{2g} orbital can interact with two π^* CO orbitals which lie *trans* to each other. This interaction results in a lowering of the t_{2g} energy level and overall an increased stability of the complex (Figure 1.2.2).

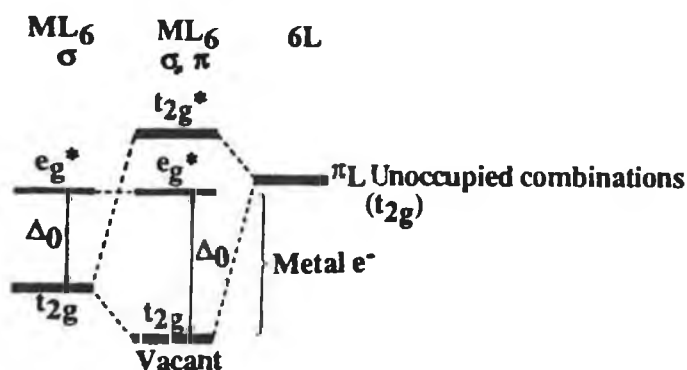


Figure 1.2.2 Interaction of π^* orbitals with metal orbitals.

The resulting molecular orbital is no longer purely metal in character but possesses some carbonyl π^* character. Therefore, electronic population of this

MO is effectively a population of the π^* orbital, thus leading to a reduction in bond order of the carbonyl bond compared with free carbon monoxide. This change in bond order is detected by infrared spectroscopy (free CO, $\nu_{\text{C=O}} = 2143 \text{ cm}^{-1}$; $\text{Cr}(\text{CO})_6$ $\nu_{\text{C=O}} = 1980 \text{ cm}^{-1}$). The charge on the metal complex also affects the CO stretching frequency. Table 1.2.1 shows that a net positive charge on the complex raises the CO frequencies while a net negative charge lowers them [5].

Complex	Frequency $\nu_{\text{C=O}} \text{ (cm}^{-1}\text{)}$	Complex	Frequency $\nu_{\text{C=O}} \text{ (cm}^{-1}\text{)}$
$\text{Mn}(\text{CO})_6^+$	2090	$\text{Mn}(\text{tren})(\text{CO})_3^+$	1960
$\text{Cr}(\text{CO})_6$	1980	$\text{Cr}(\text{tren})(\text{CO})_3$	1880
$\text{V}(\text{CO})_6^-$	1860		

Table 1.2.1 The effect of the ionic net charge and the nature of the ligands on the CO stretching frequencies of isoelectronic metal carbonyls.

Also the effect of replacing three CO's by three pure σ -donor nitrogens of the tren ligand ($\text{H}_2\text{NCH}_2\text{CH}_2\text{NHCH}_2\text{CH}_2\text{NH}_2$) is almost as great as changing the net charge by one unit. Thus, substitution of the carbonyl group by a ligand other than CO, results in a change which is reflected in the bond order of the remaining carbonyl ligands. In addition, the structure of the complex changes from octahedral, O_h in $\text{Cr}(\text{CO})_6$ to square pyramidal, C_{4v} in $\text{Cr}(\text{CO})_5(\text{L})$ (L = ligand other than CO). Again, these changes are detectable by infrared spectroscopy, for example, $\text{M}(\text{CO})_6$ $\nu_{\text{C=O}} = 1980 \text{ cm}^{-1}$; $\text{M}(\text{CO})_5(\text{pyridine})$ $\nu_{\text{C=O}} = 2060, 1940, 1910 \text{ cm}^{-1}$ and by UV/visible spectroscopy. Lower carbonyl stretching frequencies are generally indicative of more extensive metal-to-carbonyl π -bonding [6, 7].

1.2.1 Bonding in $M(\text{CO})_5(\text{L})$ complexes

The effect carbonyl ligands have on the metallic orbitals of $M(\text{CO})_6$ ($M = \text{Cr}, \text{Mo}$ or W) is shown in Figure 1.2.1 and 1.2.2. The replacement of a carbonyl ligand in the $M(\text{CO})_6$ complex results in perturbation of the molecular orbitals. The overall symmetry of the molecule is changed from octahedral (O_h) to square pyramidal (C_{4v}). This is because different ligands effect the energy levels within the molecule to varying degrees. The resultant spectra therefore may yield valuable information regarding the energy levels within the molecule.

Matrix isolation techniques and low temperature studies have provided a wealth of information regarding the structure and reactivity of the photogenerated $M(\text{CO})_5$ species. Vibrational studies concluded that the structure of the photogenerated $M(\text{CO})_5$ species was square pyramidal (C_{4v}) in symmetry [8]. The electronic spectrum of matrix isolated $M(\text{CO})_5$ is very sensitive to the matrix, because of the varying abilities of the matrices to split the d orbitals of the metal [9]. The changes observed in the metal d orbitals on the removal of a carbonyl ligand from $M(\text{CO})_6$ generating $M(\text{CO})_5$ are shown in Figure 1.2.1.1.

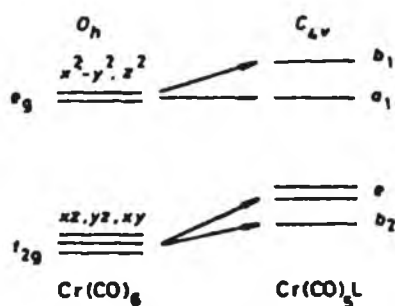


Figure 1.2.1.1 d-Orbital energy diagram for $\text{Cr}(\text{CO})_6$ and $\text{Cr}(\text{CO})_5(\text{L})$ ($\text{L} = \text{N-donor}$) complexes.

When a CO is replaced by a ligand, the t_{2g} orbital is split into e (d_{xz} , d_{yz}) and b_2 (d_{xy}). The splitting is mainly determined by the difference in π -interaction between CO and the ligand along the z-axis. Changes in σ -interaction splits the σ -antibonding e_g orbital into a_1 (d_{z^2}) and b_1 ($d_{x^2-y^2}$) respectively. Magnetic circular dichroism (M.C.D) spectra have revealed that d_{z^2} is the lowest lying orbital [10(a), (b)], thus the lowest energy spectral feature of $M(CO)_5(L)$ (for $L < CO$ in the spectrochemical series) is assigned to ${}^1A_1 (e^4b_2^2) \rightarrow {}^1E (e^3b_2^2a_1^1)$ ligand field (LF) transition [10(c)]. This band is significantly red-shifted compared to that in $M(CO)_6$, as expected from Figure 1.2.1.1. The energy difference between the d_{z^2} and $d_{x^2-y^2}$ orbitals depends on the σ donor capacity of the ligand relative to CO.

If the ligand possesses low lying π^* orbitals, the lowest energy absorption in $M(CO)_5(L)$ may be a metal to ligand charge transfer (MLCT) transition. The positioning of this band varies depending on the nature of the ligand L. The more electron-donating substituents give a higher energy MLCT absorption. MLCT bands are very sensitive to solvent, being substantially blue-shifted as the solvent polarity or polarisability increases, whereas the LF bands remain relatively unaffected [11]. Depending on the irradiation wavelength used, loss of L or another CO group may be obtained yielding coordinatively unsaturated $M(CO)_5$ or $M(CO)_4(L)$ species respectively which may undergo further reaction.

1.3 Photochemical loss of carbon monoxide

In this study, the substitution reactions of $Cr(CO)_6$ by various nucleophiles were investigated employing photolytic techniques. Photoexcitation of this complex results in dissociation of a carbonyl ligand.

This photolabilisation is directly related to the bonding interaction between the metal and the ligands (Figure 1.3.1). The d_{z^2} and the $d_{x^2-y^2}$ orbitals of e_g symmetry are antibonding (σ^*) with respect to the metal - ligand interactions whereas the d_{xy} , d_{xz} and d_{yz} orbitals of t_{2g} symmetry are weakly π -bonding between the metal and the carbonyl ligand.

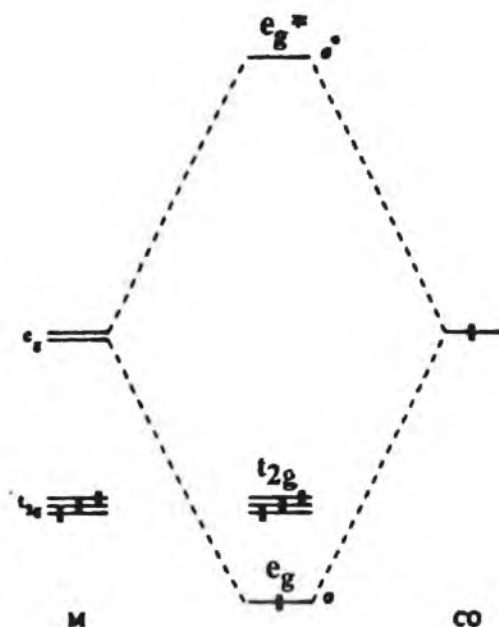
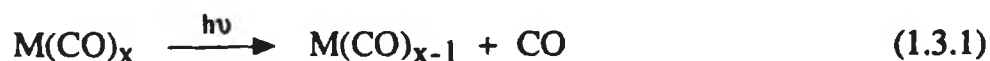


Figure 1.3.1 Photochemical loss of CO from metal carbonyl complexes.

The highest occupied molecular orbital (HOMO) of the metal carbonyl complex in its ground state is the t_{2g} ($d\pi$) metal to ligand bonding orbital. When a photon of energy is absorbed by the complex an electron is excited from the t_{2g} to the e_g (σ^*) orbital which is antibonding with respect to the metal-ligand interactions. As a result the metal loses electron density in the backbond to the CO ligand and therefore the metal-ligand bond weakens. The excitation of an electron from the t_{2g} (π) \rightarrow e_g (σ^*) is assigned as a ligand field (LF) transition. The net effect of weakening the metal-ligand bond is efficient loss of a CO

ligand (equation 1.3.1).



The changes involved in the substitution of a carbonyl ligand can be detected by IR and UV/visible spectroscopy.

1.4 Low temperature matrix isolation

Photolysis of transition metal carbonyl compounds usually results in the formation of coordinatively unsaturated species. As these intermediates are highly reactive and extremely short-lived, observation of these species is very difficult at room temperature. However, this problem was overcome by the development of the matrix isolation technique.

The principle of matrix isolation, founded by George Pimentel in 1950, lies in the trapping of a reactive intermediate in a solid inert environment at low temperature [12, 13]. This extends the lifetime of the species permitting examination of its spectroscopic properties. If the matrix is rigid enough and the temperature maintained to be sufficiently low, the reactive species will be unable to diffuse through the solid matrix and therefore is prevented from reacting with other species in the matrix. However, the photofragment may interact with the "inert" matrix material itself, for example, evidence has been found for the existence of $\text{Cr(CO)}_5(\text{Ar})$ [14], $\text{Fe(CO)}_4(\text{CH}_4)$ [15] and $\text{Cr(CO)}_5(\text{N}_2)$ [16]. Also the low temperature inhibits the only other possible decay pathway *via* unimolecular decomposition.

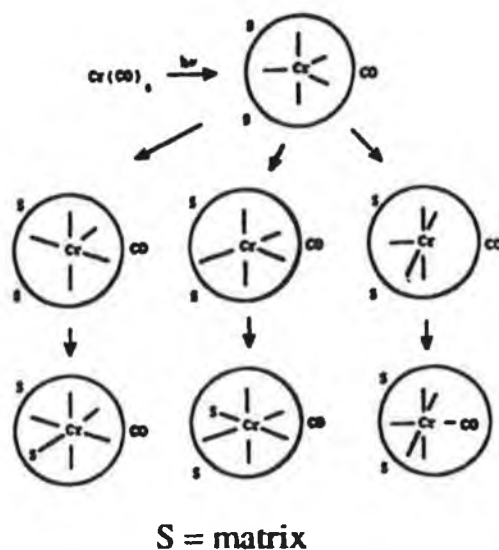
In the case of Cr(CO)_5 , although the matrix material has little effect on the infrared spectra of the photofragments, it has a remarkable effect on the UV

absorption maxima of the photofragment, (λ_{\max} for $\text{Cr}(\text{CO})_5(\text{Ne})$ and $\text{Cr}(\text{CO})_5(\text{CH}_4)$ is 624 and 489nm respectively) [8, 14]. The shift in the visible band depends on (i) the interaction of the matrix with the empty site on the metal fragment and (ii) the bond angle, θ , between the matrix and the metal fragment. Estimates of the bond angle from IR spectra, revealed that there was a substantial angle difference between $\text{Cr}(\text{CO})_5\text{---Xe}$ and $\text{Cr}(\text{CO})_5\text{---Ar}$, $\theta = 91.3^\circ$ in the former and 95.5° in the latter. The corresponding visible band maxima were $\lambda_{\max} = 492$ and 533nm , respectively [9].

In the solid matrix diffusion of the CO away from the photofragment is unlikely, but the possibility of recombination occurring is diminished by an intramolecular rearrangement of the photoproducted fragment. On UV photolysis, the excited pentacarbonyl fragment rearranges and is frozen in a spatial orientation such that there is a matrix molecule and not a CO molecule in the sixth coordination site of the metal (Scheme 1.4.1) [17]. However, upon visible photolysis of the pentacarbonyl, a photochemical rearrangement may occur to reestablish the original spatial orientation of the ligands relative to the photoejected CO such that thermal recombination is possible (equation 1.4.1).



As well as inert gas matrices, low temperature solvent glasses are also used. These consist of hydrocarbons, for example, isopentane and methylcyclohexane and are maintained at higher temperatures (77K) than the inert gas matrices. The hexacarbonyls, $\text{M}(\text{CO})_6$ ($\text{M} = \text{Cr}, \text{Mo}, \text{or W}$) were among the earliest organometallic species to be examined using this technique [18]. However, a disadvantage of this technique is that the carbonyl bands in the infrared tend to be broad and may occlude other spectral features needed for



Scheme 1.4.1

accurate structural determination. Also, the glasses may not be inert and therefore are more likely to react with the more reactive fragments produced.

Other disadvantages, concerning both matrices and glasses are (i) they yield very little kinetic information because of the restricted temperature range, (ii) they cannot be easily used for charged species and (iii) in the case of solid matrices, they can block some photochemical pathways.

Low temperature solvents have also proved to be very efficient in stabilising reactive species sufficiently to permit study with conventional techniques. The most appropriate solvents are liquid noble gases, for example, liquid Kr, Xe or doped solutions of these as they are inert and transparent to infrared radiation, thus permitting accurate structural determinations of the photofragments. This technique allows kinetics to be monitored and thermodynamic information to be extracted, for example, that of $\text{Cr}(\text{CO})_5(\text{N}_2)$ [19], thus offering greater advantages over matrix isolation techniques.

However, a limiting factor is that the species have to be relatively stable, therefore precluding the examination of highly reactive intermediates, such as coordinatively unsaturated species.

In order to investigate these species, a number of techniques have been developed, such as flash photolysis with UV monitoring or IR detection, and time - resolved infrared (TRIR) spectroscopy.

1.5 Flash Photolysis

Conventional flash photolysis was developed by Norrish and Porter in the 1950's for which they received the Nobel prize in 1967 [20]. This technique enabled reactive intermediates present in many photochemical reactions to be identified. It employs an intense flash of light, for example, a discharge tube or laser, which produces transient species, radicals or excited molecules in concentrations many thousands of times greater than in previous systems. This permits detection of intermediates, otherwise too low in concentration to be detected by spectroscopic techniques. Consequently, spectra and lifetimes of the intermediates can be obtained. Nasielski *et al.* pioneered flash photolysis coupled with UV/visible detection on metal carbonyl systems with their analysis of Cr(CO)₆ [21]. A number of factors, such as moderate solubility in non-polar solvents, large UV/visible and IR extinction coefficients and high quantum yields for photochemical reactions (equation 1.5.1) contribute to the suitability of metal carbonyl complexes for flash photolysis.



Solvent absorptions are overcome by using solvents with suitable cut-off wavelengths. The basic technique involves excitation of the sample solution with a high intensity flash of light while simultaneously passing a monitoring beam through the sample, for example, a Xenon arc lamp. Changes in absorbance in the sample solution reflect the formation of intermediates or depletion of the parent compound or both. Spectra are built up point by point by changing the wavelength of a monochromator or are recorded using a spectrograph. A schematic diagram of a conventional flash photolysis system is shown in Figure 1.5.1.

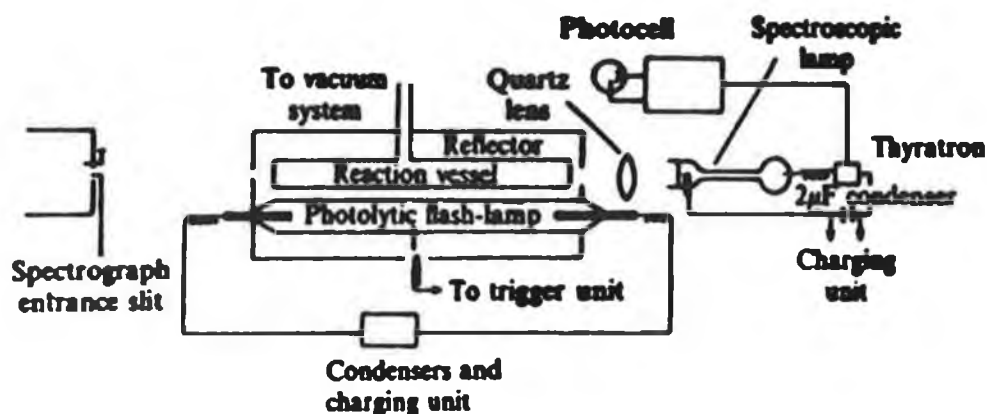


Figure 1.5.1 Schematic diagram of a conventional flash photolysis system.

UV/visible monitored flash photolysis is useful for obtaining electronic spectra, transient kinetic data and their variation with reaction conditions however, very little structural information is available from this technique.

Transient infrared spectroscopy, is a much more useful technique, particularly for metal carbonyls, as the ν_{CO} absorption bands are intense and their positions are dependent on the electron density on the metal [22, 23].

Differences between this technique and that with UV/visible monitoring lie in the absorption spectrum and the monitoring beam. As the spectrometers only measure changes in the infrared absorption, the absorption spectrum appears as positive and negative peaks corresponding to the formation of new photoproducts and the depletion of the parent compound respectively. The monitoring source may be a normal infrared source such as a glowbar or a high intensity CO laser, tunable over the carbonyl region.

As with all techniques, flash photolysis has its disadvantages also. (i) The sample must be optically clear and transparent for monitoring light, and the solvents must be of very high purity. (ii) If absorption bands of several intermediate species overlap each other, analysis of the spectra may be difficult. However, in spite of these disadvantages, flash photolysis techniques may be found in many diverse scientific fields such as, (i) atmospheric pollutants, (ii) photopolymerization, (iii) photochromism and photosensitive materials and (iv) organic and inorganic intermediates in chemistry and biology.

1.6 Structure, reactivity and photochemistry of $\text{Cr}(\text{CO})_5$

As early as 1934, Thompson *et al.* proposed that the primary photochemical step for metal carbonyl complexes was the loss of a carbon monoxide molecule, generating a coordinatively unsaturated species [24]. Further investigations into the photochemical substitution of CO by a donor ligand, L (e.g. pyridine) suggested the following scheme for Group VI hexacarbonyls (Cr, Mo or W) [25] (equation 1.6.1 and 1.6.2).

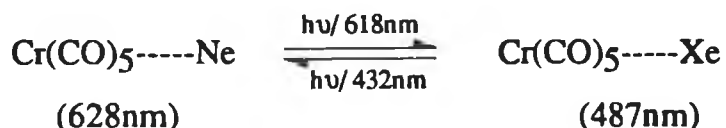


Over the last 50 years or so, many workers, employing various techniques have undertaken delicate research in the identification and determination of the structure of the coordinatively unsaturated intermediate. Stolz and co-workers, upon photolysis of the metal hexacarbonyls, $(\text{Cr}(\text{CO})_6$, $\text{Mo}(\text{CO})_6$ or $\text{W}(\text{CO})_6$) in a 1:4 isopentane-methylcyclohexane glass at -180°C , with UV light, observed three IR bands in the carbonyl stretching region, 2088 (w), 1955 (s) and 1928 (m) cm^{-1} , consistent with a molecule of C_{4v} symmetry [18]. Further evidence for the structure of the metal pentacarbonyl was obtained when the low temperature work was extended to frozen gas matrices [26-28]. Turner and colleagues, photolysed the Group VI hexacarbonyls in solid argon at 20K and the pattern of IR bands and UV spectra obtained confirmed C_{4v} symmetry for the pentacarbonyls produced. As a result of more detailed matrix studies, it was noted that the visible absorption band of $\text{Cr}(\text{CO})_5$ in argon had λ_{max} at 542nm compared to a corresponding absorption at 485nm in the pentane-methylcyclohexane glass. This difference observed lead to the investigation of the behaviour of $\text{Cr}(\text{CO})_5$ in a methane matrix at 20K. The visible absorption band was found to occur at 492nm, i.e. very close to that observed in hydrocarbon glass studies. Therefore, it was suggested that the shift of the visible band was as a result of an interaction between methane and the "vacant site" in the C_{4v} $\text{Cr}(\text{CO})_5$, as argon is assumed to be a non-interacting species. Further evidence supporting this proposal was obtained from photolysis of $\text{M}(\text{CO})_6$ in different matrices at 20K. It was found that the visible absorption band of the pentacarbonyl was extremely sensitive to the matrix while the IR spectral bands hardly changed in frequency (Table 1.6.1) [14, 8].

Matrix	Ne	SF ₆	CF ₄	Ar	Kr	Xe	CH ₄
Band max (nm)	624	560	547	533	518	492	489
cm ⁻¹ x 10 ⁻³	16.0	17.9	18.3	18.8	19.3	20.3	20.4

Table 1.6.1 Position of UV band of Cr(CO)₅ in different matrices.

The great sensitivity of the M(CO)₅ visible band is attributed to the existence of the vacant coordination site. Photolysis performed in mixed matrices, e.g. Ne matrix doped with 2% Xe, for Cr(CO)₅ resulted in the formation of two visible bands centred at 628 and 487nm corresponding to Cr(CO)₅(Ne) and Cr(CO)₅(Xe) species respectively [14]. These could be interconverted photochemically by further photolysis at selective wavelengths (Scheme 1.6.1).



Scheme 1.6.1

Since the largest proportion of the matrix environment was Ne, the shift in the visible band is further evidence that the interaction occurred with the vacant site on the metal fragment.

Conclusive evidence for the structure of the M(CO)₅ fragment came from gas phase work [29-31]. An absorption maximum at 620nm for Cr(CO)₅ correlated well with values inferred from flash photolysis experiments in fluorinated hydrocarbons [32] and in rare-gas matrices [14], while the IR

bands were virtually identical to those observed for the metal fragment in the Ne matrix, thus confirming square pyramidal C_{4v} geometry. The results also confirm the negligible interaction between $Cr(CO)_5$ and both Ne and fluorinated hydrocarbon complexes. A number of factors contribute to the variation in binding energies in complexes. It was found that the binding energy of different linear alkanes increased with the size of the alkane [31(b)], while in the case of fluorinated alkanes the trend depended on the position and degree of substitution. A bonding strength of 45.4 kJmol^{-1} was obtained for *n*-hexane with $W(CO)_5$ compared with that of $< 21 \text{ kJmol}^{-1}$ for methane. The lack of apparent bonding in the latter case may be attributed to the formation a weak 2-electron, 3-centre C-H-M bond through $\sigma \rightarrow M$ donation, or to the steric factors involved in the approach of CH_4 to the metal [33].

At about the same time, the use of flash photolysis in the observation of $Cr(CO)_5$ species was increasing. Nasielski *et al.* investigating $Cr(CO)_6$ in cyclohexane reported the presence of two transient species absorbing in the visible region (483 and 445nm) [21], however later work showed that the presence of these species was as a result of solvent impurities which reacted with $Cr(CO)_5$ [34, 35]. In pure cyclohexane the visible absorption band with maximum at 503nm is attributed to $Cr(CO)_5(\text{cyclohexane})$ and not to "naked" $Cr(CO)_5$ ($\lambda_{\text{max}} = 620\text{nm}$) [35]. The half-life of the solvated species in CO saturated cyclohexane was 25 μs , before reaction with CO and reformation of $Cr(CO)_6$ occurred.

Differences in the strength of $Cr(CO)_5$ -solvent interactions were also observed in solution studies. Kelly *et al.* compared the flash photolysis of $Cr(CO)_6$ in perfluoromethylcyclohexane (Pfcy) [32, 36] with that in cyclohexane [34, 35]. In each case a transient signal was produced within the time resolution of the apparatus (ca. 5ns), occurring at 503nm in cyclohexane

and at 620nm in Pfcy but the rate of reaction of these species with CO to yield Cr(CO)_6 was very different.

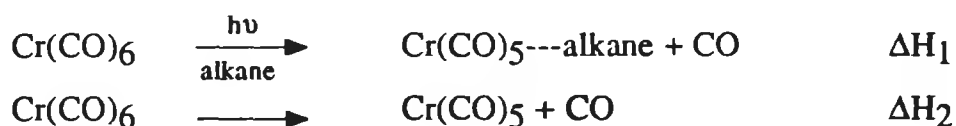


cyclohexane	503nm	$k_2 = 3 \times 10^6 \text{ dm}^3 \text{ mol}^{-1} \text{ s}^{-1}$ [35]
Pfcy	620nm	$k_2 = 3 \times 10^9 \text{ dm}^3 \text{ mol}^{-1} \text{ s}^{-1}$ [32]

The difference in rates was attributed to the binding of the respective solvents with the Cr(CO)_5 , the interaction with cyclohexane being much stronger and thus the displacement by CO being much slower. The positioning of the visible band of Cr(CO)_5 in Pfcy (624nm) [32] is very close to that observed in the gas phase (620nm) [30] and in the Ne matrix (620nm) [14], suggesting that the interactions are the same and hence essentially zero. Formation of the dinuclear species $\text{Cr(CO)}_5\text{Cr(CO)}_6$ (formed by the reaction of the fragment with the parent in the absence of CO), was observed in Pfcy but not in cyclohexane, presumably because the solvated species will have formed more rapidly in the latter solvent. Another possible reason for not observing the dinuclear species in cyclohexane, is that most of the initial studies in cyclohexane were carried out using conventional flash photolysis, and therefore the concentration of Cr(CO)_6 used would be extremely low (ca. 10^{-5}M). Thus, the possibility of dimer formation occurring was greatly reduced. As higher concentrations of Cr(CO)_6 , (ca. 10^{-3}M) were used for the laser flash photolysis studies in Pfcy, the likelihood of the dinuclear species forming was greatly enhanced. Studies in low temperature solvents [37] and liquid noble gases [19, 38] employing IR detection revealed that the metal carbonyl fragment possessed the same geometry, C_{4v} as previously

determined in matrix [9] and gas phase studies [31(b)]. Solvent impurity complexes, for example, $\text{Cr}(\text{CO})_5(\text{H}_2\text{O})$ [39] and unstable species such as $\text{Cr}(\text{CO})_5(\text{N}_2)$ [40] and $\text{Cr}(\text{CO})_5(\text{H}_2)$ [41] were also detected by TRIR spectroscopy [42].

The key feature of catalysis whether homogeneous or heterogeneous is the generation of a coordinatively unsaturated species, which is then able to react with other species. This involves the breaking and making of bonds, the strengths of which must be known, in order to understand and predict new reactions. Photoacoustic calorimetry, which involves dissociation of $\text{M}(\text{CO})_6$ and monitoring of the thermal changes generated as acoustic waves, is one method of determining bond strengths. The bond dissociation energy (ΔH_1) for $\text{Cr}(\text{CO})_6$ in alkane solvents can be determined from the difference between the ΔH 's for $\text{Cr}(\text{CO})_6$ in the gas phase reaction and in the alkane solvents provided that $\text{Cr}(\text{CO})_6$ and $\text{Cr}(\text{CO})_5(\text{alkane})$ have similar solvation energies (equation 1.6.3).



$$\Delta H_2 - \Delta H_1 = \text{measure of Cr}(\text{CO})_5\text{---alkane bond energy} \quad (1.6.3)$$

Employing a laser pyrolysis technique, Smith and co-workers obtained the gas phase dissociation energy values for $\text{M}(\text{CO})_6$ ($\text{M} = \text{Cr}, \text{Mo}$ or W : 154.6, 170.1, 193.2 kJmol^{-1} respectively) [43]. Peters [44] and later Burkey [45] using the photoacoustic technique measured the solution ΔH^\ddagger values in various hydrocarbon solvents (Table 1.6.2).

Solvent	Heptane	Pentane	Isooctane	Cyclohexane
ΔH^\ddagger (kJmol ⁻¹)	113.4 ^a	117.2 ^b	108.4 ^b	101.6 ^b
	114.2 ^b			

^a reference [44], ^b reference [45]

Table 1.6.2 Activation enthalpies for the dissociation of Cr---alkane bonds.

Thus, the bond interaction of Cr(CO)₅(alkane) is of the order of 42 kJmol⁻¹ and as this interaction is assumed to be an "agostic" interaction [46], this is taken as a measure of an "agostic" bond. The dissociation energies of alkane from W(CO)₅(alkane) in the gas phase, resulted in values for W(CO)₅(pentane) (44.5 kJmol⁻¹) which were similar to those obtained for Cr(CO)₅(pentane) (37.4 kJmol⁻¹), even though a different technique was employed [45].

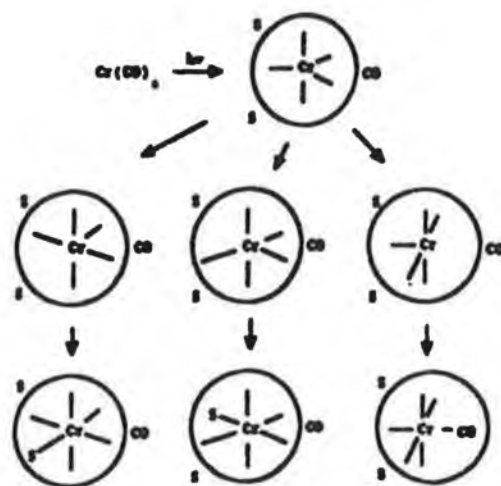
Solution flash photolysis experiments carried out initially revealed important information regarding the existence of coordinatively unsaturated metal carbonyls. A disadvantage of the techniques employed was the limit of time resolution which could be attained, at best, ca. 5ns (UV/visible detection) and 10 μ s (IR detection). On these timescales, the coordinatively, unsaturated species no longer exists and the first detectable species is Cr(CO)₅(solvent). Advances in flash photolysis covering picosecond and femtosecond timescales enabled the initial stages of the photochemistry to be studied.

Peters and colleagues investigated the formation of the solvated species, Cr(CO)₅(S) in both THF and cyclohexane and found that it was produced in less than 25ps [47]. Later, Simon and Xie showed that Cr(CO)₅(cyclohexane) formed in less than 0.8ps while a 2.5ps rise time was

observed for methanol, reflecting a longer solvent reorganisation time [48]. Faster studies on a femtosecond timescale were performed by Joly and Nelson [49] and revealed that the initially excited $\text{Cr}(\text{CO})_6$ is purely dissociative and forms "naked" $\text{Cr}(\text{CO})_5$ in about 300fs. A similar rise time, as observed by Simon and Xie was recorded for the $\text{Cr}(\text{CO})_5(\text{MeOH})$ complex [48(a)]. However, shifts in the visible band of this complex to the blue over a period of ca. 70ps suggests that $\text{Cr}(\text{CO})_5(\text{MeOH})$ is initially formed vibrationally hot and cools (relaxes) over this period. In the case of cyclohexane and THF, similar effects were observed [50]. Further evidence supporting the fact that the primary photoproduct is vibrationally hot following dissociation was obtained from transient infrared [51, 52] and Raman studies [53, 54]. The timescale on which relaxation occurs depends on the environment (i.e. solution or gas phase) and on the technique employed [54].

The first evidence that a single photon of energy can generate lower fragments of metal carbonyl complexes was obtained from the photolysis of $\text{Fe}(\text{CO})_5$ in the gas phase [55]. The degree of fragmentation depends on the laser energy. By contrast, in solution only one primary photoproduct, e.g. $\text{Cr}(\text{CO})_5$, is produced because of the rapid dissipation of excess energy into the surrounding medium before ejection of additional CO's can occur. The vibrational relaxation time of $\text{M}(\text{CO})_5(\text{S})$ is much faster when the solvated species is produced from $\text{M}(\text{CO})_5(\text{L})$ (L = pyridine, piperidine) rather than from $\text{M}(\text{CO})_6$ [56]. The explanation of this resides in the amount of energy that can be deposited in the dissociating ligand, the organic ligands absorbing more energy than the carbonyl ligand.

Despite the large number of studies conducted on the photodissociation of $\text{Cr}(\text{CO})_6$ in solution, the exact mechanism and states involved in the photodissociative process and subsequent solvation of $\text{Cr}(\text{CO})_5$ have not



S = Solvent, matrix gas

Figure 1.6.1 Relaxation of excited $\text{Cr}(\text{CO})_5$ via the Berry twist.

Spears and co-workers, in an attempt to distinguish between the C_{4v} and D_{3h} states in the early stages of the photochemistry, suggested that the unsolvated analogue of both species were in equilibrium and remained "naked" for about a hundred picoseconds and then reacted in parallel paths at different rates with the solvent molecules to produce $\text{Cr}(\text{CO})_5(\text{solvent})$ [50(c), 62, 63].

A lot of the photochemistry of $\text{Cr}(\text{CO})_5$ has been elucidated, but the more complex features still remain to be unravelled.

1.7 Kinetics and mechanisms of substitution reactions of $\text{M}(\text{CO})_6$ and $\text{M}(\text{CO})_5(\text{L})$ complexes (L = solvent or ligand)

In the 1960's, many studies on the kinetics of substitution and exchange

reactions of $\text{Cr}(\text{CO})_6$, $\text{Mo}(\text{CO})_6$ or $\text{W}(\text{CO})_6$ were reported [64].



These studies conducted in both the gas phase and in solution indicated that the Group VI metals reacted with ligand (phosphine or amine) at a rate which was governed by a simple first-order law.

$$\text{Rate} = k_1[\text{M}(\text{CO})_6] \quad (1.7.2)$$

However, in 1967 Graham and Angelici carried out similar work and they found that $\text{Mo}(\text{CO})_6$ with the proper choice of ligand and ligand concentration, reacted with phosphine and phosphite ligands at a rate which was dependent upon the concentration and nature of the ligand used [65].

$$\text{Rate} = k_1[\text{M}(\text{CO})_6] + k_2[\text{L}][\text{M}(\text{CO})_6] \quad (1.7.3)$$

The two-term rate law indicated that both S_N1 (dissociative) and S_N2 (associative) mechanisms were in operation. Positive ΔS_1^\ddagger values for k_1 path and negative ΔS_2^\ddagger values for k_2 paths supported the proposed mechanisms. The values of ΔH_1^\ddagger for the k_1 path decreased in the order $\text{Cr}(\text{CO})_6 \sim \text{W}(\text{CO})_6 > \text{Mo}(\text{CO})_6$. The magnitude of the second-order rate constant, k_2 , was found to be a function of the basicity of the ligand L and increased $\text{As}(\text{C}_6\text{H}_5)_3 < \text{P}(\text{OC}_6\text{H}_5)_3 < \text{P}(\text{C}_6\text{H}_5)_3 < \text{P}(\text{OCH}_2)_3\text{CC}_2\text{H}_5 < \text{P}(\text{n-C}_4\text{H}_9)_3$. These workers also found that as the size of the metal atom increased (from Cr to Mo to W) the S_N2 pathway was preferred, for a given ligand concentration. Since very few 18 electron complexes are known to undergo nucleophilic attack, it has been

suggested that steric crowding would reduce the possibility of attack by a ligand to form a seven-coordinated activated complex or intermediate [66]. As the $M(\text{CO})_6$ are octahedral complexes, the metal atoms have filled t_{2g} orbitals directed between the CO groups, and that the metal atom has a very low positive charge (ca. +0.35 for Cr) suggested that these complexes would be one of the least likely to undergo nucleophilic attack [67]. However, the greater tendency of $\text{Mo}(\text{CO})_6$ and $\text{W}(\text{CO})_6$, as compared to $\text{Cr}(\text{CO})_6$ to react by the S_N2 mechanism was expected when the larger sizes of Mo and W were taken into account. The S_N1 mechanism is common to all reactions of metal hexacarbonyl complexes and it is the only mechanism in which very poor nucleophiles such as amines [64, 65(a)] and CO can be used.

The first-order rate constants, k_1 , and activation parameters were determined in solution by two different research groups (Werner & Prinz [64] and Graham & Angelici [65]) and were in good agreement for the reactions of all three metal hexacarbonyls. In the gas phase the first-order rate constants of CO exchange were somewhat, though not greatly different from those obtained in hydrocarbon solutions [66]. The difference between k_1 in solution and the gas phase was small, thus emphasising the small role played by the solvent in the reactions. Within experimental error the activation parameters were the same in the two phases. The rate of substitution in $\text{Mo}(\text{CO})_6$ was observed to be 11-fold faster in tetrahydrofuran/dioxane solvent than in *n*-decane/cyclohexane. It was concluded that this acceleration was probably a result of some S_N2 attack by the nucleophilic ether solvents on $\text{Mo}(\text{CO})_6$, rather than a solvent effect on the S_N1 mechanism.

Covey and Brown reported that the substitution of amine in $\text{Mo}(\text{CO})_5(\text{amine})$ complex by phosphine ligands followed the two-term rate law also [68].

$$\text{Rate} = (k_1 + k_2[\text{L}])[\text{M}(\text{CO})_5(\text{amine})] \quad (1.7.4)$$

The rate constant k_1 was related to the first-order dissociative process leading to the intermediate $\text{M}(\text{CO})_5$, which upon reaction with L, yielded $\text{M}(\text{CO})_5(\text{L})$. Attack on the metal centre by L, displacing the amine to form the monosubstituted product, increased with increasing ligand basicity L, $\text{P}(\text{OC}_6\text{H}_5)_3 < \text{P}(\text{OCH}_3)_3 < \text{P}(\text{n-C}_4\text{H}_9)_3$ [69]. Evidence that the coordinatively unsaturated metal carbonyl intermediate $\text{M}(\text{CO})_5$ can be stabilised by the binding of rare gas atoms or CH_4 has been obtained from matrix isolation studies [28]. The first-order rate constant, k_1 decreased with increasing amine basicity, that is, primary > secondary > tertiary amine, while k_2 , the second-order rate constant was influenced by steric requirements of the leaving group [68]. The lack of influence that the steric requirements of the entering ligand have in determining the relative reactivities of the ligands towards the six-coordinate complex was noted also by Ingemanson and Angelici, in the bimolecular process for substitution of $\text{W}(\text{CO})_5(\text{amine})$ complexes [70]. However, it was found that the observed rates of dissociation of L from $\text{Cr}(\text{CO})_5(\text{L})$ were not greatly influenced by the steric requirements of ligand L. The steric requirement is measured by the cone angle [71]. In $\text{P}(\text{C}_6\text{H}_5)_3$ and $\text{As}(\text{C}_6\text{H}_5)_3$, the cone angles are almost identical but the rates obtained differed by a factor of 100. They concluded that the difference in the rates was as a result of a mixture of three factors, σ -donation, π -acceptance or steric size [70].

Since Strohmeier's pioneering work in the photochemistry of metal carbonyls, many important results on rates of substitution reactions have been achieved [4]. Dahlgren and Zink investigated the photosubstitution reactivity of $\text{W}(\text{CO})_5(\text{L})$ (L = N-, P- donor ligands, Br^- , CS) complexes [72]. Three categories of reactivity were found: (i) nitrogen donor complexes, for example,

W(CO)₅(pyridine) showed efficient ligand photosubstitution but reduced carbon monoxide replacement, while the phosphorus-donor materials underwent both efficient carbon monoxide and ligand substitution. Br⁻, CS, methyloxycarbene and phenyloxycarbene showed reduced substitution efficiency in all metal-ligand bond types.

Similar work was carried out by Atwood and Wovkulich, investigating the rate of dissociation of the ligand in Cr(CO)₅(L) complexes [73(a)].



The order of lability $\text{As(C}_6\text{H}_5)_3 > \text{P(C}_6\text{H}_5)_3 > \text{P(OC}_6\text{H}_5)_3 > \text{P(OCH}_3)_3$ was similar to that found by Dobson and Smith [74].

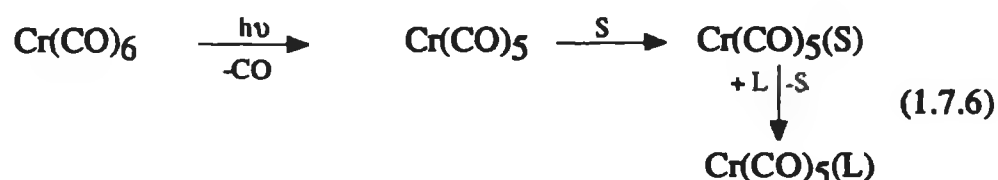
Substitution of a CO group by a ligand L has the potential to determine the mode of further substitutions, for example, the substitution of a CO in Cr(CO)₆ by PPh₃ increased the lability of the *cis* CO groups by a factor of 300 [73(b)]. This effect was found to be related to the placement of the ligands in the five-coordinate intermediate. The intermediate may have either D_{3h} or C_{4v} symmetry (trigonal bipyramidal or square pyramidal respectively), with the lowest energy form being square pyramidal [75]. The degree of labilisation observed for a given ligand was determined by the magnitude of the difference between CO and L. They concluded that ligands which were weak σ -donors and non- π -acceptors were most likely to be strongly oriented toward occupancy of the basal position in the square pyramidal intermediate, and thus strongly *cis* labilising, (e.g. Cl⁻, NO₃⁻). Ligands which were moderately good σ -donors, but weaker in π -acceptor character than CO, for example, NC₅H₅

and PPh_3 are more stable in the basal position than CO, but as the ligand becomes more strongly σ -donating or π -accepting (e.g. H^-), its preference for the basal position diminishes with the result that H^- is not a labilising ligand. If the ligand is a stronger π -acceptor than CO (for example, NO) the *trans* ligand becomes labile toward dissociation. Dobson found evidence for weaker M-C_{cis} bonding in $\text{M}(\text{CO})_5(\text{X})$ compounds in the frequencies of M-C stretching mode [76]. The extent of π -bonding between the metal and CO groups *trans* to a ligand which is a weaker π -acceptor than CO is greater than to the CO groups *cis* to that ligand. Therefore it was hypothesised that ligands which are weaker π -acceptors than CO and which upon substitution for CO labilise the complex toward dissociative ligand loss, (for example, $\text{Re}(\text{CO})_5(\text{Br})$ is labile with respect to $\text{Re}(\text{CO})_6^+$) preferentially labilise the *cis* positions.

In general, complexes of the type $\text{M}(\text{CO})_5(\text{S})$, where S = solvent and M = Cr, Mo or W can be prepared as transient species by flash photolysis techniques or as stable intermediates by conventional photochemical techniques depending on the nature of S. For weak coordinating solvents like n-alkanes, benzene, toluene and their fluorinated analogues, the $\text{M}(\text{CO})_5(\text{S})$ species are short-lived and undergo rapid substitution with the offered nucleophile. In a case of a strong coordinating solvent like THF, it is possible to prepare pure and stable complexes of the type $\text{M}(\text{CO})_5(\text{THF})$ in solution and in some instances these THF adducts can be isolated. Recently, through the study of intermediates by pulsed laser flash photolysis, it has been revealed that in many cases the species produced in predominant concentration after metal-ligand bond fission were not coordinatively unsaturated but were specifically solvated [32, 48, 50(c), 77, 78]. It has been found that upon Cr-CO bond fission in $\text{Cr}(\text{CO})_6$, the $\text{Cr}(\text{CO})_5$ produced reacted very rapidly with solvent to afford $\text{Cr}(\text{CO})_5(\text{solvent})$ species in which the solvent molecule occupied a position in the inner

coordination sphere of $\text{Cr}(\text{CO})_5$ and formed a coordinate covalent bond with the metal atom. The solvation process has been widely studied, but mechanisms of displacement have been investigated in less detail, even though the mechanism of desolvation has important bearing on catalytic selectivity.

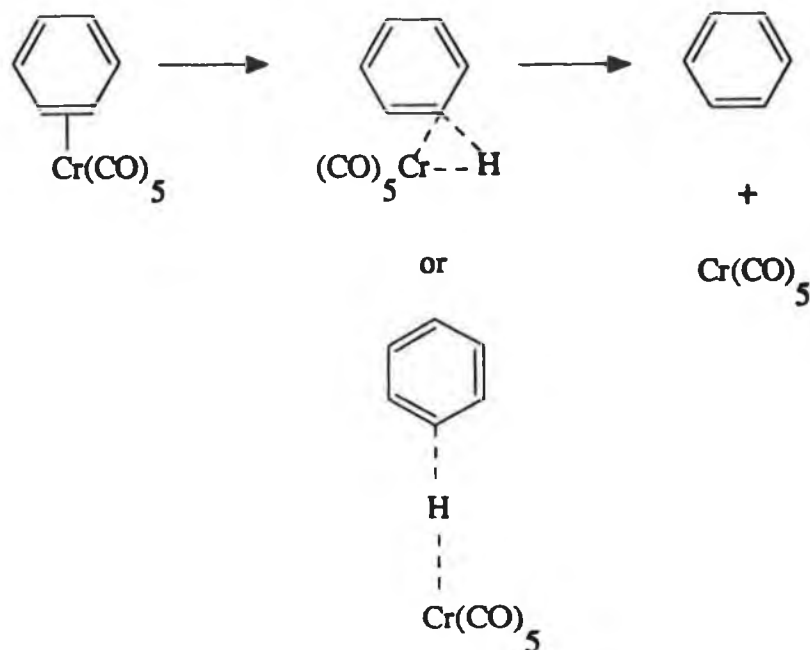
A general mechanism [79(a)] for substitution of hexacarbonyls *via* the solvated species is detailed in equation 1.7.6.



S = solvent, L = nucleophile

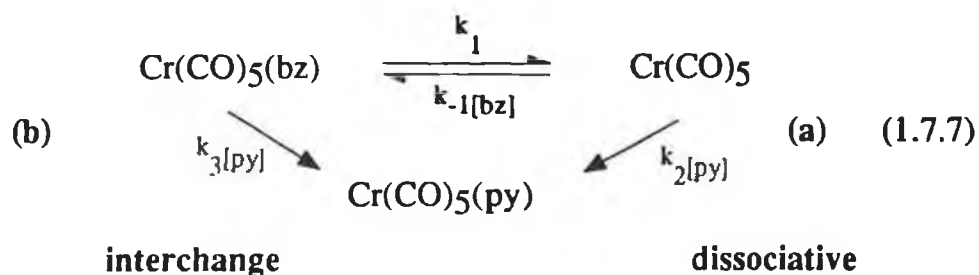
There has been much interest in the nature of metal-solvent interaction, (solvent = alkane or arene) as this interaction is the first step along the reaction coordinate to C-H bond activation by transition metals and also as $\text{Cr}(\text{CO})_6$ has been implicated as a precursor to photochemically generated catalysts involved in olefin isomerisation, hydrogenation and hydrosilylation reactions. Dobson *et al.*, found these compelling reasons to study the mechanisms of desolvation of $\text{Cr}(\text{CO})_5(\text{solvent})$ intermediates in hydrocarbon solution [80]. The displacement of benzene (bz) from photogenerated $\text{Cr}(\text{CO})_5(\text{bz})$ by Lewis bases, L, (L = 1-hexene, piperidine and pyridine) to afford $\text{Cr}(\text{CO})_5(\text{L})$ products was investigated. Coordination of benzene to Cr was *via* an "isolated" C=C bond, and reaction of the intermediate with L was on a microsecond timescale. From the results obtained it was concluded that for L = piperidine and 1-hexene, displacement of benzene occurred by a reversible dissociative mechanism (1.7.7(a)). It was also suggested that a transition state in which benzene was

bonded to Cr, by a " σ -complex", or *via* an agostic C-H-Cr interaction was involved (Scheme 1.7.1).



Scheme 1.7.1

The results obtained for L = pyridine, at very high pyridine concentrations indicated that an interchange process involving displacement of benzene may also be accessible (1.7.7(b))



Results obtained from volumes of activation studies further supported the possibility of an interchange mechanism being present for the displacement of

the solvent [79(a)]. The volume of activation represents the difference in the volume of the transition state and the ground state. It is related to the rate constant and the pressure according to equation (1.7.8).

$$-RT(\partial \ln k / \partial P)_T = \Delta V^\ddagger \quad (1.7.8)$$

and, where ΔV^\ddagger is independent of P

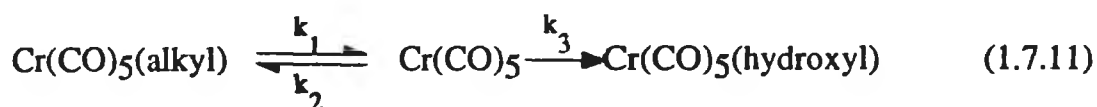
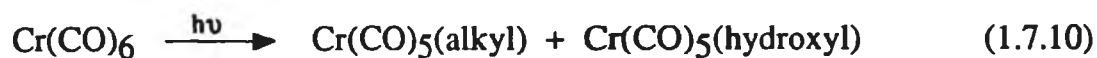
$$\ln k = \text{constant} - (\Delta V^\ddagger / RT)P \quad (1.7.9)$$

Thus, plots of $\ln k$ versus pressure should give straight line of slope = ΔV^\ddagger . The displacement mechanisms of n-heptane and substituted arenes (C_6H_5X , where $X = F, Cl, H, CH_3$) were also investigated [79]. It was found that the volumes of activation were sensitive to the identity of the coordinated solvent and suggested that bonding of chlorobenzene to Cr takes place *via* a lone pair of electrons on Cl, but through an isolated olefinic linkage for benzene, fluorobenzene and toluene. The bonding of n-heptane to Cr is through a C-H-Cr "agostic" interaction and the observed volumes of activation were consistent with the accessibility of an interchange pathway for the displacement of n-heptane from $Cr(CO)_5(\text{hep})$ while dissociative desolvation pathways for arene solvents were favoured. The displacement of the chelate ring by Lewis bases in $M(CO)_4(\text{chelate})$, chelate = chelating ligand coordinating through a sulphur atom, S, reported a significant decrease in ΔV^\ddagger values in going from Cr to Mo to W, a trend interpreted as a change in mechanism for rate-determining chelate ring-opening for Cr to chelate displacement by L for the large Mo atom [81]. In CO displacement reactions of metal carbonyls ($M = Cr, Mo$ or W) where the dissociative and interchange mechanisms are kinetically distinguishable,

particularly for reactions of $M(\text{CO})_6$ [65(a)] and $(\text{phen})M(\text{CO})_4$ [65(b)], it was also noted that the relative contribution of the interchange pathway increased in the order $\text{Cr} < \text{Mo} \sim \text{W}$, the order of increasing atomic size and related to the order of increasing effective nuclear charge ($\text{Cr} < \text{Mo} \ll \text{W}$) [66]. The inability of Mo and W to distinguish between solvents, unlike Cr, was explained by the larger atomic sizes of these atoms which would diminish the steric discrimination. The observed selectivity of $\text{Cr}(\text{CO})_5$ among various L was partly due to the contributions of the interchange pathway.

Kelly *et al.* in 1983, found that the pentacarbonyl species in perfluoromethylcyclohexane was more reactive than the pentacarbonyl species previously observed in cyclohexane [32]. The former species complexed with CO, $M(\text{CO})_6$, cyclohexane or N_2 with rate constants exceeding $10^9 \text{ dm}^3\text{mol}^{-1} \text{ s}^{-1}$. The lifetimes of any excited states in perfluoromethylcyclohexane are less than 5ns ($\tau < 5\text{ns}$). In cyclohexane, the $\text{Cr}(\text{CO})_5(\text{cyclohexane})$ complex had $\tau < 0.8\text{ps}$, however in methanol (MeOH) solution, the absorption signal of $\text{Cr}(\text{CO})_5(\text{MeOH})$ complex exhibited a 2.5ps rise time [48(a)]. The difference in rise time was attributed to the time needed for restructuring of the solvent shell in the MeOH complex, forming Cr - MeOH bond. This restructuring effect was further investigated by Simon and Xie [77] using pentanol as the solvent, as it had both alkyl and hydroxyl groups available for coordination, thus the initial intermediates formed depended on the local solvent structure around the $\text{Cr}(\text{CO})_6$ molecule. For the alcohol complex, $\lambda_{\text{max}} = 460\text{nm}$, while in hydrocarbon solvents (hexane, cyclohexane) the absorption band shifted to lower energy, $\lambda_{\text{max}} = 505\text{nm}$, reflecting the weaker interaction between the bound solvent molecule and the chromium metal [32]. Unlike the methanol complex the instantaneous rise observed suggested that the alkyl chain of the pentanol was coordinated to the vacant site in the solvated intermediate [77].

However, on a faster timescale the changes observed in the transient absorption signal during the first nanosecond were assigned to the rearrangement of the initially formed alkyl complex to the more stable hydroxyl complex. A two-step mechanism was proposed, where the first step was instantaneous ($\tau < 0.8\text{ps}$), while the second step involved either rearrangement of the coordinated ligand or exchange with another molecule.



For linear alcohols (methanol to decanol), the timescales for the restructuring process increased substantially with increasing chain length. Similar work was performed by Simon and Xie on the solution dynamics of 1- and 2-propanol [78]. The rearrangement process was considerably faster in 2-propanol than in 1-propanol despite the similar macroscopic properties, (for example, viscosities at 15°C of 1- and 2-propanol are 2.52 and 2.86cP, respectively) of the two solvents. The dynamics in 2-propanol were similar to those observed in neat ethanol solution and the data obtained revealed that the mechanism for formation of the more stable hydroxyl complex from the initially formed alkane complex depended on the structure of the coordinated solvent molecule. They concluded that the rearrangement in 2-propanol to the more stable hydroxyl complex occurred by a unimolecular displacement mechanism.

Concurrent, with the work carried out by Simon and Lee on the pentanol system, Wang *et al.*, observed the reactions of "naked" Cr(CO)_5 in tetrahydrofuran (THF) solution by picosecond infrared transient absorption [50(c)]. It was observed that THF bonded to the Cr(CO)_5 *via* both its H and O

atom sites, and the adduct with H atom bonding rearranged to the O atom bound configuration. The concept of dual binding sites was consistent with the data for $\text{Cr}(\text{CO})_6$ in pentanol [77], where the changes in transient visible absorption were interpreted as a change over several hundred picoseconds from $\text{Cr}(\text{CO})_5(\text{alkyl})$ to $\text{Cr}(\text{CO})_5(\text{hydroxyl})$ conformation. Rearrangement of the bound THF ligand occurred over a period of 700 picoseconds.

Wieland and van Eldik produced the stable intermediate $\text{M}(\text{CO})_5(\text{THF})$ complex in solution, and then monitored the rate of substitution of THF by piperidine, triethylphosphite and triphenylphosphine ligands using UV/visible spectroscopy and high pressure techniques [82]. ΔV^\ddagger values for all the systems were calculated according to equations (1.7.8) and (1.7.9). As the reactions in THF were orders of magnitude slower than in other investigated solvents, for example, n-heptane [79], substituted arenes [79] and benzene [80], indicated that THF was more strongly coordinated to the metal centre than the other solvent molecules. In $\text{Cr}(\text{CO})_5(\text{THF})$ substitution reactions, the lack of correlation with the size of the entering groups further suggested the operation of a dissociative process, whereas in the case of the Mo and W analogues the ΔV^\ddagger values became more negative, and this increased for larger entering ligands. Therefore, it was suggested that a gradual changeover from a more dissociative to a more associative mechanism occurred along the series Cr, Mo, W. A similar trend was reported for substitution reactions in aliphatic and aromatic hydrocarbon solvents [79, 80]. The decrease in ΔV^\ddagger values, that is, becomes more negative, in the series $\text{Cr} < \text{Mo} < \text{W}$ indicated that bond formation was more important for larger metal centres. Studies of the ligand displacement reactions of various $\text{Cr}(\text{CO})_5(\text{L})$ complexes have shown that generally, the mechanism follows a dissociative pathway [83, 84].

1.8 References

- 1 Masters, C.; *Homogeneous Transition-metal Catalysis*, Chapman and Hall, London, 1981.
- 2 Forster, D.; *J. Am. Chem. Soc.*, 1976, **98**, 846.
- 3 Parshall, G. W.; *Homogeneous Catalysis*, Wiley-Interscience, New York, 1980.
- 4 Strohmeier, W.; *Angew. Chem. Internat. Ed.*, 1964, **3**, 730.
- 5 Crabtree, R. H.; *The Organometallic Chemistry of the Transition Metals*, Wiley-Interscience, New York, 1987.
- 6 Brown, R. A.; Dobson, G. R.; *Inorganica Chim. Acta.*, 1972, **16**, 65.
- 7 Dobson, G. R.; *Accounts of Chem. Research*, 1976, **9**, 300.
- 8 Turner, J. J.; *Photoprocesses in Transition Metal Complexes, Biosystems and Other Molecules*, Kluwer Academic Publishers, 1992.
- 9 Turner, J. J.; Burdett, J. K.; Perutz, R. N.; Poliakoff, M.; *Pure Appl. Chem.*, 1977, **49**, 271.
- 10 (a) Boxhoorn, G.; Stufkens, D. J.; *J. Chem. Soc., Chem. Commun.*, 1979, 1075. (b) Boxhoorn, G.; Stufkens, D. J.; Oskam, A.; *Inorganica Chim. Acta.*, 1979, **33**, 215. (c) Darensbourg, D. J.; Murphy, M. A.; *Inorg. Chem.*, 1978, **17**, 884.
- 11 (a) Kolodziej, R. M.; Lees, A. J.; *Organometallics*, 1986, **5**, 450. (b) Wrighton, M. S.; Abrahamson, H. B.; Morse, D. L.; *J. Am. Chem. Soc.*, 1976, **98**, 4105. (c) Mantua, D. M.; Lees, A. J.; *Inorg. Chem.*, 1983, **22**, 3825.
- 12 Whittle, E.; Dows, D. A.; Pimentel, G. C.; *J. Chem. Phys.*, 1954, **22**, 1943.
- 13 Baldeschwieler, J. D.; Pimentel, G. C.; *J. Chem. Phys.*, 1960, **33**, 1008.

- 14 Perutz, R.N.; Turner, J. J.; *J. Am. Chem. Soc.*, 1975, **97**, 4791.
- 15 Poliakoff, M.; Turner, J. J.; *J. Chem. Soc., Dalton Trans.*, 1974, 2276.
- 16 Burdett, J. K.; Downs, A. J.; Gaskill, G. P.; Graham, M. A.; Turner, J. J.; Turner, R. F.; *Inorg. Chem.*, 1978, **17**, 523.
- 17 Burdett, J. K.; *Coord. Chem. Rev.*, 1978, **27**, 1.
- 18 (a) Stolz, I. W.; Dobson, G. R.; Sheline, R. K.; *J. Am. Chem. Soc.*, 1962, **84**, 3589. (b) *J. Am. Chem. Soc.*, 1963, **85**, 1013.
- 19 Turner, J. J.; Simpson, M. B.; Poliakoff, M.; Maier, W. B. II; Graham, M. A.; *Inorg. Chem.*, 1983, **22**, 911.
- 20 Avery, H. E.; *Basic Reaction Kinetics and Mechanisms*, Macmillan, 1974.
- 21 Nasielski, J.; Kirsh, P.; Wilputte-Steinert, L.; *J. Organomet. Chem.*, 1971, **29**, 269.
- 22 Purcell, K. F.; Kotz, J. C.; *Inorganic Chemistry*, Saunders and Co., Philadelphia, 1977.
- 23 Schaffner, K.; Grevels, F.-W.; *J. Mol. Struct.*, 1988, **173**, 51.
- 24 Thompson, H. W.; Garratt, A. P.; *J. Chem. Soc.*, 1934, **529**, 1817.
- 25 (a) Strohmeier, W.; Gerlach, K.; *Chem. Ber.*, 1961, **94**, 398. (b) Strohmeier, W.; von Hobe, D.; *Chem. Ber.*, 1961, **94**, 164.
- 26 Graham, M. A.; Rest, A. J.; Turner, J. J.; *J. Organomet. Chem.*, 1970, **24**, C54.
- 27 Graham, M. A.; Poliakoff, M.; Turner, J. J.; *J. Chem. Soc. (A)*, 1971, 2939.
- 28 Graham, M. A.; Perutz, R. N.; Poliakoff, M.; Turner, J. J.; *J. Organomet. Chem.*, 1972, **34**, C34.
- 29 Breckenridge, W. H.; Stewart, G. M.; *J. Am. Chem. Soc.*, 1986, **108**, 364.

- 30 Seder, T. A.; Church, S. P.; Ouder Kirk, A. J.; Weitz, E.; *J. Am. Chem. Soc.*, 1985, **107**, 1432.
- 31 (a) Ishikawa, Y.; Brown, C. E.; Hackett, P. A.; Rayner, D. M.; *Chem. Phys. Letts.*, 1988, **150**, 506. (b) Brown, C. E.; Ishikawa, Y.; Hackett, P. A.; Rayner, D. M.; *J. Am. Chem. Soc.*, 1990, **112**, 2530.
- 32 Kelly, J. M.; Long, C.; Bonneau, R.; *J. Phys. Chem.*, 1983, **87**, 3344.
- 33 Saillard, J.-Y.; Hoffmann, R.; *J. Am. Chem. Soc.*, 1984, **106**, 2006.
- 34 Kelly, J. M.; Hermann, H.; Koerner von Gustorf, E.; *J. Chem. Soc., Chem. Commun.*, 1973, 105.
- 35 Kelly, J. M.; Bent, D. V.; Hermann, H.; Schulte-Frohlinde, D. K.; Koerner von Gustorf, E.; *J. Organomet. Chem.*, 1974, **69**, 259.
- 36 Bonneau, R.; Kelly, J. M.; *J. Am. Chem. Soc.*, 1980, **102**, 1220.
- 37 Tyler, D. R.; Petrylak, D. P.; *J. Organomet. Chem.*, 1981, **212**, 389.
- 38 Simpson, M. B.; Poliakov, M.; Turner, J. J.; Maier, W. B. II; McLaughlin, J. G.; *J. Chem. Soc., Chem. Commun.*, 1983, 1355.
- 39 Church, S. P.; Grevels, F.-W.; Hermann, H.; Schaffner, K.; *Inorg. Chem.*, 1985, **24**, 418.
- 40 Church, S. P.; Grevels, F.-W.; Hermann, H.; Schaffner, K.; *Inorg. Chem.*, 1984, **23**, 3830.
- 41 (a) Church, S. P.; Grevels, F.-W.; Hermann, H.; Schaffner, K.; *J. Chem. Soc., Chem. Commun.*, 1985, 30. (b) Jackson, S. A.; Upmacy, R. K.; Poliakov, M.; Turner, J. J.; Burdett, J. K.; Grevels, F.-W.; *J. Chem. Soc., Chem. Commun.*, 1987, 678.
- 42 Hermann, H.; Grevels, F.-W.; Henne, A.; Schaffner, K.; *J. Phys. Chem.*, 1982, **86**, 5151.
- 43 Lewis, K. E.; Golden, D. M.; Smith, G. P.; *J. Am. Chem. Soc.*, 1984, **106**, 3905.

- 44 Yang, G. K.; Peters, K. S.; Vaida, V.; *Chem. Phys. Letters*, 1986, **125**, 566.
- 45 Morse, J. M.; Parker, G. H.; Burkey, T. J.; *Organometallics*, 1989, **8**, 2471.
- 46 (a) Brookhart, M.; Green, M. L. H.; *J. Organomet. Chem.*, 1983, **250**, 395. (b) Brookhart, M.; Green, M. L. H.; Wong, L. L.; *Prog. Inorg. Chem.*, 1988, **36**, 2.
- 47 (a) Simon, J. D.; Peters, K. S.; *Chem. Phys. Letters*, 1983, **98**, 53. (b) Welch, J. A.; Peters, K. S.; Vaida, V.; *J. Phys. Chem.*, 1982, **86**, 1941.
- 48 (a) Simon, J. D.; Xie, X.; *J. Phys. Chem.*, 1986, **90**, 6751. (b) Xie, X.; Simon, J. D.; *J. Am. Chem. Soc.*, 1990, **112**, 1130.
- 49 Joly, A. G.; Nelson, K. A.; *J. Phys. Chem.*, 1989, **93**, 2876.
- 50 (a) Lee, M.; Harris, C. B.; *J. Am. Chem. Soc.*, 1989, **111**, 8963. (b) Xie, X.; Simon, J. D.; *J. Phys. Chem.*, 1989, **93**, 4401. (c) Wang, L.; Zhu, X.; Spears, K. G.; *J. Phys. Chem.*, 1989, **93**, 2.
- 51 Seder, T. A.; Church, S. P.; Weitz, E.; *J. Am. Soc.*, 1986, **108**, 4721. (b) Seder, T. A.; Ouder Kirk, A. J.; Weitz, E.; *J. Chem. Phys.*, 1986, **85**, 1977. (c) Weitz, E.; *J. Phys. Chem.*, 1987, **91**, 3945.
- 52 Ishikawa, Y.; Brown, C. E.; Hackett, P. A.; Rayner, D. M.; *J. Phys. Chem.*, 1990, **94**, 2404.
- 53 Yu, S. C.; Xu, X.; Lingle, R.; Hopkins, J. B.; *J. Am. Chem. Soc.*, 1990, **112**, 3668.
- 54 Heilwell, E. J.; Cavanagh, R. R.; Stephenson, J. C.; *Chem. Phys. Letters*, 1987, **134**, 181.
- 55 Nathanson, G.; Gitlin, B.; Rosan, A. M.; Yardley, J. T.; *J. Chem. Phys.*, 1981, **74**, 361.

- 56 (a) Moralejo, C.; Langford, C. H.; Sharma, D. K.; *Inorg. Chem.*, 1989, **28**, 2205. (b) Moralejo, C.; Langford, C. H.; *Inorg. Chem.*, 1991, **30**, 567.
- 57 Burdett, J. K.; Grzybowski, J. M.; Perutz, R. N.; Poliakov, M.; Turner, J. J.; Turner, R. F.; *Inorg. Chem.*, 1978, **17**, 147.
- 58 Hay, P. J.; *J. Am. Chem. Soc.*, 1978, **100**, 2411.
- 59 (a) Nasielski, J.; Colas, A.; *Inorg. Chem.*, 1978, **17**, 237. (b) Nasielski, J.; Colas, A.; *J. Organomet. Chem.*, 1975, **101**, 215.
- 60 Wieland, S.; van Eldik, R.; *J. Phys. Chem.*, 1990, **94**, 5865.
- 61 Nayak, S. K.; Burkey, T. J.; *Organometallics*, 1991, **10**, 3745.
- 62 Wang, L.; Zhu, X.; Spears, K.G.; *J. Am. Chem. Soc.*, 1988, **110**, 8695.
- 63 Spears, K. G.; Wang, L.; Zhu, X.; Arrivo, S. M.; *SPIE*, 1990, **1209**, 32.
- 64 Werner, H.; Prinz, R.; *Chem. Ber.*, 1966, **99**, 3582.
- 65 (a) Graham, J. R.; Angelici, R. J.; *Inorg. Chem.*, 1967, **6**, 2082. (b) *Inorg. Chem.*, 1967, **6**, 992.
- 66 Angelici, R. J.; *Organomet. Chem. Rev.*, 1968, **3**, 173.
- 67 Gray, H. B.; Beach, N. A.; *J. Am. Chem. Soc.*, 1963, **85**, 2922.
- 68 Covey, W. D.; Brown, T. L.; *Inorg. Chem.*, 1973, **12**, 2820.
- 69 Darensbourg, D. J.; Brown, T. L.; *Inorg. Chem.*, 1968, **7**, 1679.
- 70 Ingemanson, G. M.; Angelici, R. J.; *Inorg. Chem.*, 1968, **7**, 2646.
- 71 (a) Tolman, C. A.; *J. Am. Chem. Soc.*, 1970, **92**, 2956. (b) Boyles, M. L.; Brown, D. V.; Drake, D. A.; Hostetler, C. K.; Maves, C. K.; Mosbo, J. A.; *Inorg. Chem.*, 1985, **24**, 3126.
- 72 Dahlgren, R. M.; Zink, J. I.; *Inorg. Chem.*, 1977, **16**, 3154.
- 73 (a) Wovkulich, M. J.; Atwood, J. D.; *J. Organomet. Chem.*, 1979, **184**, 77. (b) Atwood, J. D.; Brown, T. L.; *J. Am. Chem. Soc.*, 1976, **98**, 3160.

- 74 Dobson, G. R.; Smith, L. A. H.; *Inorg. Chem.*, 1970, **9**, 1001.
- 75 Perutz, R. N.; Turner, J. J.; *Inorg. Chem.*, 1975, **14**, 262.
- 76 Dobson, G. R.; Brown, R. A.; *Inorg. Nucl. Chem.*, 1972, **34**, 2785.
- 77 Simon, J. D.; Xie, X.; *J. Phys. Chem.*, 1987, **91**, 5538.
- 78 Simon, J. D.; Xie, X.; *J. Phys. Chem.*, 1989, **93**, 291.
- 79 (a) Zhang, S.; Zang, V.; Bajaj, H. C.; Dobson, G. R.; van Eldik, R.; *J. Organomet. Chem.*, 1990, **397**, 279. (b) *Organometallics*, 1992, **11**, 3901.
- 80 Zhang, S.; Dobson, G. R.; Zang, V.; Bajaj, H. C.; van Eldik, R.; *Inorg. Chem.*, 1990, **29**, 3477.
- 81 Awad, H. H.; Dobson, C. B.; Dobson, G. R.; Leipoldt, J. G.; Schneider, K.; van Eldik, R.; Wood, H. E.; *Inorg. Chem.*, 1989, **28**, 1654.
- 82 Wieland, S.; van Eldik, R.; *Organometallics*, 1991, **10**, 3110.
- 83 Geoffroy, G. L.; Wrighton, M. S.; *Organometallic Photochemistry*, Academic Press, New York, 1979.
- 84 Darensbourg, D. J.; *Advances in Organometallic Chemistry*, **21**, 113, Academic Press, New York, 1982.

CHAPTER 2

AN INVESTIGATION INTO THE EFFECT OF SOLVENT ON THE REACTION OF $\text{Cr}(\text{CO})_5(\text{SOLVENT})$ WITH CO

2.1 Introduction

The primary step in the photodissociation of $\text{Cr}(\text{CO})_6$ is the loss of a carbonyl group generating a coordinatively, unsaturated $16e^-$ species. It is the generation of these reactive intermediates which enables these compounds to play an important role in catalytic and synthetic processes. However, in solution these species quickly become solvated, yielding $\text{Cr}(\text{CO})_5(\text{solvent})$ complexes. This rapid solvation process has been investigated by many research groups [1, 2], while others have studied the strengths of the Cr---alkane bonds by photoacoustic calorimetry [3,4]. More recently attention has been focused on the rates and mechanisms of displacement of solvent molecules such as alkanes [3-7], benzene [8], chlorobenzene [7, 9, 10] and fluorobenzene [7, 10] from $\text{Cr}(\text{CO})_5(\text{solvent})$ molecules by nucleophiles (L), (equation 2.1.1)



The type of solvent displacement mechanism(s) in operation depends on the solvent being displaced and on the Lewis base (nucleophile). Both dissociative and interchange pathways have been found to be accessible for dissociation of n-heptane, while for benzene and substituted benzenes, a dissociative pathway was more pronounced [8].

In this study, we decided to investigate the strength of the $\text{Cr}(\text{CO})_5$ ---solvent interaction, for solvents such as cyclohexane (CH), methylcyclohexane (MCH), pentane (pen), hexanes (hex) and heptane (hep) by monitoring the decay of the solvated species under CO saturated conditions, in the hope of obtaining a greater understanding of the solvent displacement mechanisms.

2.2 Electronic spectrum of Cr(CO)₆

The bonding involved in this complex has been described in Section 1.2. The lowest energy absorption appearing at $\sim 30,000\text{ cm}^{-1}$ (333nm) corresponds to the ${}^1A_{1g} \rightarrow {}^1T_{1g}$ ligand field (LF) transition. This band appears only as a shoulder on the more intense Cr $\rightarrow \pi^*$ CO charge transfer (CT) absorption at $\sim 35,000\text{ cm}^{-1}$ (286nm). The second LF band, ${}^1A_{1g} \rightarrow {}^1T_{2g}$ is found at $\sim 37,500\text{ cm}^{-1}$ (266nm), while the band at $\sim 43,000\text{ cm}^{-1}$ (233nm) is assigned to the Cr $\rightarrow \pi^*$ CO CT absorption [11]. A UV/visible spectrum is shown in Figure 2.2.1.

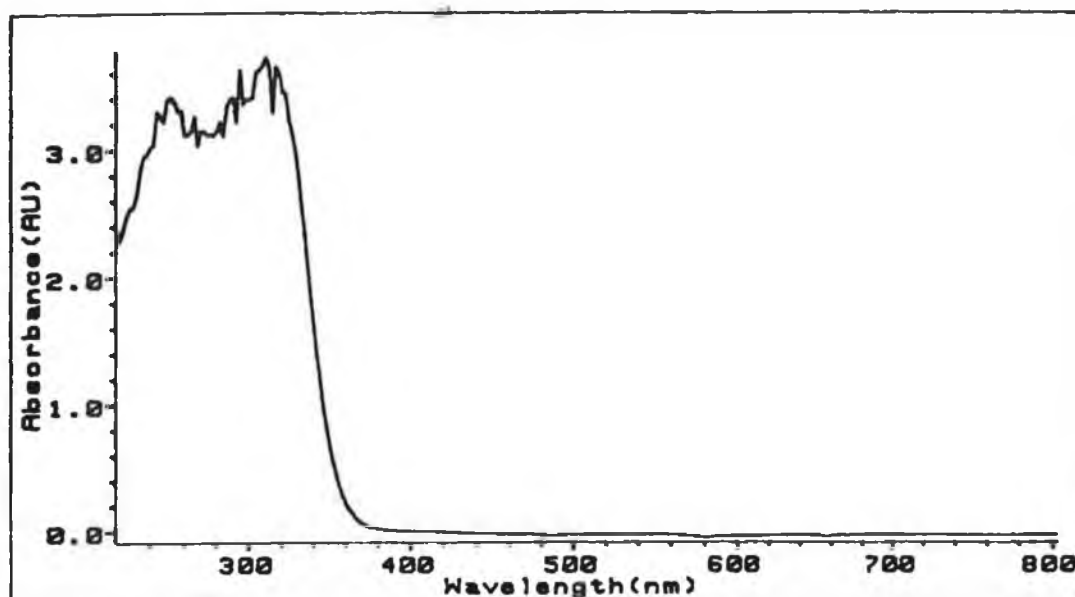


Figure 2.2.1 UV/visible spectrum of Cr(CO)₆ ($2.5 \times 10^{-3}\text{ mol dm}^{-3}$) in cyclohexane.

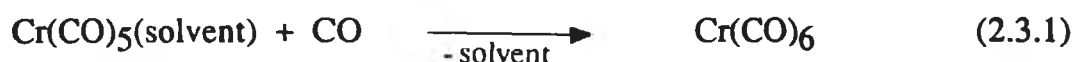
The molar extinction coefficients of Cr(CO)₆ were obtained in each solvent at the excitation wavelength of the laser (354nm). The results are tabulated in Table 2.2.1, while the experimental data is shown in Appendix C.

Solvent (S)	molar extinction coefficient $\epsilon \times 10^{-2}, \text{dm}^3\text{mol}^{-1}\text{cm}^{-1}$
Cyclohexane	2.03
Methylcyclohexane	2.31
Pentane	2.37
Hexanes	2.07
Heptane	2.29

Table 2.2.1 Extinction coefficients of $\text{Cr}(\text{CO})_6$ in various solvents, S at 354nm.

2.3 Flash photolysis of $\text{Cr}(\text{CO})_6$ in CO saturated aliphatic and cyclic hydrocarbon solvents

Flash photolysis of $\text{Cr}(\text{CO})_6$ results in the formation of a coordinatively, unsaturated species, $\text{Cr}(\text{CO})_5$ which reacts with the solvent forming $\text{Cr}(\text{CO})_5(\text{solvent})$ in less than 300fs [2(h)]. A typical transient signal observed is depicted in Figure 2.3.1 and is consistent with equation 2.3.1.



The transient is composed of two parts, (i) the rise time and (ii) the decay. The rise time, which in this study includes the formation of $\text{Cr}(\text{CO})_5(\text{solvent})$ from "naked" $\text{Cr}(\text{CO})_5$. Initial picosecond studies by Peters *et al.* indicated that the solvated species was present within 25ps [2(a), (b)], but later it was shown that the solvent coordination time was 2.5ps in methanol and less than 1ps in

cyclohexane [2(c)]. As the detection of our system is limited to nanoseconds, the solvated species forms in the pulse and hence is not observed.

The decay observed is the reaction of the solvated species with the carbon monoxide, reforming $\text{Cr}(\text{CO})_6$. Thus the rate of decay of this species is a measure of the ease of displacement of the solvent molecule and consequently a measure of the strength of the metal to solvent interaction.

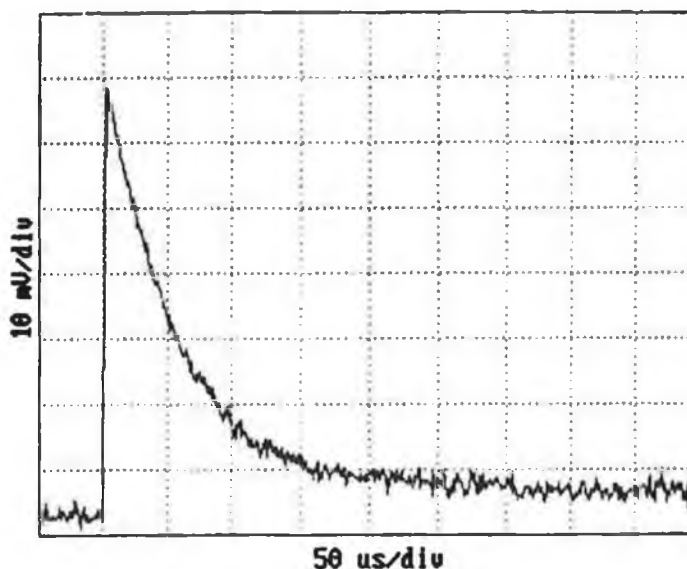


Figure 2.3.1 A typical transient signal obtained for the decay of $\text{Cr}(\text{CO})_5(\text{cyclohexane})$ at 500nm under 1 atmosphere of CO.

2.4 The effect of the power of the laser on the primary photoproduct

This experiment was performed in order to confirm that the formation of $\text{Cr}(\text{CO})_5(\text{solvent})$ species was as a result of a single photon rather than a multiple photon event. The absorbance of the primary photoproduct was measured as a function of the power of the laser. A linear relationship was obtained for the plot of the absorbance of the primary photoproduct formed

versus the relative power of the laser, indicating that a single photon event was operative. This was found to be the case for all the solvents and is graphically shown in Figure 2.4.1, for methylcyclohexane as solvent.

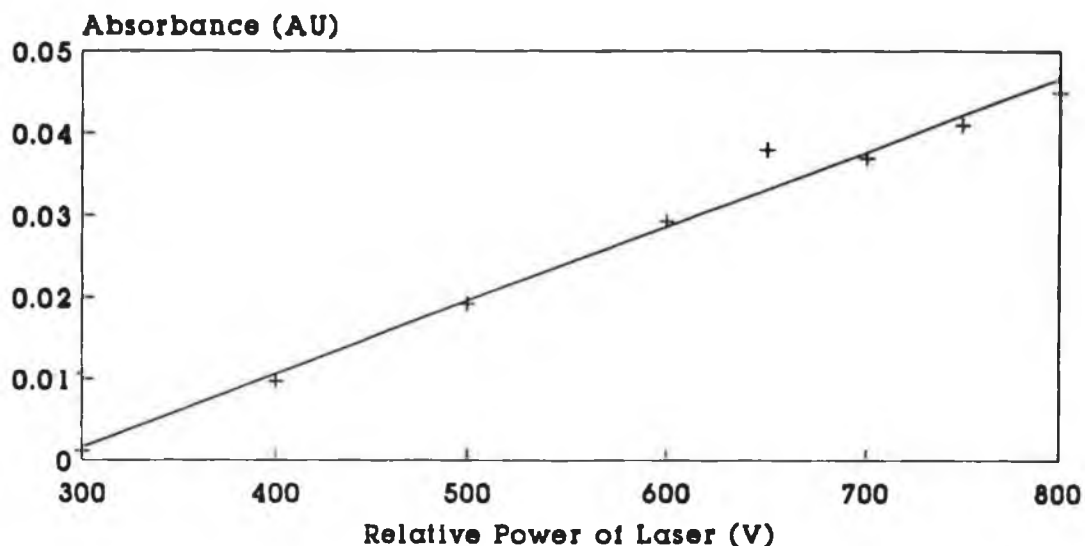


Figure 2.4.1 Plot of absorbance of $\text{Cr}(\text{CO})_5(\text{methylcyclohexane})$ *versus* relative power of laser.

2.5 UV/visible difference spectrum for formation of $\text{Cr}(\text{CO})_5(\text{solvent})$

A difference spectrum was obtained in each solvent by monitoring the reaction of $\text{Cr}(\text{CO})_5(\text{S})$ with CO at a fixed timescale over a range of wavelengths. A typical spectrum obtained, for S = cyclohexane is displayed in Figure 2.5.1.

The UV/visible difference spectrum is a good indicator of the interaction strength between the metal and the solvent [12, 13]. An absorption maximum centred at 620nm was observed for $\text{Cr}(\text{CO})_5(\text{perfluoromethylcyclohexane})$ [5(b), 5(c)], which correlated very well with that observed for $\text{Cr}(\text{CO})_5(\text{Ne})$ [13] in which the interaction between the metal and the neon molecule is suggested

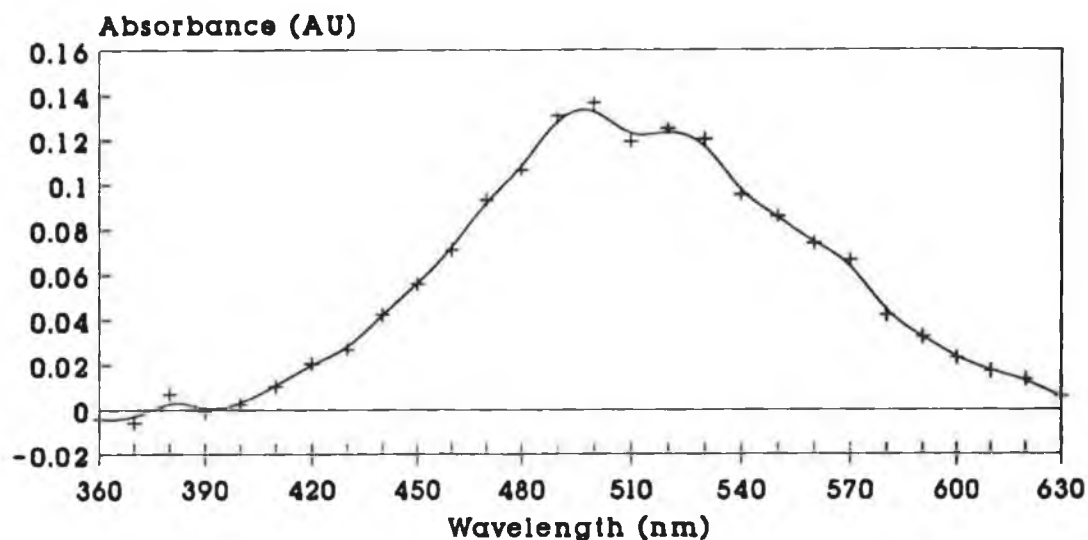
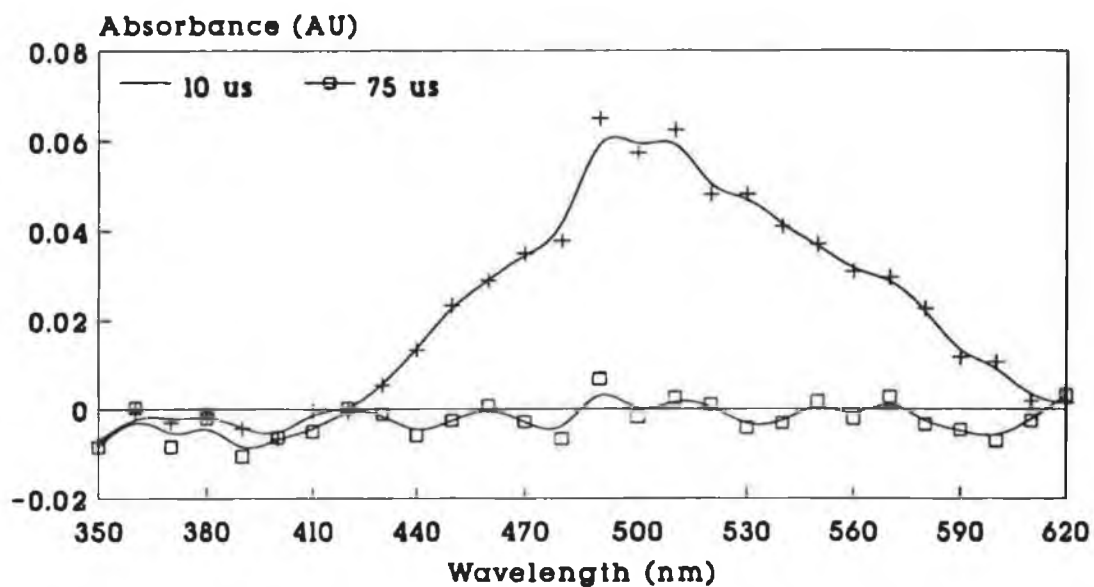


Figure 2.5.1 UV/visible difference spectrum of $\text{Cr}(\text{CO})_5$ (cyclohexane) under 1 atm CO, recorded 10 μs after the laser flash.

to be negligible, thus indicating a very weak solvent interaction, if any in the former complex. Also, gas phase studies, in which the $\text{Cr}(\text{CO})_5$ fragment is free from any interactions, have shown $\text{Cr}(\text{CO})_5$ to have λ_{max} at 620nm [14]. The maximum absorption of the solvated species is roughly the same in all the solvents, centred at $500\text{nm} \pm 5\text{nm}$, indicating that very little difference exists in the strength of the metal to solvent interaction. Similar absorption maxima, for the same system have previously been reported for cyclohexane (503nm) [5(c)] and n-hexane (505nm) [2(a)]. Simon and Xie also found that the absorption spectrum of the hydrocarbon complex was insensitive to the length of the hydrocarbon chain. A similar trend was observed in alcohol solvents [2(g)].

Some kinetic information is also available from the UV/visible difference spectra. In the case of heptane and hexanes, both solvated complexes are formed after 10 μs , but after 75 μs all of $\text{Cr}(\text{CO})_5$ (heptane) has been converted to $\text{Cr}(\text{CO})_6$ compared to only 50% of $\text{Cr}(\text{CO})_5$ (hexanes), thus indicating the

(a)



(b)

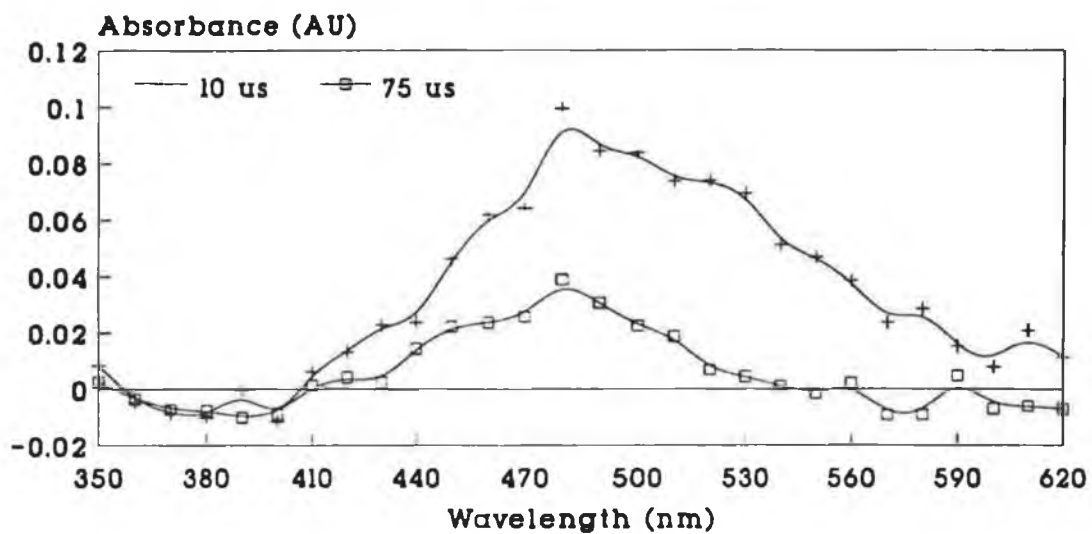


Figure 2.5.2 Comparison of UV/visible difference absorption spectra of (a) $\text{Cr(CO)}_5(\text{heptane})$ and (b) $\text{Cr(CO)}_5(\text{hexanes})$ under 1 atm CO, recorded 75 μs after the laser flash.

differences in the rates of desolvation (Figure 2.5.2). A similar trend was observed for cyclohexane and methylcyclohexane.

The presence of impurities in solvents result in secondary reactions. Usually, these impurities react so strongly with the intermediate species, that the required reaction cannot be observed. The presence of an impurity, in the form of an impurity complex may be observed in the UV/visible difference spectrum. In the desolvation process of cyclohexane from $\text{Cr}(\text{CO})_5(\text{cyclohexane})$ by CO, an absorption maximum was observed at ca. 450nm, with a smaller absorption at ca. 350nm (Figure 2.5.3). In pure cyclohexane, $\text{Cr}(\text{CO})_5(\text{cyclohexane})$ has a λ_{max} of 503nm [5(b), 5(c)], therefore the band at 450nm was assigned to be an impurity complex. As a similar absorption maximum has been reported for a water bound complex, this impurity complex was identified as that of $\text{Cr}(\text{CO})_5(\text{H}_2\text{O})$ [15].

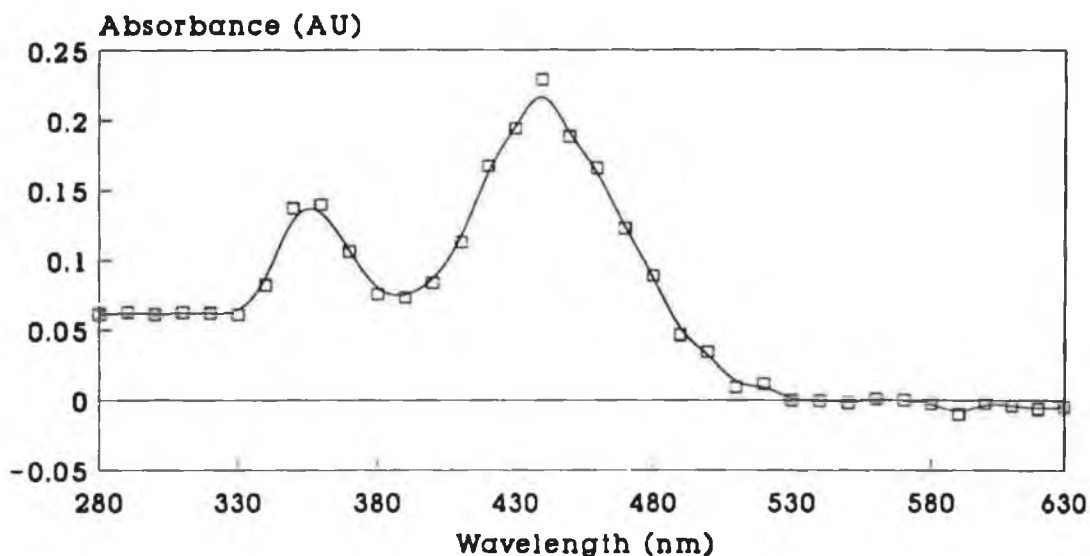


Figure 2.5.3 UV/visible difference spectrum of $\text{Cr}(\text{CO})_5(\text{impurity})$, in cyclohexane under 1 atm CO, recorded 80 μs after the laser flash.

2.6 The rate of reaction of $\text{Cr}(\text{CO})_5(\text{solvent})$ with CO

The rate of decay of the primary photoproduct, $\text{Cr}(\text{CO})_5(\text{solvent})$ upon reaction with CO was consistent with pseudo-first-order kinetics. As the absorption maxima were very similar in all the solvents, 500nm was selected as the monitoring wavelength. The rate of reaction but not the yield is dependent on the concentration of added CO (Figure 2.6.1). This confirms that no other reaction, other than that detailed in equation 2.3.1 is occurring.

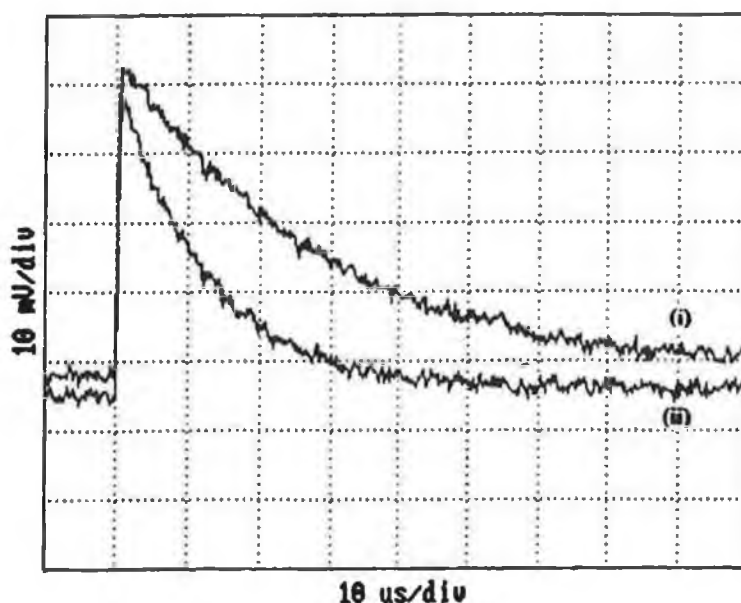


Figure 2.6.1 Decay of transient species (i) under 0.5 atm CO and (ii) under 1 atm CO, monitored at 500nm at 25°C.

The second-order rate constant (k_2) for the reaction of the transient species was obtained by varying the concentration of CO in the solvent and monitoring its rate of decay. A typical transient signal for this reaction is given in Figure 2.3.1.

Plots of the observed rate constant (s^{-1}) versus the concentration of CO

(mol dm⁻³) in aliphatic and cyclic alkane solvents are displayed in Figures 2.6.2 and 2.6.3 respectively, while the second-order rate constants are tabulated in Table 2.6.1, along with the solubility of 1 atmosphere of CO in each solvent at 298K. The data used in the construction of these plots is given in Appendix B (Table B1).

Solvent (S)	Solubility of 1 atm CO at 298K (M) (x10 ²) ^a	k ₂ x 10 ⁻⁶ (dm ³ mol ⁻¹ s ⁻¹)
Cyclohexane	0.9	2.3 ± 0.01
Methylcyclohexane	0.9 ^b	3.5 ± 0.04
Pentane	1.6	5.3 ± 0.03
Hexanes	1.3	5.9 ± 0.05
Heptane	1.2	7.6 ± 0.06

^a calculations shown in Section 5.5, ^b Solubility in MCH is taken to be the same as that in cyclohexane

Table 2.6.1 The second-order rate constants for the reaction of Cr(CO)₅(solvent) with CO at 25°C.

From the slope of the line, a second-order rate constant of 2.3 x 10⁶ dm³mol⁻¹ s⁻¹ was obtained in cyclohexane. This value is close to that of 3.0 x 10⁶ dm³mol⁻¹s⁻¹ quoted by Kelly *et al.* for the same reaction [5(c), 5(d)]. The slight discrepancy between the two values may be as a result of the different values used in each study for the concentration of CO in cyclohexane at 25°C. Kelly *et al.* used a value known for the heptane (1.1 x 10⁻² mol dm⁻³) as no value for cyclohexane had been reported at that time [5(d)]. The value used in this study was 0.9 x 10⁻² mol dm⁻³. The second-order rate constant, k₂, is a

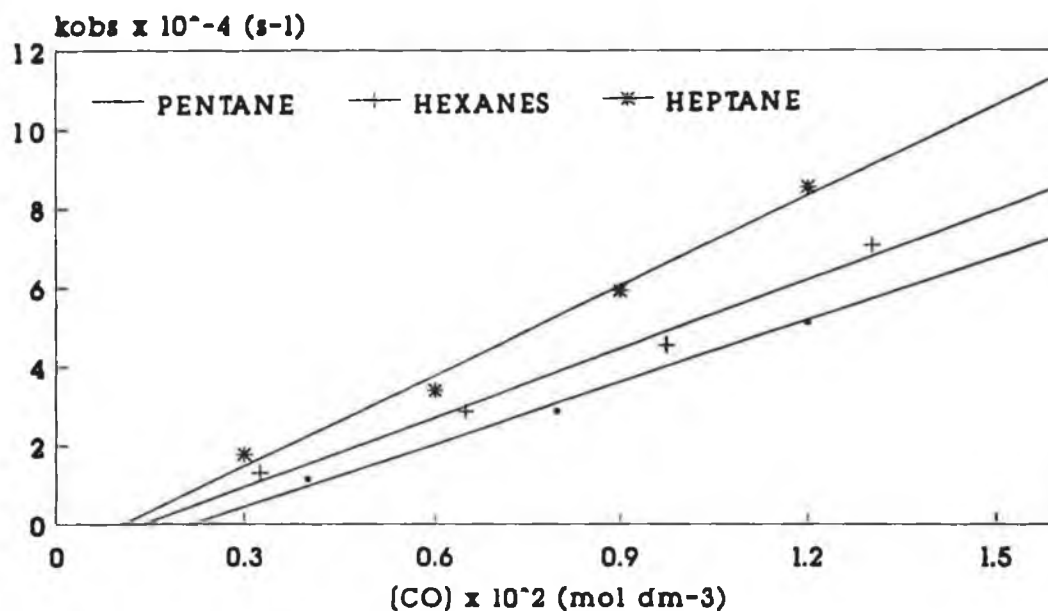


Figure 2.6.2 Plot of k_{obs} (s^{-1}) versus CO concentration (mol dm^{-3}) for the decay of $\text{Cr}(\text{CO})_5(\text{solvent})$ in aliphatic hydrocarbon solvents, monitored at 500nm at 25°C.

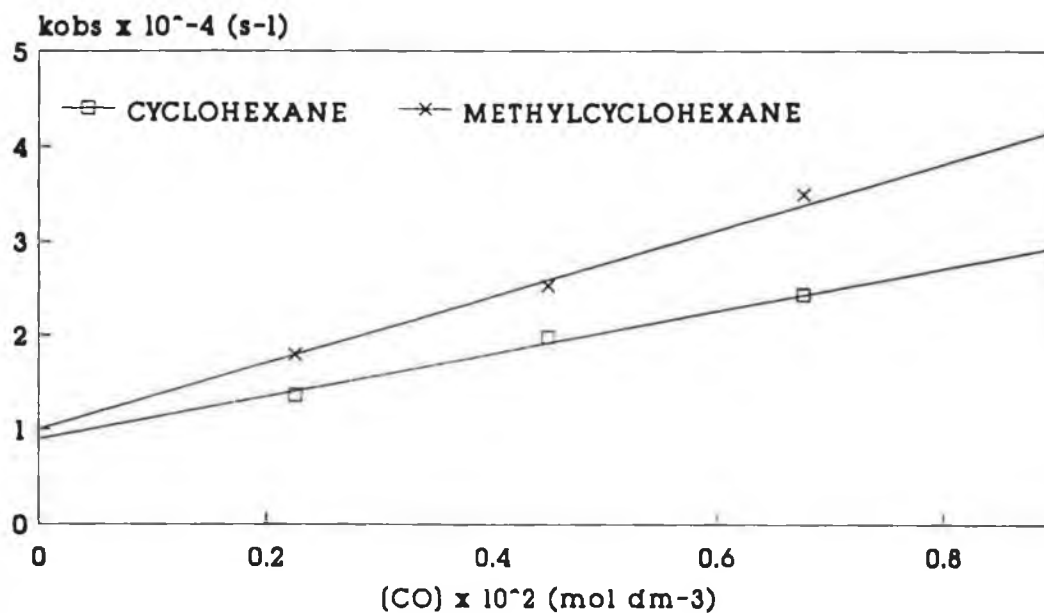


Figure 2.6.3 Plot of k_{obs} (s^{-1}) versus CO concentration (mol dm^{-3}) for the decay of $\text{Cr}(\text{CO})_5(\text{solvent})$ in cyclic hydrocarbon solvents, monitored at 500nm at 25°C.

measure of the rate at which the solvent is displaced from the $\text{Cr}(\text{CO})_5(\text{S})$ intermediate. The cyclic hydrocarbons are removed at about the same rate which is much slower than that for the aliphatic hydrocarbons. The k_2 values increase with the length of the aliphatic chain, and as heptane is the most easily displaced, a weaker bonding interaction with the metal is proposed. The difference in rates of displacement of cyclic *versus* aliphatic hydrocarbons may be attributed to the different modes of bonding to the metal. Cyclohexane has only methylene (CH_2) groups available for bonding, while the aliphatic solvents have both primary (CH_3) and secondary (CH_2) groups available through which bonding may occur. Thus, bonding of the straight chain hydrocarbons *via* the primary CH's would account for the differences observed in the rates. Methylcyclohexane has both methylene groups and a methyl group available but as the rate of displacement resembles that of cyclohexane, bonding is thought also, to occur *via* a methylene group. Also, as secondary CH's are more electron rich than primary CH's, bonding *via* the former group is more favourable [4]. The variation amongst the aliphatic hydrocarbons may be as a result of steric effects, heptane being much more bulkier than the others, thus a weaker bond interaction with the metal and hence, a faster rate of displacement. The 1000-fold increase in the rate of displacement of perfluoromethylcyclohexane compared to cyclohexane was assigned to the extremely weak bonding present in the former complex [5(c)]. This weak bonding was also reflected in the 9-fold increase in the rate of loss of fluorobenzene compared to benzene in an analogous system [10].

2.7 Activation parameter studies for the reaction of $\text{Cr}(\text{CO})_5(\text{solvent})$ with CO

In order to obtain a greater understanding of the reaction mechanisms, the activation parameters were measured. These were calculated according to equations 5.4.1 and 5.4.2. The Arrhenius and Eyring plots are shown graphically in Figures 2.7.1 and 2.7.2, while a summary of the results is detailed in Table 2.7.1. The experimental data is tabulated in Appendix A (Table A1).

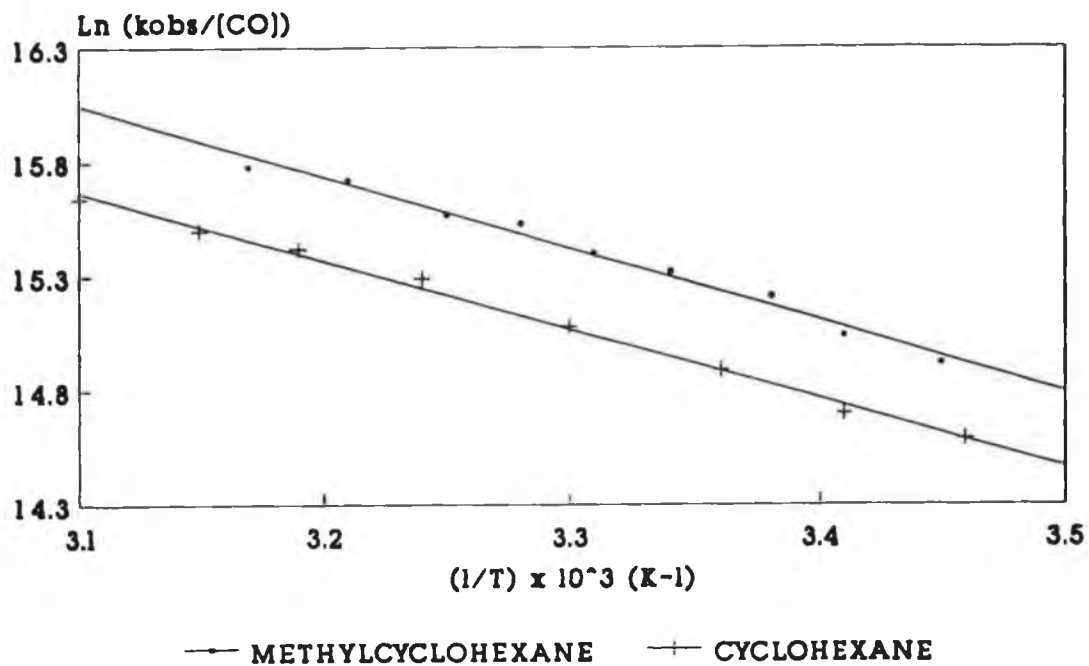
Solvent (S)	E_a^\ddagger (kJmol ⁻¹)	ΔH^\ddagger (kJmol ⁻¹)	ΔS^\ddagger ^a (Jmol ⁻¹ K ⁻¹)	ΔG_{298K}^\ddagger (kJmol ⁻¹)
Cyclohexane	25 ± 1	22 ± 1	-46	36
MCH	26 ± 1	24 ± 1	-39	35
Pentane	19 ± 1	17 ± 1	-60	35
Hexanes	24 ± 1	22 ± 1	-43	34
Heptane	25 ± 1	22 ± 1	-39	34

^a Errors associated with ΔS^\ddagger are 10 Jmol⁻¹K⁻¹

Table 2.7.1 Thermodynamic data associated with the displacement of solvent from $\text{Cr}(\text{CO})_5(\text{solvent})$ by CO.

As can be seen from Table 2.7.1, the activation energies (E_a^\ddagger) for the displacement of the solvents are very similar, within experimental error. Previously, the differences in the second-order rate constants, for the displacement of the solvents were attributed to differences in the binding energies of the solvent to the metal (*vide supra*). In such a case, this difference is expected to be reflected in the activation enthalpy (ΔH^\ddagger) values for the loss of

(a)



(b)

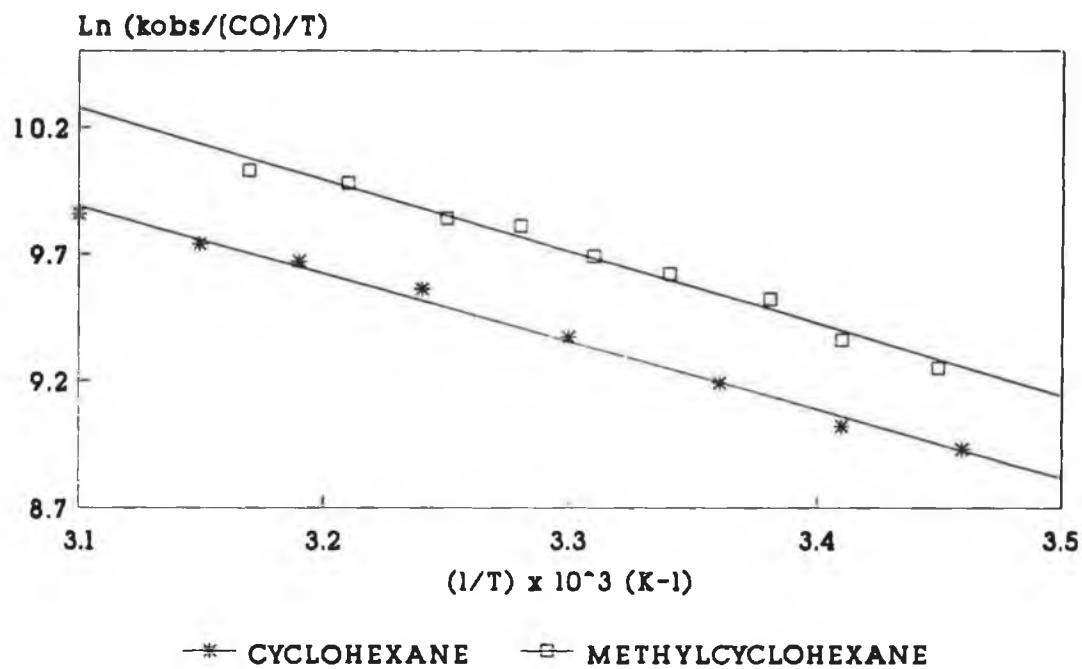
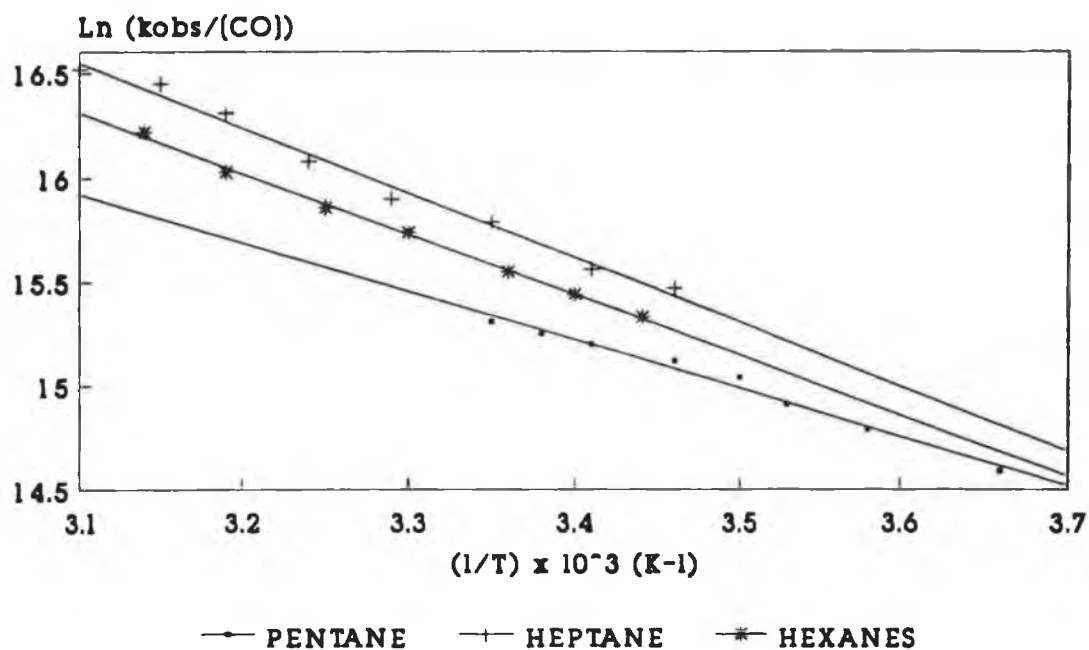


Figure 2.7.1 (a) Arrhenius and (b) Eyring plots obtained for the decay of $\text{Cr}(\text{CO})_5(\text{solvent})$, in the cyclic hydrocarbon solvents, monitored at 500nm.

(a)



(b)

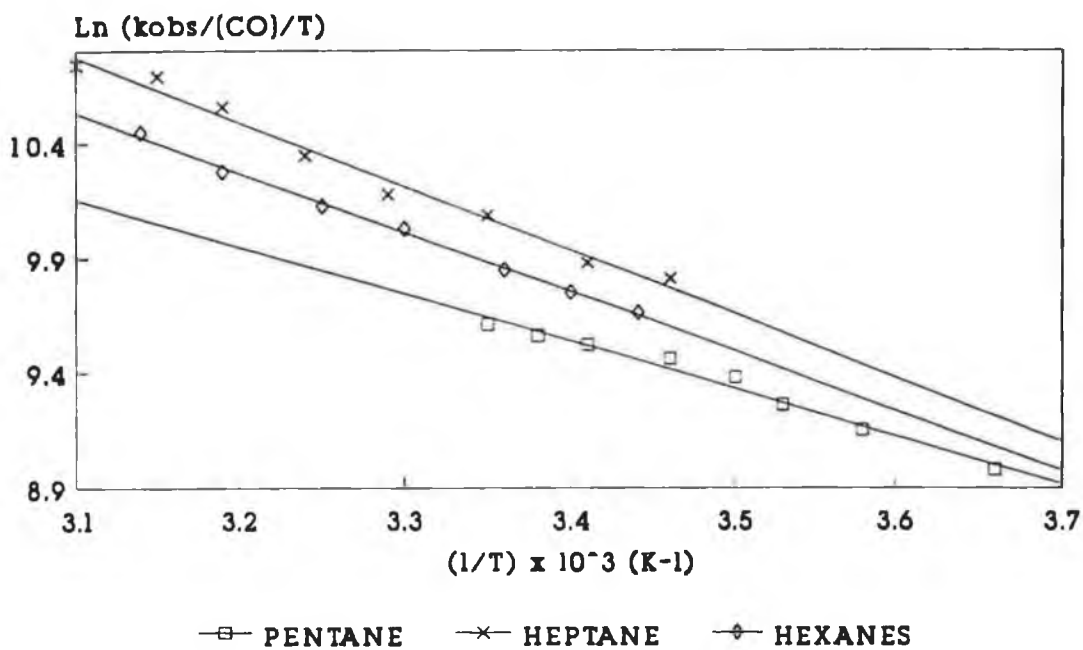
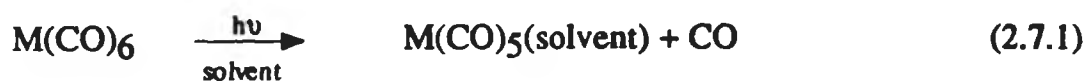


Figure 2.7.2 (a) Arrhenius and (b) Eyring plots obtained for the decay of $Cr(CO)_5(\text{solvent})$, in the aliphatic hydrocarbon solvents, monitored at 500nm.

the solvents. However, this was not found to be the case. The ΔH^\ddagger values were all very similar, being $20 \pm 4 \text{ kJmol}^{-1}$. The activation energy and enthalpy values for pentane are lower than those obtained for the other solvents. A possible reason for such low values may be the limited temperature range (0 - 30°C) over which the activation parameters could be determined, because of the low boiling point of the solvent. Also, the solubility of CO in the solvent, near its boiling point may not be the same as that at lower temperatures.

The similarities in the ΔH^\ddagger values indicate that all the metal - solvent interactions energies are very similar. The most probable mode of coordination of the solvents is *via* an agostic interaction [16]. As cyclohexane has only methylene groups available for bonding to the metal, this may also be the mode of bonding present in the other solvents, even though they have methyl groups present. Determination of metal---alkane bond strengths by photoacoustic calorimetry revealed that binding of the alkanes was *via* the secondary CH also. The reaction enthalpies obtained for the metal---alkane interaction employing this technique were much greater than that observed in this study [3, 4]. The enthalpies were calculated for equation 2.7.1 according to Scheme 2.7.1 and yielded ΔH^\ddagger 's values of 37.4, 40.3 and 52.9 kJmol^{-1} for pentane, heptane and cyclohexane, respectively. In this study it was the displacement of the solvent by a nucleophile (CO) which was used to determine the strength of the Cr to solvent bond. The enthalpy values $\Delta H^\ddagger = 20 \pm 4 \text{ kJmol}^{-1}$ correspond well with that of 21.42 kJmol^{-1} obtained for the displacement of heptane from $\text{Cr}(\text{CO})_5(\text{heptane})$ by pyridine [3]. Pyridine as a nucleophile is very similar to CO, except that it possesses reduced π^* accepting ability. More recently, the substitution of CO in metal carbonyls by silanes has been investigated [18, 19].



$$\Delta H_{\text{M-S}} = \Delta H_{\text{M-CO}} - \Delta H_1$$

where $\Delta H_{\text{M-S}}$ = M-solvent bond energy

$\Delta H_{\text{M-CO}}$ = M-CO bond dissociation energy

(154.56 kJmol⁻¹ for Cr - CO) [17]

ΔH_1 = Enthalpy of equation 2.7.1

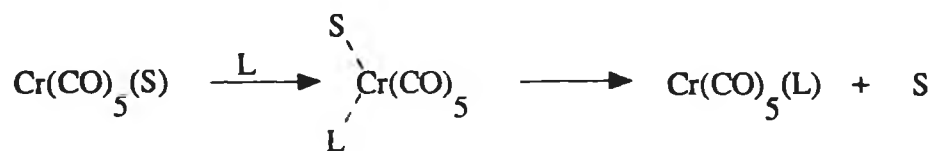
Scheme 2.7.1

As the reactivity of silanes towards metal centres is very similar to that of alkanes, the chemistry involved in metal---silane interactions may be extended to that of metal---alkane interactions. The binding of silanes to the metal is thought to be through a three-centre, two-electron bond, analogous to the agostic three-centre, two-electron bond formed between the alkanes and the metal [4, 16, 20].

As the differences in the second-order rate constants are not reflected in the ΔH^\ddagger values, they must be accounted for in the ΔS^\ddagger values. From Table 2.7.1, an increase in the activation entropy (i.e. to less negative values) is observed in the series, pentane (-60) < hexanes (-43) < heptane (-39 Jmol⁻¹K⁻¹). Thus, this gradual change towards a more dissociative character in the transition state may be attributed to more freedom of motion in the transition state in heptane, compared to that in pentane. The enthalpies calculated for the Cr - S bond, (S = pentane, heptane) further support the proposal that the differences in the k_2 values is as a result of an entropic rather than an enthalpic effect (*vide infra*). A similar trend was observed for the desolvation of alkane solvents (pentane -

dodecane) by CO in (benzene)Cr(CO)₂(solvent) [21]. In the series, pentane to dodecane, the k_2 values increased, while the entropy of activation varied from -18 to -10 Jmol⁻¹K⁻¹ for pentane to dodecane respectively, thus indicating a change in mode of solvent displacement from an interchange mechanism towards a dissociative mechanism. The entropy values are consistent with greater freedom of motion in the transition states of the longer chain alkanes (e.g. dodecane) compared to the shorter alkanes (e.g. pentane). Again, the enthalpy of activation values were very similar ($\Delta H^\ddagger = 24 \pm 2$ kJmol⁻¹) for all the solvents indicating that the difference in reaction rates must be as a result of an entropic effect. Also, it was found that a linear relationship existed between the entropy of activation and the length of the alkane chain.

There are three possible mechanisms, an associative, a dissociative or an interchange which may be involved in the desolvation process. If desolvation was by a dissociative process, the strength of the Cr - solvent bond should closely approximate the activation energies for Cr - solvent bond dissociation. The Cr---alkane bond strengths range from ca. 37 to 53 kJmol⁻¹ [4] and as the enthalpy barrier for the substitution process by CO is 20 ± 4 kJmol⁻¹, implies that the transition state must be associative in the incoming ligand, thus an interchange mechanism is proposed for the displacement of solvent from Cr(CO)₅(solvent) by CO (Scheme 2.7.2).



S = solvent, L = CO

Scheme 2.7.2

This is shown graphically in a potential energy *versus* reaction coordinate diagram, for heptane as solvent (Figure 2.7.3).

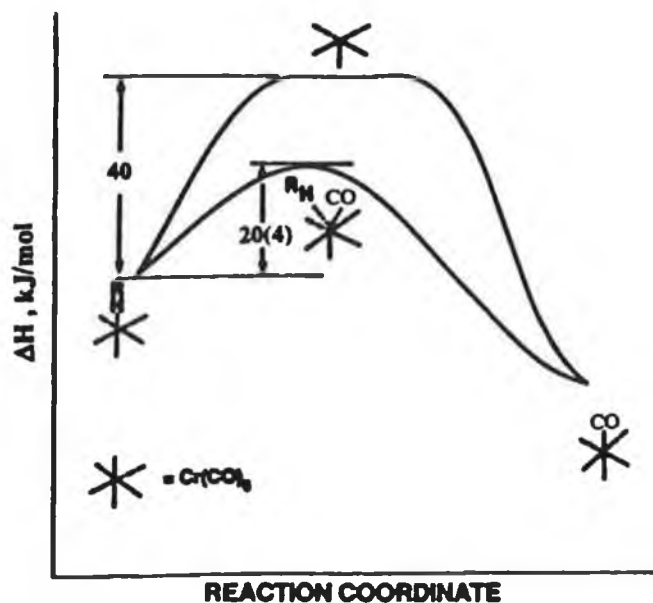


Figure 2.7.3 A potential energy *versus* reaction coordinate diagram for the desolvation of $\text{Cr}(\text{CO})_5(\text{heptane})$ by CO .

The ΔS^\ddagger values obtained support the proposed interchange mechanism. The extreme ΔS^\ddagger values were obtained for pentane and heptane. In the case of pentane, there is less freedom of motion present in the transition state, compared to that of heptane. The transition state in both solvents entails a high degree of $\text{Cr}\cdots\text{solvent}$ bond lengthening concomitant with the association of CO . A similar mechanism has been reported for the displacement of heptane by various pyridine derivatives [3]. However, Zhang *et al.* have reported the presence of a dissociative mechanism as well as the interchange mechanism in the displacement of heptane [6, 7]. The presence of the dissociative mechanism has been confirmed by volume of activation studies [20, 22], e.g. ΔV^\ddagger for the displacement of heptane from $\text{Cr}(\text{CO})_5(\text{heptane})$ by 1-hexene and piperidine are

$+6.2 \pm 0.2$ and $+1.4 \pm 0.4 \text{ cm}^3\text{mol}^{-1}$ respectively [22].

2.8 Quantum yields for the photosubstitution of $\text{Cr}(\text{CO})_6$ by pyridine

As the mechanism and strength of the metal---solvent interaction may also be obtained from the efficiency of the photochemical reaction, as quantum yield values, this is another pathway through which important mechanistic information, regarding the nature of the substitution process may be obtained. A low quantum yield obtained for $\text{Cr}(\text{CO})_6$ substitution in fluorocarbon solvents was attributed to a very efficient back reaction with CO [23]. In this study, the quantum yields for CO substitution in $\text{Cr}(\text{CO})_6$ by pyridine in each solvent were investigated. Irradiation with monochromatic light (313nm) resulted in the formation of only the monosubstituted product. This was indicated by the appearance of a band at ca. 390nm, as shown in Figure 2.8.1.

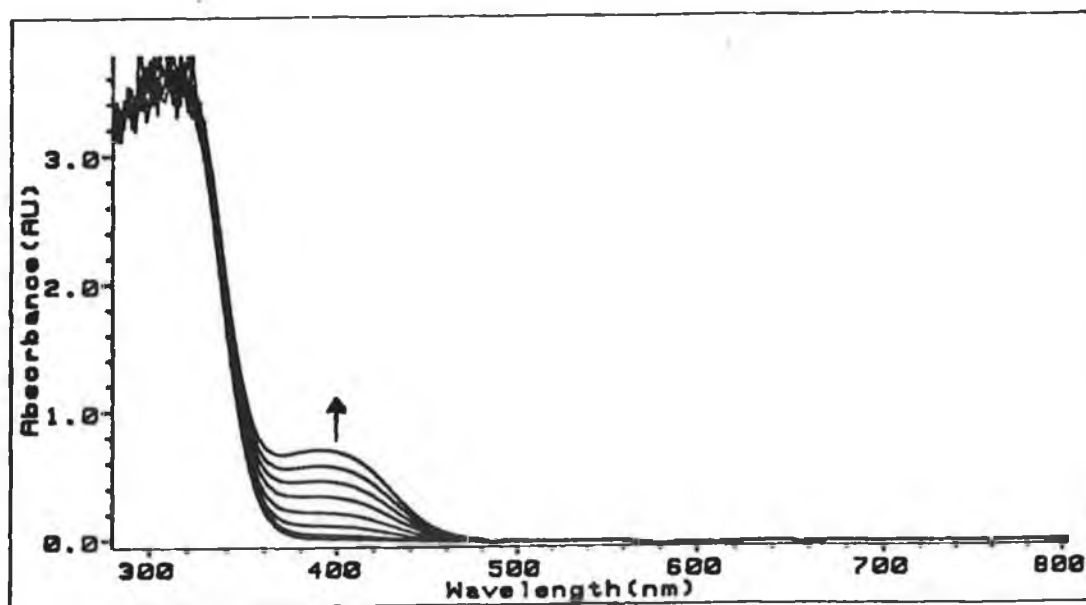
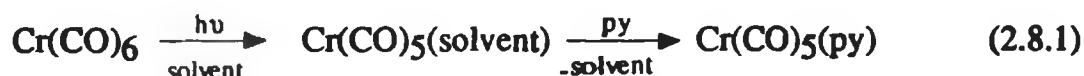


Figure 2.8.1 UV/visible spectral changes accompanying the reaction of $\text{Cr}(\text{CO})_6$ ($2 \times 10^{-3} \text{ mol dm}^{-3}$) with pyridine ($2 \times 10^{-2} \text{ mol dm}^{-3}$) in cyclohexane at 25°C.

This band is composed of overlapping LF and MLCT transitions (Section 3.1.2). The reaction involved is detailed in equation 2.8.1.



For cyclohexane as solvent, a quantum yield (Φ) of 0.67 had previously been determined for equation 2.8.1 [24]. The results obtained in this study are displayed in Table 2.8.1 and are based on the assumption that the quantum yield value of 0.67 is correct for cyclohexane.

Complex	Ligand (L)	Solvent (S)	λ_{max} (nm)	ϵ $\text{dm}^3\text{mol}^{-1}\text{cm}^{-1}$	Φ
Cr(CO)_6	pyridine	CH ^a	390	6190.3	0.67 ± 0.02^c
		MCH ^b	390	5942.2	0.69 ± 0.02
		pentane	390	4060.2	0.72 ± 0.02
		hexanes	390	5193.8	0.72 ± 0.02
		heptane	390	4151.5	0.72 ± 0.02

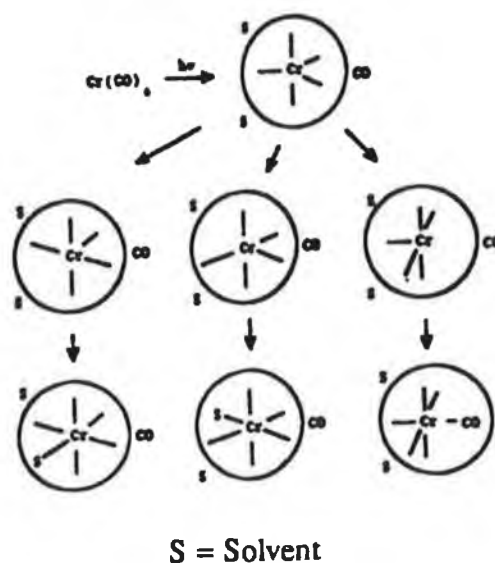
^a cyclohexane, ^b methylcyclohexane, ^c ref [24], ^d Irradiation wavelength is 313nm

Table 2.8.1 Relative quantum yields for CO substitution in Cr(CO)_6 by pyridine in the specified solvents^d.

The results in Table 2.8.1 indicate that there is very little difference in the quantum yield values among the aliphatic alkanes used, however the values are greater than that of methylcyclohexane and of that previously calculated for cyclohexane [24]. A similar value for the photosubstitution process by pyridine

in heptane was obtained by Wieland and van Eldik [25]. They also investigated the same substitution process but using piperidine instead of pyridine, in a range of alkane solvents (pentane - dodecane). The quantum yields obtained at ambient pressure decreased from 0.72 for the shorter alkanes to 0.58 for the longer chain alkanes, with a significantly lower value of 0.47 for perfluorohexane. A similar low quantum yield was found by Burkey *et al.* in perfluorodecalin [23]. Little variation was found in the values for pentane, hexane and heptane, all being ca. 0.72 ± 0.01 [25]. The decrease in quantum yield obtained for dodecane was explained in terms of a greater rate of CO recombination. A similar explanation is proposed for the increase in quantum yield observed for the shorter alkanes. This may be explained in terms of the photochemistry postulated for $\text{Cr}(\text{CO})_6$ [26]. Photolysis of $\text{Cr}(\text{CO})_6$ results in the ejection of CO and the formation of $\text{Cr}(\text{CO})_5$ with trigonal bipyramidal symmetry. This species relaxes *via* three pathways, each with equal probability to a square pyramidal geometry (Scheme 2.8.1), thus $\text{Cr}(\text{CO})_5$ ends up facing CO and promptly reforms $\text{Cr}(\text{CO})_6$ with a probability of one-third, and facing a solvent cage molecule with a probability of two-thirds. This process occurs before CO escapes from the solvent cage. In the case of alkanes as solvent, the solvent coordination is strong enough to inhibit cage recombination with the remaining CO, thus allowing the CO to diffuse away, and the solvent coordinated $\text{Cr}(\text{CO})_5$ to react with the pyridine with an overall quantum yield of two-thirds. This accounts for the quantum yield of 0.67 obtained in cyclohexane.

The increase in quantum yields in the aliphatic alkanes relative to that in cyclohexane, therefore suggests that more solvent binding or less CO recombination is occurring. A decrease in CO recombination can be accounted for by an increase in the rate of CO escape from the solvent cage or by a



Scheme 2.8.1

decrease in the rate of recombination, or both. The rate of the former process may be affected by the viscosity of the solvent. Even though, cyclohexane and heptane have similar properties, there are slight variations in their viscosity properties, the former being slightly more viscous ($\eta = 0.97\text{cP}$) than the latter ($\eta = 0.386\text{cP}$). Thus, there is a greater possibility of CO diffusion in the latter solvent, which may account for the increase in quantum yield observed. However, it is suggested that an increase in CO escape is not primarily as a result of solvent viscosity [23], but it may make an important contribution.

Also, the strength of the Cr---solvent bond ($\Delta H_{\text{Cr-S}}$) was calculated and compared to that obtained by Burkey *et al.* from photoacoustic calorimetric investigations [4]. The $\Delta H_{\text{Cr-S}}$ values were determined according to the equations described in Scheme 2.7.1. The enthalpy of CO dissociation from $\text{Cr}(\text{CO})_6$ (ΔH_1) was calculated according to equation 2.8.2.

$$\Delta H_1 = 356.16(1 - \phi) / \Phi \quad (2.8.2)$$

where, 356.16 is the energy of a mole of photons (kJmol^{-1} for 337.1nm), Φ is the quantum yield for equation 2.8.1, and ϕ is the observed heat and was calculated from the data presented by Burkey *et al.* [4]. The calculated Cr - S bond enthalpies, for the aliphatic and cyclic solvents are given in Table 2.8.2, along with the respective ϕ and ΔH_1 values, and the corresponding bond enthalpies obtained from the photoacoustic calorimetric investigations [4]. As the bond enthalpies of hexanes and methylcyclohexane with $\text{Cr}(\text{CO})_5$ were not investigated by Burkey *et al.*, a value for ϕ could not be calculated. Therefore in this study, a value of $\phi = 0.8$ which is consistent with those values calculated for the other solvents, was chosen for calculating the ΔH_1 and $\Delta H_{\text{Cr-S}}$ values for hexanes and methylcyclohexane.

Solvent (S)	ϕ	ΔH_1 (kJmol^{-1})	$-\Delta H_{\text{Cr-S}}$ (kJmol^{-1}) ^a	$-\Delta H_{\text{Cr-S}}$ (kJmol^{-1}) ^b
Pentane	0.78	108.8	45.8	37.4
Hexanes	0.80	98.9	55.6	
Heptane	0.79	103.7	50.9	40.3
Cyclohexane	0.81	101.0	53.6	52.9
MCH ^c	0.80	103.2	51.3	

^a this work, ^b reference [4], ^c methylcyclohexane

Table 2.8.2 Enthalpy of $\text{Cr}(\text{CO})_5$ - (S) bond ($\Delta H_{\text{Cr-S}}$) in alkane solvents (S).

The metal - solvent enthalpy values obtained in this study are all very similar, unlike those determined by Burkey *et al.* [4], in which they found that the

aliphatic alkanes (pentane and heptane) were more weakly bound to the metal centre than the cyclic alkane (cyclohexane). These differences in bond strengths were attributed to the presence of a stronger agostic bond in the cyclohexane complex, formed *via* secondary CH bonds. However, $\Delta H_{\text{Cr-S}}$ values obtained in this study ($\Delta H_{\text{Cr-S}} = 50 \pm 4 \text{ kJmol}^{-1}$), indicate that both the linear and cyclic alkanes bind to the chromium metal with similar energies. This suggestion is consistent with the observation of similar activation enthalpies ($\Delta H^\ddagger = 20 \pm 4 \text{ kJmol}^{-1}$) obtained for the displacement of each solvent from $\text{Cr}(\text{CO})_5(\text{S})$ by CO. Therefore, the faster rates of displacement of the aliphatic alkanes compared to the cyclic alkanes (*vide supra*), do not appear to be as a result of a difference in $\text{Cr}(\text{CO})_5$ - solvent interaction energies but rather as a result of an entropic effect. The latter may be explained in terms of freedom of motion in the transition state. As pentane is a more compact molecule than heptane, in the transition state of the former there is less freedom of motion compared to that of heptane, and hence the less negative ΔS^\ddagger values obtained for the heptane system. Cyclohexane is quite rigid in structure and therefore freedom of motion within the transition state is limited. This is reflected in the more negative entropy value ($\Delta S^\ddagger = -46 \text{ Jmol}^{-1}\text{K}^{-1}$) obtained for the system.

2.9 Conclusion

Photolysis of $\text{Cr}(\text{CO})_6$ in various cyclic and aliphatic hydrocarbon solvents, as a result of a single photon event resulted in the formation of solvated intermediates, $\text{Cr}(\text{CO})_5(\text{solvent})$, which reacted with added CO, yielding the parent compound. The absorption maxima of the solvated species were ca. 500nm, indicating that similar bonding was involved in all the solvents. The second-order rate constants indicated that the aliphatic hydrocarbons were

more easily displaced by CO than the cyclic hydrocarbons. Also an increase in quantum yield values was observed for the linear alkanes relative to that of cyclohexane. This increase may be attributed to an inefficient back reaction with CO.

An insight into the solvent displacement mechanism by CO was achieved from the activation studies, where the enthalpy values obtained were similar for all the solvents. The same trend was obtained when the Cr - S bond enthalpies were determined using the quantum yields obtained in this study and the equations involved in the determination of bond enthalpies by photoacoustic calorimetry [4]. The similar enthalpy values obtained in the aliphatic and cyclic alkane solvents indicated that all the solvents interacted with the chromium metal with similar energies. Contrary to this, Burkey *et al.* had found that the aliphatic solvents were more weakly bound than cyclohexane [4]. Therefore, in this study the differences in the rate of solvent displacement was attributed to an entropic effect rather than an enthalpic effect. The entropic values obtained were consistent with the proposed interchange mechanism, while the variation in values may be explained in terms of freedom of motion in the transition state. Similar mechanisms have been reported in other studies, for analogous systems [3, 6, 7]. However, in order to elucidate fully the mechanisms involved volume of activation studies would have to be undertaken. It has been reported that activation volumes (ΔV^\ddagger) are mechanistically more revealing than the corresponding entropy of activation (ΔS^\ddagger) values [27].

2.10 References

- 1 (a) Lee, M.; Harris, C. B.; *J. Am. Chem. Soc.*, 1989, **111**, 8963. (b) Yu, S.-C.; Xu, X.; Lingle, R.; Hopkins, J. B.; *J. Am. Chem. Soc.*, 1990, **112**, 3668. (c) Joly, A. G.; Nelson, K. A.; *Chem. Phys.*, 1991, **152**, 69.
- 2 (a) Welch, J. A.; Peters, K. S.; Vaida, V.; *J. Phys. Chem.*, 1982, **86**, 1941. (b) Simon, J. D.; Peters, K. S.; *Chem. Phys. Lett.*, 1983, **98**, 53. (c) Simon, J. D.; Xie, X.; *J. Phys. Chem.*, 1986, **90**, 6751. (d) Simon, J. D.; Xie, X.; *J. Phys. Chem.*, 1987, **91**, 5538. (e) Wang, L.; Zhu, X.; Spears, K. G.; *J. Am. Chem. Soc.*, 1988, **110**, 8695. (f) Wang, L.; Zhu, X.; Spears, K. G.; *J. Phys. Chem.*, 1989, **93**, 2. (g) Simon, J. D.; Xie, X.; *J. Phys. Chem.*, 1989, **93**, 291. (h) Joly, A. G.; Nelson, K. A.; *J. Phys. Chem.*, 1989, **93**, 2876. (i) Xie, X.; Simon, J. D.; *J. Am. Chem. Soc.*, 1990, **112**, 1130.
- 3 Yang, G. K.; Vaida, V.; Peters, K. S.; *Polyhedron*, 1988, **7**, 1619.
- 4 Morse, J. M.; Parker, G. H.; Burkey, T. J.; *Organometallics*, 1989, **8**, 2471.
- 5 (a) Kelly, J. M.; Bent, D. V.; Hermann, H.; Schulte-Frohlinde, D.; Koerner von Gustorf, E.; *J. Organomet. Chem.*, 1974, **69**, 259. (b) Bonneau, R.; Kelly, J. M.; *J. Am. Chem. Soc.*, 1980, **102**, 1220. (c) Kelly, J. M.; Long, C.; Bonneau, R.; *J. Phys. Chem.*, 1983, **87**, 3344. (d) Kelly, J. M.; Hermann, H.; Koerner von Gustorf, E.; *J. Chem. Soc., Chem. Commun.*, 1973, 105.
- 6 Zhang, S.; Dobson, G. R.; *Inorg. Chim. Acta.*, 1989, **165**, L11.
- 7 Zhang, S.; Dobson, G. R.; *Organometallics*, 1992, **11**, 2447.
- 8 Zhang, S.; Dobson, G. R.; Zang, V.; Bajaj, H. C.; van Eldik, R.; *Inorg. Chem.*, 1990, **29**, 3477.

- 9 Dobson, G. R.; Zhang, S.; *J. Coord. Chem.*, 1990, **21**, 155.
- 10 Zhang, S.; Dobson, G. R.; *Polyhedron*, 1990, **20**, 2511.
- 11 (a) Beach, N. A.; Gray, H. B.; *J. Am. Chem. Soc.*, 1968, **90**, 5713. (b) Geoffroy, G. L.; Wrighton, M. S.; *Organometallic Photochemistry*, Academic Press, New York, 1979.
- 12 Turner, J.J.; Burdett, J. K.; Perutz, R. N.; Poliakoff, M.; *Pure Appl. Chem.*, 1977, **49**, 271.
- 13 Perutz, R. N.; Turner, J. J.; *J. Am. Chem. Soc.*, 1975, **97**, 4791.
- 14 Breckenridge, W. H.; Stewart, G. M.; *J. Am. Chem. Soc.*, 1986, **108**, 364.
- 15 Church, S. P.; Grevels, F.-W.; Hermann, H.; Schaffner, K.; *Inorg. Chem.*, 1985, **24**, 418.
- 16 (a) Brookhart, M.; Green, M. L. H.; *J. Organomet. Chem.*, 1983, **250**, 395. (b) Brookhart, M.; Green, M. L. H.; Wong, L. L.; *Prog. Inorg. Chem.*, 1988, **36**, 2.
- 17 Lewis, K. E.; Golden, D. M.; Smith, G. P.; *J. Am. Chem. Soc.*, 1984, **106**, 3905.
- 18 Burkey, T. J.; *J. Am. Chem. Soc.*, 1990, **112**, 8329.
- 19 Zhang, S.; Dobson, G. R.; Brown, T. L.; *J. Am. Chem. Soc.*, 1991, **113**, 6908.
- 20 Zhang, S.; Zang, V.; Bajaj, H. C.; Dobson, G. R.; van Eldik, R.; *J. Organomet. Chem.*, 1990, **397**, 279.
- 21 Creaven, B. S.; George, M. W.; Ginzburg, A. G.; Hughes, C.; Kelly, J. M.; Long, C.; McGrath, I. M.; Pryce, M. T.; *Organometallics*, 1993, **12**, 3127.
- 22 Zhang, S.; Bajaj, H. C.; Zang, V.; Dobson, G. R.; van Eldik, R.; *Organometallics*, 1992, **11**, 3901.

- 23 Nayak, S. K.; Burkey, T. J.; *Organometallics*, 1991, **10**, 3745.
- 24 (a) Nasielski, J.; Colas, A.; *Inorg. Chem.*, 1978, **17**, 237. (b) Nasielski,
 J.; Colas, A.; *J. Organomet. Chem.*, 1975, **101**, 215.
- 25 Wieland, S.; van Eldik, R.; *J. Phys. Chem.*, 1990, **94**, 5865.
- 26 Burdett, J. K.; Grzybowski, J. M.; Perutz, R. N.; Poliakoff, M.; Turner,
 J. J.; Turner, R. F.; *Inorg. Chem.*, 1978, **17**, 147.
- 27 Brower, K. R.; Chen, T.; *Inorg. Chem.*, 1973, **12**, 2198.

CHAPTER 3

THE EFFECT OF LIGAND SUBSTITUENTS ON THE DISPLACEMENT OF SOLVENT FROM $\text{Cr}(\text{CO})_5(\text{SOLVENT})$ BY DONOR LIGANDS

3.1 Introduction

Complexes of the form $M(\text{CO})_5(\text{S})$, where S = solvent and M = Cr, Mo or W can be prepared either as transient species by flash photolysis techniques or as stable intermediates by conventional photochemical techniques depending on the nature of the solvent. For weak coordinating solvents like alkanes, benzene and toluene, the $M(\text{CO})_5(\text{S})$ species are short-lived with the solvent undergoing rapid substitution in the presence of a nucleophile. In the case of more strongly coordinating solvents, like tetrahydrofuran (THF), the species formed are much longer lived. Complexes of the form, $M(\text{CO})_5(\text{THF})$ have been isolated.

In recent years, many researchers have investigated the subsequent substitution reactions of $M(\text{CO})_5(\text{S})$ by various Lewis bases [1-7]. Such studies usually include systematic investigations of the effect of solvent, entering ligand concentration and temperature on the substitution processes. From these studies important mechanistic information regarding the substitution processes have been realised. The mechanisms involved and the rate of substitution processes are determined by the steric and electronic factors of the entering and leaving ligands [8-11]. For most ligands, the steric factors are measured as a function of the Tolman cone angle. This is defined as the apex angle of a right cylindrical cone centred 2.28Å from the centre of a phosphorus atom that just touches the van der Waals radii of the outermost atoms [12]. However, the basicity of the entering ligand also plays an important role in determining the rate of the substitution process in some systems [13-15].

In this study the rate of reaction of $\text{Cr}(\text{CO})_5(\text{S})$ with various nucleophiles L yielding $\text{Cr}(\text{CO})_5(\text{L})$ was investigated, where S = cyclohexane, toluene, THF or ethanol and L = pyridine (py), 2-, 3-, 4-picoline (pic), 2-, 4-phenylpyridine

(phpy), 2-, 3-chloropyridine (clpy) and 3-methyl-2-phenylpyridine (3-Me-2-Phpy). All the ligated complexes were formed *in situ* and thus the kinetic studies were performed without isolating the $\text{Cr}(\text{CO})_5(\text{L})$ complexes.

Also the effect that hindered rotation of a phenyl group has on the basicity of the ligand compared to when it is free to rotate was examined. This was undertaken as part of an investigation of how conformational changes of a ligand effect the basicity of that ligand. It was hoped to obtain an insight into how the conformation of 2,2'-bipyridine (bipy) may influence the formation of ligand bridged complexes, for example, $(\text{Cr}(\text{CO})_5)_2(\mu\text{-}2,2'\text{-bipy})$ [16].

Creaven *et al.* were the first to report the structural determination of a ligand bridged complex. In an attempt to isolate monodentately coordinated $\text{Cr}(\text{CO})_5(\text{bipy})$, the ligand bridged complex, $(\text{Cr}(\text{CO})_5)_2(\mu\text{-}2,2'\text{-bipy})$ was isolated [16]. The formation of the latter complex over the former was attributed to changes in the basicity of the ligand upon coordination in a monodentate fashion. It was proposed that binding of one end of the bipy ligand to the metal fragment, induced a twist in the ligand resulting in increased basicity of the uncoordinated pyridyl nitrogen, which then competes more effectively for $\text{Cr}(\text{CO})_5$ units than the free ligand. Thus, a relationship exists between the basicity and the angle between the two rings, the torsional angle, θ . This relationship was investigated by CNDO (Complete Neglect of Differential Overlap) solvation studies. Also it has been shown that bipy exists in an *s-trans* conformation in basic and inert solvents, and for such a conformation to be obtained, rotation about the C-C' bond would be necessary. This conformation would enhance the formation of the ligand bridged complex while hindering the formation of the chelate product [17].

3.1.1 CNDO calculations for 2,2'-bipyridine

The following calculations were kindly carried out for us by Dr. Tony Morton-Blake at University of Dublin [18]. The structure of 2,2'-bipyridine is shown in Figure 3.1.1.1. The angle between the two rings is denoted θ , the torsional angle.

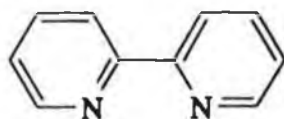


Figure 3.1.1.1 Structure of 2,2'-bipyridine.

The effect conformational changes had on the pK_a of the conjugate acid of bipy, was determined from the the energy difference between bipy and its conjugate acid, 2,2'-bipyridinium ($bipy^{2+}$) measured over a range of angles (θ). Thus, the basicity of the ligand was measured as a function of the torsional angle. Discounting solvent polarities, in general, it was found that the maximum pK_a of the conjugate acid of bipy was obtained when the rings were twisted 120° relative to each other and this tendency ($\theta \sim 120 - 150^\circ$) was maintained for most solvent polarities, but as high polarities were approached maximum pK_a was obtained for the planar, *cis* orientation, i.e. $\theta \sim 0^\circ$. The measurements were determined at 15° intervals over a range from 0° (planar with the two N atoms *cis*) to 180° (planar with the N atoms *trans*). Plots of the results obtained in both polar and non-polar media are given in Figures 3.1.1.2 and 3.1.1.3

respectively, where the Y-axis values (in eV) reflect the stability of bipyridinium ($C_{10}H_8N_2H_2$)²⁺ over bipyridyl ($C_{10}H_8N_2$).

From the plots, it was concluded that in non-polar media, the free pyridyl ring nitrogen had greatest basicity when θ - the angle between the two rings - was 120° , while in polar media, greatest basicity was obtained when the two rings were *cis*, $\theta = 0^\circ$. Therefore, in non-polar media, for example, pentane when one of the pyridyl rings becomes attached to a metal carbonyl moiety, the free pyridyl ring nitrogen has greatest basicity when it has been rotated through 120° . In the ligand bridged complex $(Cr(CO)_5)_2(\mu\text{-dmbpy})$ where pentane was used as solvent, the two pyridyl rings were found to be twisted by ca. 90° relative to each other [19]. In polar media, for example, ethanol, the free pyridyl ring nitrogen has greatest basicity when there is no twist between the rings and therefore it is predicted that chelation of the complex will be favoured over the formation of the ligand bridged complex because of steric constraints.

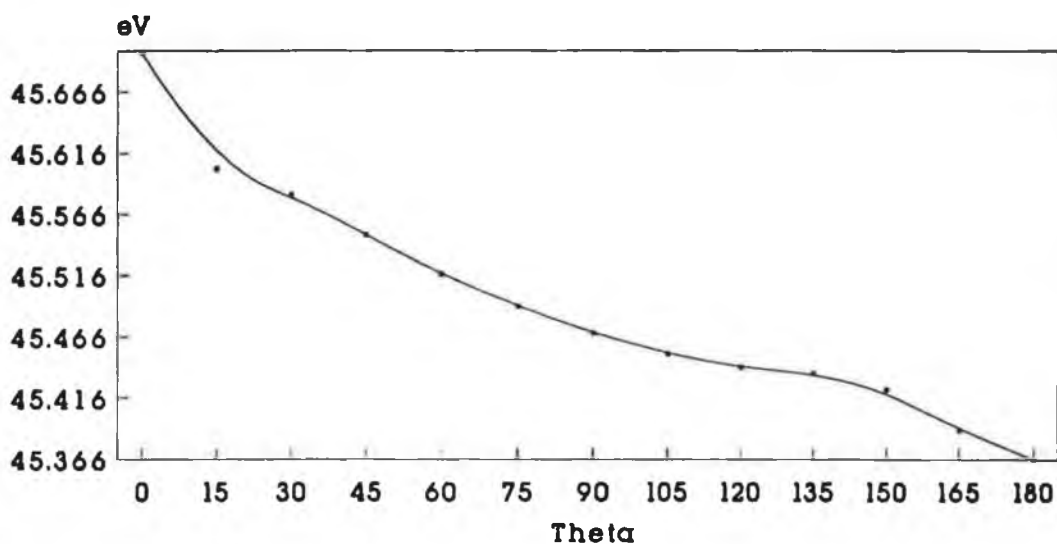


Figure 3.1.1.2 Plot of the values obtained for the stabilisation of bipyridinium over bipyridyl (eV) *versus* theta, θ , in polar media.

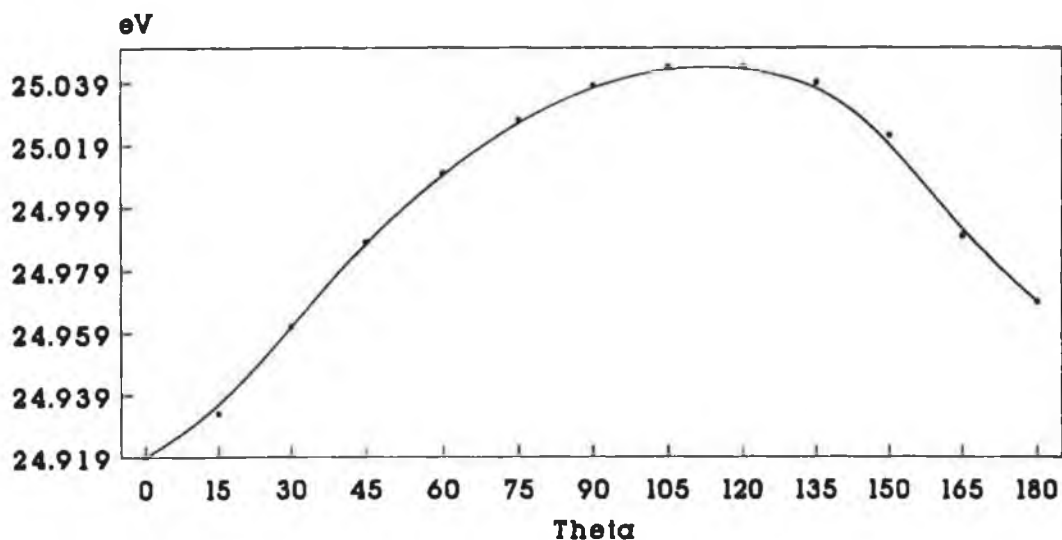


Figure 3.1.1.3 Plot of the values obtained for the stabilisation of bipyridinium over bipyridyl (eV) *versus* theta, θ , in non-polar media.

Many studies investigating the effect substituents (electron-accepting or donating) have on the basicity and reactivity of ligands have been reported [20, 21], however studies examining the effects conformational changes have on the basicity are rarely reported [18]. Therefore we decided to investigate, using 3-Me-2-Phpy as a model, the effects conformational changes had, if any, on the basicity and hence the reactivity of the ligand.

The molecular model of the lowest energy structure of 3-methyl-2-phenylpyridine, shown in Figure 3.1.1.4 is very similar to that obtained for 2-phenylpyridine (Figure 3.1.1.5). In both structures the phenyl ring is co-planar with the pyridine ring. Therefore it appears that the presence of the methyl group in 3-Me-2-Phpy does not affect the conformation of the phenyl ring.

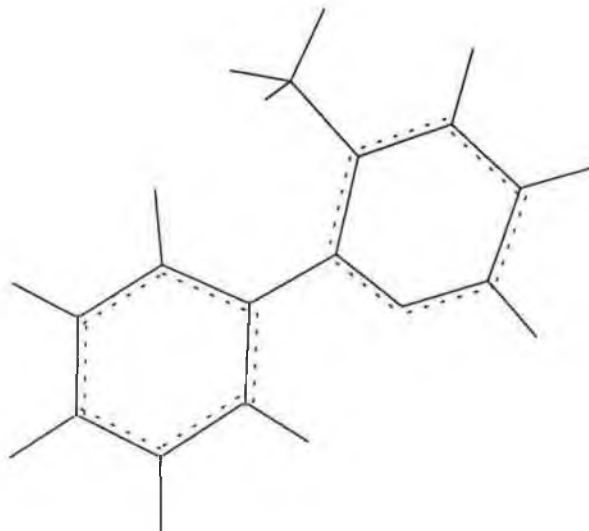
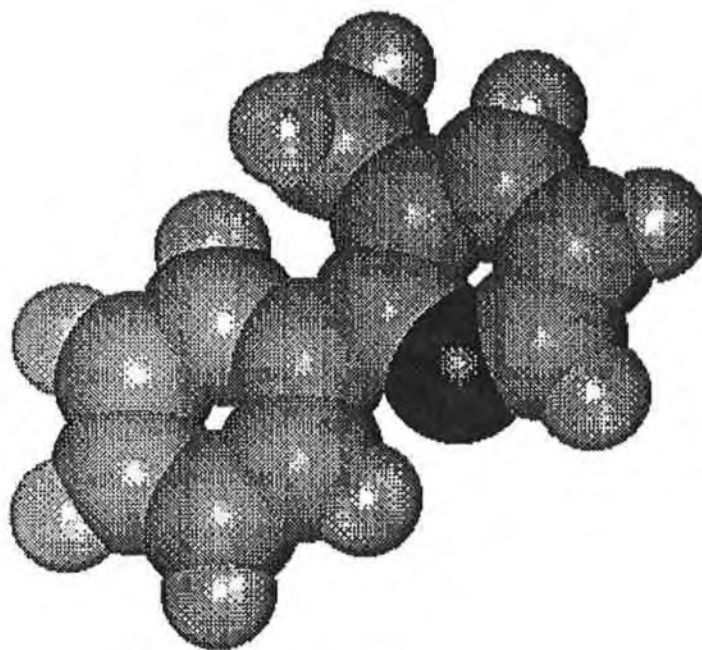


Figure 3.1.1.4 Molecular and skeletal models of the lowest energy structure of 3-methyl-2-phenylpyridine.

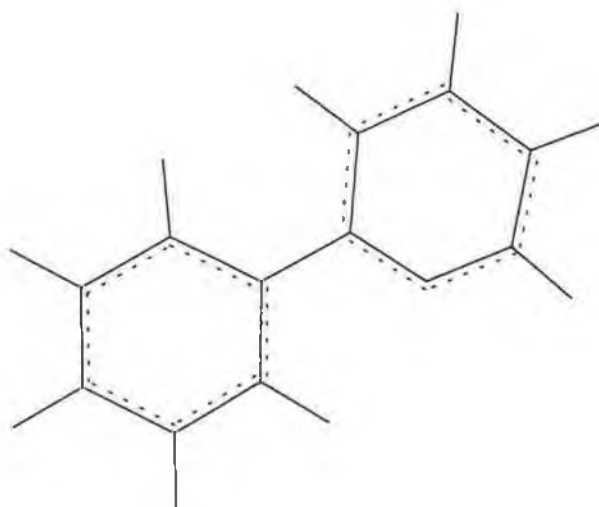
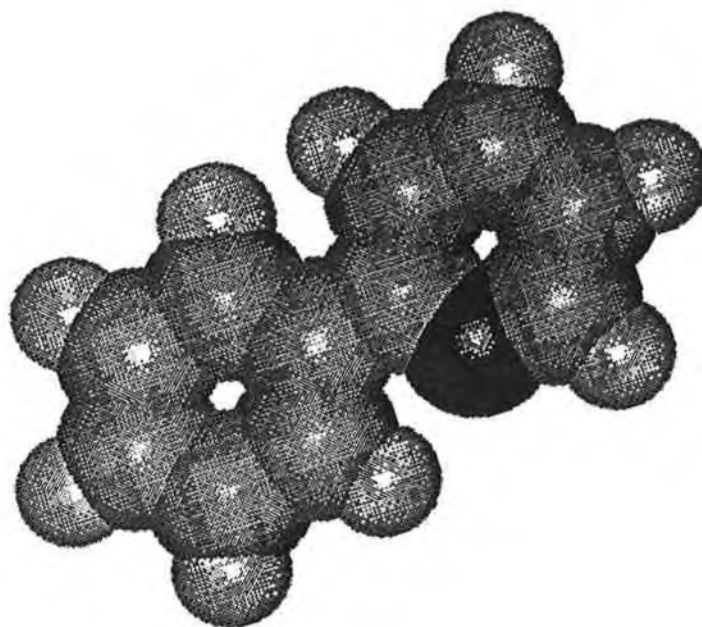


Figure 3.1.1.5 Molecular and skeletal models of the lowest energy structure of 2-phenylpyridine.

X - ray crystal structure analysis of $\text{Cr}(\text{CO})_5(2\text{-phenylpyridine})$ revealed that the phenyl ring was not co-planar with the pyridine but at an angle of 112° (Figure 3.1.1.6) [17]. As 3-methyl-2-phenylpyridine was the only ligand we could find which was substituted in both the α - and β -positions, we decided to investigate if the rate data would indicate a conformational difference between 3-methyl-2-phenylpyridine and 2-phenylpyridine.

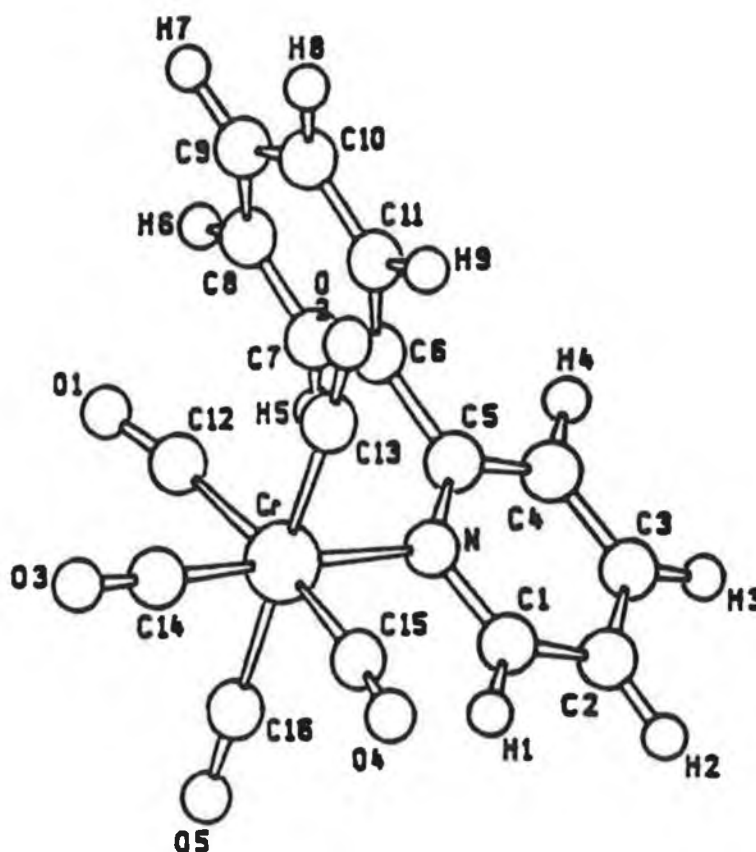


Figure 3.1.1.6 X - ray crystal structure of $\text{Cr}(\text{CO})_5(2\text{-phenylpyridine})$.

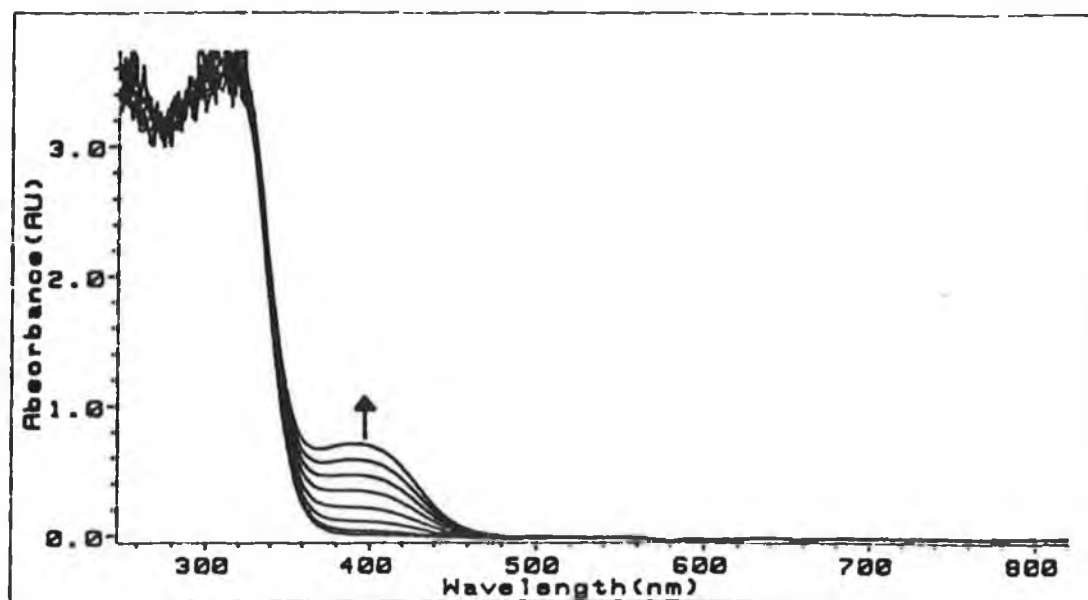
Activation parameters were also obtained for the reaction of the various ligands with $\text{Cr}(\text{CO})_5(\text{solvent})$ in the different solvents. Laser flash photolysis was employed in the investigation of the displacement of the weakly coordinating solvents, cyclohexane and toluene while stopped-flow techniques

were used for the more strongly binding solvents, THF and ethanol. Appropriate reaction mechanisms were assigned in each case and are discussed individually in the following sections.

3.1.2 Electronic spectrum of $\text{Cr}(\text{CO})_5(\text{L})$ ($\text{L} = \text{pyridine}$ or substituted pyridine)

The UV/visible spectrum for the formation of $\text{Cr}(\text{CO})_5(\text{L})$ is displayed in Figure 3.1.2.1(a), along with that of $\text{Cr}(\text{CO})_6$ (the initial spectrum). In these studies the formation of the ligated complex is evident from the grow-in of a band situated at ca. 400nm. The ultimate UV/visible spectrum obtained is identical to that for isolated, pure $\text{Cr}(\text{CO})_5(\text{py})$ (Figure 3.1.2.1(b)). The energy level diagram for $\text{Cr}(\text{CO})_5(\text{L})$ complexes is described in Section 1.2.1. The band observed at ca. 400nm is assigned to a ligand field (LF) $^1\text{A}_1 \rightarrow ^1\text{E}$ transition from d_{xz} , d_{yz} to the antibonding d_z^2 . This band coincides with the metal to ligand charge transfer (MLCT) $d \rightarrow \pi^*\text{L}$ transition. These MLCT bands can be easily resolved as they are blue-shifted relative to LF bands in solvents of increasing polarities, because of a strong interaction of the π^* ligand orbitals with the solvent. Also the MLCT transition moves to lower energy with an increasing electron-withdrawing group on the pyridine. The intense absorptions $> 300\text{nm}$ are attributed to the $\text{Cr} \rightarrow \pi^*\text{CO}$ CT transitions. As all the ligands are of the same basic structure, that is, pyridine very little difference is observed in the positioning of the ligand field bands. However, with respect to the ligand field transition $^1\text{A}_{1g} \rightarrow ^1\text{T}_{1g}$ of $\text{Cr}(\text{CO})_6$ a substantial red-shift is observed (Figure 3.1.2.1(a)).

(a)



(b)

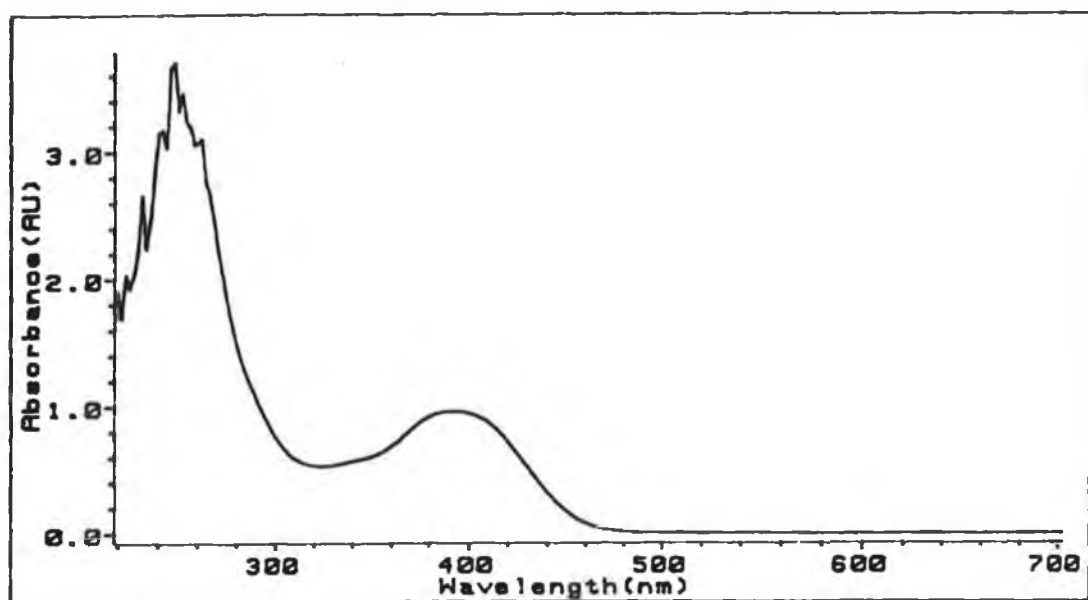


Figure 3.1.2.1 Electronic spectrum of (a) $\text{Cr}(\text{CO})_5(\text{py})$ formed *in situ*, and (b) Isolated $\text{Cr}(\text{CO})_5(\text{py})$ ($1.6 \times 10^{-4} \text{ mol dm}^{-3}$), in cyclohexane.

3.2 Laser flash photolysis of Cr(CO)₆ in the presence of excess ligand, L in cyclohexane (L = pyridine or substituted pyridine)

Intermediates formed upon photolysis of Group VI hexacarbonyls has been extensively investigated. Several studies have been conducted concerning the structure and solution of the photogenerated M(CO)₅ species in rigid-glasses [22-24] or low temperature matrix environments [25-29] while structural and kinetic information of the intermediate has been obtained from pulse radiolysis [30] and flash photolysis experiments [3(b), 3(c), 31, 32]. These results indicated that the ground state of the intermediate M(CO)₅ is square pyramidal (C_{4v}) and extremely reactive, reacting with N₂, CO, solvent and M(CO)₆ at near diffusion-controlled rates. Reaction of M(CO)₅ with solvent impurities has also been reported [3(d), 32, 33]. However, in the work presented here a minimum ten-fold excess of ligand was used, thus overcoming any interactions between M(CO)₅ and any solvent impurities.

The coordinatively unsaturated species M(CO)₅ reacts with the solvent forming a solvated complex on a picosecond timescale, or less [3, 5, 34]. In the presence of a strongly donating ligand, the solvent is easily replaced, resulting in the formation of a ligated complex (equations 3.2.1 - 3.2.3).



S = Solvent, L = Ligand

In this study, the displacement of cyclohexane, as solvent, by py, 2-, 3-, 4-pic,

2-, 4-ppy, 2-, 3-clpy and 3-methyl-2-phenylpyridine as ligands was investigated.

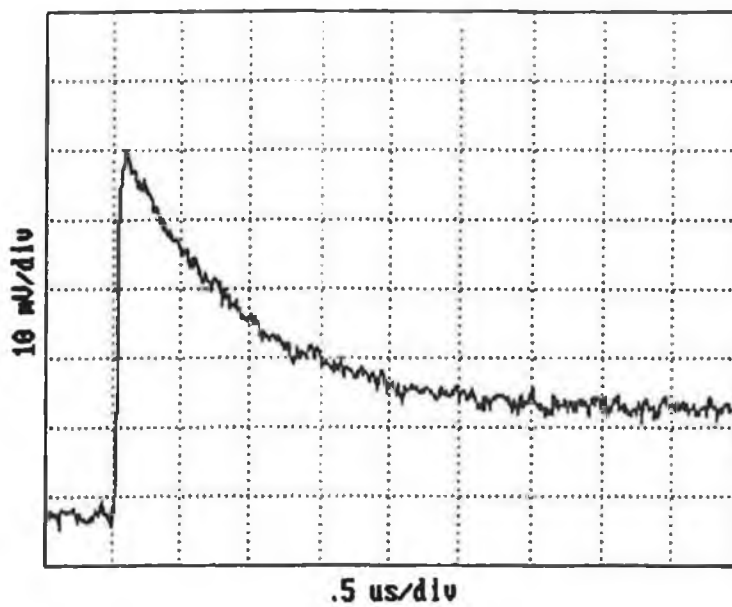
3.2.1 Flash photolysis of $\text{Cr}(\text{CO})_6$ in the presence of excess ligand, L

In accordance with equation 3.2.2, the primary photoproduct formed upon photolysis of $\text{Cr}(\text{CO})_6$ in cyclohexane is $\text{Cr}(\text{CO})_5(\text{cyclohexane})$. From previous studies this transient species has an absorption maximum at ca. 500nm [3] (see Section 2.5) and is extremely short-lived, especially in the presence of excess ligand. Therefore this solvated species decays concurrent with the formation of the ligated complex, $\text{Cr}(\text{CO})_5(\text{L})$.

Two transient species were observed in accordance with equation 3.2.3, a grow-in at 420nm and a decay at 510nm, corresponding to the formation of the ligated and the decay of the solvated complexes respectively. Similar rates were exhibited by both species (Table 3.2.4.1). The grow-in at ca. 420nm corresponds to the appearance of the band with λ_{max} at 400nm on the UV/visible spectrum. Typical transient signals for the formation of $\text{Cr}(\text{CO})_5(\text{L})$ and the decay of $\text{Cr}(\text{CO})_5(\text{cyclohexane})$ are depicted in Figure 3.2.1.1.

A residual absorbance is observed for the decay of $\text{Cr}(\text{CO})_5(\text{S})$ (S = cyclohexane) species indicating that $\text{Cr}(\text{CO})_5(\text{S})$ is reacting to form another species other than the parent complex. If the latter was being formed, no residual absorbance would be observed as obtained for the reaction of $\text{Cr}(\text{CO})_5(\text{S})$ (S = cyclohexane) with CO (Section 2.3). Both decay transient signals are compared in Figure 3.2.1.2. (The transient signals were measured on different timescales).

(a)



(b)

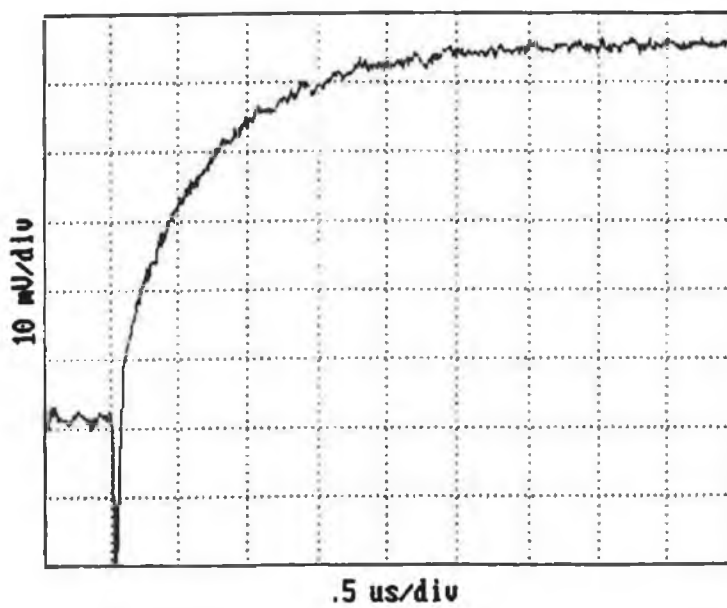


Figure 3.2.1.1 Typical transient signals for (a) the decay of $\text{Cr}(\text{CO})_5(\text{cyclohexane})$ and (b) the formation of $\text{Cr}(\text{CO})_5(\text{py})$.

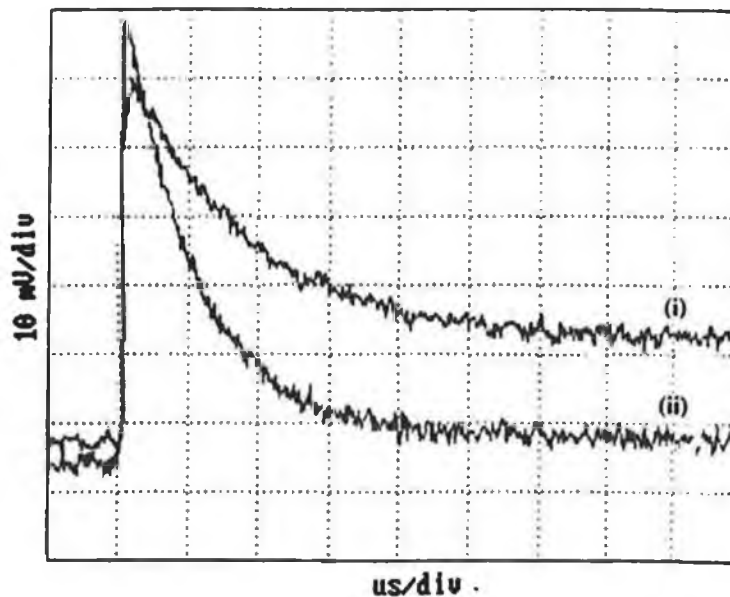


Figure 3.2.1.2 Decay transients for the reaction of $\text{Cr}(\text{CO})_5(\text{cyclohexane})$ with (i) pyridine and (ii) CO.

3.2.2 The effect of the power of the laser on the primary photoproduct

This experiment was performed to investigate whether the primary photoproduct resulted from a single photon or a multi-photon event. The primary photoproduct in all these reactions is the solvated $\text{Cr}(\text{CO})_5$ complex, thus the effect that the power of the laser had on the absorbance of the primary photoproduct, i.e on the decay of $\text{Cr}(\text{CO})_5(\text{cyclohexane})$ was investigated. The plot of absorbance of $\text{Cr}(\text{CO})_5(\text{cyclohexane})$ *versus* the relative power of the laser is displayed in Figure 3.2.2.1.

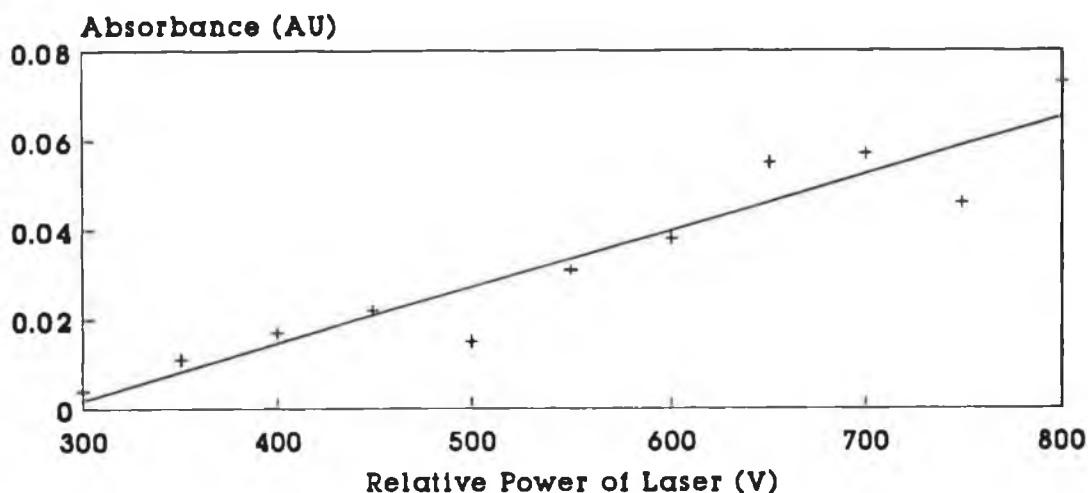


Figure 3.2.2.1 Plot of absorbance of $\text{Cr}(\text{CO})_5(\text{cyclohexane})$ *versus* relative power of the laser.

A linear relationship was obtained indicating a single photon event was in operation.

3.2.3 UV/visible difference spectrum of $\text{Cr}(\text{CO})_5(\text{L})$

The UV/visible difference spectra of all the ligated complexes in this investigation are very similar. This is a reflection of the common bonding nature present between the Cr metal and the ligands and also the energy of the π^* orbitals of the ligands. Initially, after the flash the solvated complex is formed but with time this species decays to form the ligated complex. The rate at which the solvated complex decays depends on the substituting ligand, the more reactive, less sterically hindered ligands resulting in faster rates of ligation. The UV/visible difference spectrum of the formation of $\text{Cr}(\text{CO})_5(2\text{-phenylpyridine})$ is shown in Figure 3.2.3.1. A band with λ_{max} at 460nm is formed 8 μs after the laser flash. This corresponds to the formation of $\text{Cr}(\text{CO})_5(2\text{-phenylpyridine})$.

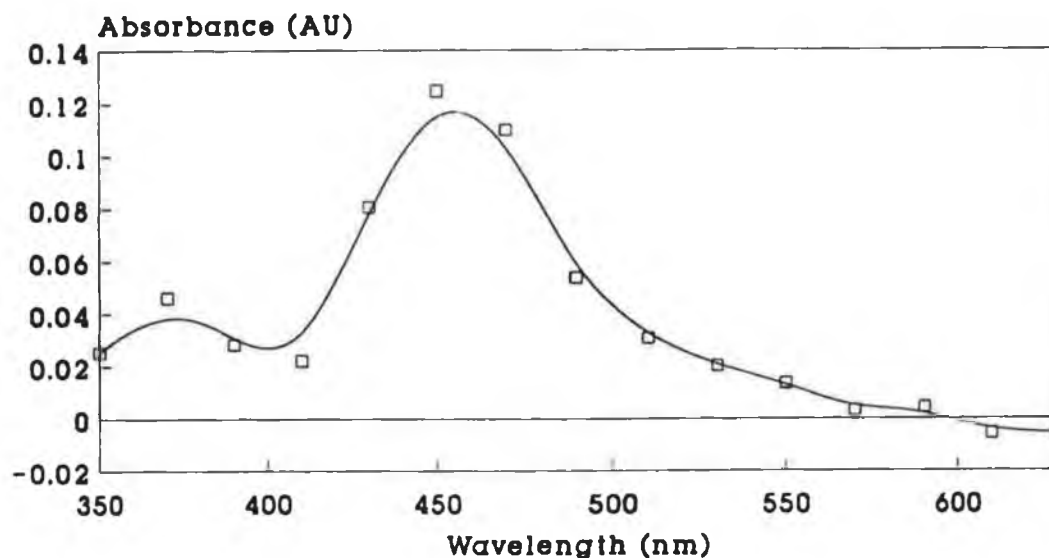


Figure 3.2.3.1 UV/visible difference spectrum of the formation of $\text{Cr}(\text{CO})_5(2\text{-phenylpyridine})$ recorded $8\mu\text{s}$ after the laser flash.

3.2.4 The rate of reaction of $\text{Cr}(\text{CO})_5(\text{S})$ with different ligand (L) concentrations

The reaction of $\text{Cr}(\text{CO})_5(\text{S})$, ($\text{S} = \text{cyclohexane}$) with the ligands *via* the transient solvated intermediate follows pseudo-first-order kinetics. From the kinetic studies, the rate constants k_{obs} for the decay of the solvated species and formation of the ligated species were obtained. The second-order rate constants, k_2 , for the reaction of $\text{Cr}(\text{CO})_5(\text{cyclohexane})$ with the various ligands were obtained from the slope of the line resulting from the plot of k_{obs} (s^{-1}) for either the formation of $\text{Cr}(\text{CO})_5(\text{L})$ or the decay of $\text{Cr}(\text{CO})_5(\text{cyclohexane})$ against the ligand concentration (mol dm^{-3}). Analysis of both the decay of $\text{Cr}(\text{CO})_5(\text{S})$ and the production of $\text{Cr}(\text{CO})_5(\text{L})$ yielded similar second-order rate constants (Table 3.2.4.1). Linear plots were obtained at both wavelengths for all the ligands.

Reaction	$\lambda(\text{nm})$	$k_2 \times 10^{-7}$ ($\text{dm}^3\text{mol}^{-1}\text{s}^{-1}$)
Decay of $\text{Cr}(\text{CO})_5(\text{cyclohexane})$	510	6.3 ± 0.3
Formation of $\text{Cr}(\text{CO})_5(\text{py})$	420	6.5 ± 0.4

Table 3.2.4.1 Second-order rate constants for the reaction of $\text{Cr}(\text{CO})_5(\text{cyclohexane})$ with pyridine.

A representative plot of k_{obs} at 510 and 420nm (decay of the solvated and formation of the ligated complexes, respectively) *versus* the ligand concentration is shown in Figure 3.2.4.1, while a summary of the second-order rate constants, along with the pK_a values of the ligands are given in Table 3.2.4.2. The data used in the construction of the plots are tabulated in Appendix B (Table B2). It is important to note that the pK_a values of the ligands quoted in Table 3.2.4.2 were measured in water and not in organic solvents, as used in this study.

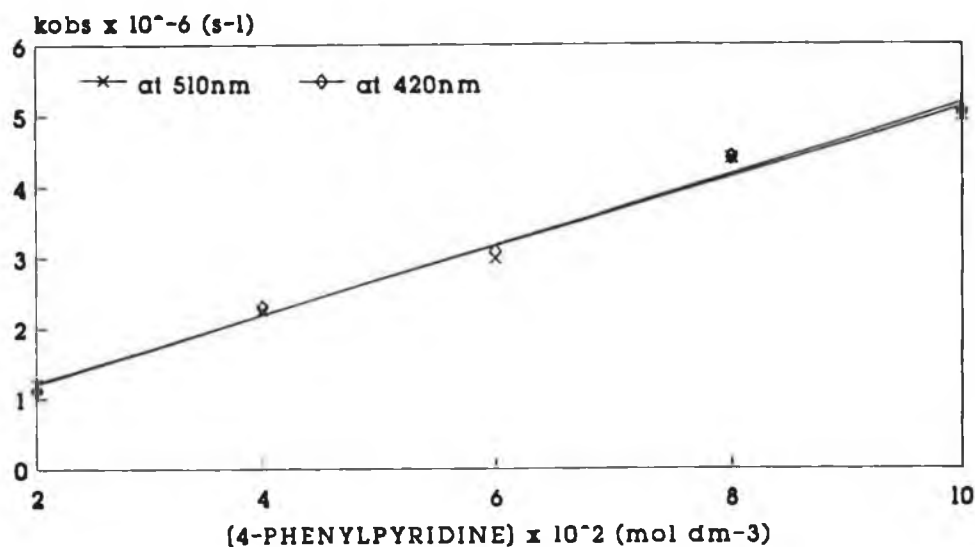


Figure 3.2.4.1 Plot of k_{obs} (s^{-1}) *versus* ligand concentration (mol dm^{-3}) monitored at 510 and 420nm, at 22°C.

Ligand (L)	$k_2 \times 10^{-7}$ (510nm) ^a (dm ³ mol ⁻¹ s ⁻¹)	$k_2 \times 10^{-7}$ (420nm) ^a (dm ³ mol ⁻¹ s ⁻¹)	pK _{a, H₂O} ^b
2-chloropyridine	2.9 ± 0.1	3.1 ± 0.1	0.76
3-chloropyridine	2.5 ± 0.2	2.4 ± 0.2	2.85
2-phenylpyridine	2.4 ± 0.2	2.4 ± 0.2	4.48
pyridine	6.3 ± 0.2	6.5 ± 0.4	5.23
4-phenylpyridine	4.9 ± 0.3	4.9 ± 0.3	5.55
3-picoline	6.9 ± 0.2	6.5 ± 0.5	5.79
2-picoline	2.9 ± 0.2	2.9 ± 0.2	6.03
4-picoline	10.8 ± 0.5	12.0 ± 0.9	6.08
3-Me-2-Phpy	2.3 ± 0.2	2.5 ± 0.2	5.04 ^c

^a obtained at 22°C, ^b reference [35], ^c estimated value

Table 3.2.4.2 Second-order rate constants for the reaction of Cr(CO)₅(cyclohexane) with the various ligands, L, monitored at 510 and 420nm at 22°C.

The second-order rate constant may be used as a measure of the nucleophilicity of the ligand, thus the larger k_2 , the better the nucleophile. However, the differences observed in the k_2 values may be attributed to both steric and electronic factors arising from the substituents on the pyridine ring. This difference is even more striking when ligands, other than those derived from pyridine are used, for example CO (Table 3.2.4.3).

Reaction	$k_2 \times 10^{-7} \text{ (dm}^3\text{mol}^{-1}\text{s}^{-1}\text{)}$
$\text{Cr(CO)}_5(\text{cyclohexane}) + \text{CO} \rightarrow \text{Cr(CO)}_6$	0.2 ± 0.01^a
$\text{Cr(CO)}_5(\text{cyclohexane}) + \text{py} \rightarrow \text{Cr(CO)}_5(\text{py})$	6.3 ± 0.2

^a Section 2.6

Table 3.2.4.3 Second-order rate constants for the displacement of cyclohexane by CO and pyridine.

The 20-fold increase in the rate of displacement of cyclohexane by pyridine compared to that by CO may be attributed to the greater σ -donating ability of the former. Thus, pyridine is a stronger nucleophile than CO. A similar k_2 value was obtained for the loss of cyclohexane from $\text{W(CO)}_5(\text{cyclohexane})$ by 4-acetylpyridine [36], $k_2 = 3.17 \times 10^7 \text{ dm}^3\text{mol}^{-1}\text{s}^{-1}$. The slightly faster rate of displacement observed for the pyridine system may be because of the smaller atomic radius of Cr compared to that of W. The atomic radii of the Group VI metals increase in the order, $\text{Cr} \ll \text{Mo} \sim \text{W}$ [37].

From Table 3.2.4.2, it can be seen that the electron-withdrawing substituents on the pyridine ring, deactivates the pyridine ring which results in reduced rate of solvent displacement. Conversely, electron-donating substituents enhance the rate of solvent displacement by further activation of the pyridine ring. The fastest rate of displacement is by 4-picoline, approximately twice as fast as that observed for pyridine. However, electronic effects are not the sole contributing factors in determining the rate at which the ligand displaces the solvent molecule. Steric effects play a major role also. 2-Picoline, based solely on electronic factors would be expected to have a rate similar to that of 3- or 4-picoline but instead a rate close to that of 2-chloropyridine was obtained. As the difference in rates cannot be attributed to electronic effects, steric effects

must be making a major contribution to the overall rate of reaction. As 2-picoline possesses a methyl group α to the coordinating nitrogen, the rate of binding of it to the $\text{Cr}(\text{CO})_5$ fragment may be affected by the interaction of the methyl group with the *cis* - carbonyl ligands. This steric interaction is also evident in other systems. The rate of displacement of n-heptane from $\text{Cr}(\text{CO})_5(\text{n-heptane})$ by pyridine is approximately twice as fast as that for 2-picoline [1, 38]. A very similar ratio was obtained for the displacement of cyclohexane by these two ligands in this study. Also, the faster rate of displacement of methylcyclohexane compared to cyclohexane by CO, from the respective $\text{Cr}(\text{CO})_5$ solvated complexes (Section 2.6) may be attributed to the weaker Cr---methylcyclohexane bond, resulting from the steric interaction of CH_3 with the carbonyl groups. The variation in the rate constants may be indicative of the selectivity present among the the ligands for the intermediate produced upon Cr---cyclohexane bond fission. Similar selectivity has also been observed in analogous systems [4(d)].

The influence steric effects have over electronic effects is reflected also in the rate of reaction of 3-methyl-2-phenylpyridine. The second-order rate constant for this ligand is very similar to that for 2-phenylpyridine, indicating that the rate of reaction is determined by the substituent present in the alpha (α) position. The similarity of rate constants also suggests that both ligands are of the same conformation, that is, the conformation of the phenyl ring in 3-methyl-2-phenylpyridine is most likely to be the same as that in 2-phenylpyridine. The most probable conformation is where the phenyl and the pyridine ring are coplanar, as represented by the molecular models of the lowest energy structures of the ligands (Figures 3.1.1 and 3.1.2). Thus in cyclohexane, the presence of the methyl group on the ligand does not appear to alter the conformation of the phenyl ring, and hence both ligands are of similar nucleophilicity.

3.2.4.1 The effect of ligand basicity on the rate of reaction of $\text{Cr}(\text{CO})_5(\text{cyclohexane})$ with L

It has been reported that the nucleophilicity of the ligands, as measured by k_2 values, increases with the basicity of the ligands [37]. Graham and Angelici, investigating the reaction of $\text{M}(\text{CO})_6$, where $\text{M} = \text{Cr}, \text{Mo}$ or W , with phosphine and phosphite ligands in decalin solvent, reported that the magnitude of the second-order rate constant, k_2 , which was found to be a function of the basicity of L (given in parentheses as ΔHNP values, i.e. the potential at half-neutralisation of the ligand) increased in the series $\text{As}(\text{C}_6\text{H}_5)_3 < \text{P}(\text{OC}_6\text{H}_5)_3$ (875) $< \text{P}(\text{C}_6\text{H}_5)_3$ (573) $< \text{P}(\text{OCH}_2)_3\text{CC}_2\text{H}_5 < \text{P}(\text{OC}_2\text{H}_5)_3$ (520) $< \text{P}(\text{n-C}_4\text{H}_9)_3$ (131) [39]. Low ΔHNP values indicate strong bases.

The basicities of the pyridine ligands used in this work are given in Table 3.2.4.2, along with the second-order rate constants. It is important to note that the basicities of the ligands were measured in water and not in alkane solvents, as used in this study. Therefore the pK_a values must be treated with caution. They can only be taken as an indicator of the general trend in the basicity present among the ligands and not as actual measurements of ligand basicity in cyclohexane. In most cases, the k_2 values increased with the ligand basicity, but the relationship between the second-order rate constants and the basicities of the ligands is not linear. This may be as a result of the pK_a values being measured in water and not cyclohexane. A plot of the k_2 values *versus* pK_a of the ligand is given in Figure 3.2.4.1.1.

However, if ligands with similar steric requirements are investigated, a linear relationship is observed. A plot of the k_2 values *versus* pK_a of these ligands is given in Figure 3.2.4.1.2, for L = 3-chloropyridine (3-clpy), pyridine (py) and 3-picoline (3-pic).

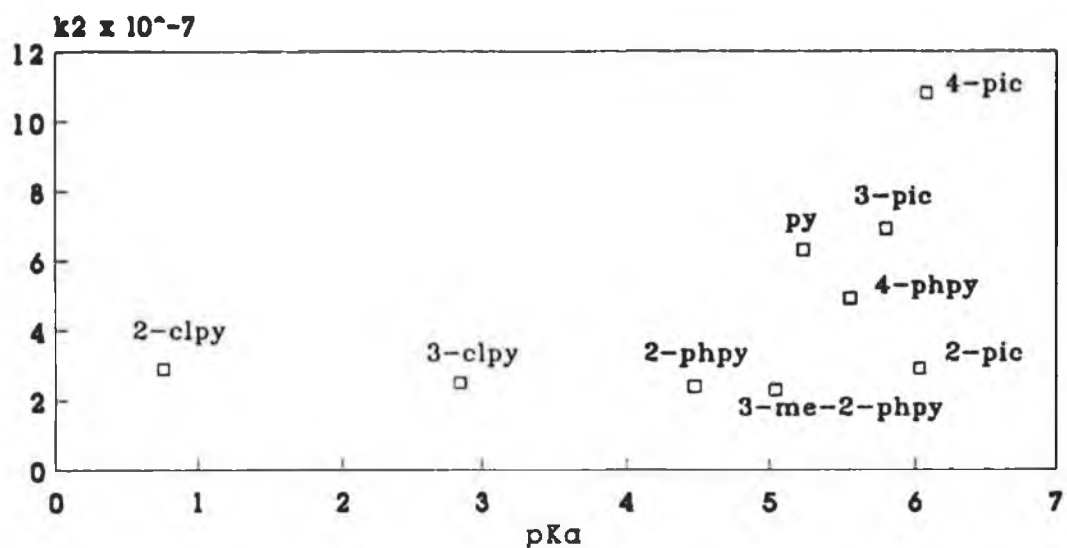


Figure 3.2.4.1.1 Plot of k_2 values at 510nm versus pK_a of the ligands, L for the reaction of $Cr(CO)_5$ (cyclohexane) with L.

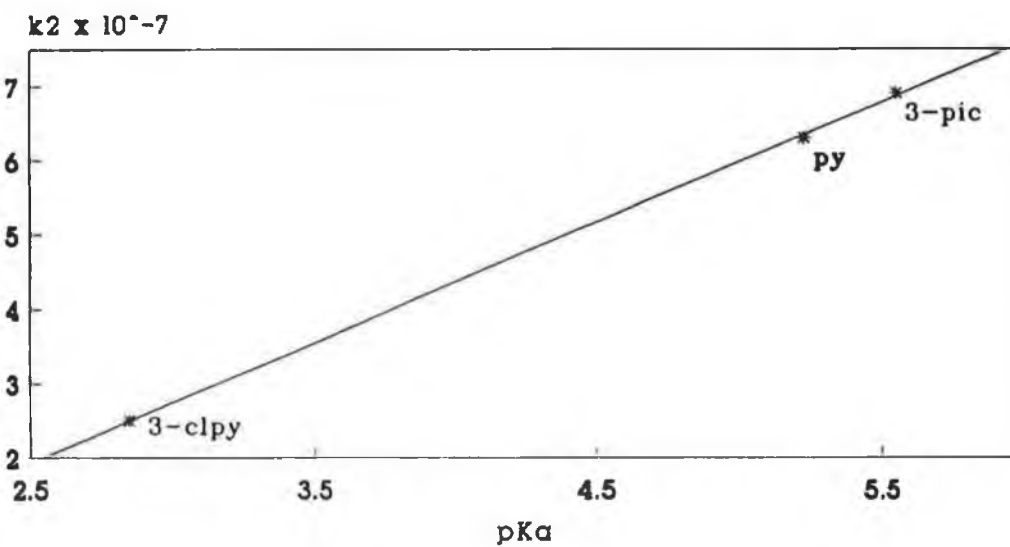


Figure 3.2.4.1.2 Plot of k_2 values at 510nm versus the pK_a for 3-chloropyridine, pyridine and 3-picoline.

A similar linear relationship was obtained for the reaction of $\text{CoNO}(\text{CO})_3$ with these three nucleophiles [13(a)]. No deviations from such a linear relationship were observed by Thorstein as the pyridine ligands investigated did not possess substituents in the α - position. Thus, the rate of attack of pyridines increases as the basicity of the ligand increases provided that the ligands have similar steric requirements [15]. This suggests that the transition state is selective amongst the ligands for those with similar steric constraints, suggesting the operation of an associative or interchange process rather than a dissociative one.

3.2.5 Activation parameter studies for the reaction of $\text{Cr}(\text{CO})_5(\text{cyclohexane})$ with L

Activation parameter studies were carried out for the reaction of $\text{Cr}(\text{CO})_5(\text{S})$ with the pyridine and substituted pyridine ligands. The results obtained revealed mechanistic information about the reaction pathway. As both, the rate of formation of $\text{Cr}(\text{CO})_5(\text{L})$ and the decay of $\text{Cr}(\text{CO})_5(\text{cyclohexane})$ are the same within experimental error (Section 3.2.4), we decided to determine the activation parameters of only one of these processes. In this case, the decay of the solvated species, monitored at 510nm was investigated. The activation parameters were calculated according to the equations given in Section 5.4, and are tabulated in Table 3.2.5.1. Representative Arrhenius and Eyring plots are displayed in Figure 3.2.5.1. Similar plots were obtained for the reaction with the other ligands. The data involved in the construction of these plots is tabulated in Appendix A (Table A2).

Ligand (L)	E_a^\ddagger (kJmol ⁻¹) ^a	ΔH^\ddagger (kJmol ⁻¹) ^a	ΔS^\ddagger (JK ⁻¹ mol ⁻¹) ^a	ΔG_{298K}^\ddagger (kJmol ⁻¹) ^a
Pyridine	14 ± 1	12 ± 1	-57 ± 10	29
2-Phpy	22 ± 1	20 ± 1	-39 ± 10	32
4-Phpy	16 ± 1	14 ± 1	-48 ± 10	28
3-Me-2-Phpy	17 ± 1	15 ± 1	-49 ± 10	30
2-Picoline	18 ± 1	16 ± 1	-49 ± 10	30
3-Picoline	17 ± 1	14 ± 1	-47 ± 10	28
4-Picoline	16 ± 1	13 ± 1	-43 ± 10	26
2-Clpy	23 ± 1	20 ± 1	-28 ± 10	29
3-Clpy	21 ± 1	18 ± 1	-40 ± 10	30

^a monitored at 510nm

Table 3.2.5.1 Activation parameters for the reaction of Cr(CO)₅(cyclohexane) with pyridine and substituted pyridine ligands, L ([L] = 6 x 10⁻²M).

From Table 3.2.5.1, the activation energy (E_a^\ddagger), the energy required for the reaction to occur, is lowest for pyridine. The more reactive ligands, those with electron-donating substituents (e.g. picolines) have slightly greater activation energies than that of pyridine, thus indicating that the substituent position rather than its electronic ability is influencing the rate of reaction. The largest E_a^\ddagger values within each group of ligands (picolines, chloro- and phenylpyridines) were obtained for the ligands in the 2-position.

Similar trends were found in the enthalpy of activation values (ΔH^\ddagger). The greater ΔH^\ddagger values were associated with the more hindered ligands. This trend

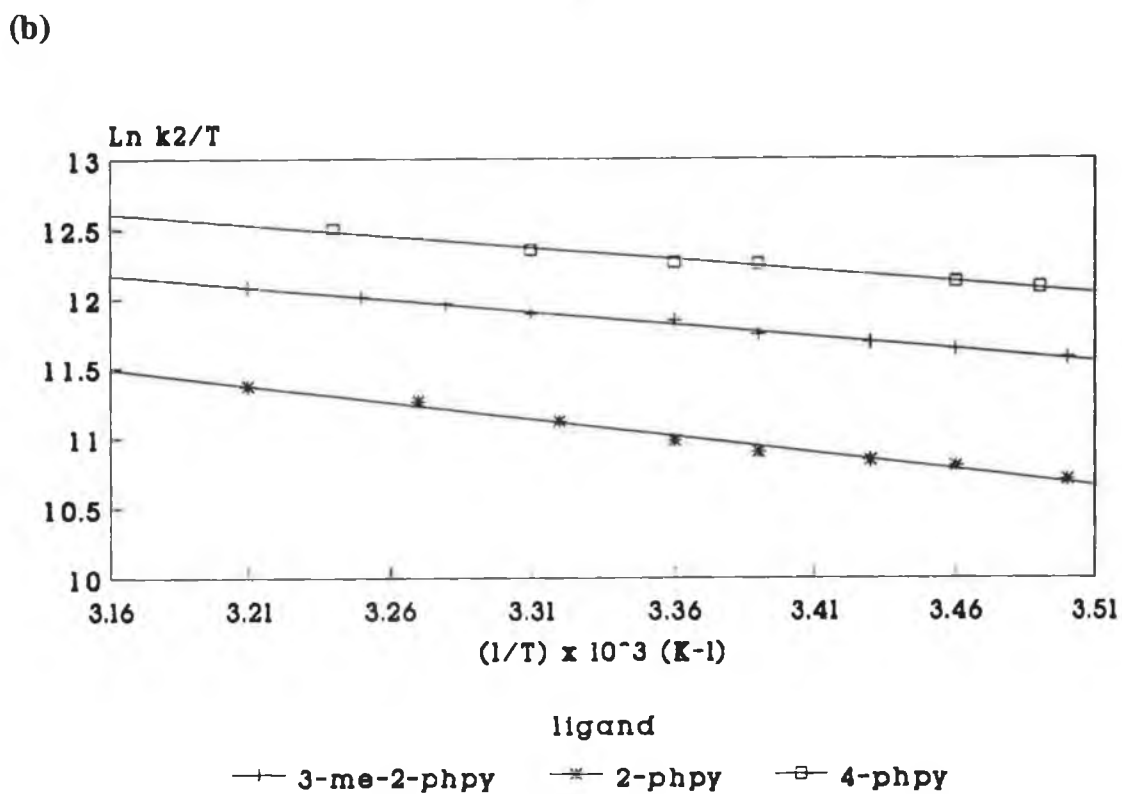
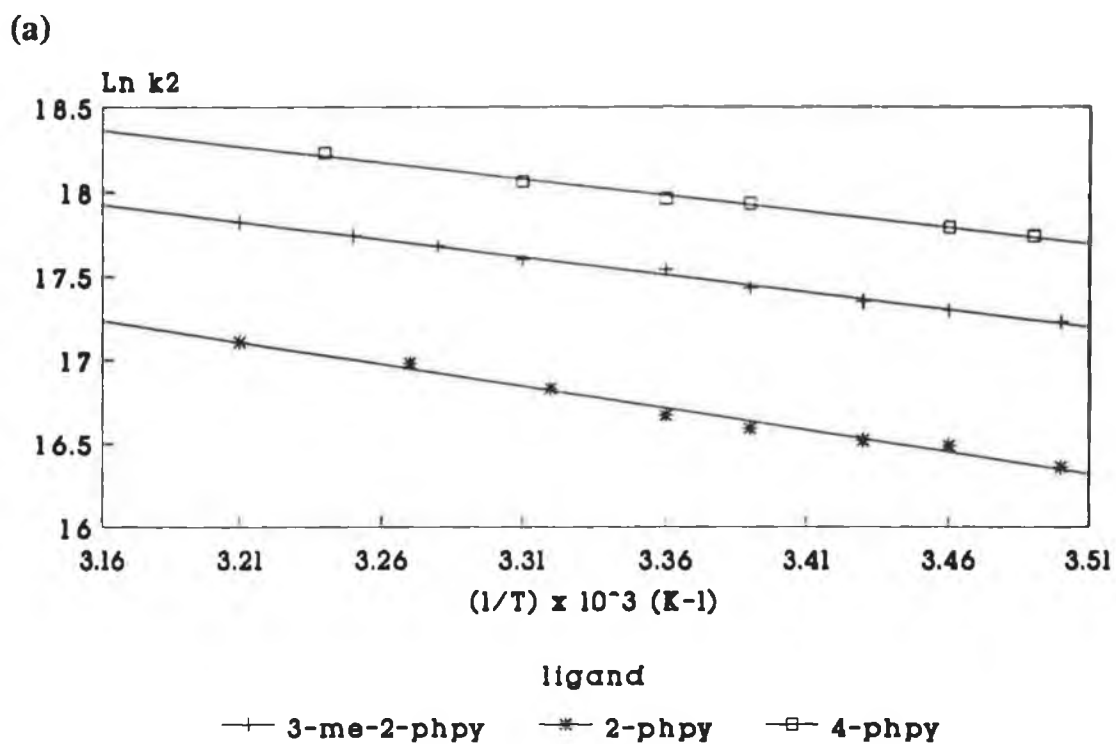


Figure 3.2.5.1 (a) Arrhenius and (b) Eyring plots for the reaction of $\text{Cr}(\text{CO})_5(\text{cyclohexane})$ with 2-phpy, 4-phpy and 3-me-2-phpy.

was also found by Yang *et al.* in the displacement of n-heptane from $\text{Cr}(\text{CO})_5(\text{n-heptane})$ by pyridine and 2-picoline [1]. The increase in value was assigned to the increasing steric hinderance about the coordinating nitrogen atom. In this case, it is afforded by the chloro, methyl and phenyl groups. The enthalpy of activation for 3- and 4-picoline is less than that for 2-picoline, indicating the contibution the steric effects make to this value. A similar trend is observed for the phenylpyridines.

Photoacoustic calorimetric studies have estimated the Cr---cyclohexane bond strength to be approximately 52 kJmol^{-1} [2]. As the enthalpy barrier for the substitution processes investigated is considerably less, at $15 \pm 5 \text{ kJmol}^{-1}$, the transition state must be associative in the incoming ligand. As expected, for the more sterically demanding incoming ligands, a larger ΔH^\ddagger was observed. The enthalpy of activation for the displacement of cyclohexane from $\text{Cr}(\text{CO})_5(\text{cyclohexane})$ by CO is approximately twice that for the same displacement by pyridine, $\Delta H_{\text{CO}}^\ddagger = 22.31$ cf. $\Delta H_{\text{py}}^\ddagger = 11.98 \text{ kJmol}^{-1}$ (Section 2.7). In both cases an interchange mechanism is proposed, in which Cr---L bond making is important in the transition state. A potential energy *versus* reaction coordinate diagram for the displacement of cyclohexane from $\text{Cr}(\text{CO})_5(\text{cyclohexane})$ by the pyridines is presented in Figure 3.2.5.4. If a dissociative process was operative, the Cr---cyclohexane bond strength should closely approximate the activation energies for Cr---cyclohexane bond dissociation.

The entropies of activation values (ΔS^\ddagger) for all the reactions are very similar, $-40 \pm 15 \text{ JK}^{-1}\text{mol}^{-1}$, and are indicative of an interchange mechanism. Thus, the transition state entails the formation of a seven-coordinate complex, involving displacement of cyclohexane with simultaneous binding of the ligand to the metal centre. A mechanism for the substitution reaction is detailed in

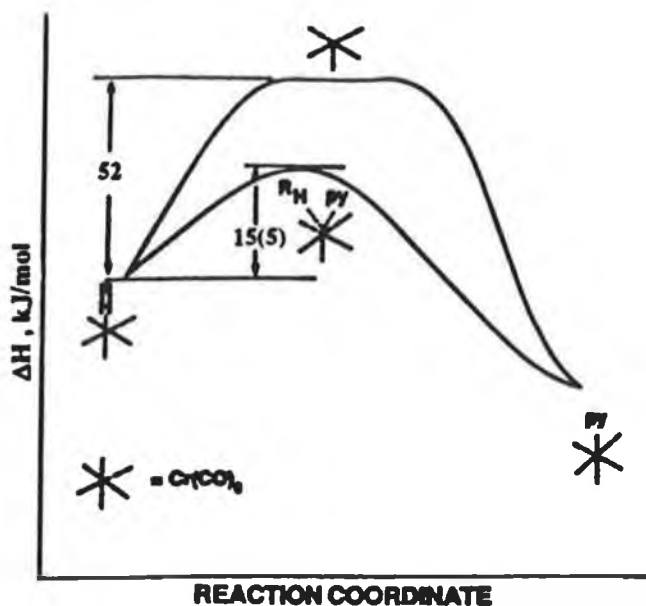
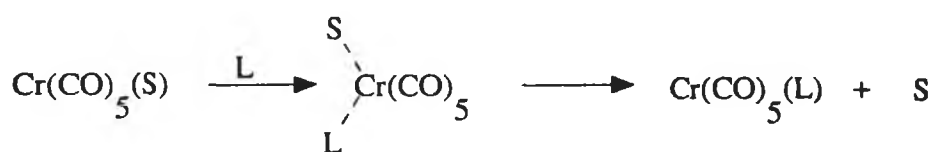


Figure 3.2.5.4 Plots of enthalpy *versus* reaction coordinate of $\text{Cr}(\text{CO})_5(\text{cyclohexane})$ with the pyridines *via* a dissociative pathway (top) and *via* an interchange pathway.



L = nucleophile, S = cyclohexane

Scheme 3.2.5.1

Scheme 3.2.5.1. The enthalpy and entropy of activation for the displacement of cyclohexane and methylcyclohexane from the respective solvated $W(CO)_5$ complexes by 4-acetylpyridine are very similar to the values obtained in this study [36], $\Delta H^\ddagger = 14.28 \text{ kJmol}^{-1}$ and $\Delta S^\ddagger = -54.6 \text{ JK}^{-1}\text{mol}^{-1}$. These results were consistent with the proposed interchange mechanism but contradictory with that proposed by Lees and Adamson in an earlier study [31]. They had proposed a dissociative mechanism for the same reaction. Mixed solvent studies indicated that the displacement of n-heptane from $W(CO)_5(\text{n-heptane})$ by 1-hexene occurred *via* an interchange mechanism even though 1-hexene is a much weaker nucleophile than 4-acetylpyridine [4(a)]. $Mo(CO)_6$ and $W(CO)_6$ complexes have a greater tendency than $Cr(CO)_6$ to undergo an associative process owing to their larger covalent radii ($Cr < Mo \sim W$) and to the related increase in effective nuclear charge ($Cr < Mo < W$). Therefore, the most likely mechanism through which the substitution processes in this study take place is an interchange mechanism.

3.3 Laser flash photolysis of $Cr(CO)_6$ in the presence of excess ligand L, in toluene, (L = pyridine or substituted pyridine)

The rate of reaction of $Cr(CO)_5(S)$, (S = toluene) with pyridine, 2-, 3-, 4-picoline, 2-, 3-chloropyridine, 2-, 4-phenylpyridine and 3-methyl-2-phenylpyridine in toluene was investigated. The reaction scheme is the same as that described in Section 3.2, except that the solvated species is $Cr(CO)_5(\text{toluene})$. Toluene is classified as a weak coordinating solvent compared to THF, however in comparison with cyclohexane, it is more strongly coordinating. Bonding of toluene to the coordinatively, unsaturated species may occur *via* an "agostic" interaction, that is, through the formation of a

three-centre, two electron C-H-Cr bond, or *via* "edge-on" coordination through an isolated olefinic linkage [4(b), 40]. The latter has been reported as being the dominant mode of coordination. As the strength of the metal - solvent interaction has a major influence on the reactivity of the solvated intermediates, we decided to investigate the reactivity of the toluene solvated intermediate with the various pyridine-based nucleophiles, and to compare its reactivity with that obtained for the cyclohexane solvated intermediate previously studied in Section 3.2. Also, the effect conformational changes have on the basicity and hence the reactivity of a ligand were investigated. This part of the study was undertaken to obtain an insight into how the conformation of 2,2'-bipyridine (bipy) influences the formation of the ligand bridged complex, $(\text{Cr}(\text{CO})_5)_2(\mu\text{-}2,2'\text{-bipy})$. In this investigation, 3-methyl-2-phenylpyridine was used as a model, and the effect conformational changes had, if any on the reactivity of the ligand was examined (see Section 3.1).

3.3.1 Electronic spectrum of $\text{Cr}(\text{CO})_5(\text{L})$

The UV/visible spectrum for the formation of $\text{Cr}(\text{CO})_5(\text{L})$ is shown in Figure 3.3.1.1. In these studies, the formation of the ligated complex is evident from the very broad band appearing at ca. 410nm. This is composed of overlapping ligand field (LF) and metal to ligand charge transfer (MLCT) bands. The LF band is assigned to a $^1\text{A}_1 \rightarrow ^1\text{E}$ transition from d_{xz} , d_{yz} to the antibonding d_z^2 , while the MLCT is as a result of a $\text{Cr} \rightarrow \pi^*\text{L}$ transition. The MLCT bands are blue-shifted relative to LF bands in solvents of increasing polarities, because of a strong interaction of the π^* ligand orbitals with the solvent. They are also sensitive to substituents, shifting to lower energy as the substituent on the pyridine ring becomes more electron-withdrawing. The

intense absorptions $> 300\text{nm}$ are attributed to the $\text{Cr} \rightarrow \pi^*\text{CO}$ CT transitions. As the ligands involved in this study are pyridine and pyridine derivatives, very little difference is observed in the positioning of the ligand field bands.

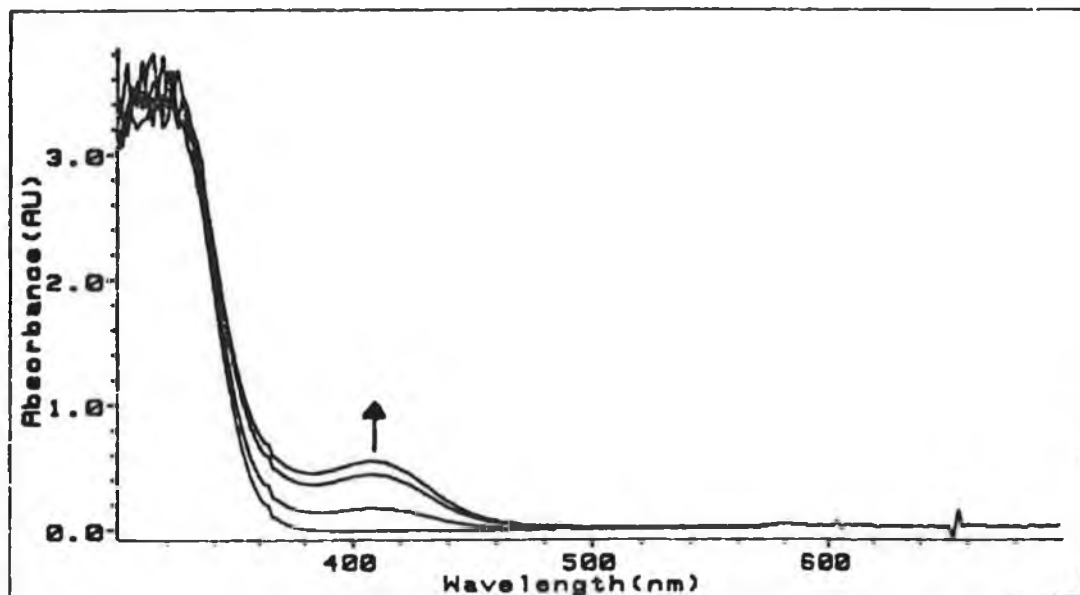
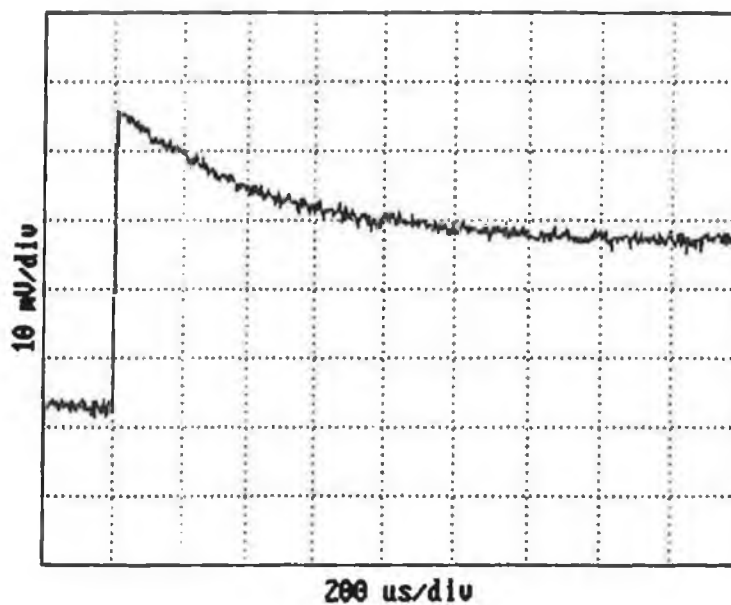


Figure 3.3.1.1 Electronic spectrum of the formation of $\text{Cr}(\text{CO})_5(2\text{-picoline})$ in toluene.

3.3.2 Flash photolysis of $\text{Cr}(\text{CO})_6$ in the presence of excess ligand L

Photolysis of $\text{Cr}(\text{CO})_6$ in toluene, produces the solvated intermediate $\text{Cr}(\text{CO})_5(\text{toluene})$ (λ_{max} at 480nm), which in the presence of excess ligand is rapidly converted to the $\text{Cr}(\text{CO})_5(\text{L})$ complex. Typical transients for the decay of the solvated intermediate and the formation of the ligated complex are presented in Figure 3.3.2.1. The rates at which these processes occur are much slower than those observed in cyclohexane, indicating the stronger bonding present in the Cr -toluene complex, and hence the slower rate of displacement. The differences in the rates of decay of the two solvated species are shown in

(a)



(b)

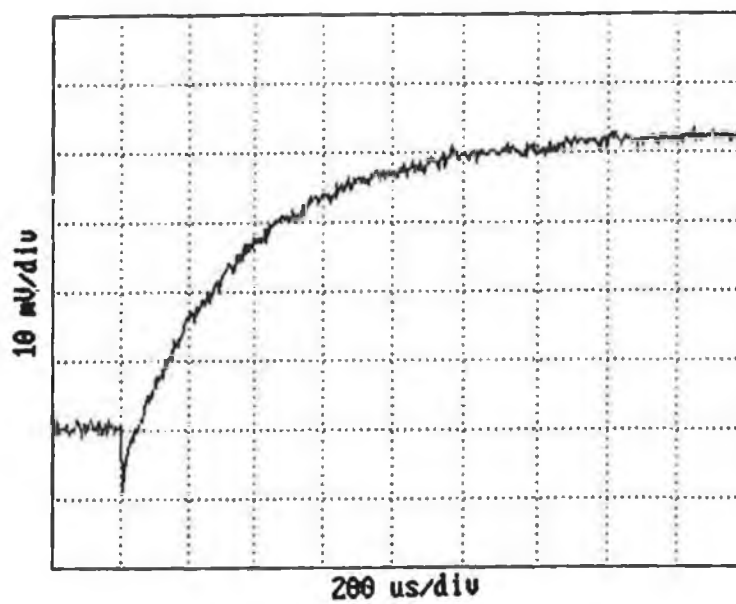
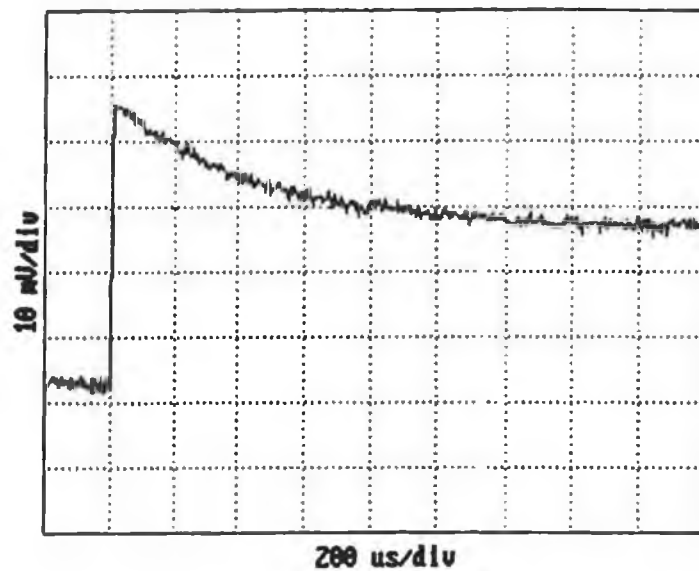


Figure 3.3.2.1 Typical transient signals for (a) the decay of $\text{Cr}(\text{CO})_5(\text{toluene})$ at 480nm and (b) the formation of $\text{Cr}(\text{CO})_5(\text{py})$ at 410nm.

(a)



(b)

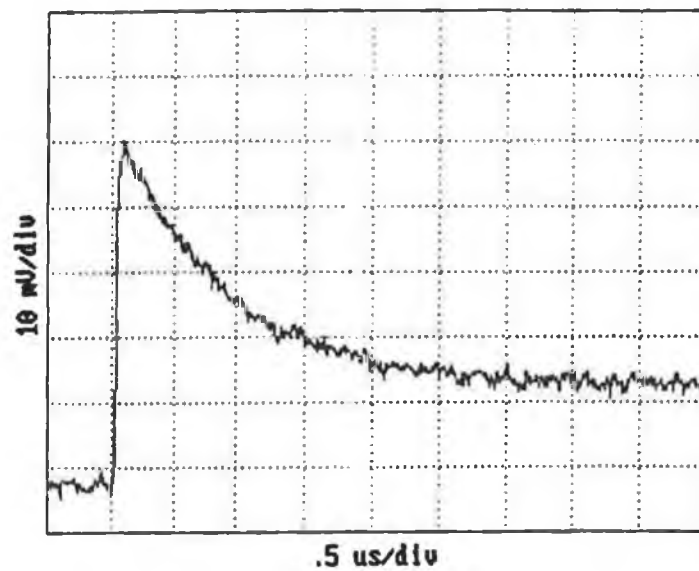


Figure 3.3.2.2 Transient signals observed for the decay of (a) $\text{Cr}(\text{CO})_5(\text{toluene})$ at 480nm and (b) $\text{Cr}(\text{CO})_5(\text{cyclohexane})$ at 510nm.

Figure 3.3.2.2. Again, the rate of decay of the solvated species and the rate of formation of the ligated complex were approximately the same (monitored at 480 and 410nm respectively). As the band for the formation of the ligated complexes is very broad, 410nm was chosen as the monitoring wavelength for investigating the formation of the complexes in this study.

3.3.3 The effect of the power of the laser on the primary photoproduct

As the primary photoproduct may arise from a single photon or multiple photon event, the power of the laser was varied and the corresponding absorbance of the primary photoproduct measured to determine which event was operative. A plot of absorbance of the primary photoproduct, $\text{Cr}(\text{CO})_5(\text{toluene})$ versus relative power of the laser is given in Figure 3.3.3.1.

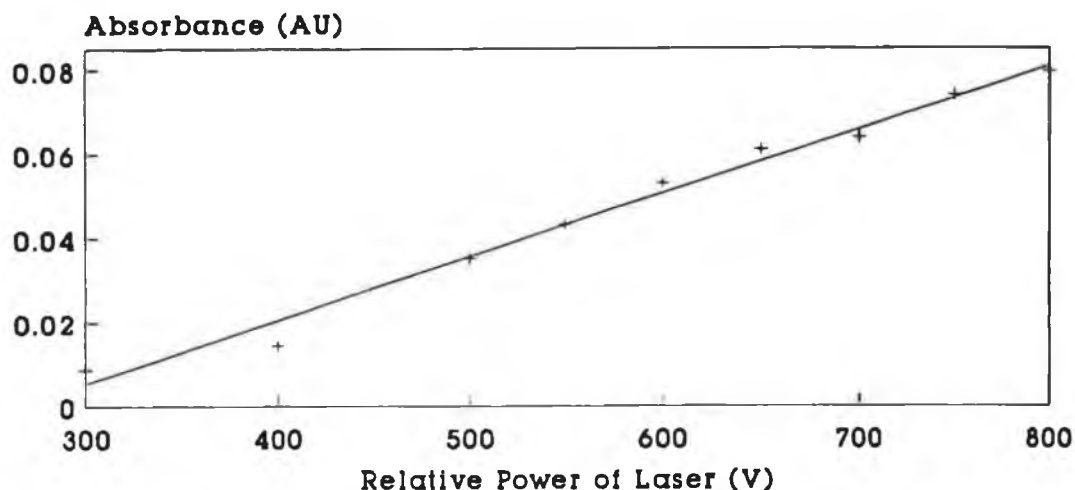


Figure 3.3.3.1 Plot of absorbance of $\text{Cr}(\text{CO})_5(\text{toluene})$ versus power of the laser.

The linear relationship obtained indicates that the formation of the primary photoproduct is as a result of a single photon event.

3.3.4 UV/visible difference spectrum of Cr(CO)₅(L)

The UV/visible difference spectrum shows the presence of the Cr(CO)₅(toluene) species with λ_{max} at 480nm, zero microseconds after the flash. The positioning of this band is shifted approximately 30nm to the blue compared to that of cyclohexane. Such shifts are indicative of stronger bonding being present in the complex [28, 29]. With time, the solvated complex reacts with the ligand, for example, 4-phenylpyridine, forming the Cr(CO)₅(4-ppy) complex whose absorption occurs at ca. 400nm (Figure 3.3.4.1). As all the ligands are pyridine derivatives, the Cr(CO)₅(L) complexes absorb in the same region ca. 380 - 430nm.

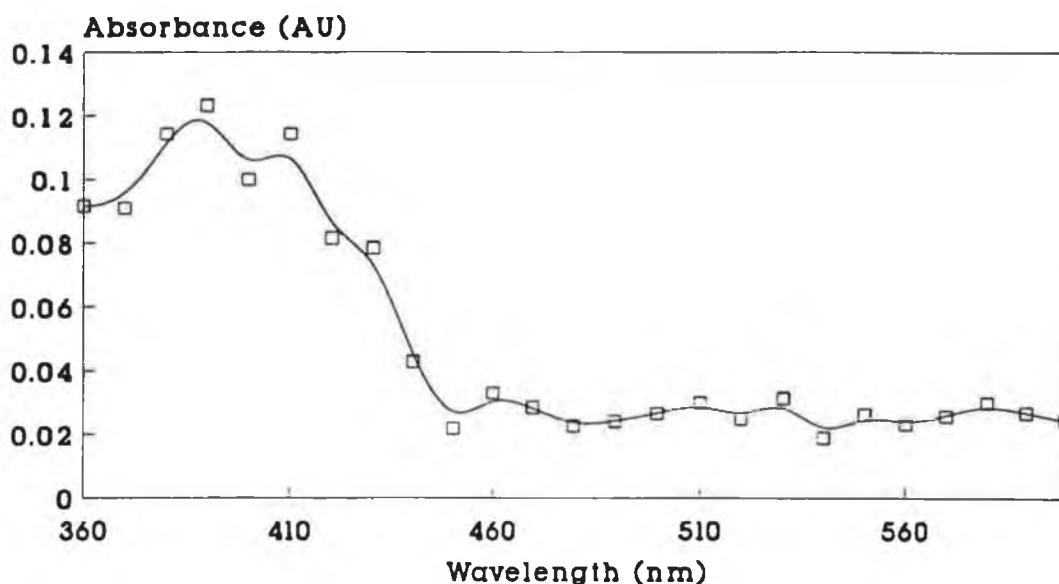


Figure 3.3.4.1 UV/visible difference spectrum for the reaction of Cr(CO)₅(toluene) with 4-phenylpyridine, recorded 400 μ s after the laser flash.

3.3.5 The rate of reaction of $\text{Cr}(\text{CO})_5(\text{S})$ with different ligand (L) concentrations

The reaction of $\text{Cr}(\text{CO})_5(\text{toluene})$ with each of the ligands, yielding $\text{Cr}(\text{CO})_5(\text{L})$ followed pseudo-first-order kinetics. The rate of decay of the solvated complex and the formation of the ligated complex were the same within error (Table 3.3.5.1).

Reaction	$\lambda(\text{nm})$	$k_{\text{obs}} (\text{s}^{-1}) \times 10^{-3}$
Decay of $\text{Cr}(\text{CO})_5(\text{toluene})$	480	2.8 ± 0.5
Formation of $\text{Cr}(\text{CO})_5(\text{pyridine})$	410	2.8 ± 0.3

Table 3.3.5.1 Rate constants for the formation of $\text{Cr}(\text{CO})_5(\text{pyridine})$ and the decay of $\text{Cr}(\text{CO})_5(\text{toluene})$.

Plots of k_{obs} versus ligand concentration, for each ligand at 480 and 410nm were obtained. Linear plots were observed in all cases. A representative example is presented in Figure 3.3.5.1. From the slope of the line of such plots, the second-order rate constants, k_2 were obtained. The experimental data is tabulated in Appendix B (Table B3), while a summary of the second-order rate constants, along with the pK_a values of the ligands are given in Table 3.3.5.2. It is important to note that the pK_a values of the ligands quoted in Table 3.3.5.2 were measured in water and not aromatic solvents, and therefore may not reflect the actual basicities of the ligands in toluene.

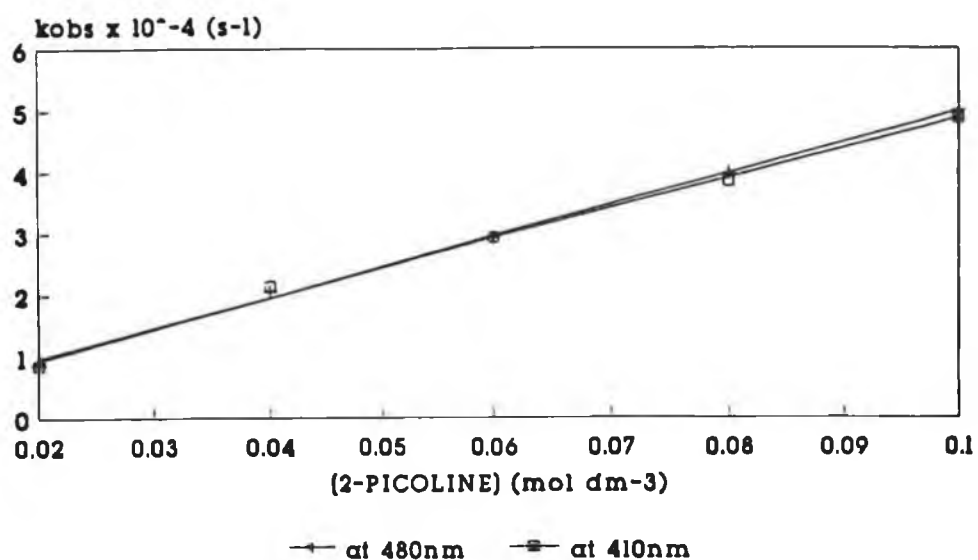


Figure 3.3.5.1 Plot of k_{obs} (s^{-1}) versus ligand concentration (mol dm^{-3}) monitored at 480 and 410nm, at 22°C.

The fastest rate of displacement was obtained for the pyridine ligands with substituents in the 4-position. As with cyclohexane as solvent, the greatest rates were obtained for ligands with electron-donating substituents while the slowest rates were for those with electron-withdrawing substituents. Again, the rate of displacement of toluene was influenced by the steric factors associated with the substituents on the pyridine ring. The rate of displacement of toluene in $\text{Cr}(\text{CO})_5(\text{toluene})$ by pyridine, $k_2 = 8.3 \times 10^4 \text{ dm}^3\text{mol}^{-1}\text{s}^{-1}$, is very close to that obtained by Zhang *et al.* using piperidine [38] and 1-hexene [40] as nucleophiles, $k_2 = 2.26 \times 10^4$ and $0.506 \times 10^4 \text{ dm}^3\text{mol}^{-1}\text{s}^{-1}$, respectively. Nucleophilicity among these ligands increases in the order 1-hexene < piperidine < pyridine [4(b), 41].

Toluene being an aromatic solvent, with a methyl group present may coordinate to the coordinatively unsaturated $\text{Cr}(\text{CO})_5$ by either an "agostic" interaction between a methyl hydrogen and the Cr metal or by "edge-on"

Ligand (L)	$k_2 \times 10^{-4}$ (480nm) ($\text{dm}^3\text{mol}^{-1}\text{s}^{-1}$) ^a	$k_2 \times 10^{-4}$ (410nm) ($\text{dm}^3\text{mol}^{-1}\text{s}^{-1}$) ^a	$\text{pK}_{\text{a, H}_2\text{O}}$ ^b
2-chloropyridine	5.3 ± 0.3	5.5 ± 0.3	0.76
3-chloropyridine	2.9 ± 0.2	3.2 ± 0.1	2.85
2-phenylpyridine	1.6 ± 0.3	1.7 ± 0.1	4.48
pyridine	8.4 ± 0.5	8.3 ± 0.4	5.23
4-phenylpyridine	9.8 ± 0.7	9.1 ± 0.6	5.55
2-picoline	5.1 ± 0.2	4.9 ± 0.5	6.03
3-picoline	7.5 ± 0.4	7.7 ± 0.2	5.79
4-picoline	9.9 ± 0.7	10.7 ± 0.3	6.08
3-Me-2-Phpy	3.9 ± 0.2	3.9 ± 0.1	5.04 ^c

^a at 22°C, ^b reference [35], ^c estimated value

Table 3.3.5.2 Second-order rate constants for the reaction of $\text{Cr}(\text{CO})_5(\text{toluene})$ with the various ligands, L, monitored at 480 and 410nm at 22°C.

coordination *via* an olefinic linkage [4(b), 40]. Previous studies support the latter mode of coordination. Rate of displacement of n-heptane from $\text{Cr}(\text{CO})_5(\text{n-heptane})$ was approximately 2,500 times faster than the rate of displacement of toluene by the same ligand [38]. The differences in rates suggest that the bonding mode present in toluene is not the same as that in n-heptane, i.e. not an "agostic" interaction. Thus, bonding most likely occurs through an isolated double bond. Similar bonding mechanisms have been proposed for benzene, fluorobenzene and xylenes [4(b), 4(c), 38, 40, 41]. The rate of displacement of cyclohexane by pyridine is $6.3 \times 10^7 \text{ dm}^3\text{mol}^{-1}\text{s}^{-1}$, in which bonding is known to occur *via* an "agostic" interaction involving a

methylene hydrogen. This rate is approximately 1000-fold faster than that observed in toluene, thus suggesting the presence of a different bonding mechanism in the toluene complex.

The second-order rate constants, k_2 , for the reaction of 3-methyl-2-phenylpyridine with $\text{Cr}(\text{CO})_5(\text{toluene})$ is approximately twice that of 2-phenylpyridine. This significant difference in rates is in contrast to the similar k_2 values obtained in cyclohexane. In the latter case it was concluded that both ligands possessed the same structural conformation (Section 3.2.4). The differences in rates observed in this study suggest that in toluene, the methyl group may be altering the conformation of the phenyl ring so that it is no longer the same as that in 2-phenylpyridine. As the basicity of a ligand may be taken as a measure of its nucleophilicity [21(a)], the increase observed in the reactivity of 3-methyl-2-phenylpyridine may be as a result of an increase in the basicity of the ligand owing to a change in conformation of the phenyl ring.

In the formation of the ligand bridged complex $(\text{Cr}(\text{CO})_5)_2(\mu\text{-}2,2'\text{-bipyridine})$, it was proposed that binding of 2,2'-bipyridine (bipy) to one $\text{Cr}(\text{CO})_5$ fragment induced a conformational change in the ligand, which resulted in increased basicity of the uncoordinated pyridine ring. This then reacted with another $\text{Cr}(\text{CO})_5$ fragment forming the bridging complex [16] (Section 3.1). The relationship between the basicity and the angle between the two rings, θ , for 2,2'-bipyridine was investigated by CNDO solvation studies [18] (Section 3.1.1). It was found that the lowest pK_b was obtained when θ was 0° in polar media and 120° in non-polar media. Therefore, the the angle θ and the basicity of the ligand were influenced by the solvent used.

Thus, the variation in the k_2 values of 3-methyl-2-phenylpyridine and 2-phenylpyridine in toluene and the lack of such a variation in cyclohexane suggest that the solvent may also be influencing the time-averaged conformation

of the ligand in solution. Such time-averaged collision complexes are known to influence the ^1H NMR spectrum of aromatic moieties. Toluene unlike cyclohexane may interact strongly with the phenyl ring. This may account for the differences observed in the rates of the two ligands in the different solvents.

3.3.5.1 The effect of ligand basicity on the rate of reaction of $\text{Cr}(\text{CO})_5(\text{toluene})$ with L

Even though 2-picoline and 4-picoline have approximately the same basicity, the rate of reaction of the former is only half that of the latter. This indicates the role steric effects are playing in the substitution process. As for cyclohexane, in general, no linear relationship was evident between the second-order rate constants and the basicities of the ligands. One reason for absence of linearity may be because the pK_a values used were measured in water rather than in toluene. A plot of k_2 versus pK_a of the ligands is displayed in Figure 3.3.5.1.1. However, a linear relationship is observed when only ligands of the same steric nature are examined, for example, 4-picoline, pyridine and 3-chloropyridine. This is shown in Figure 3.3.5.1.2. Thus the transition state appears to be selective, for ligands with similar steric constraints, suggesting the operation of an associative or interchange process rather than a dissociative one. A similar relationship was obtained for the reaction of $\text{CoNO}(\text{CO})_3$ with these three ligands [13(a)]. In $\text{Mo}(\text{CO})_5(4\text{-picoline})$, the rate of displacement of CO decreased with decreasing ligand basicity in the order, 3,4-lutidine > 4-picoline > 3-chloropyridine. All three entering ligands have the same steric requirements but different σ -donating abilities [15].

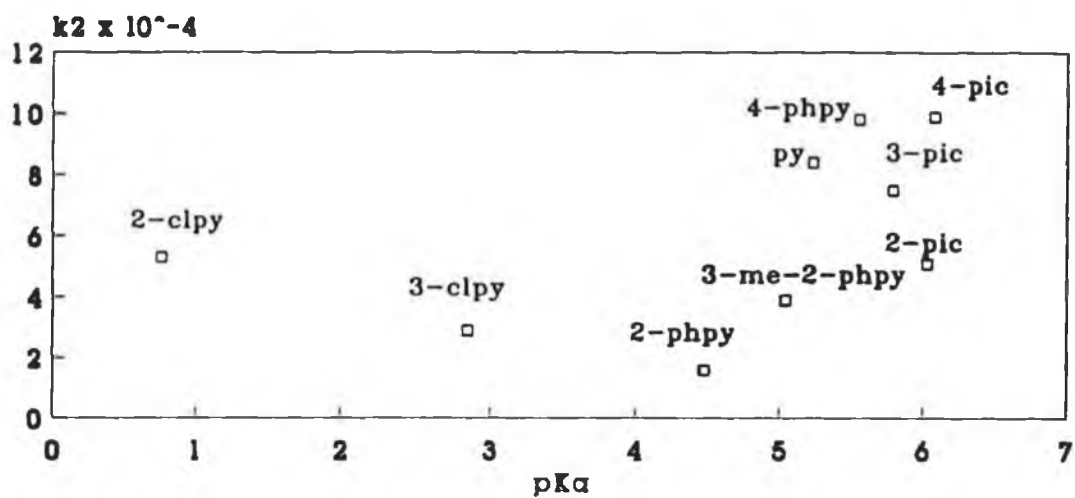


Figure 3.3.5.1.1 Plot of k_2 values at 480nm versus pK_a of the ligands, L for the reaction of $Cr(CO)_5(\text{toluene})$ with L.

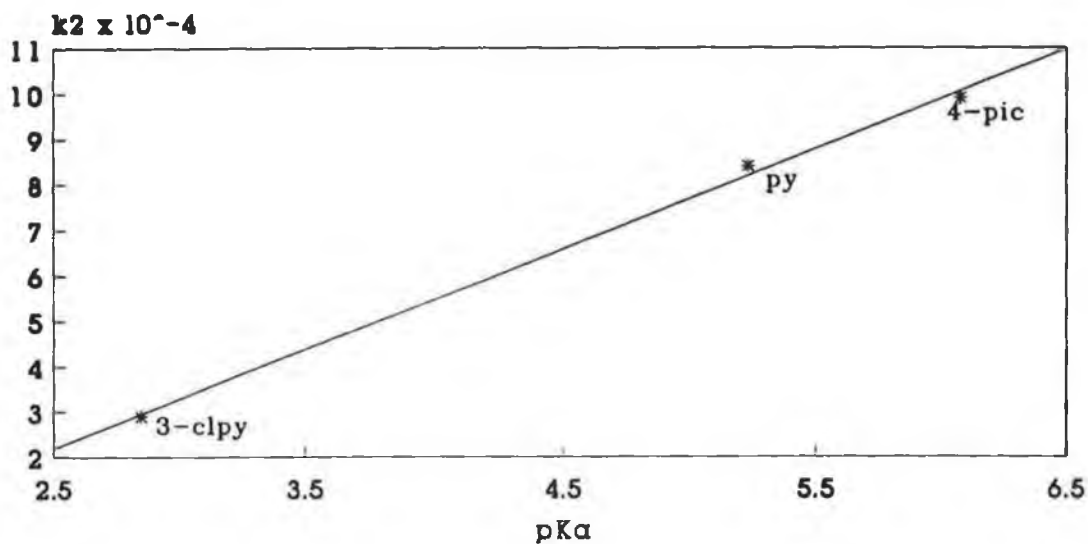


Figure 3.3.5.1.2 Plot of k_2 values at 480nm versus pK_a of 4-picoline, pyridine and 3-chloropyridine.

3.3.6 Activation parameter studies for the reaction of Cr(CO)₅(toluene) with L

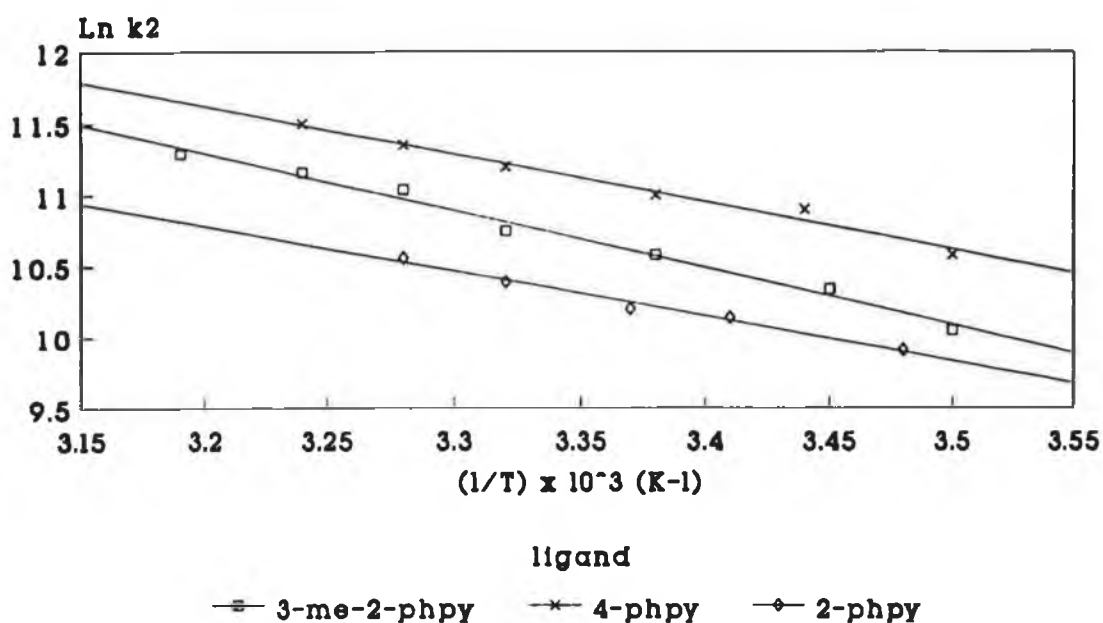
As the rate of decay of the solvated species and the formation of the ligated species were the same within error, the activation parameters were determined for only one of the processes. In this study, the rate of decay of Cr(CO)₅(toluene) was monitored at 480nm. The activation parameters were calculated according to equations 5.4.1 and 5.4.2 and are tabulated in Table 3.3.6.1. Representative Arrhenius and Eyring plots are presented in Figure 3.3.6.1. Similar plots were obtained for all the ligands. The experimental data used in the construction of these plots is tabulated in Appendix A (Table A3).

Ligand (L)	E _a [‡] (kJmol ⁻¹) ^a	ΔH [‡] (kJmol ⁻¹) ^a	ΔS [‡] (JK ⁻¹ mol ⁻¹) ^a	ΔG _{298K} [‡] (kJmol ⁻¹) ^a
Pyridine	26 ± 1	23 ± 1	-73 ± 10	45
2-Phpy	26 ± 2	24 ± 2	-79 ± 10	47
4-Phpy	28 ± 2	25 ± 2	-67 ± 10	45
3-Me-2-Phpy	33 ± 2	31 ± 2	-52 ± 10	47
2-Picoline	33 ± 1	30 ± 1	-53 ± 10	46
3-Picoline	29 ± 1	26 ± 1	-63 ± 10	45
4-Picoline	22 ± 2	20 ± 1	-81 ± 10	44
2-Clpy	26 ± 2	23 ± 2	-77 ± 10	46
3-Clpy	26 ± 1	23 ± 1	-80 ± 10	47

^a monitored at 480nm

Table 3.3.6.1 Activation parameters for the reaction of Cr(CO)₅(toluene) with L (6 x 10⁻²M), monitored at 480nm.

(a)



(b)

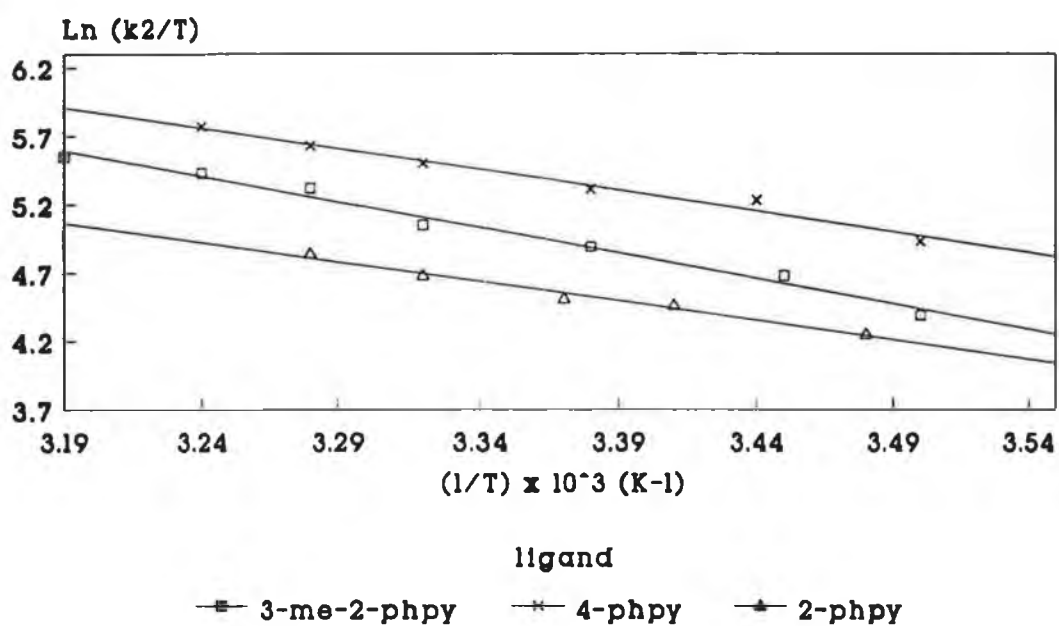
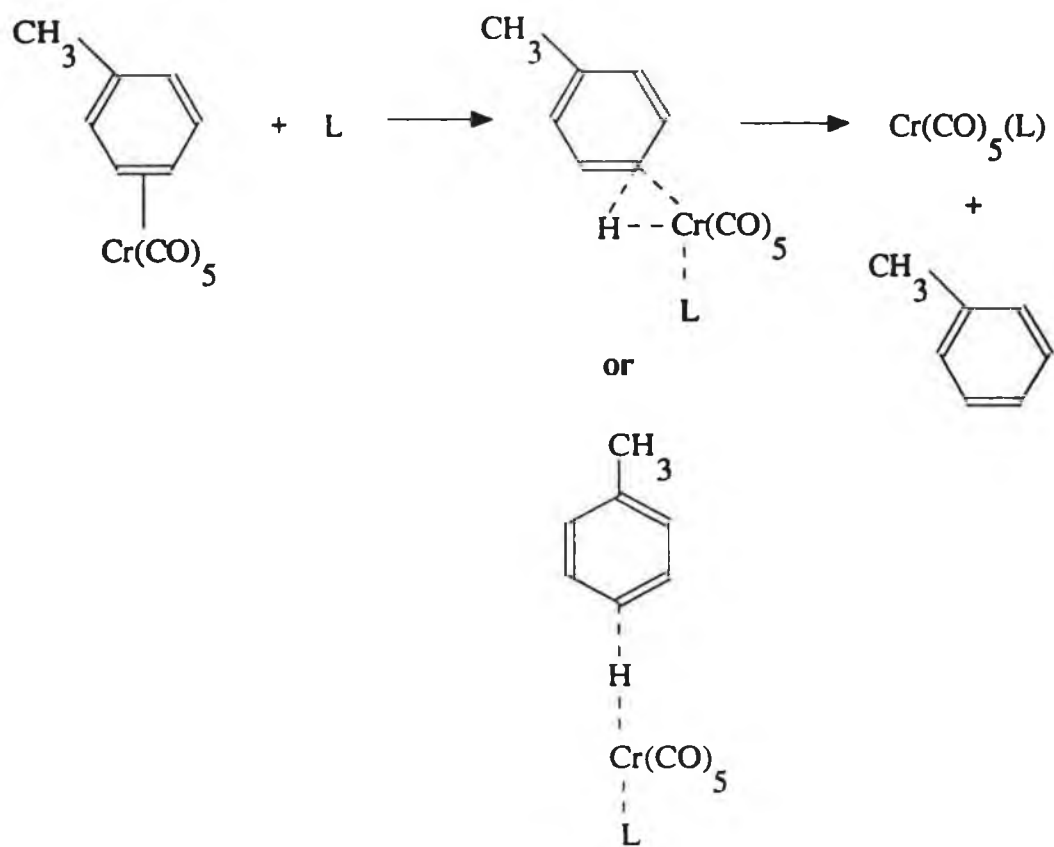


Figure 3.3.6.1 (a) Arrhenius and (b) Eyring plots for the reaction of $\text{Cr}(\text{CO})_5(\text{toluene})$ with 2-ppy, 4-ppy and 3-me-2-ppy.

The activation energy (E_a^\ddagger) and activation enthalpy (ΔH^\ddagger) values are very similar between most of the ligands. The ΔH^\ddagger values of $25 \pm 5 \text{ kJmol}^{-1}$, are significantly smaller than that estimated for Cr---toluene bond strength, which is assumed to be greater than ΔH^\ddagger of ca. 40 kJmol^{-1} reported for the Cr---benzene bond strength [4(b), 42, 43]. Within the individual groups of ligands, that is, picolines, chloropyridines and phenylpyridines, the greatest variation in ΔH^\ddagger values is for the picolines. The decrease in activation enthalpies in the order, 2-picoline (30 ± 1) > 3-picoline (26 ± 1) > 4-picoline ($20 \pm 1 \text{ kJmol}^{-1}$), complies well with weaker bond formation for the more sterically hindered ligands. Thus compared to pyridine, the differences in the activation parameters may be attributed to steric rather than electronic effects. On the contrary, chloro- and phenyl-substituted ligands, show little variation in the results upon varying the position of the substituent. Therefore, in the latter case any differences compared to pyridine are more as a result of electronic rather than steric effects.

The large negative entropies of activation ($\Delta S^\ddagger = -72 \pm 10 \text{ JK}^{-1}\text{mol}^{-1}$) suggest that associative processes are operative in the displacement of toluene from $\text{Cr}(\text{CO})_5(\text{toluene})$ by the ligands. For the more bulky ligands, 2-picoline and 3-methyl-2-phenylpyridine ($\Delta S^\ddagger = -52 \text{ JK}^{-1}\text{mol}^{-1}$), an interchange mechanism may also be accessible in the displacement of toluene. Bonding of toluene to $\text{Cr}(\text{CO})_5$ is reported to be through an isolated double bond, the same mode as suggested for benzene [40, 43]. However, in the latter case, upon reaction with a ligand a transition state is formed in which benzene is bonded to Cr forming a σ -complex or *via* an "agostic" C-H-Cr interaction [4(b)]. Thus, the displacement of toluene by the pyridine ligands may possess such a transition state. A possible reaction mechanism is outlined in Scheme 3.3.6.1.



L = nucleophile

Scheme 3.3.6.1

3.4 Conclusion

A comparison of the cyclohexane and toluene solvated systems upon reaction with pyridine and the substituted pyridine ligands is outlined below.

The rate of reaction of the cyclohexane complex with the ligands was 1000-fold greater than that for the toluene complex. This difference in rates is a reflection of the mode and strength of binding of these solvents to the Cr metal. Cyclohexane binds *via* an "agostic" C-H-Cr interaction while toluene coordinates *via* an isolated double bond. Similar trends were also observed in analogous systems [38, 40, 41].

The difference in binding is also reflected in the activation parameters, with E_a^\ddagger and ΔH^\ddagger values being much greater in toluene than in cyclohexane. The entropies of activation suggest that an associative or an interchange mechanism is operative in the displacement of toluene, while an interchange mechanism is most likely for the displacement of cyclohexane.

In both solvents, the rate of reaction is not determined by the nucleophilicity of the ligand alone but rather as a combination of both steric and electronic factors. It has been reported that the pK_a values and ionization potentials of the lone pairs of the free ligands are not good parameters for describing the σ -bond system [44].

Also, in cyclohexane it appears that the methyl group in 3-methyl-2-phenylpyridine does not affect the conformation of the phenyl group, as its rate of reaction is the same as that of 2-phenylpyridine. However, in toluene a significant difference between the two k_2 values was observed. This difference may be attributed to the influence the methyl group may have in determining the interaction of the toluene solvent with the phenyl ring. Cyclohexane, unlike toluene is not able to interact with the phenyl ring.

3.5 An investigation of the rate of reaction of $\text{Cr}(\text{CO})_6$ with L, in THF or ethanol using the stopped-flow technique, L = pyridine or substituted pyridine

Mechanistic studies on the substitution behaviour of coordinated solvent molecules in transition metal complexes are of utmost importance to the understanding of the general substitution behaviour and reactivity patterns of metal complexes in solution. Even though the solvent coordinated complexes may be present in very low concentrations, but as they are extremely labile, they may represent the main reaction pathway for all the ligand substitution processes. Therefore we decided to investigate the substitution process of $\text{Cr}(\text{CO})_5(\text{S})$, where S = THF or ethanol by various pyridine and substituted pyridine ligands, mainly 2-, 3-, 4-picoline, 2-, 3-chloropyridine, 2-, 4-phenylpyridine and 3-methyl-2-phenylpyridine. Also, the effect conformational changes had, if any, on the reactivity of 3-methyl-2-phenylpyridine was investigated. This part of the study was undertaken to obtain more information on how the conformation of 2,2'-bipyridine may influence the formation the ligand bridged complex, $(\text{Cr}(\text{CO})_5)_2(\mu\text{-}2,2'\text{-bipyridine})$ (Section 3.1).

The reactions being investigated are very similar to those discussed previously in Sections 3.2 and 3.3. The general reaction scheme involved is detailed in equation 3.5.1.



where S = THF, ethanol

L = pyridine or substituted pyridine

As both THF and ethanol are strong binding solvents compared to cyclohexane and toluene, their rates of displacement by the various ligands are slower. In the case of some of the ligands, reaction takes place on a timescale of seconds and thus such systems are not suitable for investigation by laser flash photolysis. Stopped-flow techniques are ideal for reactions on such timescales. The apparatus used is described in Section 5.3.1. The solvated complex, $\text{Cr}(\text{CO})_5(\text{S})$ was formed upon photolysis of $\text{Cr}(\text{CO})_6$ in the appropriate solvent, THF or ethanol. This was then reacted with the ligand, forming the ligated complex, $\text{Cr}(\text{CO})_5(\text{L})$. All the ligation reactions were performed *in situ* (i.e. not isolated) and were monitored by UV/visible spectroscopy.

3.5.1 UV/visible spectrum for the formation of $\text{Cr}(\text{CO})_5(\text{L})$

The spectral changes shown in Figure 3.5.1.1 were recorded upon the reaction of $\text{Cr}(\text{CO})_5(\text{S})$ with L, where S = THF or ethanol and L = pyridine or substituted pyridine. The $\text{Cr}(\text{CO})_5(\text{S})$ band at ca. 460nm decays with concomitant growth of a band centred at ca. 400nm, in accordance with the reaction described in equation 3.5.1. The maintenance of an isosbestic point at ca. 430nm indicates that the reaction is uncomplicated by side or subsequent reactions. The ultimate spectrum given in Figure 3.5.1.2 for the formation of $\text{Cr}(\text{CO})_5(\text{py})$ *in situ* is identical to that of an authentic sample of $\text{Cr}(\text{CO})_5(\text{py})$.

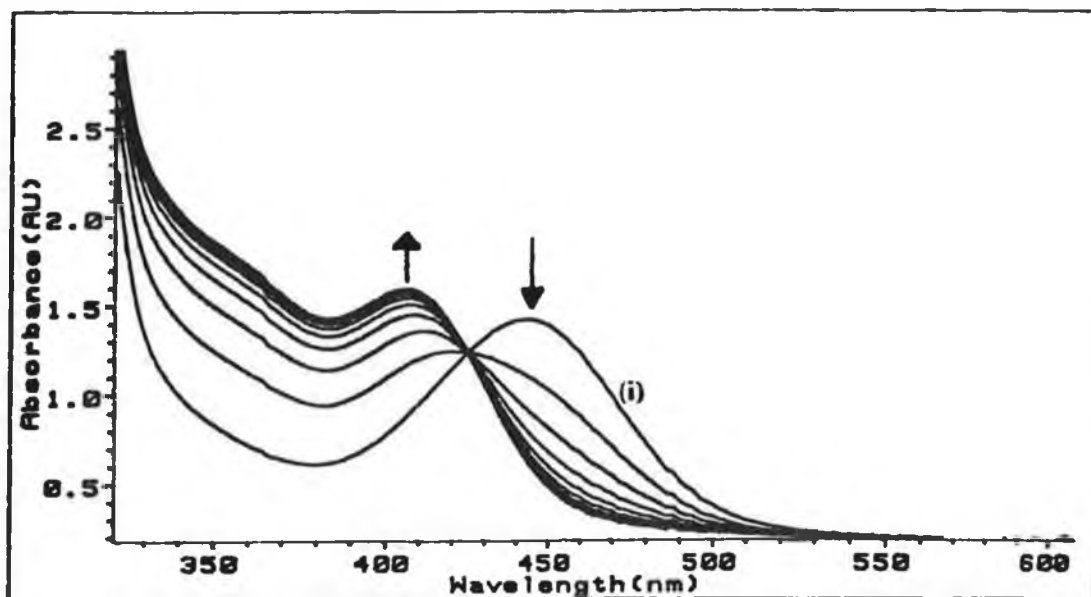
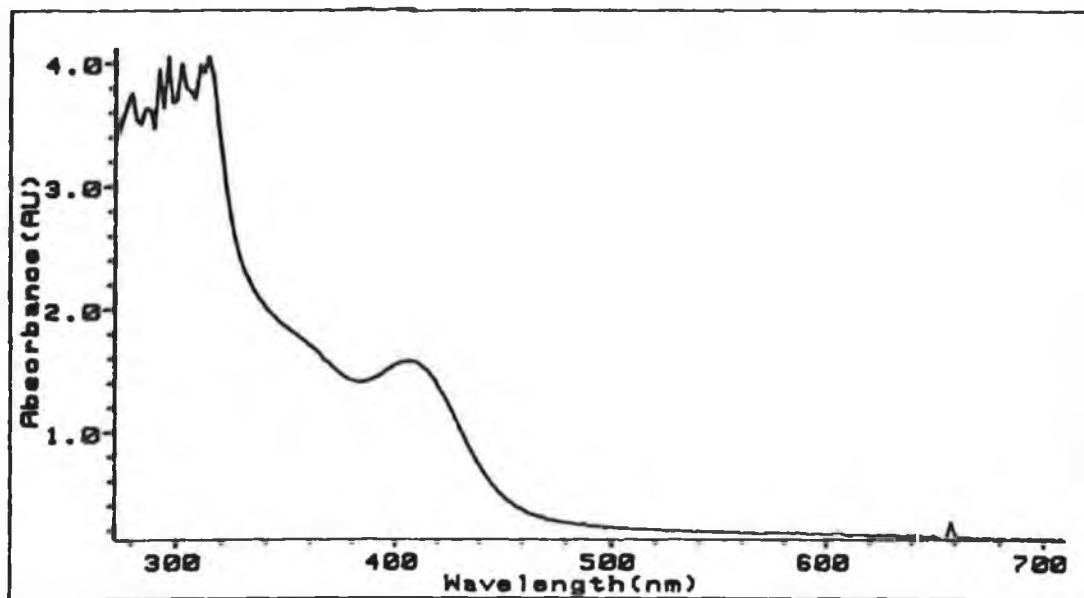


Figure 3.5.1.1 UV/visible spectral changes observed during the reaction of $\text{Cr}(\text{CO})_5(\text{THF})$ with pyridine in THF. $[\text{Pyridine}] = 5 \times 10^{-2}\text{M}$, time interval between successive spectra = 15s. (i) initial spectrum of $\text{Cr}(\text{CO})_5(\text{THF})$.

UV/visible spectra are good indicators of the strength and nature of bonding present between the metal atom and ligands in complexes [28, 29]. The similar positioning of the bands of the solvated species at ca. 460nm, in both THF and ethanol is evidence of the common bonding present in both complexes, however that of ethanol is slightly blue-shifted compared to that of THF. Thus, the bonding in the latter complex is slightly weaker. In comparison with the analogous complexes of toluene and cyclohexane, the band associated with the solvated species is blue-shifted ca. 20 and 50nm respectively, (Table 3.5.1.1). Thus the strength of the Cr---solvent interaction decreases in the order, ethanol \sim THF > toluene > cyclohexane.

(a)



(b)

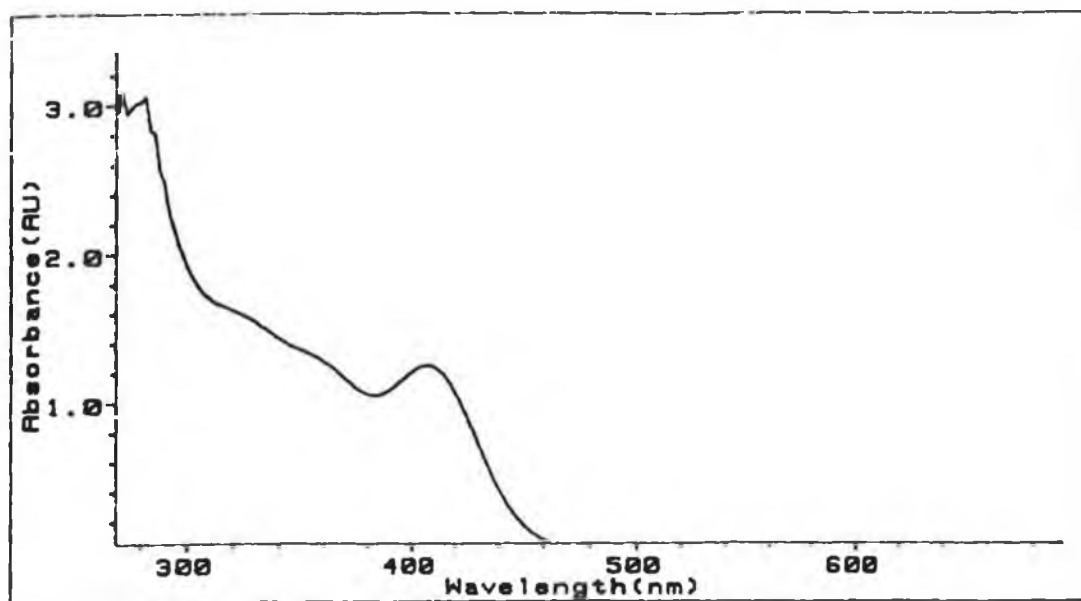


Figure 3.5.1.2 Comparison of the UV/visible spectra of $\text{Cr}(\text{CO})_5(\text{py})$, (a) formed *in situ* (b) an authentic sample of $\text{Cr}(\text{CO})_5(\text{py})$ (ca. $2.5 \times 10^4 \text{ mol dm}^{-3}$) in THF.

Cr(CO) ₅ (S)	λ_{max} (nm)
S = ethanol	456
THF	460
toluene ^a	480
cyclohexane ^b	504

^a Section 3.3, ^b Section 3.2 and ref [3(c)]

Table 3.5.1.1 λ_{max} (nm) of Cr(CO)₅(S) in different solvents.

The positioning of the ligated band is roughly the same for all the ligands, λ_{max} at $400 \pm 10\text{nm}$, suggesting similar bonding patterns. However, the slight variations in positioning compared to that of pyridine, may be attributed to the electronic and steric properties of the attached substituents.

3.5.2 Rate of reaction of Cr(CO)₅(S) with different ligand (L) concentrations

Similar rates within error were obtained for the formation of the ligated complex and the decay of the solvated species in both solvents (Table 3.5.2.1). The rate constant for the formation of the ligated product was determined from the "grow-in" of the overlapping LF and MLCT band of Cr(CO)₅(L) at 380nm. Figure 3.5.2.1 shows the plot of absorbance at 380 and 460nm *versus* time for the formation of Cr(CO)₅(L) and the decay of Cr(CO)₅(S) respectively. In each case a single exponential is fitted to the curve in accordance with the expression $A = a_1 + a_2e^{-kt}$, where A is the absorbance at time t, a_1 and a_2 are constants related to the initial and final absorbances at the monitoring wavelength, and k is the observed first-order rate constant (k_{obs}).

Reaction	k_{obs} (s^{-1})	
	S = THF	S = ethanol
Formation of $\text{Cr}(\text{CO})_5(\text{L})^{\text{a}}$	0.280	0.047
Decay of $\text{Cr}(\text{CO})_5(\text{S})^{\text{b}}$	0.300	0.050

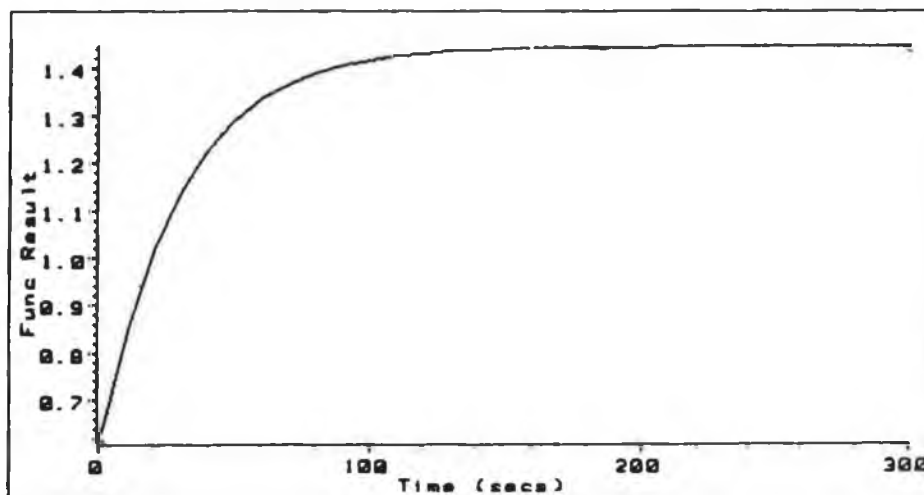
^a monitored at 380nm, ^b monitored at 460nm

Table 3.5.2.1 Rates of formation of ligated complex and decay of the solvated species in THF and ethanol for L = pyridine (1M) at 25°C.

The effect variations in ligand concentration had on the rate of reaction of $\text{Cr}(\text{CO})_5(\text{S})$ was investigated. In all cases, a minimum 10-fold excess of ligand concentration (10^{-2} ----> 2M) over $\text{Cr}(\text{CO})_6$ concentration (10^{-3}M) was used to ensure pseudo-first-order conditions were maintained (equation 3.5.2.1). Formation of $\text{Cr}(\text{CO})_5(\text{L})$ was not observed for L = 3-Me-2-Phpy and 2-phpy in THF, and 3-Me-2-Phpy, 2-phpy and 2-clpy in ethanol, even at high ligand concentrations. Also, in both solvents, for L = 3-pic and 4-phpy, the rate of formation of $\text{Cr}(\text{CO})_5(\text{L})$, at high ligand concentrations was too rapid for the instrumentation employed, and therefore the rate constants at these concentrations could not be determined by the stopped-flow technique.

$$k_{\text{obs}} = k[\text{L}] \quad (3.5.2.1)$$

(a)



(b)

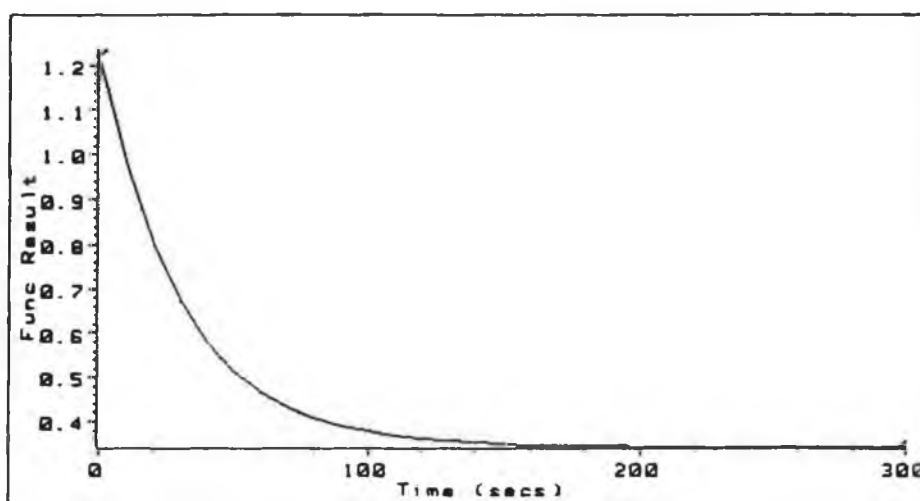
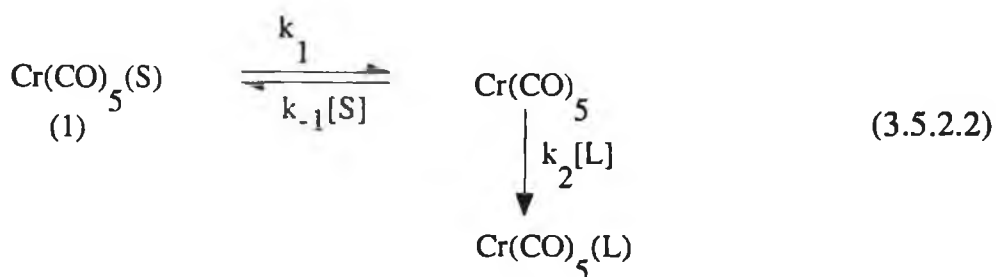


Figure 3.5.2.1 Plots of absorbance *versus* time for (a) the formation of $\text{Cr}(\text{CO})_5(\text{py})$ and (b) the decay of $\text{Cr}(\text{CO})_5(\text{THF})$, monitored at 380 and 460nm respectively.

Thus, plots of k_{obs} versus $[L]$ should yield straight lines of slope k_2 , the second-order rate constant. However, in this study, these reactions failed to follow pseudo-first-order behaviour. For all the systems studied, in both THF and ethanol, curved plots were obtained. The graphs tended to be linear at low ligand concentration but as higher concentrations were approached, deviations from linearity were obtained as the graphs reached a limiting rate. Plots of k_{obs} versus ligand concentration are presented in Figures 3.5.2.2 and 3.5.2.3 for THF and ethanol as solvents respectively. The experimental data is tabulated in Appendix B (Tables B4 and B5). Similar trends were observed by Lees and Adamson, when they investigated the substitution of solvent in $\text{W}(\text{CO})_5(\text{S})$ complexes by 4-acetylpyridine, where $\text{S} = \text{methylcyclohexane}$ [31], and also in the displacement of benzene by pyridine in analogous systems [4(b)].

Plot curvature is suggestive of a mechanism which involves consecutive steps one or more of which are reversible [4(b)]. Thus a plausible mechanism is one which involves reversible dissociation of the solvent from $\text{Cr}(\text{CO})_5(\text{S})$, where $\text{S} = \text{THF}$ or ethanol, followed by nucleophilic attack of L at the coordinatively unsaturated $\text{Cr}(\text{CO})_5$, as described in equation 3.5.2.2. The corresponding rate law is given in equation 3.5.2.3.



where $\text{S} = \text{THF, ethanol}$

$\text{L} = \text{pyridine or substituted pyridine}$

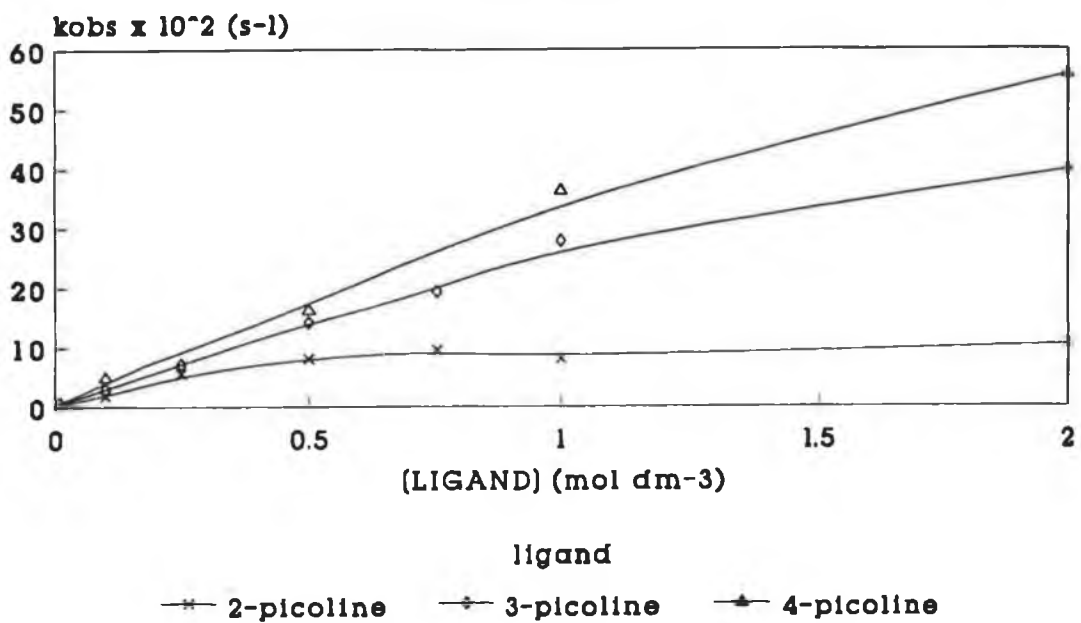
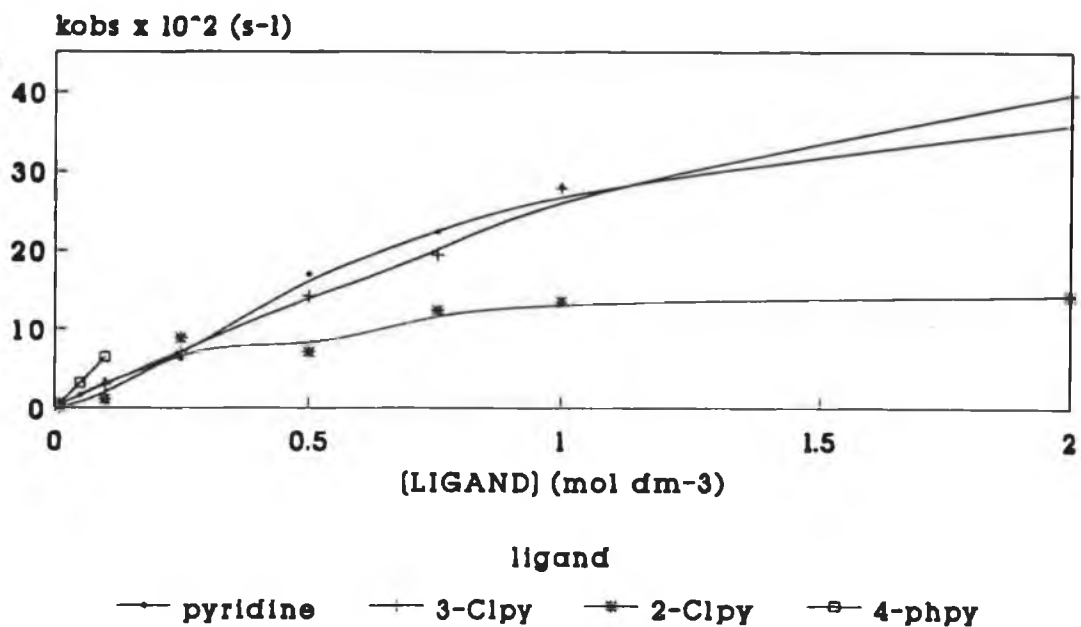


Figure 3.5.2.2 Plot of $k_{obs} (s^{-1})$ versus [L] for the reaction $Cr(CO)_5(THF)$ with L in THF at $25^{\circ}C$, monitored at 380nm.

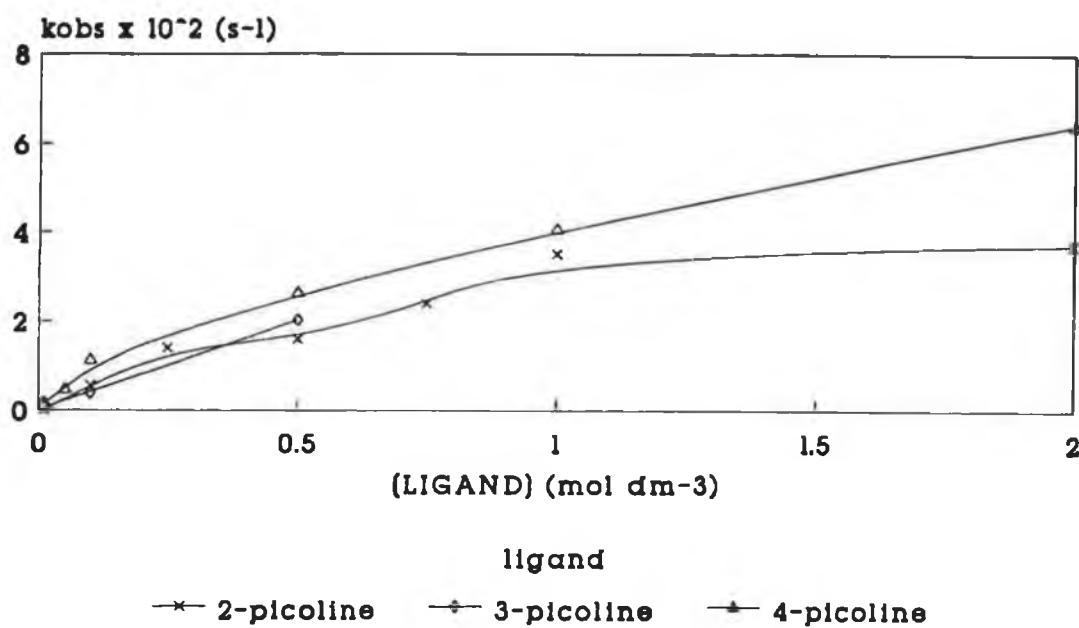
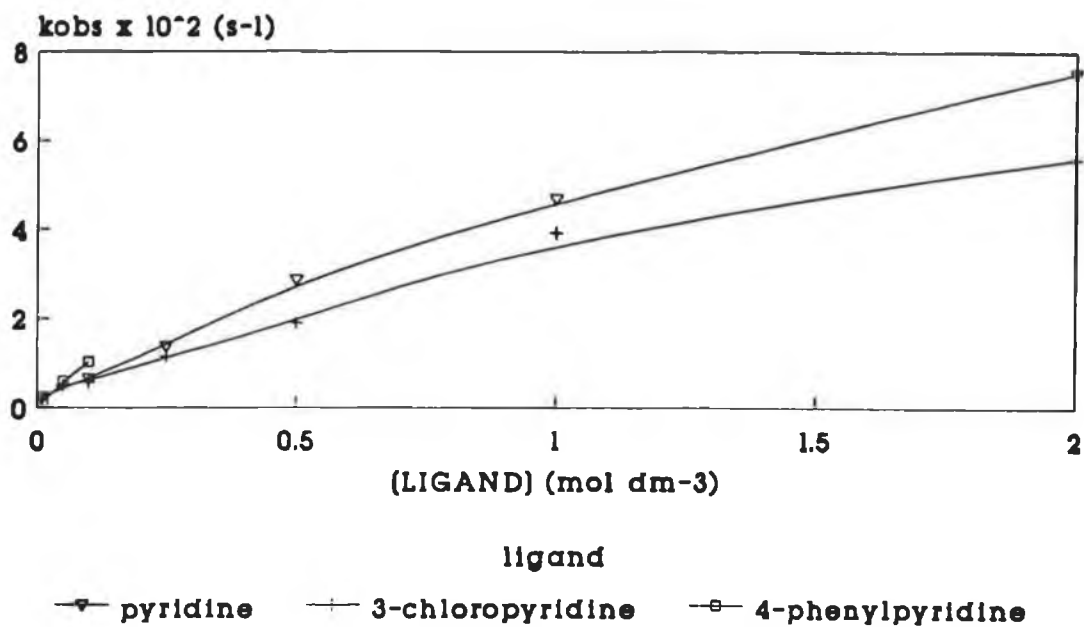


Figure 3.5.2.3 Plot of $k_{obs} (s^{-1})$ versus $[L]$ for the reaction $Cr(CO)_5(ethanol)$ with L in ethanol at $25^{\circ}C$, monitored at $380nm$.

Assuming a steady-state concentration of $\text{Cr}(\text{CO})_5$, the corresponding rate law is

$$-d[1]/dt = k_1 k_2 [L] [1] / \{k_{-1} [S] + k_2 [L]\} \quad (3.5.2.3)$$

In terms of the pseudo-first-order rate constant, k_{obs}

$$1/k_{\text{obs}} = 1/k_1 + (k_{-1}/k_1 k_2) [S]/[L] \quad (3.5.2.4)$$

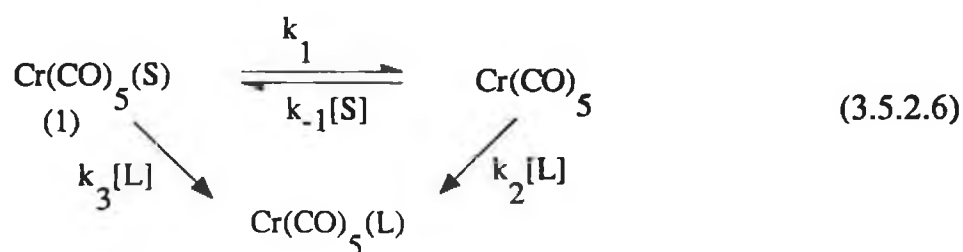
However, in the presence of neat solvent, the $[S]$ is constant [46],

$$1/k_{\text{obs}} = 1/k_1 + (k_{-1}/k_1 k_2) / [L] \quad (3.5.2.5)$$

Thus, plots of $1/k_{\text{obs}}$ versus $1/[L]$ should yield straight lines of slope $k_{-1}/k_1 k_2$ and intercept $1/k_1$. Such plots were linear for all the ligands at high ligand concentrations, but at lower concentrations (ca. 10^{-2}M), slight non-linearity was observed in some cases, for example, pyridine and 3-chloropyridine. Representative examples of the curved and linear plots obtained are shown in Figure 3.5.2.4, while a subsection of the plot at higher ligand concentrations is illustrated in Figure 3.5.2.5, for THF as solvent. Similar trends were observed in ethanol and these are shown in Figures 3.5.2.6 and 3.5.2.7. The relative rates of attack by the various ligands L at the $\text{Cr}(\text{CO})_5$ can be determined from values of k_2/k_{-1} obtained as intercept/slope of the reciprocal plots. The slope of the lines, yield the rate constants, $k_1 k_2/k_{-1}$. The deviations from non-linearity (for py and 3-clpy) may be as a result of a competing mechanism [4(b)]. This mechanism is most likely to be associative or interchange in nature. An interchange mechanism was found to be accessible in the displacement of

benzene by pyridine from $\text{Cr}(\text{CO})_5(\text{benzene})$ [4(b)]. Linear dependence of the rate constants on the entering ligand concentration is indicative of an associative process, thus in the substitution processes investigated the rate-determining step was interpreted as being associative (ligand dependent) at low ligand concentrations while rate-limiting conditions were approached at high ligand concentrations. Therefore depending on the ligand concentration different reaction pathways may be in operation. Such competing reaction paths are present in analogous systems [4(b), 38].

The inclusion of an associative reaction path results in the mechanism shown in equation 3.5.2.6 and the corresponding rate law given in equation 3.5.2.7.



$$-d[1]/dt = k_3[\text{L}] + k_1k_2[\text{L}]/\{k_{-1}[\text{S}] + k_2[\text{L}]\} \quad (3.5.2.7)$$

Both rate laws given in equations 3.5.2.3 and 3.5.2.7, at high ligand concentrations predict a nonlinear dependence of k_{obs} on $[\text{L}]$, as was observed in Figures 3.5.2.2 and 3.5.2.3. The linear dependence of k_{obs} on $[\text{L}]$ observed by Wieland and van Eldik, for the displacement of THF from $\text{Cr}(\text{CO})_5(\text{THF})$ by piperidine was attributed to $k_{-1}[\text{THF}] \gg k_2[\text{L}]$ [41]. Therefore, in neat solvent where the concentration of S is constant, linear or nonlinear dependence of k_{obs} on $[\text{L}]$ depends on the competition ratio $k_{-1}[\text{S}]/k_2[\text{L}]$. Thus the contributions

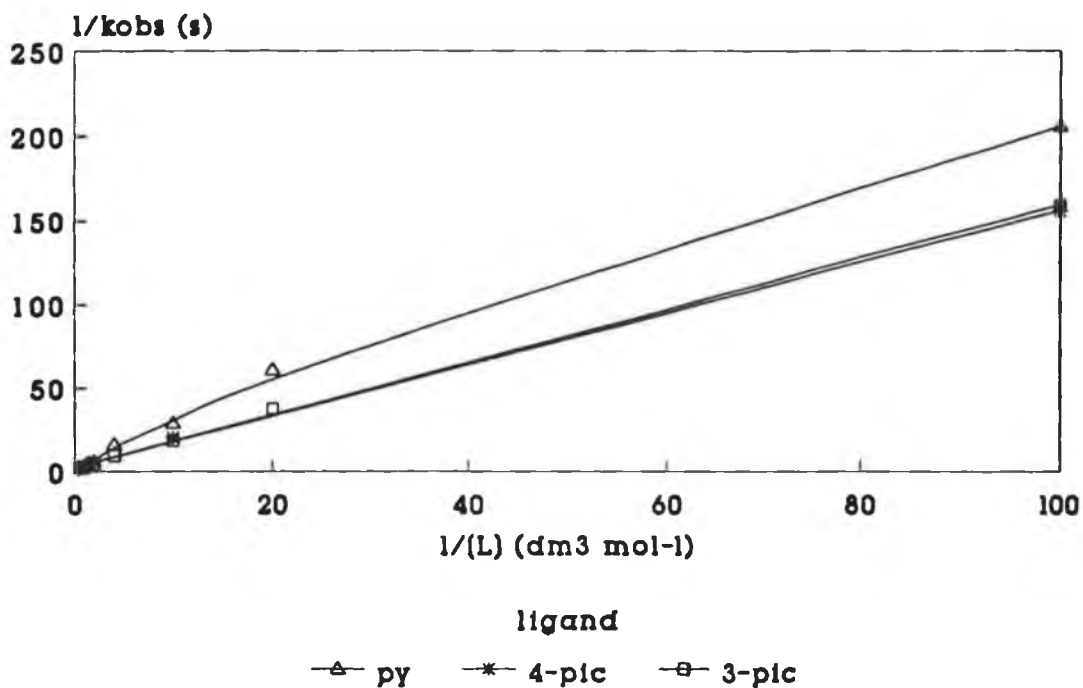


Figure 3.5.2.4 Plot of $1/k_{obs}$ versus $1/[L]$ in THF at lower ligand concentrations.

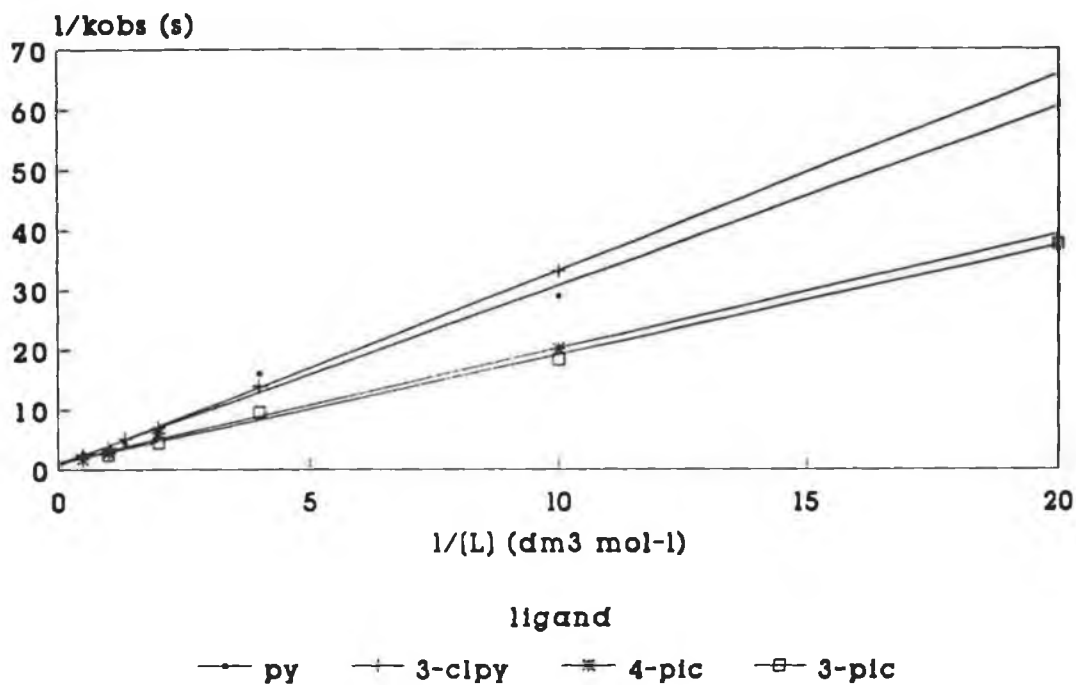


Figure 3.5.2.5 Plot of $1/k_{obs}$ versus $1/[L]$ in THF at higher ligand concentrations.

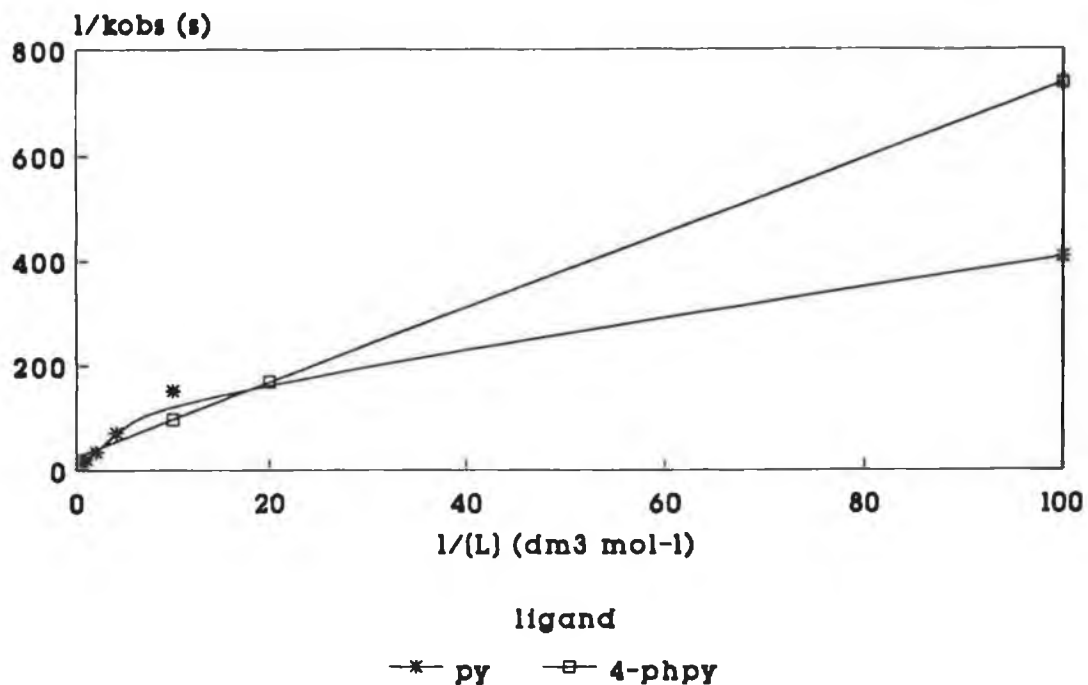


Figure 3.5.2.6 Plot of $1/k_{\text{obs}}$ versus $1/[L]$ in ethanol at lower ligand concentrations.

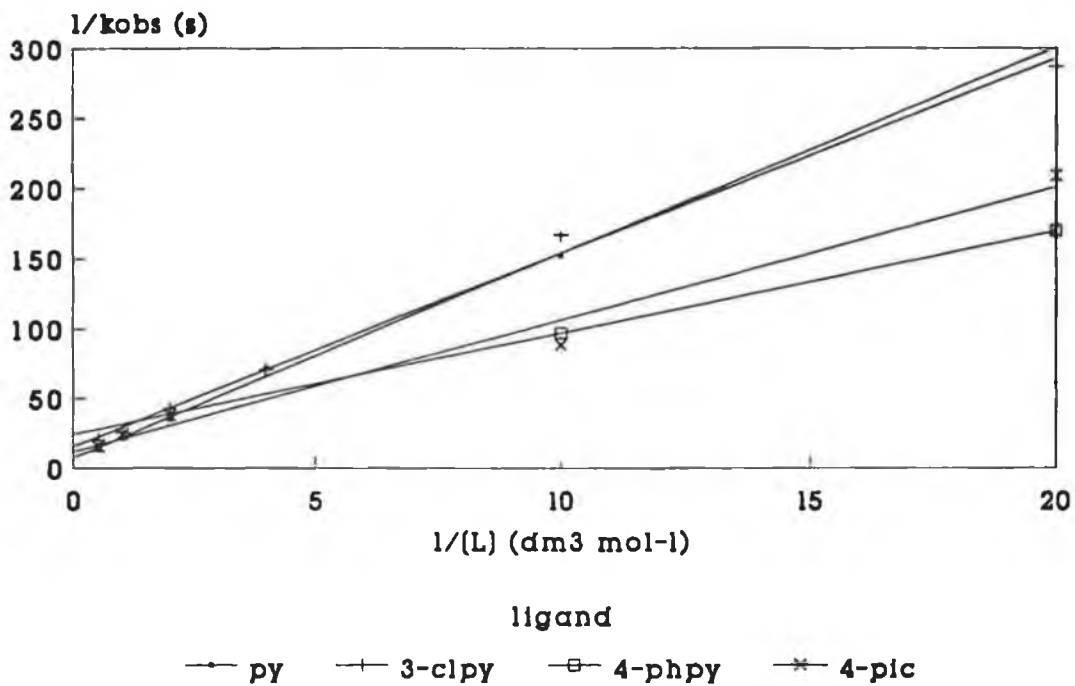


Figure 3.5.2.7 Plot of $1/k_{\text{obs}}$ versus $1/[L]$ in ethanol at higher ligand concentrations.

from the parallel reaction paths cannot be separated and consequently the second-order rate constants and the associated activation parameters are composite quantities, possessing contributions from both the associative and dissociative reaction pathways. The accessibility of two competing pathways has been suggested for other systems [4(a), 46]. The presence of such pathways have been confirmed by volume of activation studies [38].

From the reciprocal plots, the rate constant (k_1k_2/k_{-1}), the first-order dissociation rate constant (k_1) and the "competition ratios" (k_2/k_{-1}), that is the ratio of the rate constants for attack at $\text{Cr}(\text{CO})_5$ by the solvent and ligand were determined and are summarised in Tables 3.5.2.2 and 3.5.2.3 for reactions in THF and ethanol respectively.

Ligand (L)	k_1k_2/k_{-1} (s^{-1})	k_1 (s^{-1})	k_2/k_{-1}
Pyridine	0.34	0.34	0.98
2-Picoline	0.20	0.30	0.68
3-Picoline	0.63	0.36	1.76
4-Picoline	0.65	0.41	1.60
2-Chloropyridine	0.16	0.34	0.46
3-Chloropyridine	0.51	0.21	2.39
4-Phenylpyridine	0.56	0.32	1.76

Table 3.5.2.2 Rate constants for the reaction of $\text{Cr}(\text{CO})_5(\text{THF})$ with L in THF, monitored at 380nm at 25°C.

Ligand (L)	k_1k_2/k_{-1} (s ⁻¹)	k_1 (s ⁻¹)	k_2/k_{-1}
Pyridine	0.07	0.13	0.51
2-Picoline	0.01	0.005	2.25
3-Picoline	0.07	0.01	5.29
4-Picoline	0.18	0.03	6.39
3-Chloropyridine	0.07	0.06	1.12
4-Phenylpyridine	0.13	0.12	1.13

Table 3.5.2.3 Rate constants for the reaction of Cr(CO)₅(ethanol) with L in ethanol, monitored at 380nm at 25°C.

The rate constants, k_1k_2/k_{-1} obtained at 25°C for the displacement of THF and ethanol by the nucleophiles indicate that the rate of displacement of THF is faster than that of ethanol. Thus, THF is more weakly bound to the Cr(CO)₅ fragment than ethanol. The variations observed in the rate constants between the two solvents may be a reflection of the differences in the binding abilities of the solvents to the metal atom. The mode of binding of each solvent has been extensively investigated by many workers. It was concluded that both THF [5] and ethanol [47] initially bind to the metal atom *via* the alkane ends of the molecules and then rapidly rearranges to a more stable structure where binding is *via* the oxygen atom in THF and the hydroxyl group in ethanol. As ethanol is more polar than THF, binding to the Cr atom is much stronger and thus displacement of it is more difficult. The rate constants within each solvent followed similar trends, with the reaction being fastest with 4-picoline and slowest with 2-picoline. The trend followed the order,

(i) in THF



(ii) in ethanol



Therefore, the determining factors in the rate of reaction of the ligands with $\text{Cr}(\text{CO})_5$, appears to be a mixture of both electronic and steric effects. Also, the reactivity is not solely influenced by the basicity of the ligand as 2-picoline ($\text{pK}_a = 6.03$) is one of the least reactive ligands, however it probably has a contributing effect. The major influence seems to arise from steric effects. The reactivity decreases in both solvents as the substituents attached to the pyridine ring are moved from the 4-, to the 3-, to the 2-position. Also the observed lack of reactivity of 2-chloropyridine with $\text{Cr}(\text{CO})_6$ in ethanol was probably as a result of steric hindrance as well as electronic factors. The variation in the rate constants may be indicative of some selectivity among the ligands for the intermediate produced *via* $\text{Cr}(\text{CO})_5$ -solvent bond fission. Such a situation was observed in the analogous $\text{W}(\text{CO})_6$ system [4(d)].

The rate constant, k_1 for the dissociation of THF from $\text{Cr}(\text{CO})_5(\text{THF})$ in the presence of pyridine at 25°C , 0.34 s^{-1} , is approximately three times that for ethanol dissociation from the pentacarbonyl, 0.13 s^{-1} , in the presence of the same ligand. This difference may be attributed partly to the weaker Cr -THF bond. However, in the presence of picolines this difference is much greater (a 30-fold decrease in the k_1 value in ethanol compared with THF is obtained, in the presence of 3-picoline). One possible explanation may be that in the presence of the picolines in ethanol, one of the competing pathways (most

probably the associative/interchange path) is favoured over the other. The k_1 values in THF for all the ligands are similar, $0.30 \pm 0.1 \text{ s}^{-1}$.

In ethanol, the picolines have the greatest "competition ratio". This feature, coupled with the slower rates of displacement of ethanol, suggests further the likelihood of an interchange/associative mechanism. In general, in both solvents the "competition ratio" varies with the steric and electronic properties of the ligands

Within the picoline group, in both THF and ethanol, the k_1k_2/k_{-1} , k_1 and k_2/k_{-1} values decreased in moving the methyl substituent from the 4-, to the 3-, to the 2-position on the pyridine ring. This further indicates the role that steric effects are playing in the substitution process.

3.5.3 Activation parameter studies for the reaction of $\text{Cr}(\text{CO})_5(\text{S})$ with L

The activation parameters were determined at both low ligand concentrations ($5 \times 10^{-2}\text{M}$) where the rate-determining step is ligand dependent and at high ligand concentrations (1M) where rate-limiting conditions were approached. They were calculated according to equations 5.4.1 and 5.4.2, and are summarised in Tables 3.5.3.1 and 3.5.3.2. As the rate of formation of $\text{Cr}(\text{CO})_5(\text{L})$ and the rate of decay of $\text{Cr}(\text{CO})_5(\text{S})$, ($\text{S} = \text{THF}$ or ethanol) were the same within error (Table 3.5.2.1) the activation parameters were only calculated for one of the processes. In this study, the rate of formation of $\text{Cr}(\text{CO})_5(\text{L})$ monitored at 380nm was investigated. Representative examples of the Arrhenius and Eyring plots are displayed in Figures 3.5.3.1 and 3.5.3.2 for the reactions at high and low ligand concentrations in THF and ethanol respectively. All the plots obtained were linear. The experimental data used in the

determination of the activation parameters is given in Appendix A (Tables A4 and A5).

Ligand (L)	E_a^\ddagger (kJmol ⁻¹)	ΔH^\ddagger (kJmol ⁻¹)	ΔS^\ddagger (JK ⁻¹ mol ⁻¹)	ΔG_{298K}^\ddagger (kJmol ⁻¹)
Pyridine	53 ± 2 ^a	50 ± 2 ^a	-81 ± 10	74
	36 ± 1	33 ± 2	-146 ± 10	76
2-Picoline	46 ± 3 ^a	43 ± 3 ^a	-113 ± 10	76
	53 ± 4	50 ± 5	-92 ± 10	77
3-Picoline	44 ± 4 ^a	42 ± 4 ^a	-105 ± 10	73
	31 ± 3	29 ± 3	-157 ± 10	75
4-Picoline	67 ± 9 ^a	64 ± 9 ^a	-30 ± 10	73
	65 ± 4	64 ± 4	-40 ± 10	76
2-Chloropyridine ^b	-	-	-	-
	50 ± 4	47 ± 4	-101 ± 10	77
3-Chloropyridine	58 ± 2 ^a	56 ± 2 ^a	-66 ± 10	75
	45 ± 2	42 ± 2	-117 ± 10	77
4-Phenylpyridine	58 ± 4 ^a	55 ± 4 ^a	-63 ± 10	74

^a at low ligand concentration (5 x 10⁻²M)

^b no reaction at low ligand concentration (5 x 10⁻²M)

Table 3.5.3.1 Activation parameters for the reaction of Cr(CO)₅(THF) with L in THF, for [L] = 5 x 10⁻²M and 1.0M, monitored at 380nm.

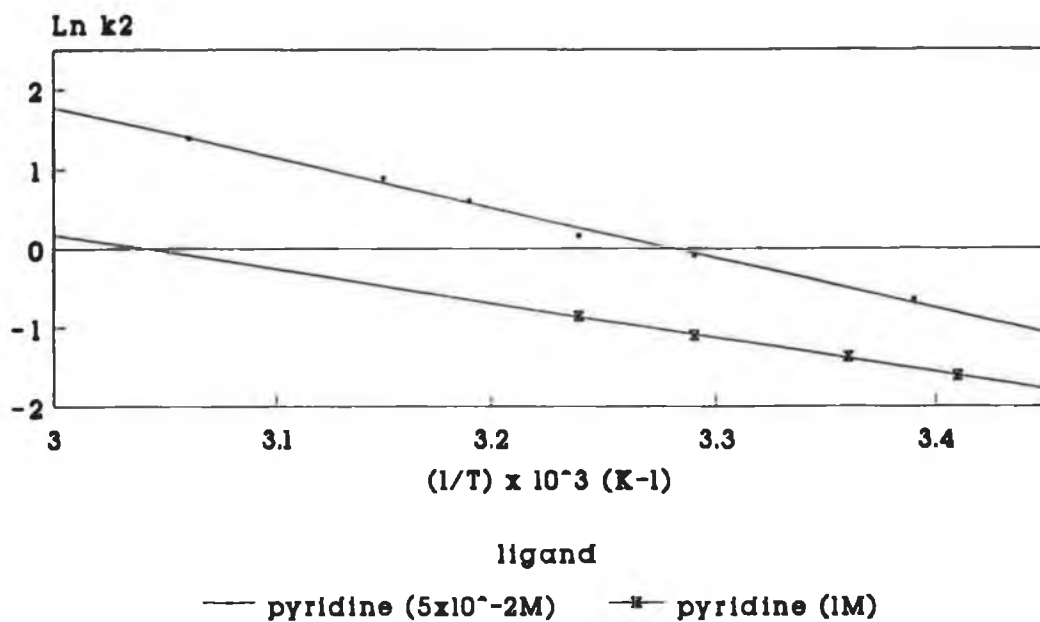
Ligand (L)	E_a^\ddagger (kJmol ⁻¹)	ΔH^\ddagger (kJmol ⁻¹)	ΔS^\ddagger (JK ⁻¹ mol ⁻¹)	ΔG_{298K}^\ddagger (kJmol ⁻¹)
Pyridine	73 ± 4 ^a	70 ± 4 ^a	-34 ± 10	80
	73 ± 4	71 ± 3	-39 ± 10	82
2-Picoline ^b	-	-	-	-
	28 ± 2	26 ± 2	-190 ± 10	83
3-Picoline	52 ± 2 ^a	50 ± 2 ^a	-100 ± 10	80
	47 ± 5	45 ± 5	-121 ± 10	81
4-Picoline	42 ± 2 ^a	40 ± 2 ^a	-132 ± 10	79
	47 ± 2	44 ± 2	-129 ± 10	83
3-Chloropyridine	66 ± 5 ^a	63 ± 5 ^a	-55 ± 10	80
	47 ± 3	47 ± 2	-117 ± 10	81
4-Phenylpyridine	44 ± 3 ^a	42 ± 3 ^a	-126 ± 10	79

^a at low ligand concentration (5 x 10⁻²M)

^b no reaction at low ligand concentration (5 x 10⁻²M)

Table 3.5.3.2 Activation parameters for the reaction of Cr(CO)₅(ethanol) with L in ethanol, for [L] = 5 x 10⁻²M and 1.0M, monitored at 380nm.

(a)



(b)

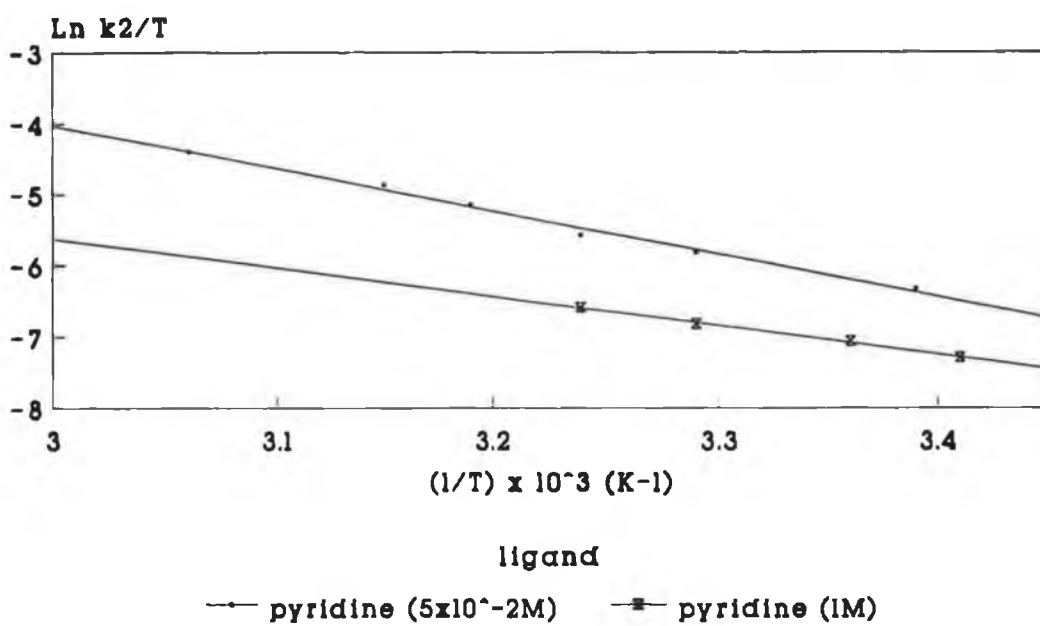
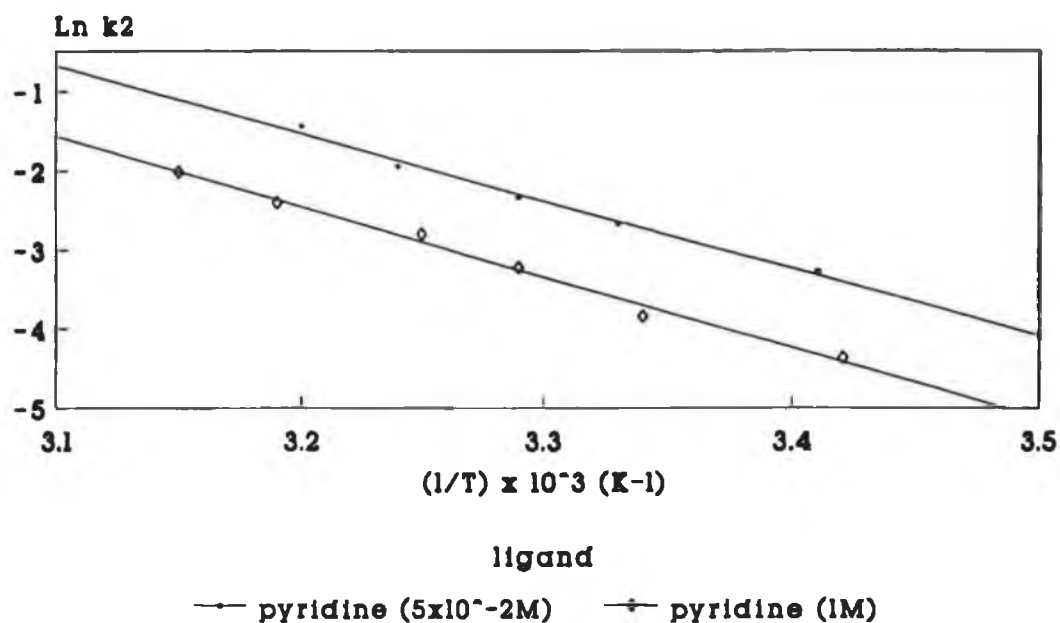


Figure 3.5.3.1 (a) Arrhenius and (b) Eyring plots for the formation of $\text{Cr}(\text{CO})_5(\text{L})$ complexes in THF, monitored at 380nm.

(a)



(b)

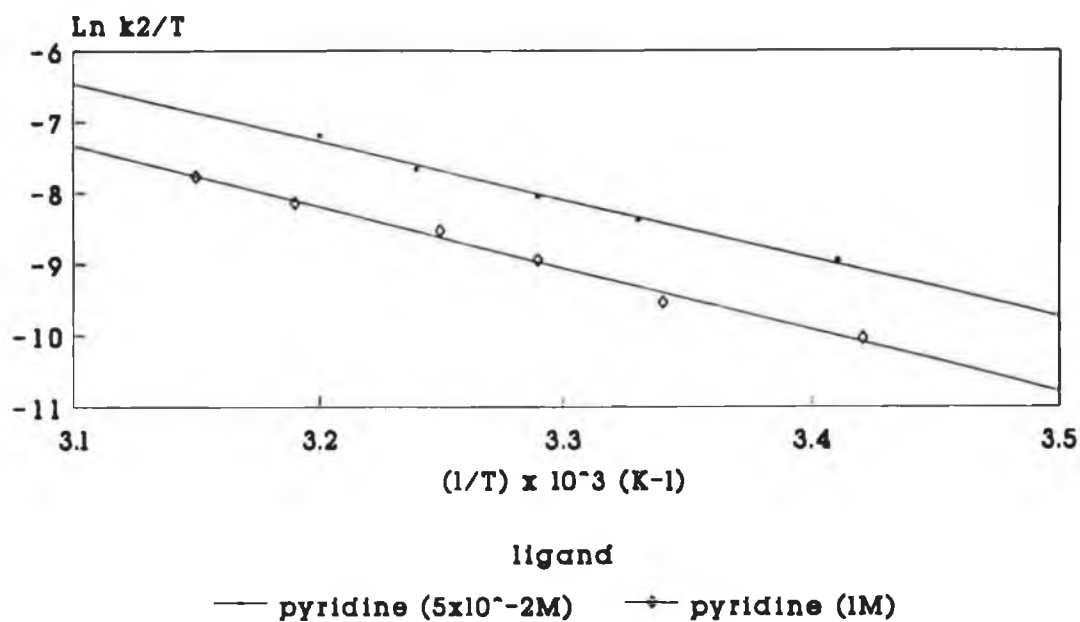


Figure 3.5.3.2 (a) Arrhenius and (b) Eyring plots for the formation of $\text{Cr}(\text{CO})_5(\text{L})$ in ethanol, monitored at 380nm.

The activation parameters were determined in both THF and ethanol at high (1M) and low (5×10^{-2} M) ligand concentrations, in the hope of obtaining a further insight into the reaction mechanisms involved at these ligand concentrations. The low ligand concentration studies were unsuitable for some ligands such as 2-picoline in ethanol and 2-clpy in THF. The rates at which these ligands reacted, at such low concentrations, were too slow to permit accurate measurements of the rates. In contrast, high concentration studies proved difficult to obtain for 4-phenylpyridine in both solvents as the rate of formation of $\text{Cr}(\text{CO})_5(4\text{-phenylpyridine})$ was too rapid for the instrumentation employed. In both THF and ethanol, reaction of $\text{Cr}(\text{CO})_5(\text{S})$, with 3-methyl-2-phenylpyridine was not observed, even at high ligand concentrations. Therefore the effect conformational changes may have on the reactivity of the ligand, could not be determined in this study.

In THF, at low ligand concentrations, the activation energy (E_a^\ddagger) and enthalpy of activation (ΔH^\ddagger) values are greater for ligands with electron-withdrawing substituents and less for those with electron-donating substituents. This is to be expected as the former reduces the availability of the lone pair on the N-atom while the latter increases its availability. The enthalpy of activation for displacement of THF by pyridine, $\Delta H^\ddagger = 50 \pm 2 \text{ kJmol}^{-1}$ is very similar to that for the displacement of THF by piperidine, $\Delta H^\ddagger = 45 \pm 2 \text{ kJmol}^{-1}$ [45]. The ΔH^\ddagger values in ethanol are greater than those in THF. This is a reflection of the difference in binding strengths of the solvents to the Cr atom.

The activation entropies (ΔS^\ddagger) for THF and ethanol substitution reactions are significantly negative for most ligands, which indicates an associative reaction path. Thus the most likely intermediate present in the substitution process is a 20-electron species. This is in accordance with the rate equation given in equation 3.5.2.6. The proposed reaction scheme is that described in

equation 3.5.2.6, and is composed of competing associative (or interchange) and dissociative reaction paths.

3.6 Conclusion

The substitution processes involved in the displacement of THF and ethanol from $\text{Cr}(\text{CO})_5(\text{S})$ species by various pyridine ligands are influenced by the steric and electronic nature of the ligands. THF is a weaker binding solvent than ethanol as evident from the reaction rates and lack of reaction of some ligands with the latter solvated species. The similar bonding nature of both solvents and ligands is reflected in the positioning of the appropriate bands in the UV/visible spectrum. Both solvents bind to the $\text{Cr}(\text{CO})_5$ fragment *via* the lone pairs on the oxygen atoms [5, 47].

The proposed mechanism for the displacement of the solvents is that of parallel dissociative and associative/interchange reaction paths. The activation parameters and reaction rates are consistent with such a mechanism. These parameters represent an overview of the whole mechanism, and not the individual contributions made to the mechanism by the parallel reaction paths. These contributions made by the parallel paths may be resolved by undertaking solvent concentration studies, in which the solvent concentration, as well as the ligand concentration is varied over a wide range. Also, volume of activation studies, which investigates the effect high pressure has on the rate of reaction, is of fundamental importance in determining the intimate mechanism involved in substitution processes. From many studies, it has been concluded that ΔV^\ddagger parameters are mechanistically more revealing than ΔS^\ddagger values [48]. Many studies have been conducted in which the latter two techniques have been individually employed [4(b), 38, 41, 46], however more recently combined

pressure and solvent dependence studies have been performed in order to resolve the intimate nature of the parallel solvent displacement mechanisms [49]. In the systems investigated, as we are dealing with a very fine tuning effect between various contributions, such as the nucleophilicity of the entering and departing ligands, the degree of bond formation and bond cleavage in the transition state, and steric hindrance, that such studies would have to be conducted to permit elucidation of the intimate mechanisms involved in these systems.

3.7 References

- 1 Yang, G. K.; Vaida, V.; Peters, K. S.; *Polyhedron*, 1988, **7**, 1619.
- 2 Morse, J. M.; Parker, G. H.; Burkey, T. J.; *Organometallics*, 1989, **8**, 2471.
- 3 (a) Kelly, J. M.; Bent, D. V.; Hermann, H.; Schulte-Frohlinde, D.; Koerner von Gustorf, E. A.; *J. Organomet. Chem.*, 1974, **69**, 259. (b) Bonneau, R.; Kelly, J. M.; *J. Am. Chem. Soc.*, 1980, **102**, 1220. (c) Kelly, J. M.; Long, C.; Bonneau, R.; *J. Phys. Chem.*, 1983, **87**, 3344. (d) Kelly, J. M.; Hermann, H.; Koerner von Gustorf, E.; *J. Chem. Soc., Chem. Commun.*, 1973, 105.
- 4 (a) Zhang, S.; Dobson, G. R.; *Inorg. Chim. Acta.*, 1989, **165**, L11. (b) Zhang, S.; Dobson, G. R.; Zang, V.; Bajaj, H. C.; van Eldik, R.; *Inorg. Chem.*, 1990, **29**, 3477. (c) Dobson, G. R.; Zhang, S.; *J. Coord. Chem.*, 1990, **21**, 155. (d) Dobson, G. R.; Asali, K. J.; Cate, C. D.; Cate, C. W.; *Inorg. Chem.*, 1991, **30**, 4471.
- 5 Wang, L.; Zhu, X.; Spears, K. G.; *J. Phys. Chem.*, 1989, **93**, 2.
- 6 Oishi, S.; *Organometallics*, 1988, **7**, 1237.
- 7 Kalyanasundaram, K.; *J. Phys. Chem.*, 1988, **92**, 2219.
- 8 Schadt, M. J.; Lees, A. J.; *Inorg. Chem.*, 1986, **25**, 672.
- 9 Marx, D.E.; Lees, A. J.; *Inorg. Chem.*, 1987, **26**, 2254.
- 10 (a) Darensbourg, D. J.; Gray, R. L.; *Inorg. Chem.*, 1984, **23**, 2993. (b) Darensbourg, D. J.; Graves, A. H.; *Inorg. Chem.*, 1979, **18**, 1257.
- 11 Wovkulich, T. L.; Atwood, J. D.; *J. Organomet. Chem.*, 1979, **184**, 77.
- 12 (a) Tolman, C.A.; *J. Am. Chem. Soc.*, 1970, **92**, 2956. (b) Boyles, M. L.; Brown, D. V.; Drake, D. A.; Hostetler, C. K.; Maves, C. K.; Mosbo, J. A.; *Inorg. Chem.* 1985, **24**, 3126.

- 13 (a) Thorsteinson, E. M.; Basolo, F.; *J. Am. Chem. Soc.*, 1966, **88**, 3929. (b) Schuster-Woldan, H.; Basolo, F.; *J. Am. Chem. Soc.*, 1966, **88**, 1657.
- 14 Zingales, F.; Canziani, F.; Basolo, F.; *J. Organomet. Chem.*, 1967, **7**, 461.
- 15 Zingales, F.; Faraone, F.; Uguagliati, P.; Belluco, U.; *Inorg. Chem.*, 1968, **7**, 1653.
- 16 Creaven, B. S.; Grevels, F.-W.; Long, C.; *Inorg. Chem.*, 1989, **28**, 2231.
- 17 Creaven, B. S.; Ph. D. Thesis, Dublin City University, 1989.
- 18 Morton-Blake, T.; University of Dublin, private communication.
- 19 Creaven, B. S.; Howie, R. A.; Long, C.; Low, J.; McQuillan, G. P.; *Inorg. Chim. Acta.*, 1989, **157**, 151.
- 20 Dennenberg, R. J.; Darensbourg, D. J.; *Inorg. Chem.*, 1972, **11**, 72.
- 21 (a) Angelici, R. J.; *Organomet. Chem. Rev.*, 1968, **3**, 173. (b) Angelici, R. J.; Graham, J. R.; *J. Am. Chem. Soc.*, 1965, **87**, 5586. (c) *J. Am. Chem. Soc.*, 1966, **6**, 988.
- 22 (a) Stolz, I. W.; Dobson, G. R.; Sheline, R. K.; *J. Am. Chem. Soc.*, 1962, **84**, 3589. (b) *J. Am. Chem. Soc.*, 1963, **85**, 1013.
- 23 Tyler, D. R.; Petrylak, D. P.; *J. Organomet. Chem.*, 1981, **212**, 389.
- 24 Dobson, G. R.; *J. Phys. Chem.*, 1965, **69**, 677.
- 25 Graham, M. A.; Rest, A. J.; Turner, J. J.; *J. Organomet. Chem.*, 1970, **24**, C54.
- 26 Graham, M. A.; Perutz, R. N.; Poliakoff, M.; Turner, J. J.; *J. Organomet. Chem.*, 1972, **34**, C34.
- 27 Graham, M. A.; Poliakoff, M.; Turner, J. J.; *J. Chem. Soc. (A)*, 1971, 2939.

- 28 Perutz, R. N.; Turner, J. J.; *J. Am. Chem. Soc.*, 1975, **97**, 4791.
- 29 Turner, J. J.; Burdett, J. K.; Perutz, R. N.; Poliakoff, M.; *Pure Appl. Chem.*, 1977, **49**, 271.
- 30 Flamigni, L.; *Radiat. Phys. Chem.*, 1979, **13**, 133.
- 31 Lees, A. J.; Adamson, A. W.; *Inorg. Chem.*, 1981, **20**, 4381.
- 32 Church, S. P.; Grevels, F.-W.; Hermann, H.; Schaffner, K.; *Inorg. Chem.*, 1984, **23**, 3830.
- 33 Schadt, M. J.; Gresalfi, N. J.; Lees, A. J.; *Inorg. Chem.*, 1985, **24**, 2942.
- 34 (a) Simon, J. D.; Peters, K. S.; *Chem. Phys. Lett.*, 1983, **98**, 53. (b) Welch, J. A.; Peters, K. S.; Vaida, V.; *J. Phys. Chem.*, 1982, **90**, 6751. (c) Simon, J. D.; Xie, X.; *J. Phys. Chem.*, 1986, **90**, 6751. (d) Xie, X.; Simon, J. D.; *J. Am. Chem. Soc.*, 1990, **112**, 1130. (e) Joly, A. G.; Nelson, K. A.; *J. Phys. Chem.*, 1989, **93**, 2876.
- 35 Tomasik, P.; Zalewski, R.; *Chem. Zvesti.*, 1977, **31**, 246.
- 36 Dobson, G. R.; Spradling, M. D.; *Inorg. Chem.*, 1990, **29**, 880.
- 37 Howell, J. A. S.; Burkinshaw, P. M.; *Chem. Rev.*, 1983, **83**, 557.
- 38 Zhang, S.; Zang, V.; Bajaj, H. C.; Dobson, G. R.; van Eldik, R.; *J. Organomet. Chem.*, 1990, **397**, 279.
- 39 Graham, J. R.; Angelici, R. J.; *Inorg. Chem.*, 1967, **6**, 2082.
- 40 Zhang, S.; Dobson, G. R.; *Polyhedron*, 1990, **20**, 2511.
- 41 Zhang, S.; Bajaj, H. C.; Zang, V.; Dobson, G. R.; van Eldik, R.; *Organometallics*, 1992, **11**, 3901.
- 42 Asali, K. J.; Basson, S. S.; Tucker, J. S.; Hester, B. C.; Cortes, J. E.; Awad, H. H.; Dobson, G. R.; *J. Am. Chem. Soc.*, 1987, **109**, 5386.
- 43 Asali, K. J.; van Zyl, G. J.; Dobson, G. R.; *Inorg. Chem.*, 1988, **27**, 3314.

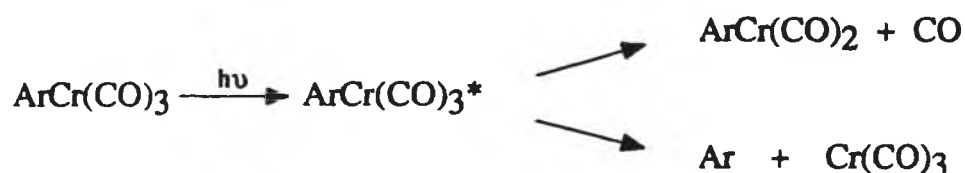
- 44 Daamen, H.; Oskam, A.; *Inorg. Chim. Acta.*, 1978, 26, 81.
- 45 Wieland, S.; van Eldik, R.; *Organometallics*, 1991, 10, 3110.
- 46 Zhang, S.; Dobson, G. R.; *Organometallics*, 1992, 11, 2447.
- 47 Simon, J. D.; Xie, X.; *J. Phys. Chem.*, 1989, 93, 291.
- 48 Brower, K. R.; Chen, T.; *Inorg. Chem.*, 1973, 12, 2198.
- 49 Zang, V.; Zhang, S.; Dobson, C. B.; Dobson, G. R.; van Eldik, R.;
Organometallics, 1992, 11, 1154.

CHAPTER 4

**LASER FLASH PHOTOLYSIS OF $\text{ArCr}(\text{CO})_2(\text{L})$, (L = CO, PYRIDINE, 4-
ACETILPYRIDINE) COMPLEXES IN THE PRESENCE OF
PYRIDINE OR 4-ACETILPYRIDINE**

4.1 Photochemistry of $\text{ArCr}(\text{CO})_3$

The photochemistry of $\text{ArCr}(\text{CO})_3$ ($\text{Ar} = \eta^6 - \text{C}_6\text{H}_6$) has been investigated in a number of different media, namely, low temperature matrices, gas matrices, gas phase and in solution. The earliest observations of the photoreactivity of $\text{ArCr}(\text{CO})_3$ were made by Strohmeier and von Hobe who proposed the reaction mechanism described in Scheme 4.1.1 [1].



Scheme 4.1.1

This scheme was concluded based on experiments in which the complexes were irradiated in the presence of both ^{14}CO and ^{14}C - labelled arene. Incorporation of the labelled species was observed in both cases.

Rest *et al.*, investigated the photochemistry of $\text{ArCr}(\text{CO})_3$ in argon, methane and N_2 matrices at 12K [2]. Photolysis of $\text{ArCr}(\text{CO})_3$ in argon and methane matrices, produced bands in the infrared spectrum which could be assigned to the coordinatively unsaturated $\text{ArCr}(\text{CO})_2(\text{matrix})$ species and free CO. Photolysis of the tricarbonyl compound in an N_2 matrix gave rise to bands assignable to $\text{ArCr}(\text{CO})_2(\text{N}_2)$. However, this complex, unlike the argon and methane analogues failed to undergo photoreversal upon irradiation at longer wavelengths. There was no evidence for the photolabilisation of the arene ligand even when $\text{ArCr}(\text{CO})_3$ was photolysed in a CO matrix.

Hill and Wrighton studied the thermal reactivity of trisubstituted silanes (R_3SiH) with the photochemically generated coordinatively unsaturated $ArCr(CO)_2$ species at low temperatures (85 - 157K) [3]. Photolysis of $ArCr(CO)_3$ in inert organic solvents, resulted in dissociative loss of CO, forming the 16 electron dicarbonyl $ArCr(CO)_2$ species which could be spectroscopically characterised. Upon annealing of the matrix doped with R_3SiH , the dicarbonyl species reacted to form the 18 electron oxidative addition products, $ArCr(CO)_2(H)(SiR_3)$. More recently, it has been reported that arene exchange may occur upon photolysis of silylated $ArCr(CO)_2$ complexes at room temperature [4]. Photolysis of $ArCr(CO)_3$ in the presence of $HSiCl_3$ yielded $ArCr(CO)_2(H)(SiCl_3)$ as reported by Hill and Wrighton [3]. However, further photolysis of this complex resulted in the elimination of H_2 and the formation of $ArCr(CO)_2(SiCl_3)_2$. During this process it has been reported that the arene ligand becomes labilised and undergoes exchange with other arene ligands present.

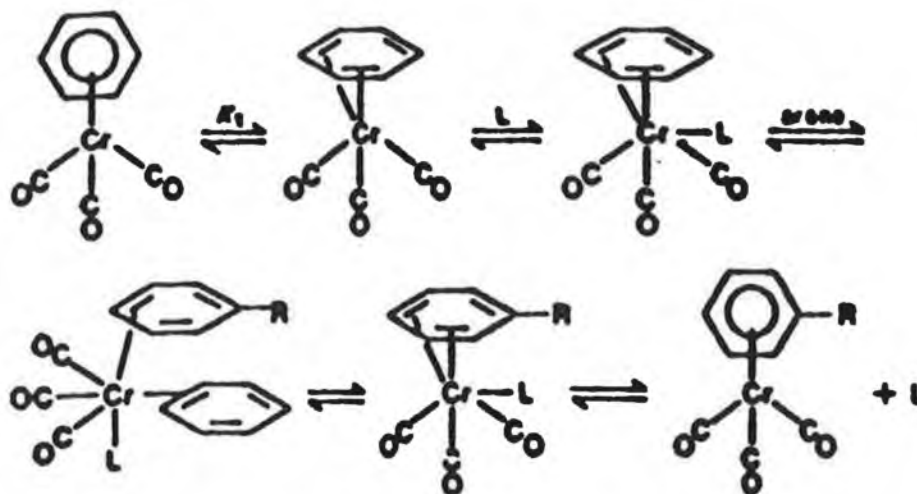
Many studies investigating the photochemistry of $ArCr(CO)_3$ have been conducted in solution. Yavorskii *et al.* [5] and Trembovler and co-workers [6] studied the spectral changes which occurred during the irradiation of $ArCr(CO)_3$ in cyclohexane solution. They concluded that the spectral changes observed were compatible with the formation of arene and chromium hexacarbonyl. Trembovler *et al.* also determined the quantum yield of photodecomposition as a function of light intensity and proposed the simultaneous occurrence of three photodecay processes, with different dependencies on light intensity. At low intensities the decomposition had negligible dependence on the incident light intensity, while at high incident light intensities the decomposition was determined by deactivation of an excited molecule and by a biquantum

photodecay. Monoquantum decomposition was observed at the intermediate light intensities.

The thermal reaction of $\text{ArCr}(\text{CO})_3$ with various substituted arene ligands results in the exchange of the Ar moiety [7]. These exchange reactions are equilibrium processes and were carried out at high temperatures in sealed NMR tubes. However, the addition of donor solvents such as THF, acetone or benzonitrile catalysed the process allowing arene exchange to occur at reasonable rates and lower temperatures (140°C or below) upon attaining equilibrium. The exchange process can also be self catalysed by arene chromium tricarbonyls. The replacement of *p*-xylene from its tricarbonylchromium complex by benzene is catalysed by (hexamethylbenzene)tricarbonylchromium [8]. Also, the rate of the arene exchange process is influenced by the substituents on the arene being substituted. Electron-accepting substituents (for example, chloro group) accelerate the process while electron-donating substituents slow down the rate of exchange.

More recently, Traylor *et al.* investigated the thermal exchange of arene ligands [9]. A kinetic study was performed on the displacement of arene and substituted arenes from their chromium carbonyl complexes by other substituted arenes. The reactions were carried out at 170°C in vacuum sealed NMR tubes. They concluded that the exchange process occurred *via* a η^6 to η^4 hapticity change of the arene ligand resulting in a simple stepwise displacement of the arene ligand. The catalytic ligand L present may be any two electron Lewis base, such as ketones, nitriles, alkenes or even another molecule of arene (Scheme 4.1.2).

Although both the arene and carbonyl ligands can be replaced, arene displacement is generally favoured under thermal conditions while photolysis usually results in CO loss.



Scheme 4.1.2

UV irradiation of $\text{ArCr}(\text{CO})_3$ complexes in the presence of suitable nucleophiles in hydrocarbon solvents is a convenient route for the formation of carbonyl-substituted complexes (Scheme 4.1.3) [10, 11].



S = solvent, L = nucleophile

Scheme 4.1.3

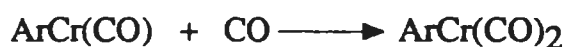
A number of studies have been carried out on the mechanisms of photosubstitution. Wrighton and Ginley investigated the quantum efficiency for the formation of $\text{ArCr}(\text{CO})_2(\text{pyridine})$ from $\text{ArCr}(\text{CO})_3$ and pyridine, and found that it was independent of both the irradiating wavelength ($\Phi_{\text{CO}} = 0.72 \pm 0.007$ at 313, 366, or 436nm) and the concentration of pyridine [12]. Similarly, the quantum yield for the photosubstitution of a CO ligand in $(1,3,5\text{-Me}_3\text{C}_6\text{H}_3)\text{Cr}(\text{CO})_3$ by *N*-dodecylmaleimide was 0.9 ± 0.009 at 313nm and no evidence was found for the photolabilisation of the mesitylene ligand [13]. These results are consistent with dissociative loss of one molecule of CO as the primary photoprocess. Disubstituted complexes of the form $\text{ArCr}(\text{CO})(\text{L})_2$ only seem to result from the irradiation of $\text{ArCr}(\text{CO})_2(\text{L})$ when L is a good π -acceptor ligand, for example, a phosphite ligand [14].

Wrighton and Haverty investigated the photosubstitution of $\text{ArCr}(\text{CO})_3$ in the presence of pyridine (Ar = benzene or mesitylene) [15]. The results observed were consistent with dissociative loss of CO as the primary photoreaction (Scheme 4.1.3). Also, the nearly quantitative chemical yield (0.72 ± 0.007) of $\text{ArCr}(\text{CO})_2(\text{pyridine})$ obtained implied that if arene exchange was occurring at all under these conditions it was only a very minor component of the photochemistry. Exchange of arene ligands was believed to proceed *via* the one step dissociation of the excited molecule to give $\text{Cr}(\text{CO})_3$ and arene (Scheme 4.1.1). Photoinduced CO exchange studies of $\text{ArCr}(\text{CO})_3$ [16] resulted in a quantum yield similar to that obtained by Wrighton and Haverty [15], however the efficiency of the arene exchange was found to be approximately one-sixth the efficiency of CO loss ($\Phi_{\text{C}_6\text{H}_6} = 0.12$ compared with $\Phi_{\text{CO}} = 0.72$) [17]. Competition studies suggest that $\text{ArCr}(\text{CO})_2$ species may be the precursor in the exchange of the arene ligand as well as the exchange of CO. Flash photolysis of $\text{ArCr}(\text{CO})_3$ (Ar = benzene) in cyclohexane solution produced a

weakly absorbing transient species which reacted within one millisecond to form a second species [16, 18]. The formation of both species was quenched when the solution was saturated with CO at one atmosphere pressure. Thus, it was proposed that the primary species observed was $\text{ArCr}(\text{CO})_2$ and that exchange of the arene group was through this intermediate and not *via* a one-step dissociation of the excited molecule as previously thought.

Conclusions reached by Bamford *et al.* [17], from studies of $\text{ArCr}(\text{CO})_3$ in isooctane and methyl methacrylate solutions were consistent with those of other workers [15, 16].

More recently, time-resolved infrared spectroscopic studies of gas phase unsaturated metal carbonyl photofragments have been investigated. These have revealed large amounts of information on the structure and reactivity of the reactive species free from the interference of host matrix or solvent molecules [19-21]. Wang *et al.* studied the photofragments produced upon photolysis of gas phase $\text{ArCr}(\text{CO})_3$ at 355 and 266nm [22]. $\text{ArCr}(\text{CO})_2$ was the predominant product upon irradiation at 355nm, while both $\text{ArCr}(\text{CO})_2$ and $\text{ArCr}(\text{CO})$ were produced upon 266nm photolysis, with a ratio of $\text{ArCr}(\text{CO})_2:\text{ArCr}(\text{CO})$ of approximately 2:5. The reactivity of photofragments with CO was also investigated according to equations 4.1.1 and 4.1.2.



The rate constants for the reaction of $\text{ArCr}(\text{CO})_2$ and $\text{ArCr}(\text{CO})$ with CO were determined to be $(6.3 \pm 0.3) \times 10^{12}$ and $(1.4 \pm 0.2) \times 10^{12} \text{ dm}^3\text{mol}^{-1}\text{s}^{-1}$,

respectively. Evidence was also reported for the formation of a dinuclear species in the absence of CO [18, 23]. This species was formed by the reaction of the dicarbonyl species with the parent complex (equation 4.1.3).

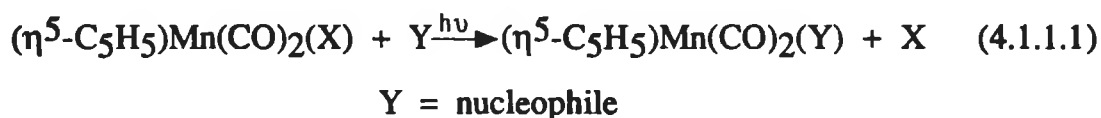


The dinuclear species has also been observed by other workers who determined its rate of formation to be ca. $4.8 \times 10^7 \text{ dm}^3\text{mol}^{-1}\text{s}^{-1}$, in cyclohexane solution [24].

4.1.1 Photochemistry of $\text{ArCr(CO)}_2(\text{L})$ complexes

Irradiation of ArCr(CO)_3 complexes in the presence of an entering nucleophile, results in photosubstitution of CO and the formation of $\text{ArCr(CO)}_2(\text{L})$ complexes [10, 14]. Very few studies investigating the photochemistry of the substituted complexes have been reported. Photochemical reactions of $\text{ArCr(CO)}_2(\text{L})$ ($\text{L} = \text{pyridine, 4-acetylpyridine}$) are rarely reported, however many more studies have been carried out on the isoelectronic $\text{CpMn(CO)}_2(\text{L})$, ($\text{Cp} = \eta^5\text{-C}_5\text{H}_5$, $\text{L} = \text{pyridine or substituted pyridine}$) system.

Wrighton *et al.* examined the photosubstitution behaviour in $\text{CpMn(CO)}_2(\text{X})$, ($\text{X} = \text{pyridine and substituted pyridine}$) complexes, and the results showed that the only observed reaction was pyridine substitution (equation 4.1.1.1) [25].



This is as a result of the lowest ligand field states populating σ^* states directed along the L-M-X (X = ligand) axis for X < CO in LF strength [26]. The quantum yields for these reactions were very high ($\Phi = 0.65$) and were independent of the concentration of the entering group. However, unlike the manganese complexes, the substitution process for the analogous rhenium complexes depended to a great extent on the electron-accepting ability of the ligand. Lowest quantum yields were obtained for complexes of substituted pyridines having strongly electron-withdrawing groups and hence lowest energy absorptions. The variation in substitution was attributed to the presence of a low lying MLCT state which could lie above or below the LF excited state depending on the nature of the ligand. Similar conclusions were reached for the observed photochemistry of the $W(CO)_5(X)$, (X = pyridine or substituted pyridine) complex [26(a)]. For the manganese complexes it was concluded that the reactivity was consistent with a LF state, even though irradiation into the MLCT states produced photochemical substitution reactions of the pyridine ligands. These reactions were independent of the nature and the concentration of the entering nucleophile but dependent on the nature of the metal and the leaving group. $ArCr(CO)_2(trans-4\text{-styrylpyridine})$, even though it possesses a MLCT absorption at very low energies, it undergoes efficient photosubstitution of the styrylpyridine ligand. This is attributed to the complex possessing relaxed reactive LF states which lie below the MLCT state [27].

As very little information is available on the photochemistry of substituted chromium dicarbonyl complexes, we decided to synthesise and investigate the photochemistry of two $ArCr(CO)_2(L)$ complexes, L = pyridine (py) and 4-acetylpyridine (4-Acpy). It was hoped to determine the origin of the reactivity of the complexes, that is, whether the lowest excited state was LF or

MLCT in nature. However, because of the high absorptivities of these complexes in the visible region of the spectrum, solutions of these compounds were very unstable upon exposure to air and visible light and thus the photochemistry was extremely difficult to investigate. The instability of the complexes in solution was surmounted by the addition of excess ligand, but at the expense of the "true" photochemistry of the $\text{ArCr}(\text{CO})_2(\text{L})$ complexes. Initially, the photochemical reactions of $\text{ArCr}(\text{CO})_3$ with both pyridine and 4-acetylpyridine were investigated.

4.2 UV/visible electronic spectrum of $\text{ArCr}(\text{CO})_3$

The electronic spectra of arene metal tricarbonyls has been reported by several workers [28, 29]. The UV/visible spectrum of $\text{ArCr}(\text{CO})_3$ is shown in Figure 4.2.1.

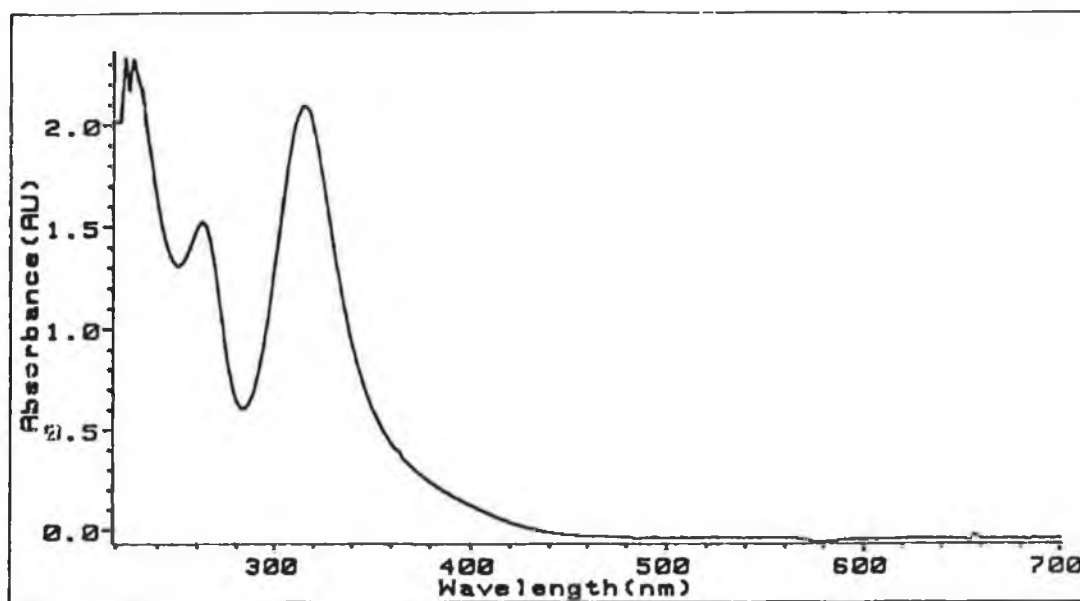


Figure 4.2.1 UV/visible spectrum of $\text{ArCr}(\text{CO})_3$ (ca. 1.9×10^{-4} mol dm^{-3}) in cyclohexane.

It is composed of four main transitions. In the region below 290nm, an intense peak at ~ 320nm and a shoulder at ~ 370nm are found. Both transitions are assigned to charge transfer from the chromium to the arene ring and the carbonyl groups, with the latter occurring to a lesser extent. The transition occurring at ~ 260nm is assigned to a chromium-carbonyl charge transfer band, while that at ~ 230nm arises from charge transitions from the ring and the chromium metal to the carbonyls.

The extinction coefficient of $\text{ArCr}(\text{CO})_3$ in cyclohexane was calculated to be $3676.7 \text{ dm}^3\text{mol}^{-1}\text{cm}^{-1}$ at 354nm, the excitation wavelength used in this study (Section 5.7).

4.3 Laser flash photolysis of $\text{ArCr}(\text{CO})_3$ in the presence of L, (L = py, 4-Acpy), in cyclohexane

Photolysis of $\text{ArCr}(\text{CO})_3$ results in the dissociation of a carbonyl group forming a coordinatively unsaturated $\text{ArCr}(\text{CO})_2$ species, which in the presence of solvent, (S) rapidly forms the solvated complex, $\text{ArCr}(\text{CO})_2(\text{S})$, (equations 4.3.1 - 4.3.3).



The formation of the solvated complex is evident from the decay transient monitored at 290nm for the reaction of $\text{ArCr}(\text{CO})_2(\text{S})$ in CO saturated cyclohexane (equation 4.3.4). A typical decay transient is shown in Figure 4.3.1.

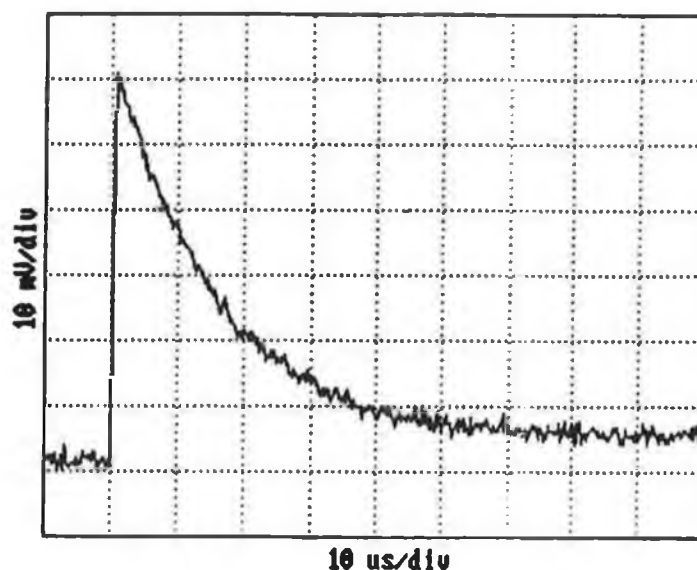
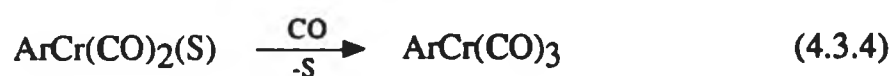
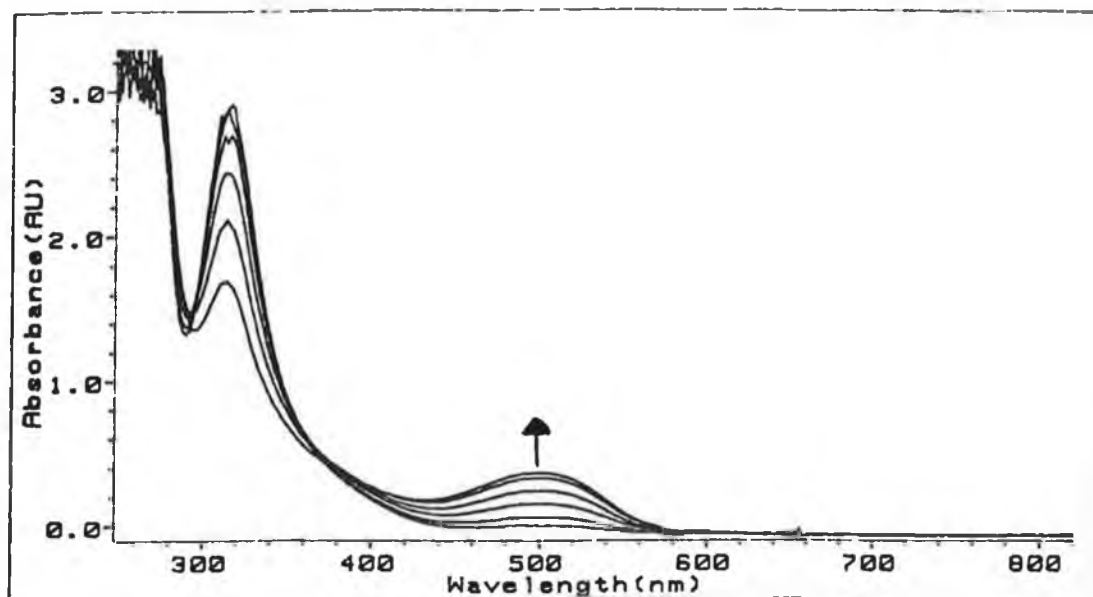


Figure 4.3.1 Decay transient of $\text{ArCr(CO)}_2(\text{cyclohexane})$ monitored at 290nm under 1 atm CO, at 25°C.

In the presence of excess ligand, the solvated complex disappears concomitant with the formation of the ligated complex. However, this decay transient is not observed in the presence of excess ligand, as it is occluded by the absorption of the ligand in that region of the UV/visible spectrum. The spectral changes involved in the formation of (a) $\text{ArCr(CO)}_2(\text{py})$ and (b) $\text{ArCr(CO)}_2(4\text{-Acpy})$ are shown in Figure 4.3.2.

(a)



(b)

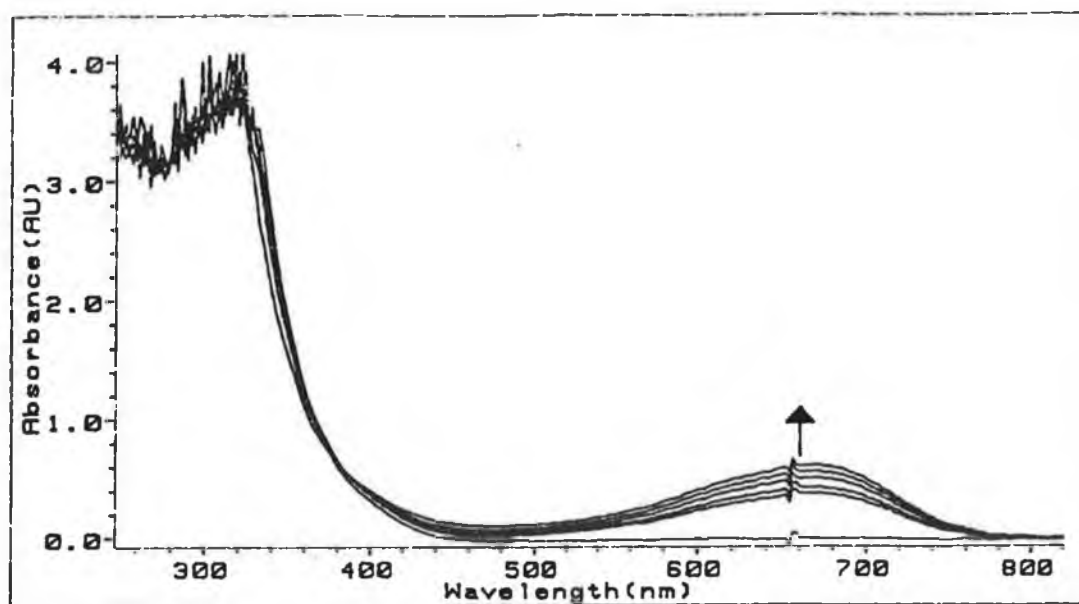


Figure 4.3.2 Spectral changes involved in the formation of (a) $\text{ArCr}(\text{CO})_2(\text{py})$ and (b) $\text{ArCr}(\text{CO})_2(4\text{-Acpy})$ in cyclohexane, $[\text{ArCr}(\text{CO})_3] = \text{ca. } 3 \times 10^{-4} \text{ mol dm}^{-3}$, $[\text{py}] = 5 \times 10^{-3} \text{ mol dm}^{-3}$, $[4\text{-Acpy}] = 1 \times 10^{-2} \text{ mol dm}^{-3}$.

In the pyridine complex a band appears at ca. 500nm. An isosbestic point at 360nm is maintained to very high fractional conversions. This rules out any other possible side reactions of the $\text{ArCr(CO)}_2(\text{pyridine})$ complex on the same timescale. There is no evidence to suggest that arene exchange occurs in the presence of pyridine. Wrighton and Haverty reported a nearly quantitative quantum yield of $\text{ArCr(CO)}_2(\text{pyridine})$ indicating that if arene group exchange occurs at all, it is only a minor component of the photochemistry [15].

The spectral changes involved in the formation of $\text{ArCr(CO)}_2(4\text{-Acpy})$ are shown in Figure 4.3.2(b). In this case a band "grows-in" at ca. 670nm with the maintenance of an isosbestic point at ca. 380nm. This indicates that the photoreaction is clean and free from any undesired side reactions. Spectral changes in the high energy region of the spectrum are undetected because of the high absorptivity of 4-acetylpyridine ligand which overlaps that of ArCr(CO)_3 .

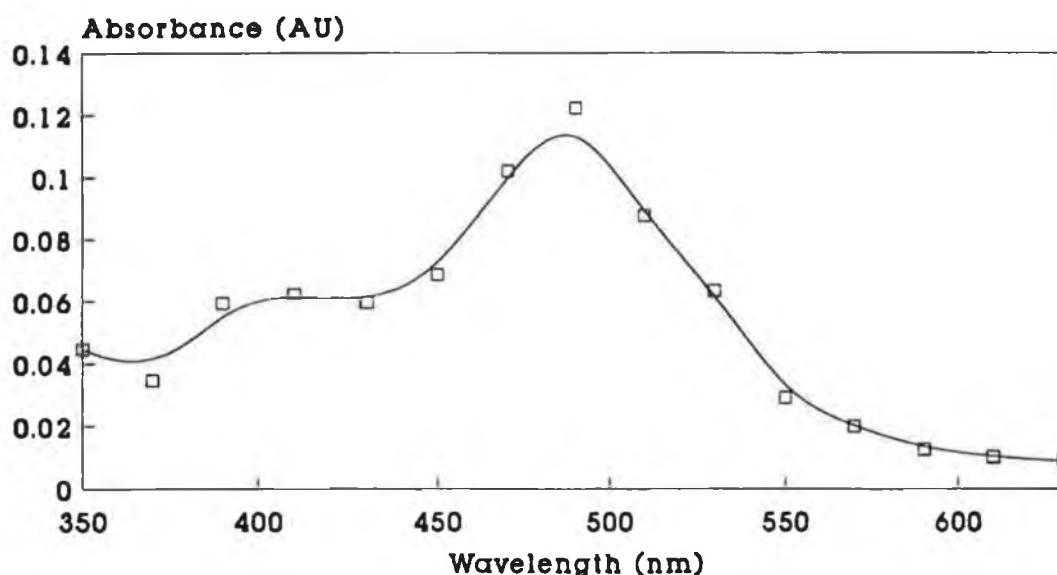
The substitution of a CO molecule in ArCr(CO)_3 resulted in a red-shift in the bands compared to those of the parent. Comparison of the UV/visible spectra of the two complexes formed revealed that both complexes have fairly intense visible absorption bands whose maxima depends on the nature of the substituent on the pyridine ring. The more electron-accepting substituent red-shifts the band relative to that of pyridine. Also, both low energy absorptions in the complexes are solvent sensitive, shifting to the blue in more polar or polarisable solvents, (see Section 4.4.1 and 4.5.1), thus these bands are assigned as $\text{Cr} \rightarrow \text{L}\pi^*\text{CT}$ transitions. Similar trends have been observed in the $\text{W(CO)}_5(\text{X})$ [26] and isoelectronic $(\eta^5\text{-C}_5\text{H}_5)\text{M(CO)}_2(\text{X})$ [15] systems where $\text{M} = \text{Mn, Re}$ and $\text{X} = \text{pyridine and substituted pyridine}$.

4.3.1 The reactions of photogenerated $\text{ArCr(CO)}_2(\text{S})$ with L

The reaction of photogenerated $\text{ArCr(CO)}_2(\text{cyclohexane})$, with the nucleophiles upon excitation at 355nm resulted in the formation of $\text{ArCr(CO)}_2(\text{L})$ complexes. The formation of these species is observed in the UV/visible difference spectra as shown in Figure 4.3.1.1(a) and 4.3.1.1(b) for the respective pyridine and 4-acetylpyridine complexes.

Transient signals were observed at 500 and 670nm for the formation of $\text{ArCr(CO)}_2(\text{py})$ and $\text{ArCr(CO)}_2(4\text{-Acpy})$ respectively. In addition, a transient decay was detected at 420nm in the presence of 4-acetylpyridine. No such decay was found in the pyridine system. A diffraction grating blazed at 500nm was used to investigate the photochemistry of the 4-acetylpyridine system at longer wavelengths. In all other studies, a grating blazed at 300nm was used, which covered a working range of 200-600nm. Typical transients observed are illustrated in Figures 4.3.1.2 and 4.3.1.3(a) and (b) for the formation of $\text{ArCr(CO)}_2(\text{py})$ and $\text{ArCr(CO)}_2(4\text{-Acpy})$ respectively.

(a)



(b)

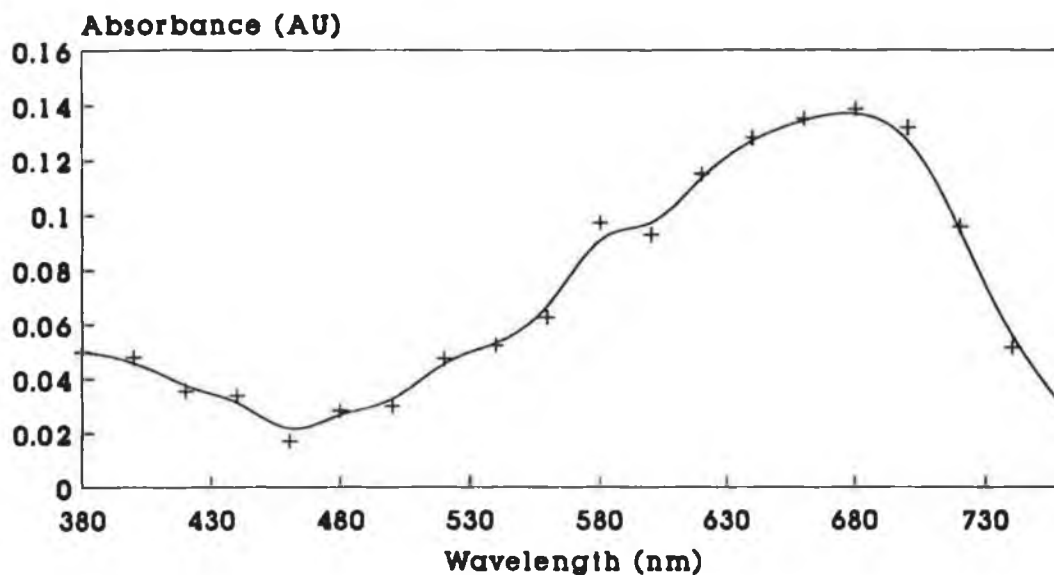


Figure 4.3.1.1 UV/visible difference spectra for the formation of (a) $\text{ArCr(CO)}_2(\text{py})$ and (b) $\text{ArCr(CO)}_2(4\text{-AcPy})$ in cyclohexane at 25°C, recorded 40 μs and 5 μs respectively after the laser flash.

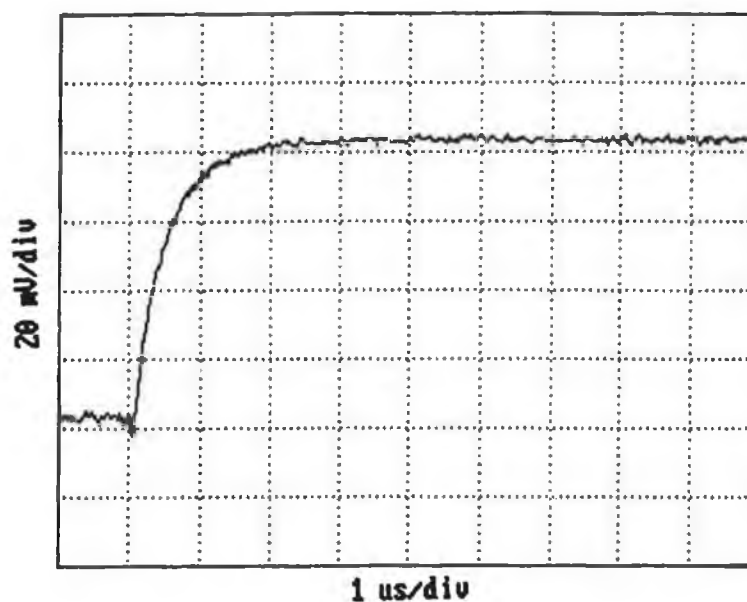
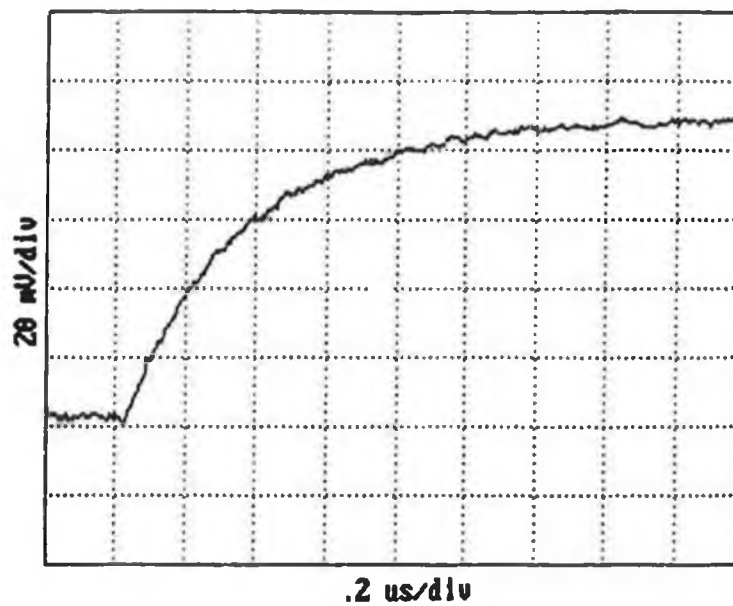


Figure 4.3.1.2 Transient signal monitored at 500 nm for the formation of $\text{ArCr(CO)}_2(\text{py})$ at 25°C.

(a)



(b)

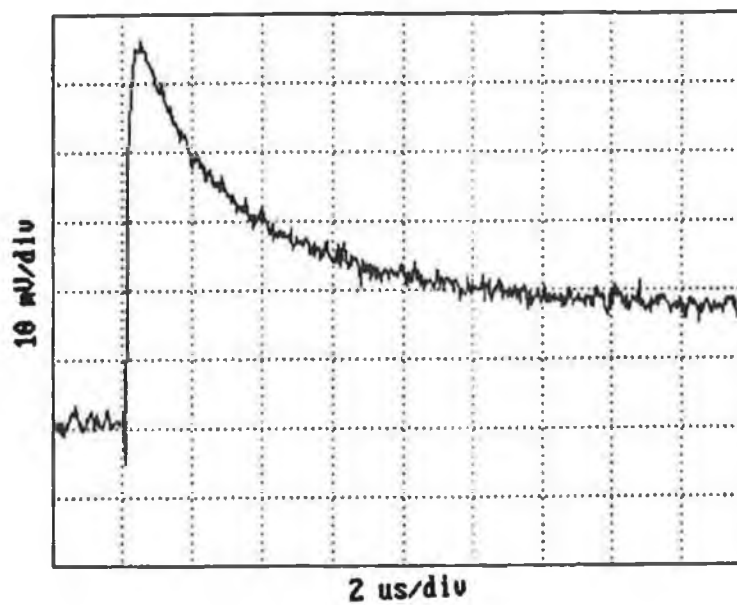


Figure 4.3.1.3 Transient signals observed at (a) 670nm and (b) 420nm in the $\text{ArCr}(\text{CO})_2(4\text{-Acpy})$ system, at 25°C.

4.3.2 The rate of reaction of $\text{ArCr}(\text{CO})_2(\text{S})$ with L

The reaction of $\text{ArCr}(\text{CO})_2(\text{cyclohexane})$ with pyridine and 4-acetylpyridine followed pseudo-first-order kinetics. The second-order rate constants, k_2 , were obtained from the plot of k_{obs} (the observed rate constant) versus ligand concentration for both pyridine and 4-acetylpyridine. The k_{obs} values were determined for the formation of the ligated complexes. The data and plots are shown in Figures 4.3.2.1 and 4.3.2.2 for pyridine and 4-acetylpyridine as ligands, respectively. A summary of the results is given in Table 4.3.2.1.

Ligand (L)	Monitoring λ (nm)	$k_2 \times 10^{-7}$ ($\text{dm}^3\text{mol}^{-1}\text{s}^{-1}$)
pyridine	500	3.7 ± 0.2
4-acetylpyridine	670	4.3 ± 0.1
"	420	0.7 ± 0.3

Table 4.3.2.1 Second-order rate constants for the reaction of $\text{ArCr}(\text{CO})_2(\text{S})$ with pyridine and 4-acetylpyridine at 25°C.

The k_2 values for the formation of the ligated complexes are quite similar, with that of 4-acetylpyridine being slightly larger. This similarity in rates suggests that both coordinate to the chromium metal in a similar manner. The most likely mode of coordination is *via* the lone pair on the nitrogen atom. The second-order rate constant for the decay, determined at 420nm was approximately 6 times smaller than that measured at 670nm. As the decay is not evident in the absence of 4-acetylpyridine (see Section 4.5.2.1), this suggests

that it is directly associated with the ligand. As 4-acetylpyridine possesses two potential binding sites (i) *via* the nitrogen lone pair and (ii) *via* the oxygen lone

[L] x 10 ² (mol dm ⁻³)	k _{obs} (s ⁻¹)
1.0	468996
2.0	879287
3.0	1171412
4.0	1561184
5.0	2003006

$$\text{Slope} = 3.7 \times 10^7 \pm 1.4 \times 10^6 \text{ dm}^3 \text{ mol}^{-1} \text{ s}^{-1}$$

$$\text{Intercept} = 91802 \pm 43659 \text{ s}^{-1}$$

$$\text{Corr. coeff.} = 0.99$$

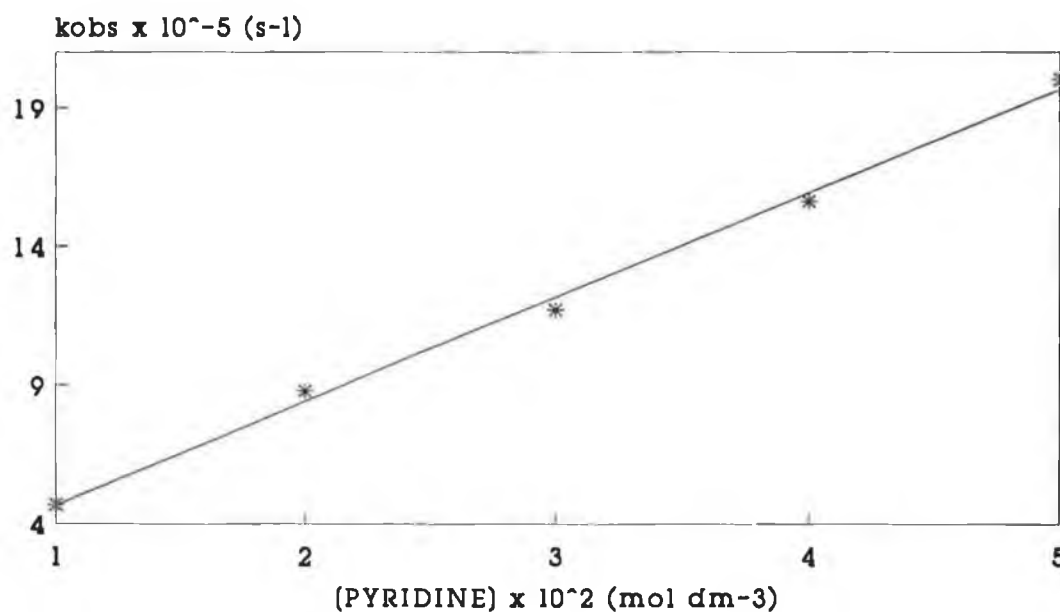


Figure 4.3.2.1 Second-order rate constant data for the formation of $\text{ArCr}(\text{CO})_2(\text{py})$ monitored at 500nm at 25°C.

[L] x 10 ² (mol dm ⁻³)	k _{obs} at 420nm (s ⁻¹)	k _{obs} at 670nm (s ⁻¹)
1.0	89168	491169
2.0	166007	861165
3.0	238792	1360451
4.0	298958	1796131
5.0	392470	2175614

at 670nm

$$\text{Slope} = 4.3 \times 10^7 \pm 1.2 \times 10^6$$

$$\text{Intercept} = 45749 \pm 37220$$

$$\text{Corr. coeff.} = 0.99$$

at 420nm

$$7.4 \times 10^6 \pm 2.7 \times 10^6 \text{ dm}^3 \text{ mol}^{-1} \text{ s}^{-1}$$

$$15213 \pm 8426.9 \text{ s}^{-1}$$

$$0.99$$

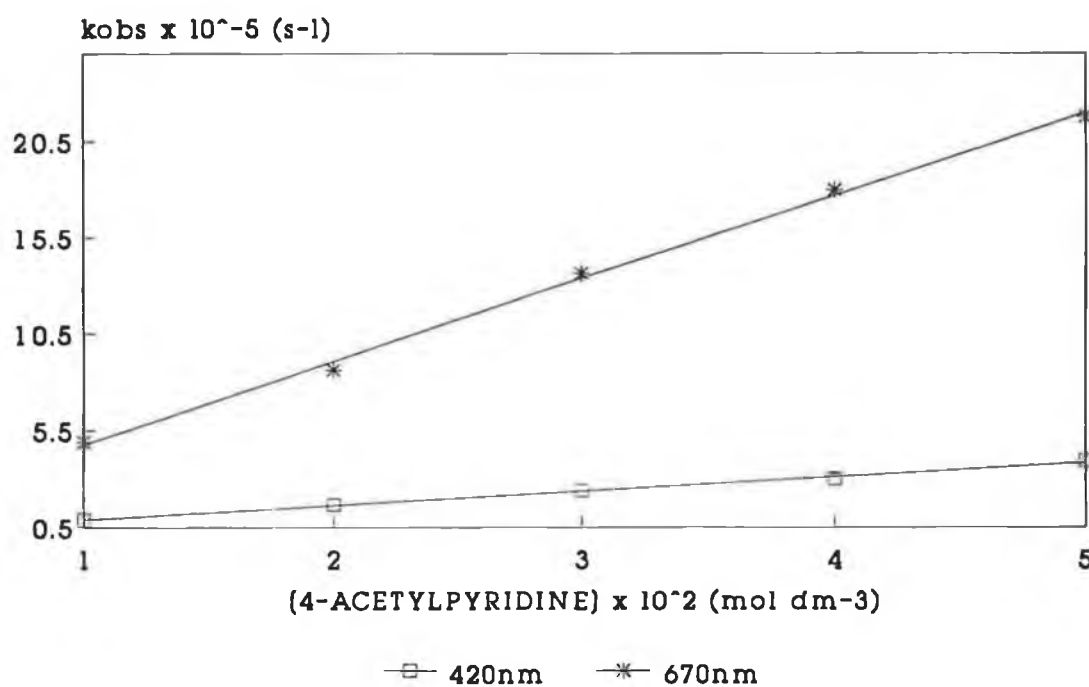
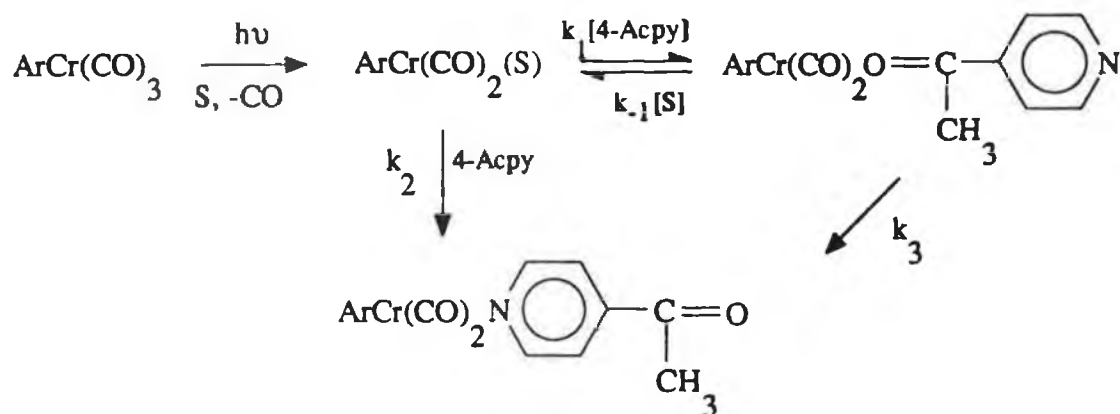


Figure 4.3.2.2 Second-order rate constant data for the species monitored at 670 and 420nm in the ArCr(CO)₂(4-Acpy) system, at 25°C.

pair, two isomeric complexes of the form $\text{ArCr(CO)}_2(4\text{-Acpy})$ can be produced. As no transient signal was observed for the formation of the oxygen bound complex, it is assumed that it is formed on a very fast timescale, too fast to be detected by laser system used in this study. The oxygen bound $\text{Cr(CO)}_5(\text{THF})$ complex is produced in less than 25ps [30] and has a λ_{max} at ca. 450nm [30(b)]. Thus, the decay transient signal observed at ca. 420nm most probably corresponds to the decay of the oxygen coordinated complex.

A possible reaction scheme is detailed in Scheme 4.3.2.1. Photolysis of ArCr(CO)_3 in cyclohexane produces the primary photoproduct, $\text{ArCr(CO)}_2(\text{cyclohexane})$. This then reacts with 4-acetylpyridine, forming both the oxygen and nitrogen bound complexes. These are represented by the k_1 and k_2 pathways respectively. Formation of the latter complex is evident from the "grow-in" observed at 670nm. The O-bound complex is short-lived, decaying to form, most likely, the primary photoproduct again (k_{-1} pathway). Another possibility for the decay, is the rearrangement of the O-bound complex to form the N-linked isomer (k_3 pathway). This process was observed by Dobson and Spradling upon flash photolysis of W(CO)_6 with 4-Acyp in cyclohexane [32]. Initially, O-bonded $\text{W(CO)}_5(4\text{-Acpy})$ was produced upon displacement of cyclohexane from the solvated complex. This then rearranged within several minutes to form the N-bound linkage isomer. However, no evidence was obtained in this study to support the presence of such a rearrangement. A second-order rate constant of $3.1 \times 10^7 \text{ dm}^3\text{mol}^{-1}\text{s}^{-1}$ was obtained for the displacement of cyclohexane from the solvated W(CO)_5 complex by 4-acetylpyridine [32]. The slightly faster rate obtained in this study may be a reflection of the difference in reactivity of the two types of complexes. Tungsten complexes are generally more stable than chromium analogues. Rearrangements of ligands are known to occur in other systems, for example,

aliphatic alcohols. Initial coordination of these solvents to the metal fragment is *via* the hydroxyl end of the chain forming unstable complexes which undergo rapid rearrangements on a very fast timescale, forming more stable complexes where bonding is *via* the aliphatic end of the alcohol [31].



S = cyclohexane

Scheme 4.3.2.1

As there is excess ligand present (10-fold at least), any back reaction by the photoliberated CO is very unlikely.

4.3.3 Activation parameter studies for the formation of $\text{ArCr(CO)}_2(\text{L})$

The activation parameters for the formation of $\text{ArCr(CO)}_2(\text{py})$ and $\text{ArCr(CO)}_2(4\text{-Acpy})$ were calculated according to equations 5.4.1 and 5.4.2. The data is displayed in Tables 4.3.3.1 - 4.3.3.3 while the Arrhenius and Eyring plots are presented in Figures 4.3.3.1 and 4.3.3.2 for the formation of the

pyridine and 4-acetylpyridine complexes, respectively. A summary of the activation parameters is given in Table 4.3.3.4.

$1/T \times 10^3 \text{ (K}^{-1}\text{)}$	$\text{Ln } k_2^a$	$\text{Ln } k_2^a/T$
3.48	17.42	11.76
3.44	17.70	12.02
3.38	17.76	12.07
3.36	17.90	12.20
3.31	18.14	12.43
3.27	18.28	12.56
3.23	18.42	12.69
3.17	18.55	12.80

$$^a k_2 = k_{\text{obs}}/[\text{py}], [\text{py}] = 5 \times 10^{-3}\text{M}$$

Arrhenius Plot

$$\text{Slope} = -3667.5 \pm 224.7$$

$$\text{Intercept} = 30.23 \pm 0.06$$

$$\text{Corr. coeff.} = 0.99$$

Eyring Plot

$$\text{Slope} = -3395.6 \pm 220.5$$

$$\text{Intercept} = 23.62 \pm 0.06$$

$$\text{Corr. coeff.} = 0.99$$

$$E_a^\ddagger = 30 \pm 1 \text{ kJmol}^{-1}, \Delta H^\ddagger = 28 \pm 1 \text{ kJmol}^{-1}, \Delta S^\ddagger = -1 \pm 10 \text{ JK}^{-1}\text{mol}^{-1}$$

Table 4.3.3.1 Experimental data for the determination of activation energy, enthalpy and entropy for the formation of $\text{ArCr(CO)}_2(\text{py})$ in cyclohexane, monitored at 500nm.

$1/T \times 10^3 \text{ (K}^{-1}\text{)}$	$\text{Ln } k_2^a$	$\text{Ln } k_2^a/T$
3.47	18.52	12.85
3.42	18.74	13.06
3.36	18.81	13.11
3.32	18.95	13.24
3.26	19.19	13.46
3.21	19.33	13.59

^a $k_2 = k_{\text{obs}}/[4\text{-Acpy}]$, $[4\text{-Acpy}] = 5 \times 10^{-3}\text{M}$

Arrhenius Plot

Slope = -3040.1 ± 208.7

Intercept = 29.08 ± 0.45

Corr. coeff. = 0.99

Eyring Plot

Slope = -2759.5 ± 212.3

Intercept = 22.44 ± 0.05

Corr. coeff. = 0.99

$$E_a^\ddagger = 25 \pm 1 \text{ kJmol}^{-1}, \Delta H^\ddagger = 23 \pm 1 \text{ kJmol}^{-1}, \Delta S^\ddagger = -11 \pm 10 \text{ JK}^{-1}\text{mol}^{-1}$$

Table 4.3.3.2 Experimental data for the determination of activation energy, enthalpy and entropy for the formation of $\text{ArCr(CO)}_2(4\text{-Acpy})$ in cyclohexane, monitored at 670nm.

$1/T \times 10^3 \text{ (K}^{-1}\text{)}$	$\text{Ln } k_2^a$	$\text{Ln } k_2^a/T$
3.48	16.25	10.59
3.42	16.42	10.74
3.38	16.58	10.89
3.32	16.70	10.99
3.26	17.04	11.32
3.21	17.23	11.49
3.15	17.33	11.57

$$^a k_2 = k_{\text{obs}}/[4\text{-Acpy}], [4\text{-Acpy}] = 2.49 \times 10^{-2}\text{M}$$

Arrhenius Plot

$$\text{Slope} = -3476.6 \pm 196.4$$

$$\text{Intercept} = 28.33 \pm 0.57$$

$$\text{Corr. coeff.} = 0.99$$

Eyring Plot

$$\text{Slope} = -3182.5 \pm 203.7$$

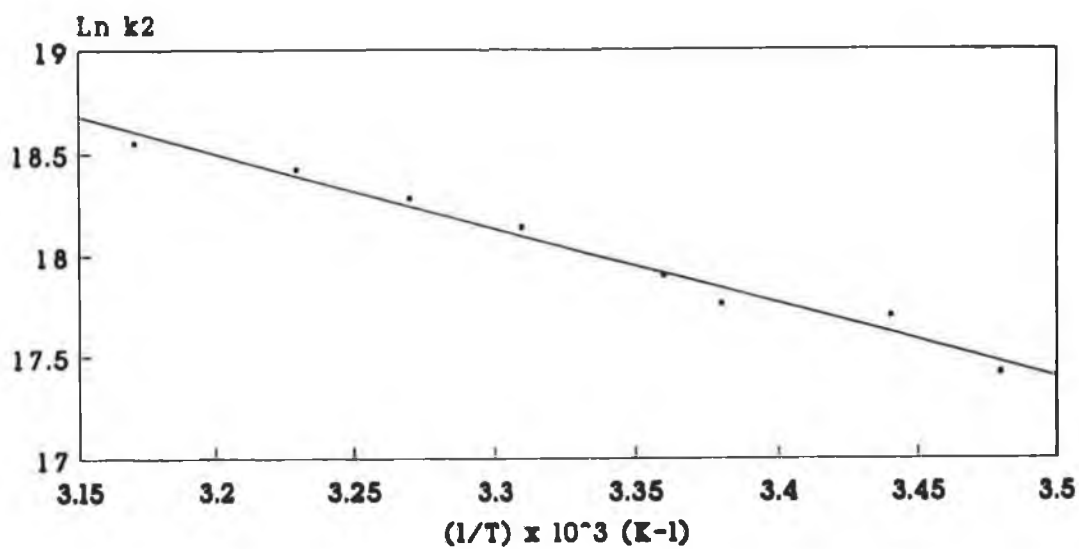
$$\text{Intercept} = 21.64 \pm 0.06$$

$$\text{Corr. coeff.} = 0.99$$

$$E_a^\ddagger = 29 \pm 1 \text{ kJmol}^{-1}, \Delta H^\ddagger = 26 \pm 1 \text{ kJmol}^{-1}, \Delta S^\ddagger = -18 \pm 10 \text{ JK}^{-1}\text{mol}^{-1}$$

Table 4.3.3.3 Experimental data for the determination of activation energy, enthalpy and entropy for the decay of the species, monitored at 420nm.

(a)



(b)

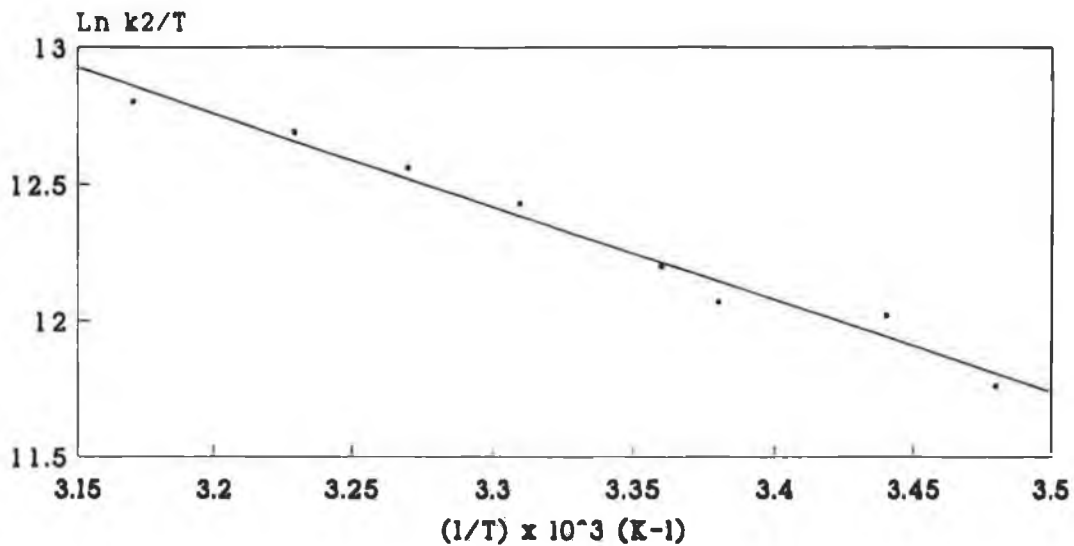
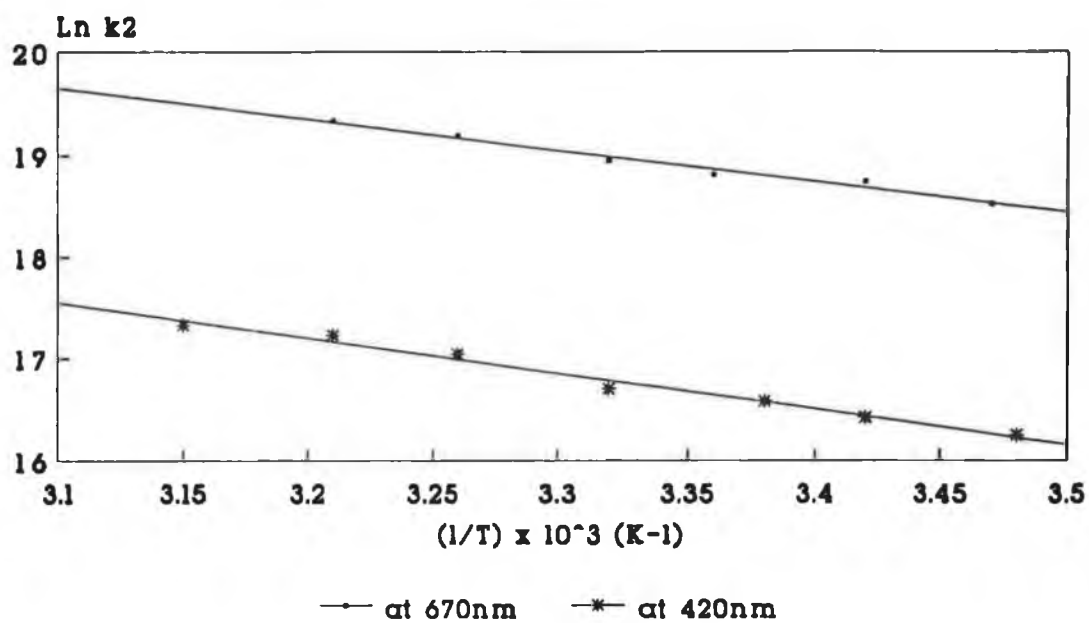


Figure 4.3.3.1 (a) Arrhenius and (b) Eyring plots for the formation of $\text{ArCr}(\text{CO})_2(\text{py})$, monitored at 500nm.

(a)



(b)

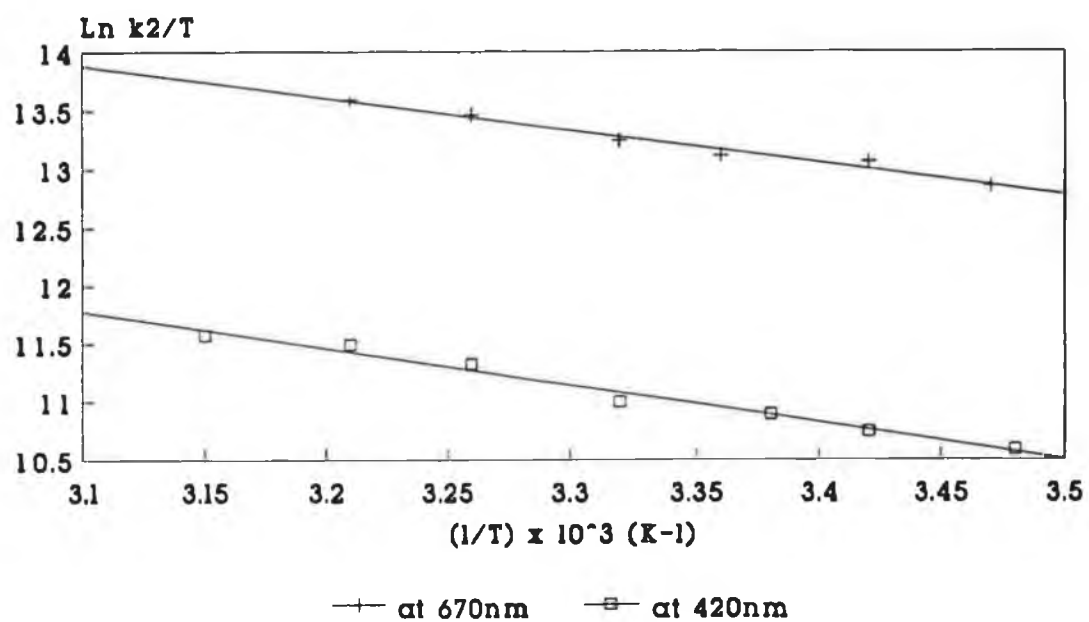


Figure 4.3.3.2 (a) Arrhenius and (b) Eyring plots for the formation of $\text{ArCr}(\text{CO})_2(4\text{-Acpy})$ at 670nm and the decay of the species at 420nm.

Ligand (L)	λ (nm)	E_a^\ddagger (kJmol ⁻¹)	ΔH^\ddagger (kJmol ⁻¹)	ΔS^\ddagger (Jmol ⁻¹ K ⁻¹)	ΔG_{298K}^\ddagger (kJmol ⁻¹)
Pyridine ^a	500	30	28	-1	29
4-Acpy ^a	670	25	23	-11	26
4-Acpy ^b	670	21	18	-28	27
4-Acpy ^b	420 ^c	29	26	-18	32

^a [L] = 5 x 10⁻³M, ^b [L] = 2.49 x 10⁻²M, ^c decay of transient species at 420nm

Table 4.3.3.4 Activation parameters for the reaction of ArCr(CO)₃ with pyridine and 4-acetylpyridine in cyclohexane.

The activation energy (E_a^\ddagger) and enthalpy (ΔH^\ddagger) values for bonding of 4-acetylpyridine are slightly lower than those of pyridine. The ΔH^\ddagger for the displacement of cyclohexane by CO is ca. 22 kJmol⁻¹ [33]. The low negative values for the activation entropies (ΔS^\ddagger) indicates the presence of an interchange mechanism for the displacement of cyclohexane and the formation of the ligated complexes. Similar mechanistic pathways have been proposed for the loss of solvent in hexacarbonyl systems [32, 34].

4.4 Laser flash photolysis of (η^6 -C₆H₆)Cr(CO)₂(pyridine)

The photochemical reactions of arene chromium tricarbonyls (ArCr(CO)₃) with nitrogen, phosphorus, sulphur or olefinic ligands, forming ArCr(CO)₂(L) are well known [35-37], but the photochemistry of these

complexes have not been extensively studied. As many of these complexes, particularly those with nitrogen-donor ligands exhibit low lying energy absorptions, they are extremely sensitive to visible light and unstable in solution upon exposure to air. The lifetime of the complexes may be prolonged in solution by the addition of excess ligand, but at the expense of the photochemistry of the pure complex.

4.4.1 UV/visible electronic spectrum of $\text{ArCr}(\text{CO})_2(\text{pyridine})$

The UV/visible spectrum of $\text{ArCr}(\text{CO})_2(\text{py})$ in cyclohexane is displayed in Figure 4.4.1.1 and shows the presence of a strong visible absorption band at ca. 500nm, with a less intense band at ca. 350nm.

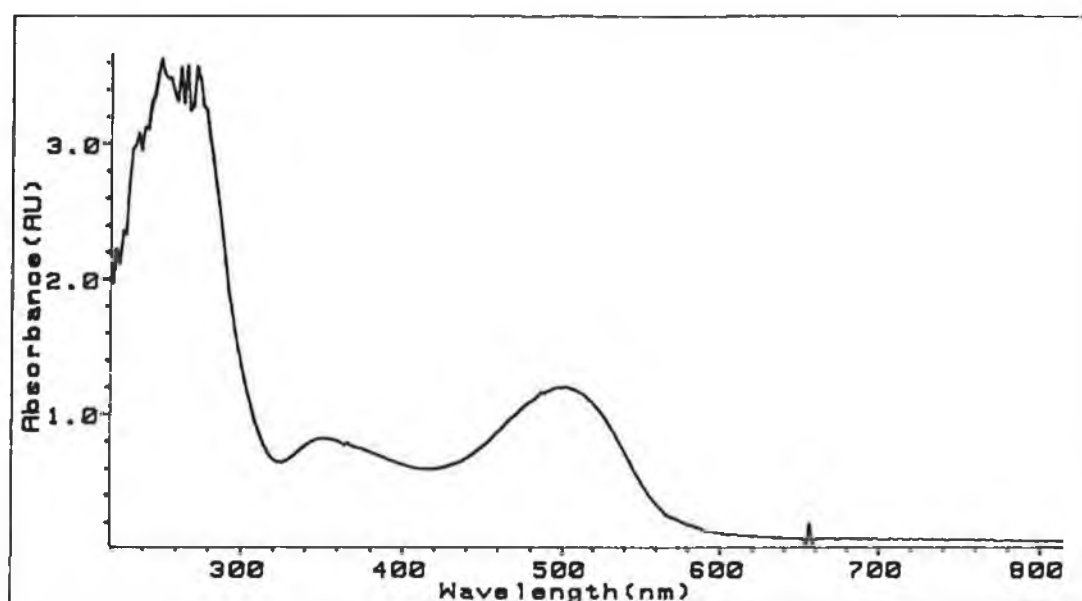


Figure 4.4.1.1 UV/visible spectrum of $\text{ArCr}(\text{CO})_2(\text{py})$ ($4.7 \times 10^{-4} \text{ mol dm}^{-3}$) in cyclohexane.

The band at ~500nm is most likely a Cr \rightarrow py π^* CT band as it is both solvent and substituent sensitive. The UV/visible spectrum in different solvents is given in Figure 4.4.1.2, while the variation in band maxima in the various solvents are given in Table 4.4.1.1 along with the solvent polarities. The differences in the intensities of the bands are as a result of differing complex concentrations in each solvent. The low energy absorption is blue-shifted in more polar or polarisable solvents, while the addition of an electron-withdrawing group to the pyridine ring resulted in a red-shift of that band compared to that of pyridine. As LF bands are insensitive to such changes the lowest energy band was assigned as a Cr \rightarrow py π^* CT band. The less intense band at ~350nm was little affected by all these changes and was assigned as a LF band.

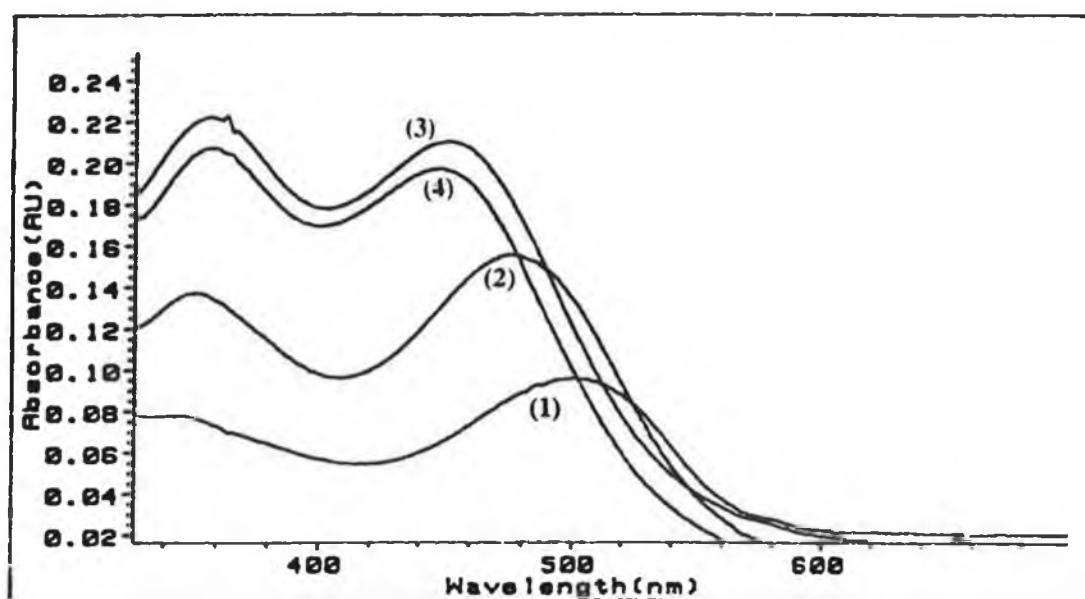


Figure 4.4.1.2 UV/visible spectrum of $\text{ArCr}(\text{CO})_2(\text{py})$ in cyclohexane (1), toluene (2), dichloromethane (3) and acetone (4).

Solvent	Solvent polarity	λ_{\max} (nm)
Cyclohexane	0.0	500
Toluene	2.3	476
Dichloromethane	3.4	452
Acetone	5.4	446

Table 4.4.1.1 Solvent dependence of the lowest energy absorption band in $\text{ArCr}(\text{CO})_2(\text{pyridine})$.

The extinction coefficient of $\text{ArCr}(\text{CO})_2(\text{py})$ in cyclohexane was calculated to be 1697.3 and 2532.3 $\text{dm}^3\text{mol}^{-1}\text{cm}^{-1}$ at 354 and 500nm respectively (Section 5.7).

4.4.2 Flash photolysis of $\text{ArCr}(\text{CO})_2(\text{py})$ in cyclohexane

In the absence of excess ligand, $\text{ArCr}(\text{CO})_2(\text{py})$ is unstable in solution and has a very short lifetime, decomposing to form $\text{ArCr}(\text{CO})_3$, free pyridine and decomposition products. Flash photolysis under argon results in the decomposition products, while in CO saturated cyclohexane $\text{ArCr}(\text{CO})_2(\text{py})$ is totally converted to $\text{ArCr}(\text{CO})_3$. There is no obvious "grow-in" observed at 500nm. The UV/visible difference spectrum is shown in Figure 4.4.2.1. The formation of $\text{ArCr}(\text{CO})_3$ in both cases is evident from the UV/visible electronic spectra (Figure 4.4.2.2).

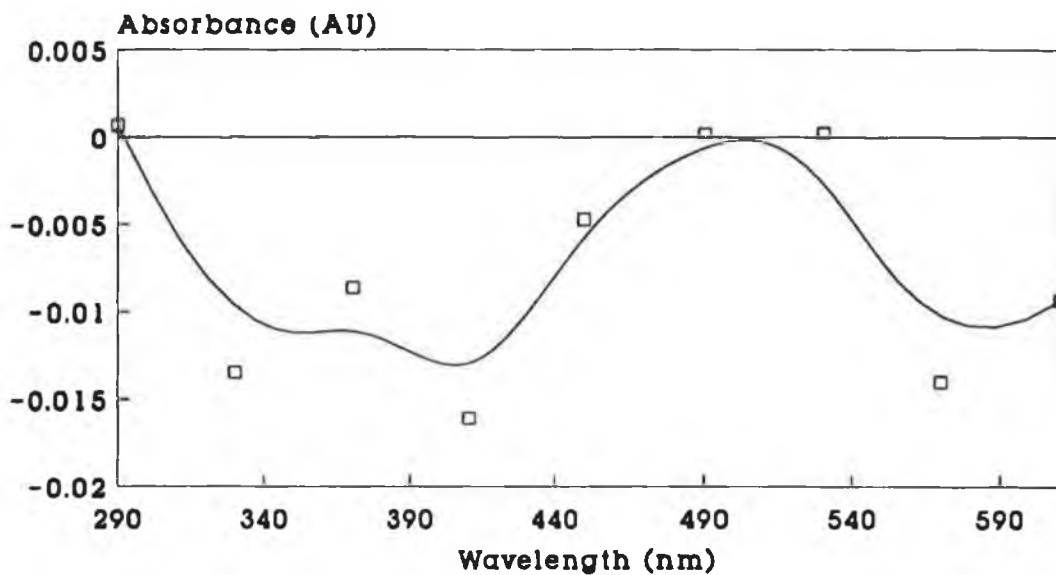
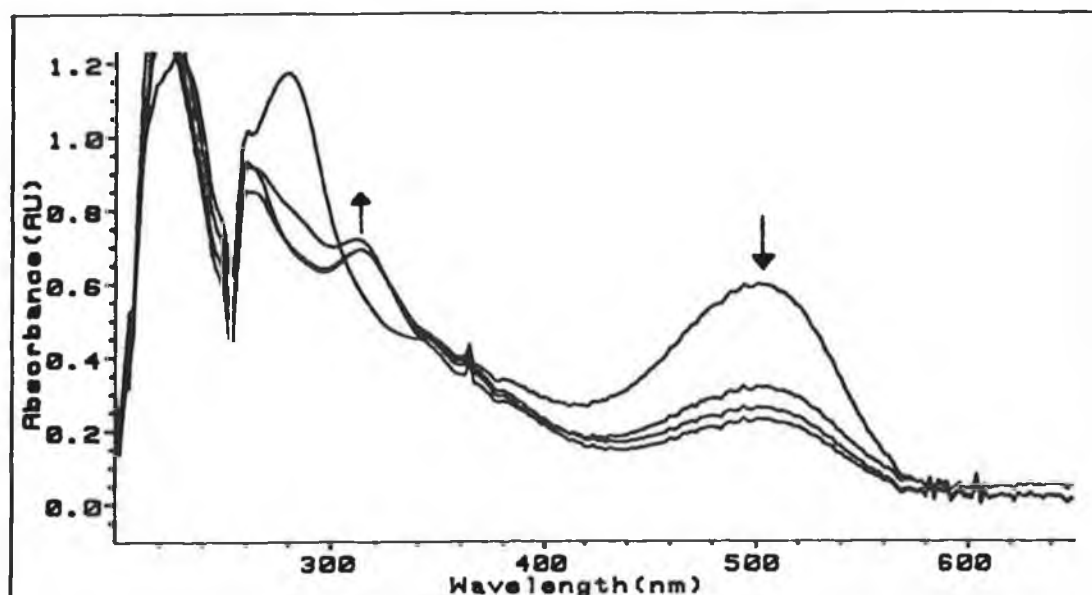


Figure 4.4.2.1 UV/visible difference spectrum of $\text{ArCr}(\text{CO})_2(\text{py})$ in CO saturated cyclohexane (no excess ligand present), recorded $80\mu\text{s}$ after the laser flash.

(a)



(b)

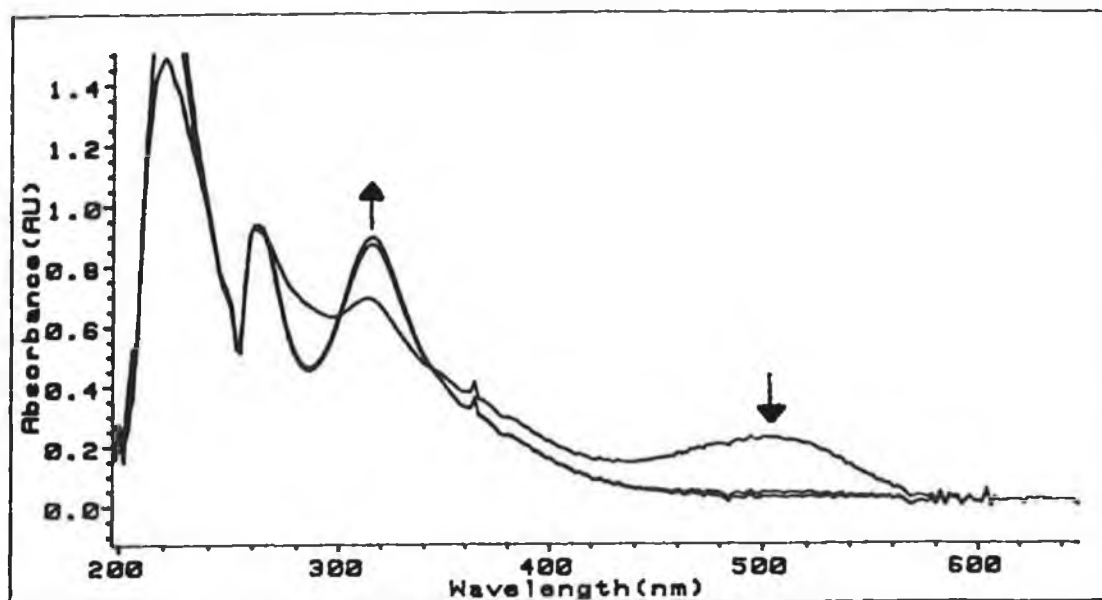


Figure 4.4.2.2 UV/visible electronic spectra of ArCr(CO)₂(py) (ca. 1×10^{-4} mol dm⁻³) upon flash photolysis in (a) argon and (b) CO saturated cyclohexane.

As a result of the instability of the complex in solution, the photochemistry of ArCr(CO)₂(pyridine) was investigated in the presence of a known concentration of excess ligand, in both argon and carbon monoxide saturated cyclohexane at 355nm.

4.4.2.1 Flash photolysis of ArCr(CO)₂(py) in argon saturated cyclohexane solution containing pyridine

The UV/visible difference spectrum obtained for the reaction of ArCr(CO)₂(py) in the presence of excess pyridine is displayed in Figure 4.4.2.1.1.

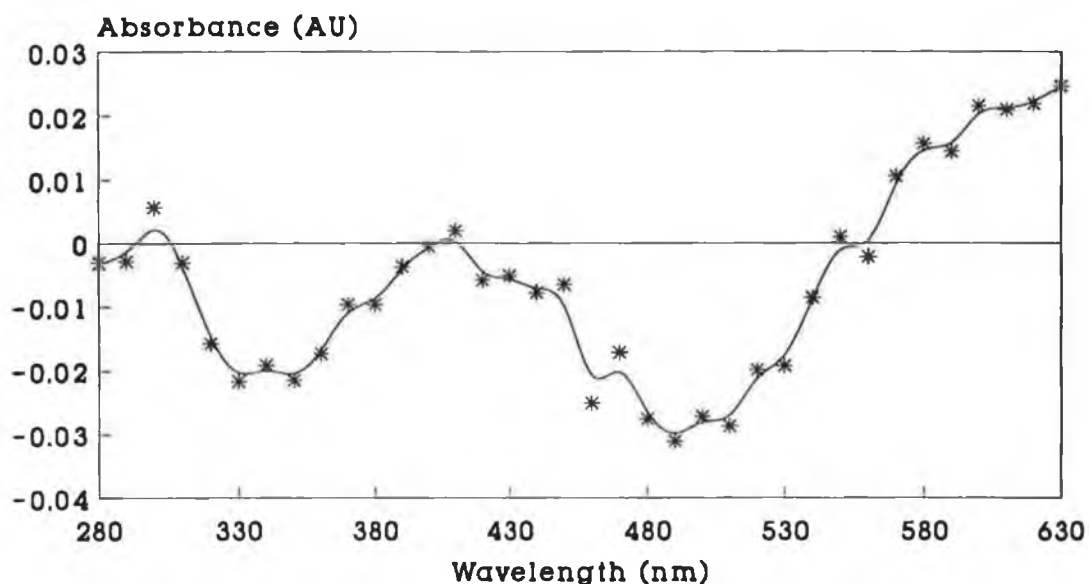


Figure 4.4.2.1.1 UV/visible difference spectrum for the reaction of $\text{ArCr}(\text{CO})_2(\text{py})$ in degassed cyclohexane in the presence of excess pyridine, recorded $10\mu\text{s}$ after the laser flash.

In argon saturated cyclohexane and in the presence of excess ligand (pyridine), depletions were observed at 350 and 500nm, the latter being the greater. These depletions correspond to the absorptions of the parent compound in the UV/visible electronic spectrum (Figure 4.4.1.1). In addition, a positive absorption was observed at ca. 600nm, which may be as a result of some other species being formed. However, the possibility of it being an artefact of the system could not be ruled out as the absorption lies close to the upper limit of the diffraction grating used. This grating blazed at 300nm covered a working range of 200-600nm. In order to verify the source of the absorption, the grating was changed to one blazed at 500nm so that the photochemistry could be investigated at longer wavelengths (350-900nm). As transient signals corresponding to the formation of a species at ca. 600nm were not observed

using this grating, it was postulated that the positive absorption observed in Figure 4.4.1.1 was an artefact of the system. Thus, in an inert atmosphere, the spectrum suggests that the pyridine ligand is displaced in the flash, forming a coordinatively unsaturated $\text{ArCr}(\text{CO})_2$ species which in turn reacts with the excess pyridine ligand, regenerating the parent complex (equation 4.4.2.1.1). A typical transient signal for the reformation of the parent complex monitored at 500nm is displayed in Figure 4.4.2.1.2. All the transient signals observed were consistent with pseudo-first-order kinetics.

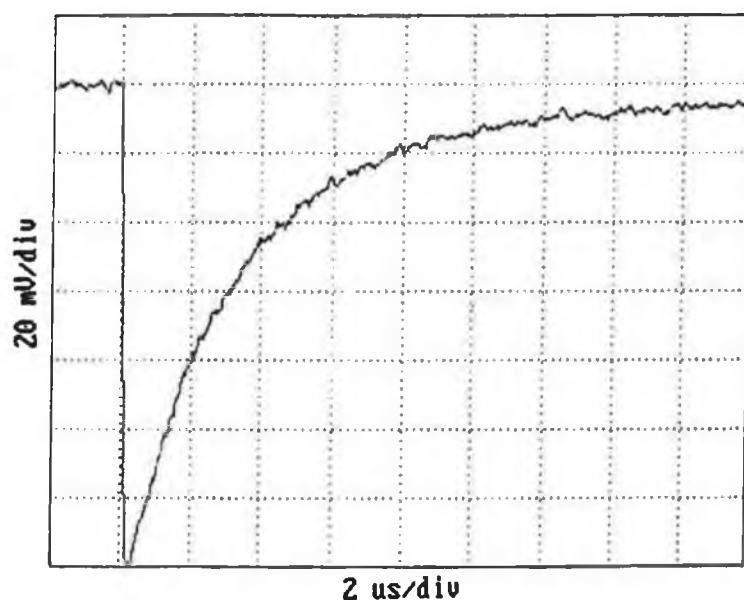
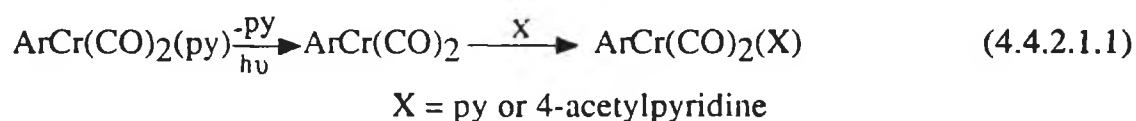


Figure 4.4.2.1.2 Typical transient observed for the regeneration of $\text{ArCr}(\text{CO})_2(\text{py})$ in cyclohexane, monitored at 500nm.

The lack of change observed in the electronic spectrum upon flash photolysis is in accordance with equation 4.4.2.1.1 (Figure 4.4.2.1.3).

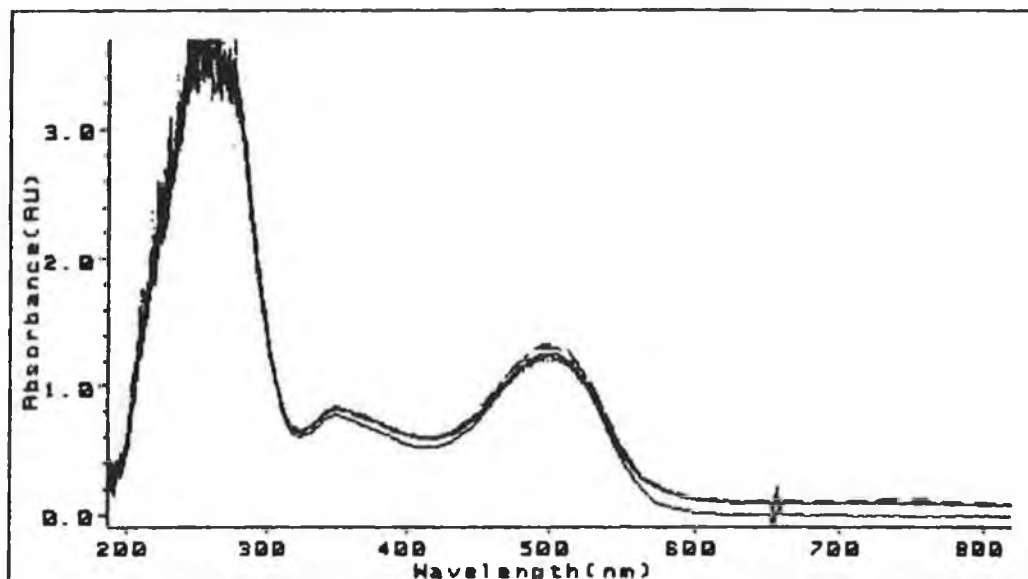


Figure 4.4.2.1.3 Electronic spectrum obtained upon flash photolysis of $\text{ArCr}(\text{CO})_2(\text{py})$ in degassed cyclohexane solution containing pyridine.

The reaction of $\text{ArCr}(\text{CO})_2(\text{py})$ in the presence of 4-acetylpyridine was also examined. The electronic spectral changes accompanying the photosubstitution are shown in Figure 4.4.2.1.4. A decrease in the Cr \rightarrow py π^* CT band at 500nm with concomitant growth of a band at ca. 670nm is observed. This band is assigned to Cr \rightarrow 4-Acpy π^* CT transition (see Section 4.5.1). The presence of the isosbestic point at ca. 550nm is indicative of a clean, efficient photoreaction, free from any undesired side reactions. The spectral changes are consistent with the loss of the pyridine ligand as detailed in equation 4.4.2.1.1, for X = 4-acetylpyridine. This seems to be the dominant reaction in the photochemistry of these dicarbonyl complexes. Similar conclusions were attained for the photochemistry of the isoelectronic

$\text{CpMn(CO)}_2(\text{L})$ complexes, where $\text{Cp} = (\eta^5\text{-C}_5\text{H}_5)$, $\text{L} = \text{pyridine}$ or substituted pyridine [25].

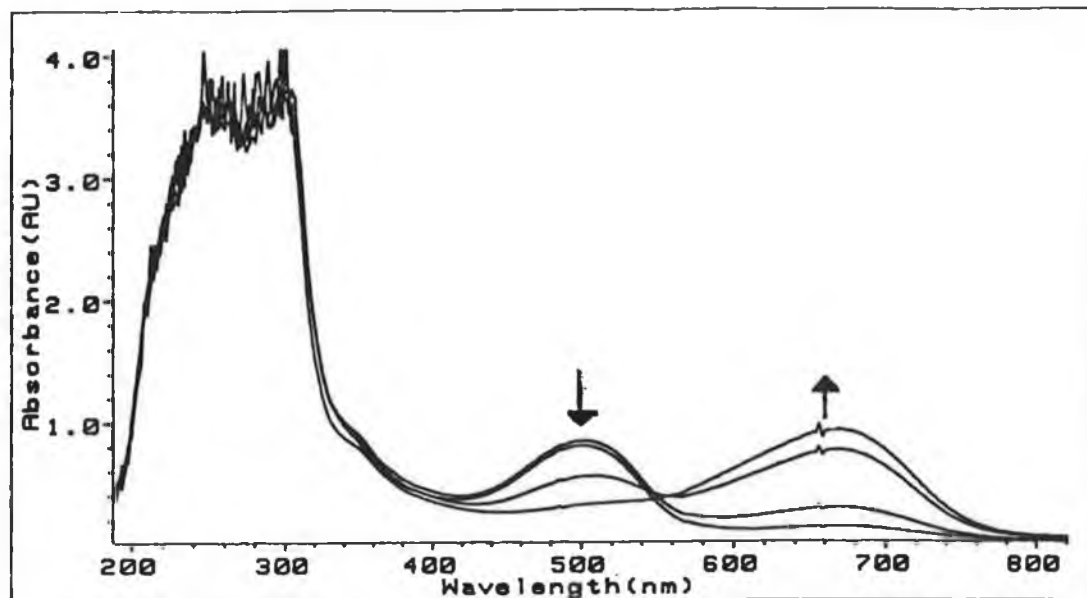


Figure 4.4.2.1.4 Spectral changes accompanying the reaction of $\text{ArCr(CO)}_2(\text{py})$ ($3.5 \times 10^{-4} \text{ mol dm}^{-3}$) with 4-acetylpyridine ($4 \times 10^{-3} \text{ mol dm}^{-3}$) in degassed cyclohexane solution.

4.4.2.2 Flash photolysis of $\text{ArCr(CO)}_2(\text{py})$ in CO saturated cyclohexane solution containing pyridine

The spectral changes observed during the reaction of $\text{ArCr(CO)}_2(\text{py})$ in CO saturated cyclohexane solution containing pyridine, indicate the formation of ArCr(CO)_3 (Figure 4.4.2.2.1). During the reaction the MLCT band of the dicarbonyl complex at $\sim 500\text{nm}$ decays with concurrent formation of a band at $\sim 310\text{nm}$. This latter band is characteristic of arene chromium tricarbonyl

complexes (see Section 4.1). The conversion of the dicarbonyl complex to the tricarbonyl is a very clean reaction as evident from the two isosbestic points maintained at ~300 and ~340nm to high fractional conversions.

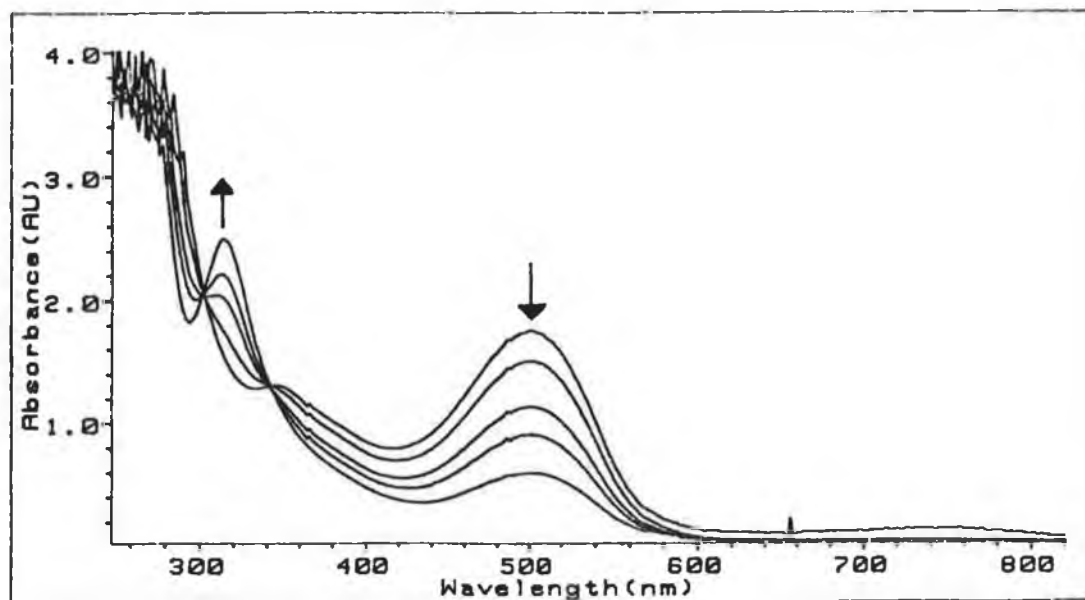
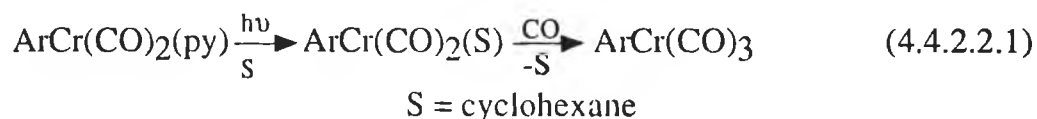


Figure 4.4.2.1 Spectral changes accompanying the reaction of $\text{ArCr}(\text{CO})_2(\text{py})$ ($7 \times 10^{-4} \text{ mol dm}^{-3}$) in CO saturated cyclohexane solution containing pyridine.

The spectral changes are consistent with the reaction detailed in equation 4.4.2.2.1.



Based on the electronic spectrum of the photoproduct (Figure 4.4.2.2.1) $\text{ArCr}(\text{CO})_3$ is being formed in this process. As the extinction coefficient of $\text{ArCr}(\text{CO})_3$ is much larger than that of $\text{ArCr}(\text{CO})_2(\text{py})$ at 354nm (the excitation

wavelength used), as the experiment proceeds, the photochemistry of $\text{ArCr}(\text{CO})_3$ becomes dominant. This results in the formation of the solvated species which then reacts with the pyridine present, again yielding $\text{ArCr}(\text{CO})_2(\text{py})$. This accounts for the absorption at ca. 500nm and the depletion at ca. 320nm observed in the UV/visible difference spectrum (Figure 4.4.2.2.2). The band at 500nm also corresponds with that obtained for the formation of $\text{ArCr}(\text{CO})_2(\text{py})$ from $\text{ArCr}(\text{CO})_3$ and pyridine (Figure 4.3.1.1(a)).

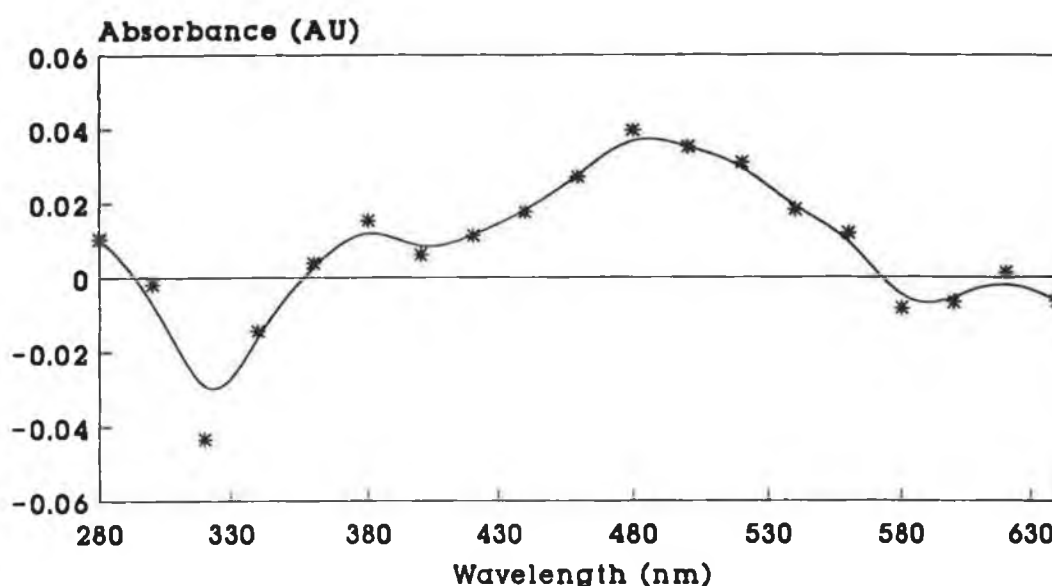


Figure 4.4.2.2.2 UV/visible difference spectrum for the reaction of $\text{ArCr}(\text{CO})_2(\text{py})$ in CO saturated cyclohexane solution containing pyridine, recorded 10 μs after the laser flash.

The effect the presence of CO had on the rate and yield of this species forming at ca. 500nm was investigated. It was found that the yield decreased while the rate of formation of the species increased with increasing CO concentrations. Figure 4.4.2.2.3 illustrates the change in transient signals in the presence of CO, monitored at 500nm. This indicates that under argon, only depletion of

$\text{ArCr}(\text{CO})_2(\text{py})$ is observed which then reacts with pyridine regenerating the parent complex. However under CO, depletions of both $\text{ArCr}(\text{CO})_2(\text{py})$ and $\text{ArCr}(\text{CO})_3$ are occurring with $\text{ArCr}(\text{CO})_2$ reacting with the pyridine forming $\text{ArCr}(\text{CO})_2(\text{py})$. The "grow-in" is observed because $\text{ArCr}(\text{CO})_2(\text{py})$ is being formed rather than $\text{ArCr}(\text{CO})_3$ being regenerated.

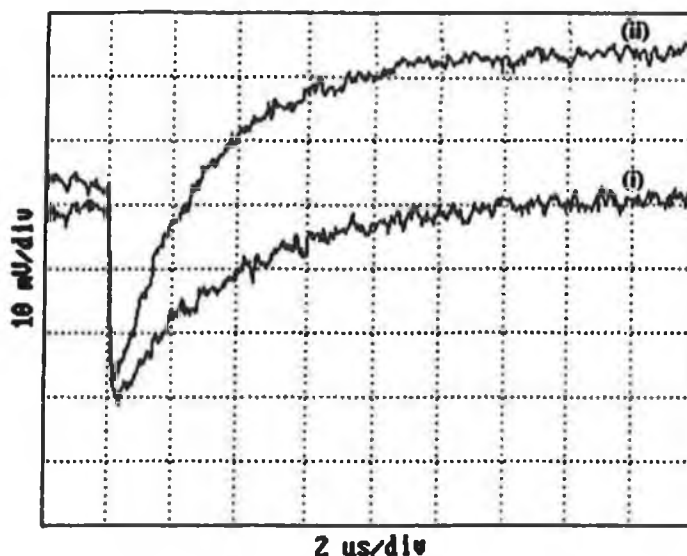
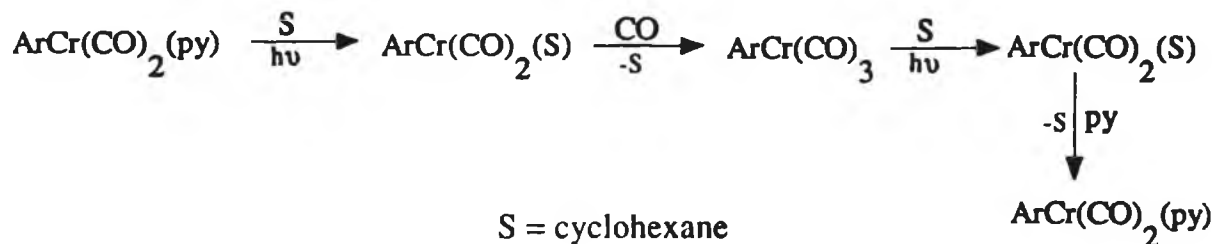


Figure 4.4.2.2.3 The variation in yield and lifetime of the species monitored at 500nm, under (i) 1 atm argon, (ii) 1 atm CO.

A possible reaction mechanism for the system is proposed in Scheme 4.4.2.2.1.



Scheme 4.4.2.2.1

Flash photolysis of $\text{ArCr}(\text{CO})_2(\text{py})$ in CO saturated cyclohexane containing pyridine results in the displacement of pyridine and the formation of $\text{ArCr}(\text{CO})_2(\text{S})$, (S = cyclohexane) as the primary photoproduct. The weakly bound cyclohexane is then replaced by the more nucleophilic CO ligand forming $\text{ArCr}(\text{CO})_3$. Even though the latter complex may be present in smaller concentrations, as its extinction coefficient at 354nm (the excitation wavelength) is greater than that of $\text{ArCr}(\text{CO})_2(\text{py})$, its photochemistry becomes dominant. Thus, further flash photolysis at 354nm produces the solvated species which then reacts with the excess pyridine, regenerating $\text{ArCr}(\text{CO})_2(\text{py})$. This accounts for the band forming at 500nm in the absorption spectrum under CO saturated conditions.

In the presence of argon, the primary photoproduct reacts with the excess ligand regenerating the parent complex (equation 4.4.2.1.1).

Other photochemical studies of $\text{ArCr}(\text{CO})_3$ in both low temperature matrices [2, 23] and solution [33, 38] have reported observations of a dinuclear species ($\text{Ar}_2\text{Cr}_2(\text{CO})_5$) at ca. 510nm [39]. These dinuclear species were formed from the reaction of parent ($\text{ArCr}(\text{CO})_3$) with the primary photoproduct ($\text{ArCr}(\text{CO})_2$). This is another possibility for the band observed at 500nm, however the likelihood of such a species forming in this system is very low as it would require reaction of the primary photoproduct with $\text{ArCr}(\text{CO})_3$ (formed from the primary photoproduct).

4.4.3 Activation parameter studies for $\text{ArCr}(\text{CO})_2(\text{py})$ system

The activation parameters for the reaction of $\text{ArCr}(\text{CO})_2(\text{py})$ with pyridine were determined at 500nm in both degassed and CO saturated cyclohexane. The parameters were calculated according to equations 5.4.1 and

5.4.2 and are tabulated in Tables 4.4.3.1 and 4.4.3.2, while the Arrhenius and Eyring plots are displayed in Figures 4.4.3.1 and 4.4.3.2 for the species monitored at 500nm in argon and CO saturated solutions respectively. A summary of the activation parameters is given in Table 4.4.3.3.

$1/T \times 10^3(\text{K}^{-1})$	$\text{Ln } k_2^a$	$\text{Ln } k_2^a/T$
3.51	16.40	10.74
3.47	16.61	10.95
3.42	16.83	11.15
3.39	16.90	11.22
3.34	17.05	11.34
3.31	17.11	11.40
3.28	17.24	11.52
3.25	17.35	11.62
3.21	17.49	11.75

$$^a k_2 = k_{\text{obs}}/[\text{py}], [\text{py}] = 12.02 \times 10^{-3}\text{M}$$

Arrhenius Plot

$$\text{Slope} = -3437.4 \pm 129.9$$

$$\text{Intercept} = 28.53 \pm 0.04$$

$$\text{Corr. coeff.} = 0.99$$

Eyring Plot

$$\text{Slope} = -3148.5 \pm 138.4$$

$$\text{Intercept} = 21.86 \pm 0.04$$

$$\text{Corr. coeff.} = 0.99$$

$$E_a^\ddagger = 29 \pm 1 \text{ kJmol}^{-1}, \Delta H^\ddagger = 27 \pm 1 \text{ kJmol}^{-1}, \Delta S^\ddagger = -13 \pm 10 \text{ Jmol}^{-1}\text{K}^{-1}$$

Table 4.4.3.1 Experimental data for the determination of activation energy, enthalpy and entropy for the regeneration of $\text{ArCr}(\text{CO})_2(\text{py})$ under 1 atm argon, monitored at 500nm.

$1/T \times 10^3(\text{K}^{-1})$	$\text{Ln } k_2^a$	$\text{Ln } k_2^a/T$
3.47	16.96	11.30
3.42	17.04	11.36
3.39	17.18	11.50
3.36	17.30	11.60
3.32	17.41	11.71
3.28	17.53	11.81
3.24	17.69	11.96
3.19	17.81	12.07

^a $k_2 = k_{\text{obs}}/[\text{py}]$, $[\text{py}] = 12.02 \times 10^{-3}\text{M}$

Arrhenius Plot

Slope = $-3.193.7 \pm 111.4$

Intercept = 28.01 ± 0.3

Corr. coeff. = 0.99

Eyring Plot

Slope = -2906.2 ± 113.8

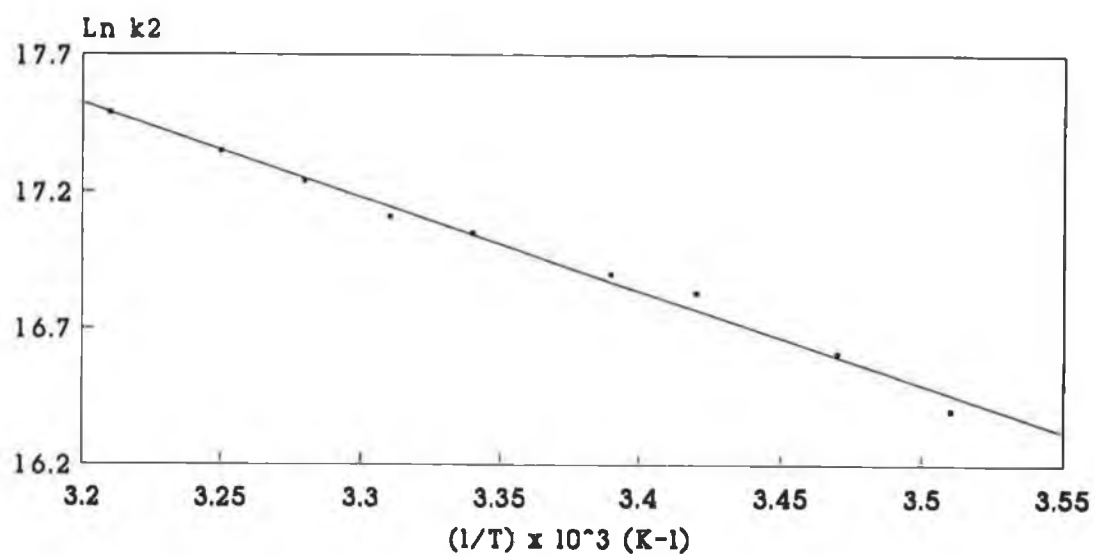
Intercept = 21.35 ± 0.03

Corr. coeff. = 0.99

$E_a^\ddagger = 27 \pm 1 \text{ kJmol}^{-1}$, $\Delta H^\ddagger = 24 \pm 1 \text{ kJmol}^{-1}$, $\Delta S^\ddagger = -20 \pm 10 \text{ Jmol}^{-1}\text{K}^{-1}$

Table 4.4.3.2 Experimental data for the determination of activation energy, enthalpy and entropy for the reaction of photoproducted $\text{ArCr}(\text{CO})_3$ with pyridine, regenerating $\text{ArCr}(\text{CO})_2(\text{py})$ under 1 atm CO, monitored at 500nm.

(a)



(b)

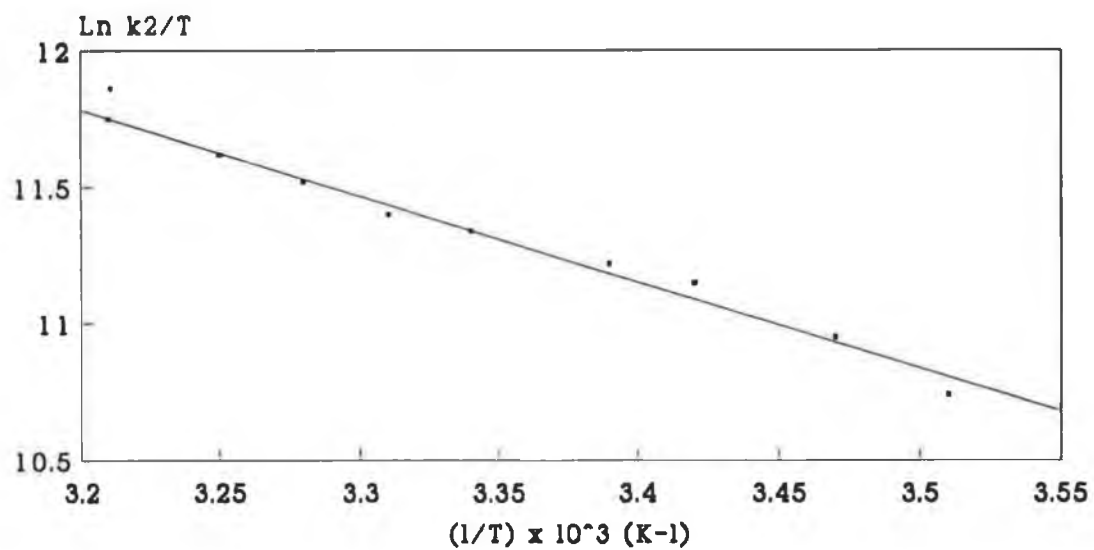
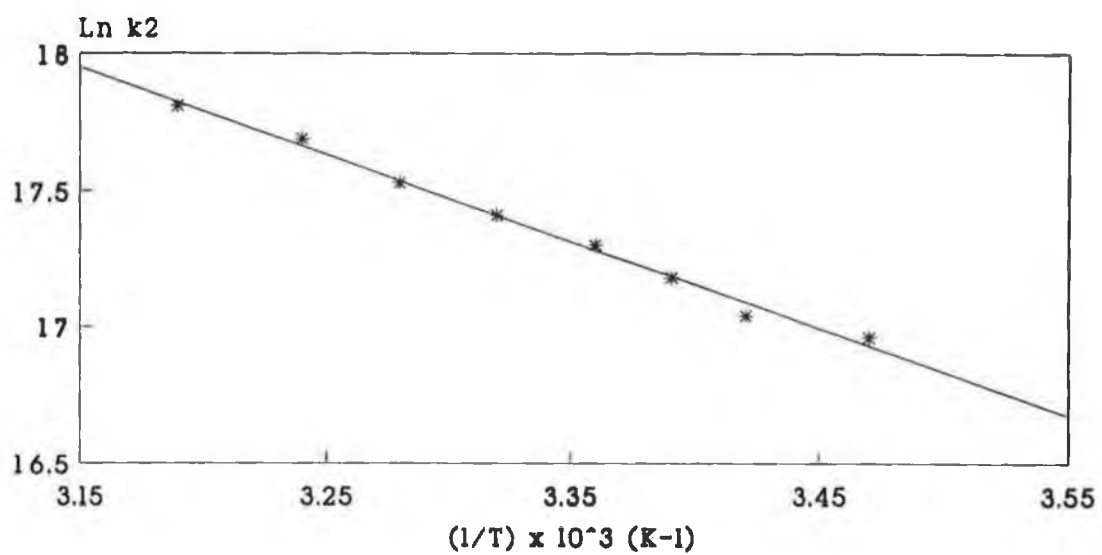


Figure 4.4.3.1 (a) Arrhenius and (b) Eyring plots for the regeneration of $\text{ArCr}(\text{CO})_2(\text{py})$ under 1 atm argon, monitored at 500nm.

(a)



(b)

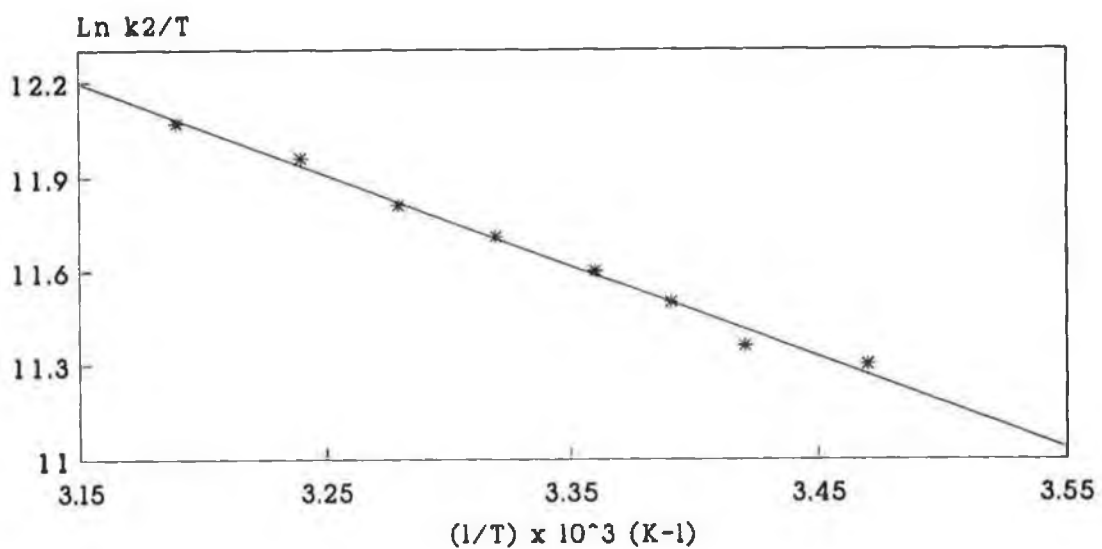


Figure 4.4.3.2 (a) Arrhenius and (b) Eyring plots for the reaction of photoproducted $\text{ArCr}(\text{CO})_3$ with pyridine under 1 atm CO, monitored at 500nm.

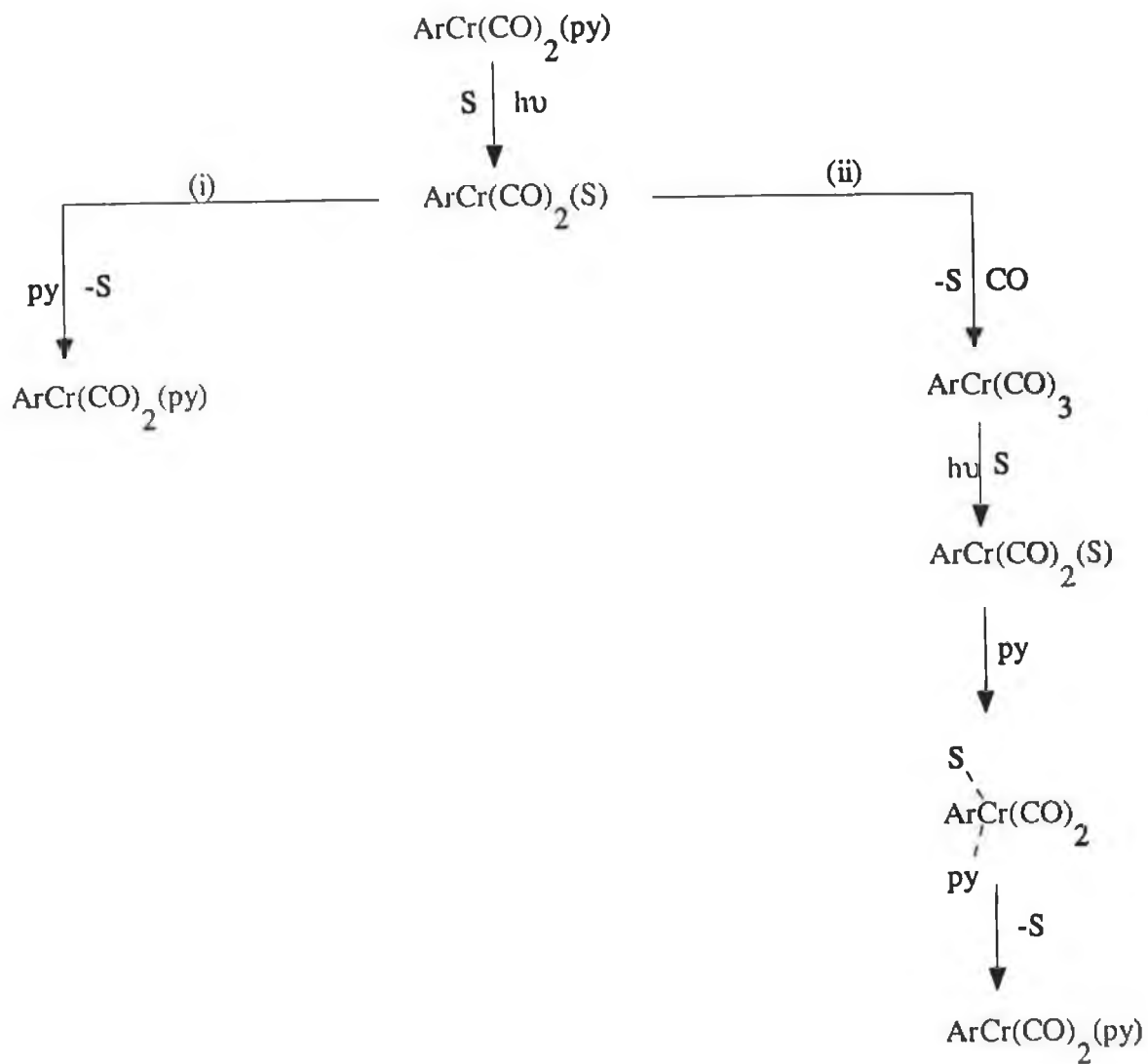
ArCr(CO) ₂ (L) + py	E _a [‡] (kJmol ⁻¹)	ΔH [‡] (kJmol ⁻¹)	ΔS [‡] (JK ⁻¹ mol ⁻¹)	ΔG _{298K} [‡] (kJmol ⁻¹)
L = py ^a	29	27	-13	31
= py ^b	27	24	-20	30
= CO ^c	30	28	-1	29

^a argon saturated solution, ^b CO saturated solution, ^c Section 4.3.3

Table 4.4.3.4 Summary of the activation parameters for the formation of the species at 500nm.

As shown in Table 4.4.3.4, the activation energy (E_a[‡]) and enthalpy (ΔH[‡]) values for the species occurring at 500nm are very similar under both argon and CO conditions suggesting that similar complexes are being formed in both cases. As ArCr(CO)₂(py) is regenerated under argon, this suggests that this is the complex forming under CO also. Thus the photoproduct, ArCr(CO)₃ formed under CO, reacts with the excess pyridine, yielding ArCr(CO)₂(py). The ΔH[‡] value is also close to that obtained for the reaction of ArCr(CO)₃ with pyridine (Table 4.4.3.4). The values obtained in this study are also similar to the activation enthalpy value of ca. 22 kJmol⁻¹ which was obtained for the displacement of cyclohexane from ArCr(CO)₂(cyclohexane) by CO [33]. The slightly negative ΔS[‡] values suggest that an interchange mechanism is the most likely process involved in the displacement of cyclohexane from the solvated complexes by the pyridine ligand.

A possible reaction scheme for the photochemical reactions observed under both (i) argon and (ii) CO saturated conditions are detailed in Scheme 4.4.3.2.



S = cyclohexane

Scheme 4.4.3.2

4.5 Laser flash photolysis of (η^6 -C₆H₆)Cr(CO)₂(4-acetylpyridine)

Even though many substituted arene chromium dicarbonyl complexes have been synthesised, photochemical studies of these complexes are rarely reported [27]. This may be attributed to the photosensitivity of these complexes, in particular those with nitrogen-donor ligands as they possess low lying energy absorptions. The photochemistry of the isoelectronic CpMn(CO)₂(L) complex, (Cp = (η^5 -C₅H₅), L = phosphorus and nitrogen-donor ligands) has been investigated in some detail [25, 40]. Manganese complexes in general are more stable than the chromium analogues.

ArCr(CO)₂(4-acetylpyridine), (Ar = η^6 -C₆H₆) is very air and light sensitive, decomposing rapidly in solution forming ArCr(CO)₃, free 4-Acpy (4-acetylpyridine) and decomposition products, thus rendering photochemical studies almost impossible. In the presence of excess ligand the lifetime of the complex is prolonged, therefore in this study the photochemistry of ArCr(CO)₂(4-acetylpyridine) was investigated in the presence of a known concentration of excess ligand.

4.5.1 UV/visible electronic spectrum of ArCr(CO)₂(4-acetylpyridine)

The UV/visible spectrum of ArCr(CO)₂(4-Acpy) in cyclohexane is displayed in Figure 4.5.1.1. The band at ca. 230nm is assigned to charge transitions from the ring and the chromium metal to the carbonyl ligands, while that at ca. 280nm is attributed to a chromium - carbonyl charge transfer band. The lowest energy band having λ_{max} at ca. 670nm arises from a Cr \rightarrow 4-Acpy π^* CT transition. The deep blue colour of the complex is as a result of this transition, which is also responsible for its absorption of visible light and

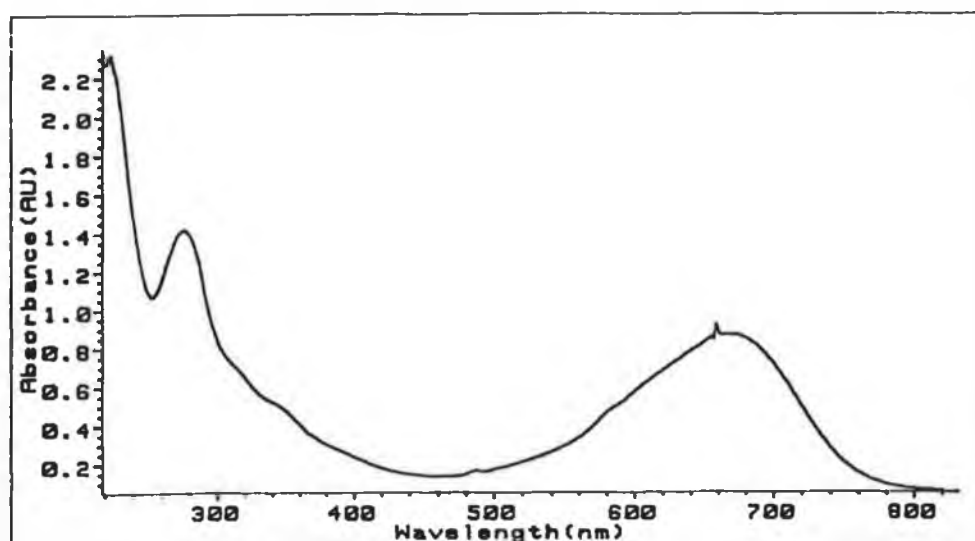


Figure 4.5.1.1 UV/visible electronic spectrum of $\text{ArCr}(\text{CO})_2(4\text{-acetylpyridine})$ (ca. $9 \times 10^{-4} \text{ mol dm}^{-3}$) in cyclohexane.

consequently its instability in solution.

The UV/visible spectrum of $(\eta^6\text{-C}_6\text{H}_6)\text{Cr}(\text{CO})_2(4\text{-acetylpyridine})$ in solvents of different polarities is given in Figure 4.5.1.2. The lowest energy band is blue-shifted in solvents of increasing polarities. Differences in the intensities of the band were as a result of differing complex concentrations in each solvent. The variation in band maxima in the different solvents is given in Table 4.5.1.1, along with the polarities of the solvents.

Solvent	Solvent polarity	λ_{max} (nm)
Cyclohexane	0.0	666
Toluene	2.3	640
Dichloromethane	3.4	614
Acetone	5.4	596

Table 4.5.1.1 Solvent dependence of the lowest energy band in $\text{ArCr}(\text{CO})_2(4\text{-Acpy})$.

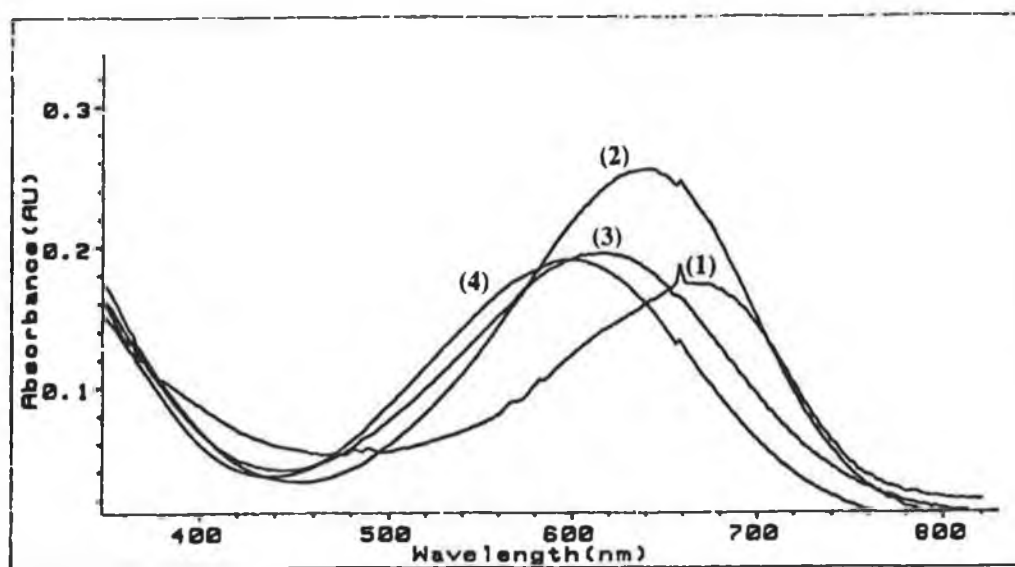


Figure 4.5.1.2 UV/visible spectrum of $\text{ArCr}(\text{CO})_2(4\text{-AcPy})$ in cyclohexane (1), toluene (2), dichloromethane (3) and acetone (4).

As LF bands are insensitive to changes in solvent polarities, the lowest energy band was assigned as a $\text{Cr} \rightarrow 4\text{-AcPy} \pi^* \text{CT}$ band. The addition of an electron-accepting group to the pyridine ring resulted in a red-shift of approximately 120nm of the lowest energy band compared to that of the pyridine complex. LF bands are little affected by variation of substituents. This was further supported by comparison of the electronic spectra of $\text{ArCr}(\text{CO})_2(\text{py})$ and $\text{ArCr}(\text{CO})_2(4\text{-AcPy})$, (Figures 4.4.1.1 and 4.5.1.1 respectively).

The extinction coefficient of $\text{ArCr}(\text{CO})_2(4\text{-AcPy})$ in cyclohexane was calculated to be 713 and 978 $\text{dm}^3\text{mol}^{-1}\text{cm}^{-1}$ at 354 and 670nm respectively (Section 5.7).

As 4-acetylpyridine absorbs strongly in the ultraviolet region of the electronic spectrum, when added to the dicarbonyl complex it occludes the high

energy region of UV/visible spectrum of the dicarbonyl complex, thus prohibiting observations of photochemical reactions occurring in that region.

4.5.2 Flash photolysis of $\text{ArCr}(\text{CO})_2(4\text{-acetylpyridine})$ in cyclohexane

In argon saturated cyclohexane, flash photolysis of $\text{ArCr}(\text{CO})_2(4\text{-acetylpyridine})$ in the absence of excess ligand resulted in decomposition of the complex, forming $\text{ArCr}(\text{CO})_3$, free 4-acetylpyridine and decomposition products. The spectral changes are shown in Figure 4.5.2.1. The final spectrum correlates well with that of pure $\text{ArCr}(\text{CO})_3$ in cyclohexane (Figure 4.3.1.1).

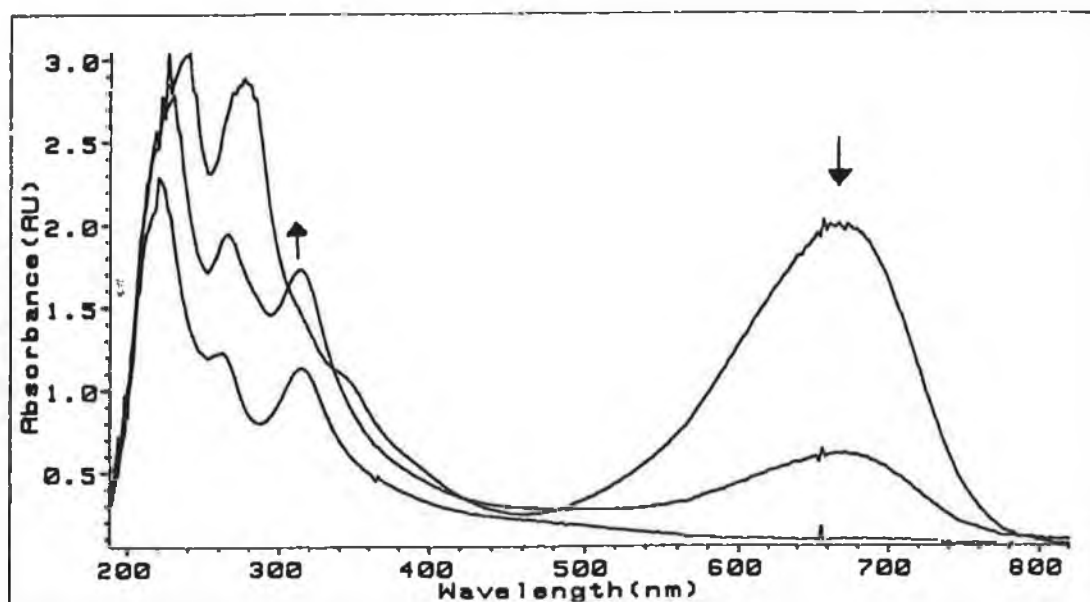


Figure 4.5.2.1 Spectral changes observed upon flash photolysis of $\text{ArCr}(\text{CO})_2(4\text{-Acpy})$ ($2 \times 10^{-3} \text{ mol dm}^{-3}$) in degassed cyclohexane.

In CO saturated cyclohexane $\text{ArCr}(\text{CO})_2(4\text{-Acpy})$ is cleanly converted to $\text{ArCr}(\text{CO})_3$ as evident from the UV/visible spectrum displayed in Figure 4.5.2.2.

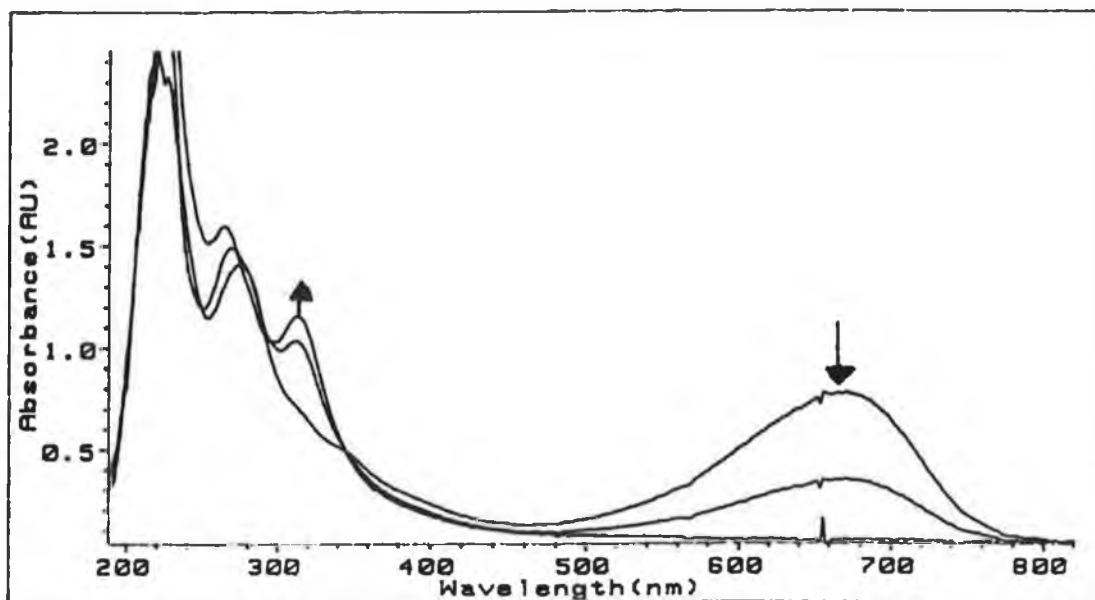


Figure 4.5.2.2 Spectral changes observed during flash photolysis of $\text{ArCr}(\text{CO})_2(4\text{-Acpy})$ ($8 \times 10^{-4} \text{ mol dm}^{-3}$) in CO saturated cyclohexane.

As a result of the rapid decomposition of the complex and conversion to $\text{ArCr}(\text{CO})_3$, under argon and CO respectively, we decided to investigate the photochemistry in the presence of excess ligand.

4.5.2.1 Flash photolysis of $\text{ArCr}(\text{CO})_2(4\text{-Acpy})$ in argon saturated cyclohexane solution containing 4-acetylpyridine

The UV/visible difference spectrum obtained as a result of flash photolysis of the system is shown in Figure 4.5.2.1.1. In contrast, with the analogous pyridine complex, regeneration of the parent complex was not observed. Instead, a band formed ca. $2\mu\text{s}$ after the flash decays away with concomitant formation of a band at ca. 670nm.

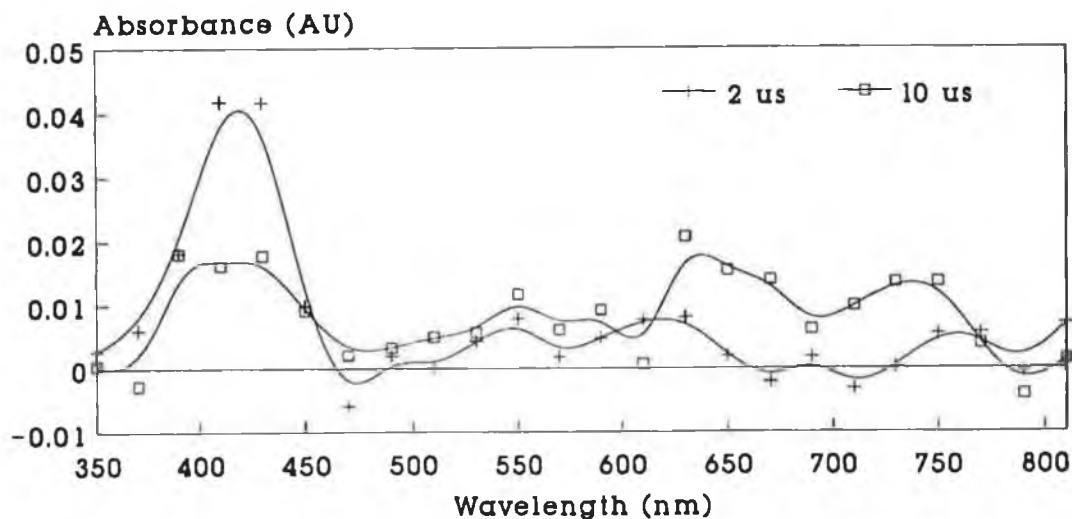


Figure 4.5.2.1.1 UV/visible difference spectrum of $\text{ArCr}(\text{CO})_2(4\text{-Acpy})$ in degassed cyclohexane solution containing 4-Acpy, recorded $2\mu\text{s}$ and $10\mu\text{s}$ after the laser flash.

Transient signals of the decay and the "grow-in" monitored at 420 and 670nm respectively are represented in Figure 4.5.2.1.2. A grating blazed at 500nm was used in this work to investigate the photochemistry at longer wavelengths (350-900nm). The rate of decay of the species at 420nm is approximately 8 times slower than the rate of formation of that at 670nm (Table 4.5.2.1.1). All the transient signals followed pseudo-first-order kinetics.

In the absence of excess ligand the decay transient signal is not observed, thus it is proposed that this decay is directly associated with the presence of unbound ligand. As 4-acetylpyridine possesses two potential binding sites *via* (i) the nitrogen lone pair and (ii) the oxygen lone pair, reaction with the solvated complex results in the formation of two isomeric complexes of the form $\text{ArCr}(\text{CO})_2(4\text{-Acpy})$. The decay observed at ca. 420nm is attributed to the decay of the oxygen bound complex. This complex is short-lived and possibly

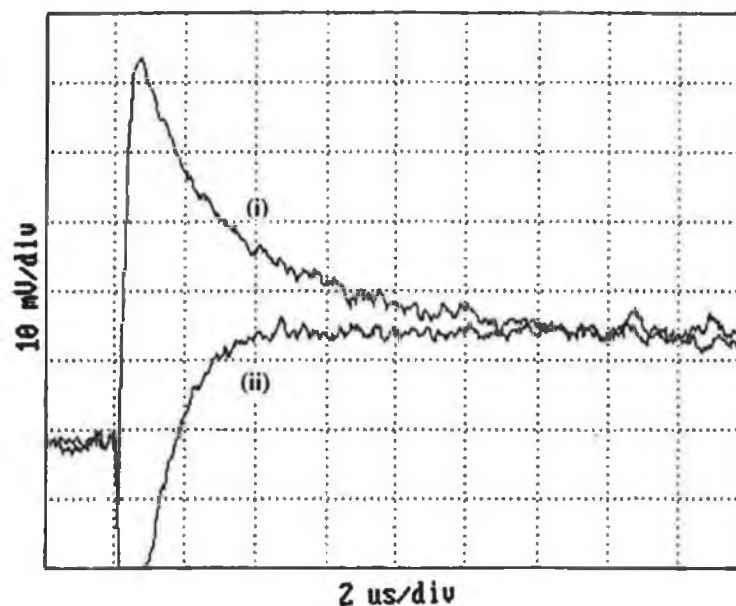


Figure 4.5.2.1.2 Typical transient signals of (i) the decay at 420nm and (ii) the "grow-in" at 670nm, obtained upon flash photolysis of $\text{ArCr}(\text{CO})_2(4\text{-Acpy})$ in degassed cyclohexane containing 4-acetylpyridine.

Wavelength (nm)	$k_{\text{obs}} \times 10^{-4} (\text{s}^{-1})^{\text{a}}$
420	8.2
670	63.6

^a $[4\text{-Acpy}] = 4.5 \times 10^{-3}\text{M}$

Table 4.5.2.1.1 Rates of formation and decay of species monitored at 670 and 420nm, respectively.

reforms the solvated species. Another possible mechanism consistent with the decay observed, is the rearrangement of the O-linked complex to the N-linked isomer. No evidence for such a rearrangement was obtained in this study, but Dobson and Spralding have reported such a rearrangement for the formation of

$W(CO)_5(4\text{-Acpy})$ [32]. Aliphatic alcohols have also been reported to undergo rearrangements, from the initially formed unstable complex where bonding is *via* the aliphatic end of the chain, to the more stable complex where bonding is *via* the hydroxyl end of the alcohol [31].

The reaction of $ArCr(CO)_2(4\text{-Acpy})$ in the presence of pyridine in degassed cyclohexane was also investigated. The photosubstitution which occurred was consistent with that described in equation 4.5.2.1.1, while the spectral changes accompanying this photoreaction are shown in Figure 4.5.2.1.3. The net reaction, as for the analogous pyridine and isoelectronic manganese complexes, was dissociative loss of the ligand ($X = 4\text{-Acpy}$ in this case).

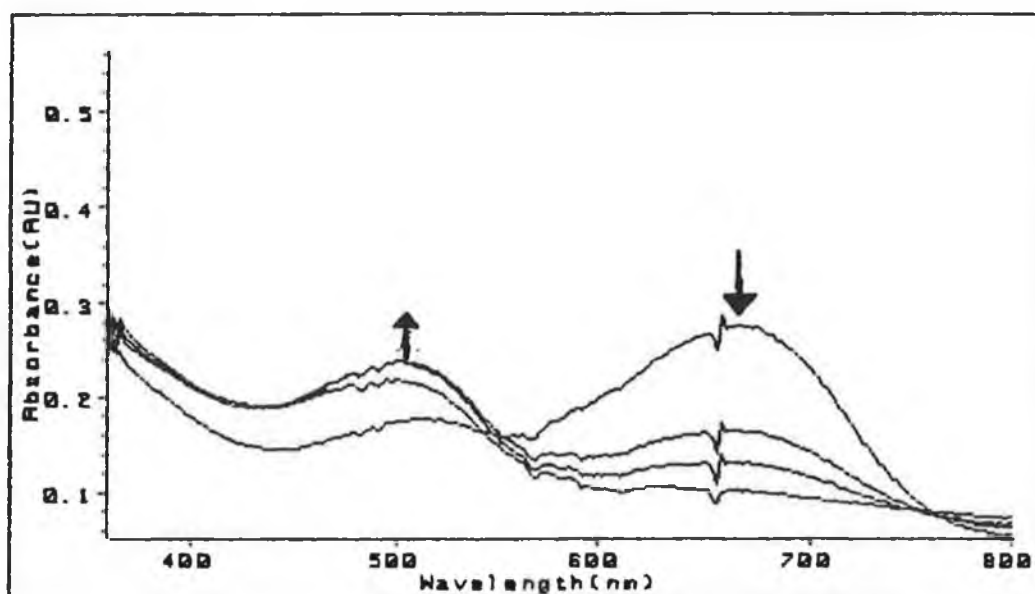
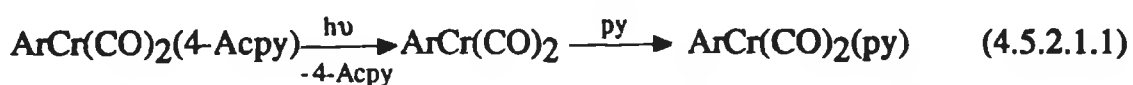


Figure 4.5.2.1.3 Spectral changes accompanying the reaction of $ArCr(CO)_2(4\text{-Acpy})$ ($4.3 \times 10^{-4} \text{ mol dm}^{-3}$) with pyridine ($5 \times 10^{-3} \text{ mol dm}^{-3}$) in degassed cyclohexane.

4.5.2.2 Flash photolysis of $\text{ArCr}(\text{CO})_2(4\text{-Acpy})$ in CO saturated cyclohexane solution containing 4-acetylpyridine

In CO saturated cyclohexane, the UV/visible difference spectrum recorded $2\mu\text{s}$ and $40\mu\text{s}$ after the laser flash is shown in Figure 4.5.2.2.1. A weak band at ca. 420nm and a more intense band at ca. 670nm were observed $2\mu\text{s}$ after the flash. However, after $40\mu\text{s}$ the band at ca. 420nm had decayed while that at ca. 670nm had increased in intensity. Thus, the band at ca. 420nm is only a short-lived species. The band at 670nm correlates well with that in Figure 4.3.1.1(b).

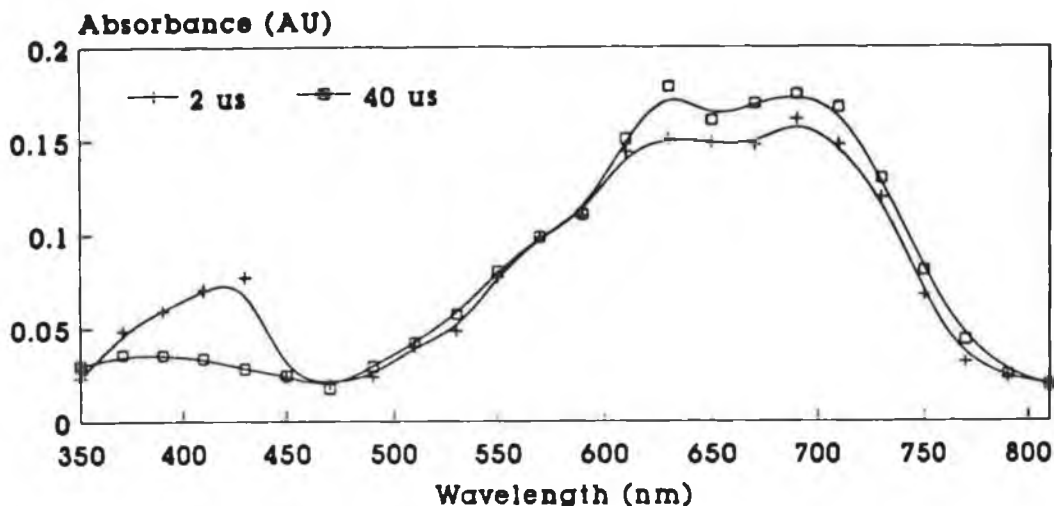
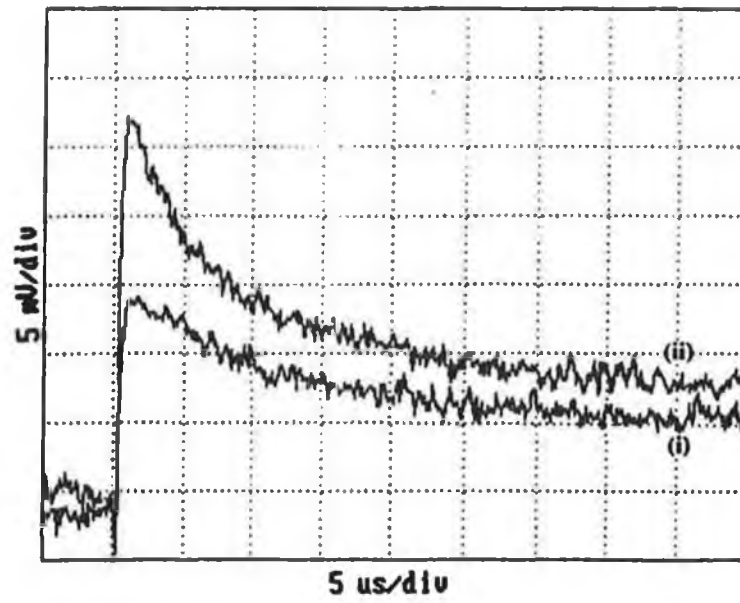


Figure 4.5.2.2.1 UV/visible difference spectrum of $\text{ArCr}(\text{CO})_2(4\text{-Acpi})$ in CO saturated cyclohexane solution containing 4-Acpi, recorded $2\mu\text{s}$ and $40\mu\text{s}$ after the laser flash.

An increase in both the yield and the rate of decay of the species at 420nm was observed upon the addition of CO. A similar trend was found for the species forming at 670nm . Typical transients signals observed are shown in Figure 4.5.2.2.2.

(a)



(b)

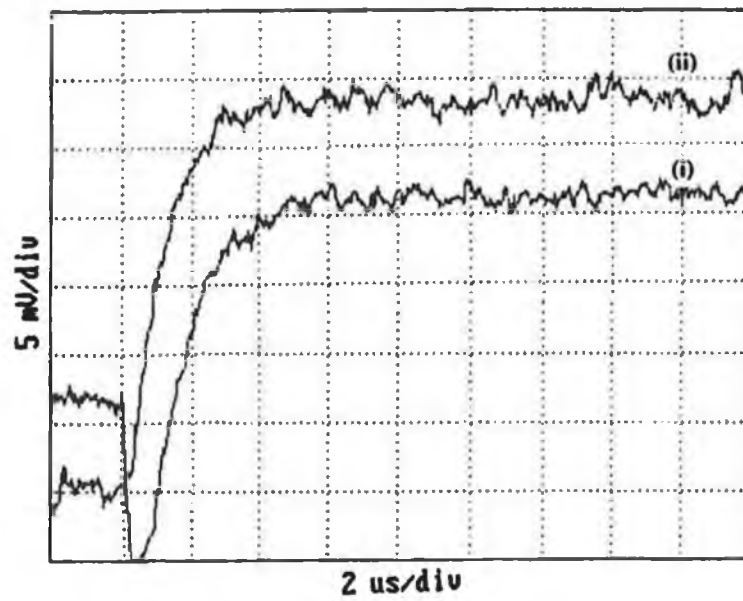


Figure 4.5.2.2.2 Transient signals observed at (a) 420nm and (b) 670nm, (i) under 1 atm argon, (ii) under 1 atm CO.

As the yields are affected by the concentration of CO, this indicates that neither species are primary photoproducts. The primary photoproduct is most probably the solvated $\text{ArCr}(\text{CO})_2(\text{cyclohexane})$ complex, formed upon dissociation of 4-Acpy. However in CO saturated conditions, the primary photoproduct reacts with CO, producing $\text{ArCr}(\text{CO})_3$. This is evident from the UV/visible electronic spectrum recorded in the absence of excess ligand (Figure 4.5.2.2). These changes cannot be observed on the UV/visible spectrum in the presence of excess ligand, (as the high energy portion of the spectrum is occluded by the absorption of the ligand), however they most probably occur. As was the case under argon, the "grow-in" is proposed to be that of $\text{ArCr}(\text{CO})_2(4\text{-Acpy})$ bonded *via* the N-atom while the decay corresponds to that of $\text{ArCr}(\text{CO})_2(4\text{-Acpy})$ coordinated through the O-atom. The decay may also be that of the O-bound complex rearranging so that coordination is *via* the N-atom [32]. Therefore it is proposed that as $\text{ArCr}(\text{CO})_3$ is formed from the reaction of the primary photoproduct with CO, and as its extinction coefficient at the excitation wavelength (354nm) is greater than that of $\text{ArCr}(\text{CO})_2(4\text{-Acpy})$, it becomes the active chromophore, resulting in dissociative loss of a CO molecule from $\text{ArCr}(\text{CO})_3$ and formation of a solvated complex. This then reacts with 4-acetylpyridine, forming (i) the O-bound complex (k_1 path) and (ii) the N-bound isomer (k_2 path). The transient signal observed at 420nm is attributed to the decay of the short-lived O-bound complex. This may reform the solvated complex (k_{-1} path). It may also be as a result of O-linked complex rearranging so that coordination is *via* the N-atom (k_3 path), as proposed by Dobson *et al.* for a similar system [32]. No evidence was found in this study to confirm such a rearrangement. A possible reaction scheme is detailed in Scheme 4.5.3.1.

4.5.3 Activation parameter studies for ArCr(CO)₂(4-Acpy) system

Activation parameters were determined at 420nm in argon saturated solution and at both 420 and 670nm in CO saturated solution. The experimental data is given in Tables 4.5.3.1 - 4.5.3.3, while the Arrhenius and Eyring plots are displayed in Figures 4.5.3.1 and 4.5.3.2. A summary of the activation parameters is tabulated in Table 4.5.3.4. The parameters were calculated according to equations 5.4.1 and 5.4.2.

$1/T \times 10^3 \text{ (K}^{-1}\text{)}$	$\text{Ln } k_2^a$	$\text{Ln } k_2^a/T$
3.47	16.59	10.93
3.44	16.87	11.19
3.39	16.94	11.24
3.34	17.08	11.37
3.30	17.20	11.48
3.27	17.29	11.56
3.23	17.39	11.66
3.18	17.52	11.79

$$^a k_2 = k_{\text{obs}}/[4\text{-Acpy}], [4\text{-Acpy}] = 4.52 \times 10^{-3}\text{M}$$

Arrhenius Plot

$$\text{Slope} = -3019.4 \pm 309.5$$

$$\text{Intercept} = 27.16 \pm 0.08$$

$$\text{Corr. coeff.} = 0.98$$

Eyring Plot

$$\text{Slope} = -2737.8 \pm 290.7$$

$$\text{Intercept} = 20.52 \pm 0.08$$

$$\text{Corr. coeff.} = 0.98$$

$$E_a^\ddagger = 25 \pm 1 \text{ kJmol}^{-1}, \Delta H^\ddagger = 23 \pm 1 \text{ kJmol}^{-1}, \Delta S^\ddagger = -27 \pm 10 \text{ Jmol}^{-1}\text{K}^{-1}$$

Table 4.5.3.1 Experimental data for the determination of activation energy, enthalpy and entropy for the decay monitored at 420nm in argon saturated solution.

$1/T \times 10^3 \text{ (K}^{-1}\text{)}$	$\text{Ln } k_2^a$	$\text{Ln } k_2^a/T$
3.47	17.72	12.05
3.44	17.88	12.20
3.39	17.92	12.23
3.34	18.04	12.34
3.30	18.30	12.59
3.27	18.36	12.64
3.24	18.47	12.74
3.18	18.59	12.84

$$^a k_2 = k_{\text{obs}}/[4\text{-Acpy}], [4\text{-Acpy}] = 10.76 \times 10^{-3}\text{M}$$

Arrhenius Plot

$$\text{Slope} = -3072.9 \pm 212.0$$

$$\text{Intercept} = 28.39 \pm 0.06$$

$$\text{Corr. coeff.} = 0.99$$

Eyring Plot

$$\text{Slope} = -2808.5 \pm 210.9$$

$$\text{Intercept} = 21.80 \pm 0.06$$

$$\text{Corr. coeff.} = 0.98$$

$$E_a^\ddagger = 26 \pm 2 \text{ kJmol}^{-1}, \Delta H^\ddagger = 23 \pm 2 \text{ kJmol}^{-1}, \Delta S^\ddagger = -16 \pm 10 \text{ Jmol}^{-1}\text{K}^{-1}$$

Table 4.5.3.2 Experimental data for the determination of activation energy, enthalpy and entropy for the "grow-in" monitored at 670nm in CO saturated solution.

$1/T \times 10^3 \text{ (K}^{-1}\text{)}$	$\text{Ln } k_2^a$	$\text{Ln } k_2^a/T$
3.47	16.09	10.42
3.44	16.17	10.49
3.39	16.32	10.64
3.34	16.39	10.68
3.30	16.47	10.75
3.27	16.54	10.81
3.24	16.59	10.85

$$^a k_2 = k_{\text{obs}}/[4\text{-Acpy}], [4\text{-Acpy}] = 4.52 \times 10^{-3}\text{M}$$

Arrhenius Plot

$$\text{Slope} = -2142.3 \pm 128.4$$

$$\text{Intercept} = 23.54 \pm 0.03$$

$$\text{Corr. coeff.} = 0.995$$

Eyring Plot

$$\text{Slope} = -1831.9 \pm 162.9$$

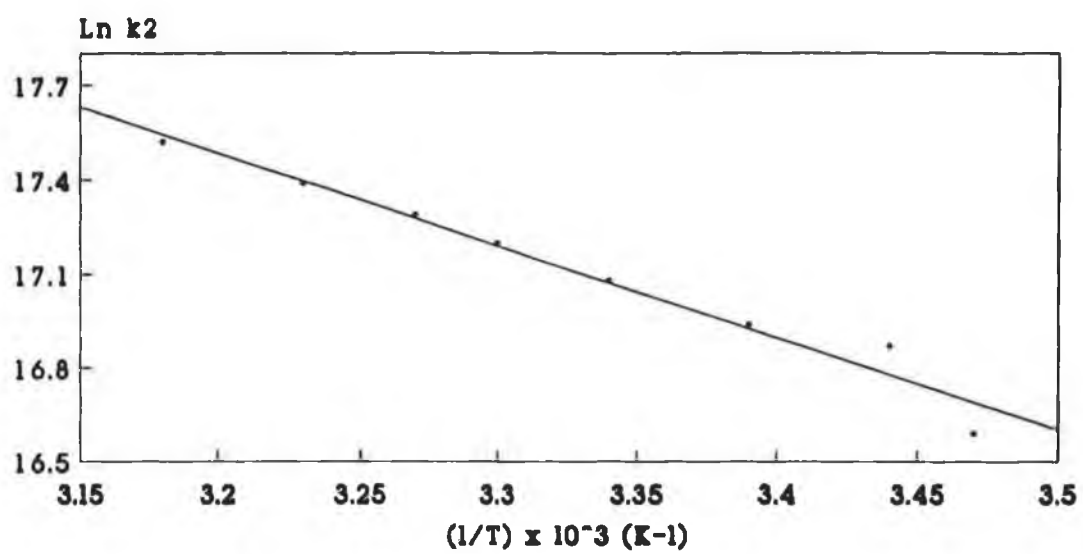
$$\text{Intercept} = 16.80 \pm 0.03$$

$$\text{Corr. coeff.} = 0.99$$

$$E_a^\ddagger = 18 \pm 2 \text{ kJmol}^{-1}, \Delta H^\ddagger = 15 \pm 2 \text{ kJmol}^{-1}, \Delta S^\ddagger = -58 \pm 10 \text{ Jmol}^{-1}\text{K}^{-1}$$

Table 4.5.3.3 Experimental data for the determination of activation energy, enthalpy and entropy for the decay monitored at 420nm in CO saturated solution.

(a)



(b)

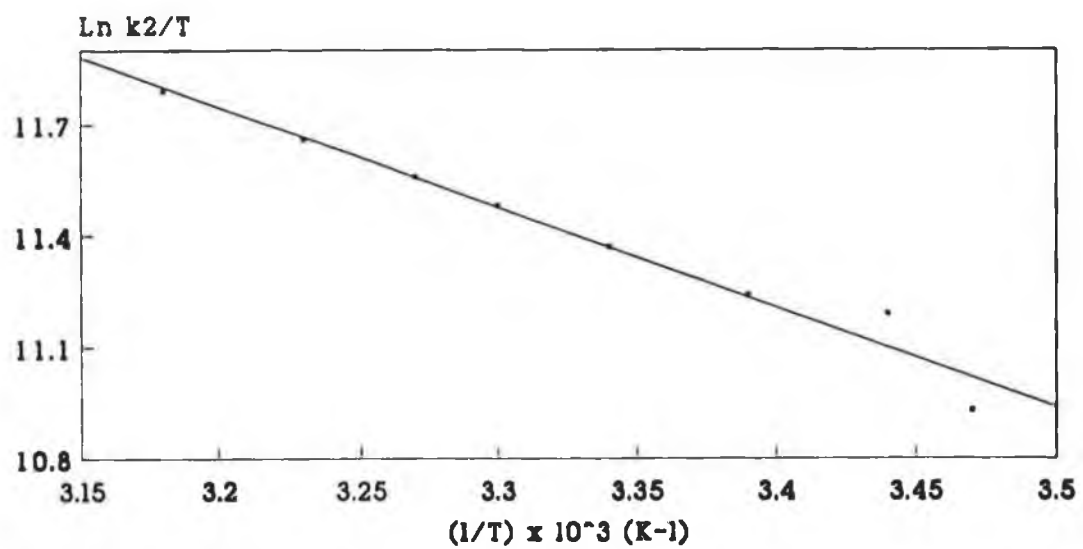
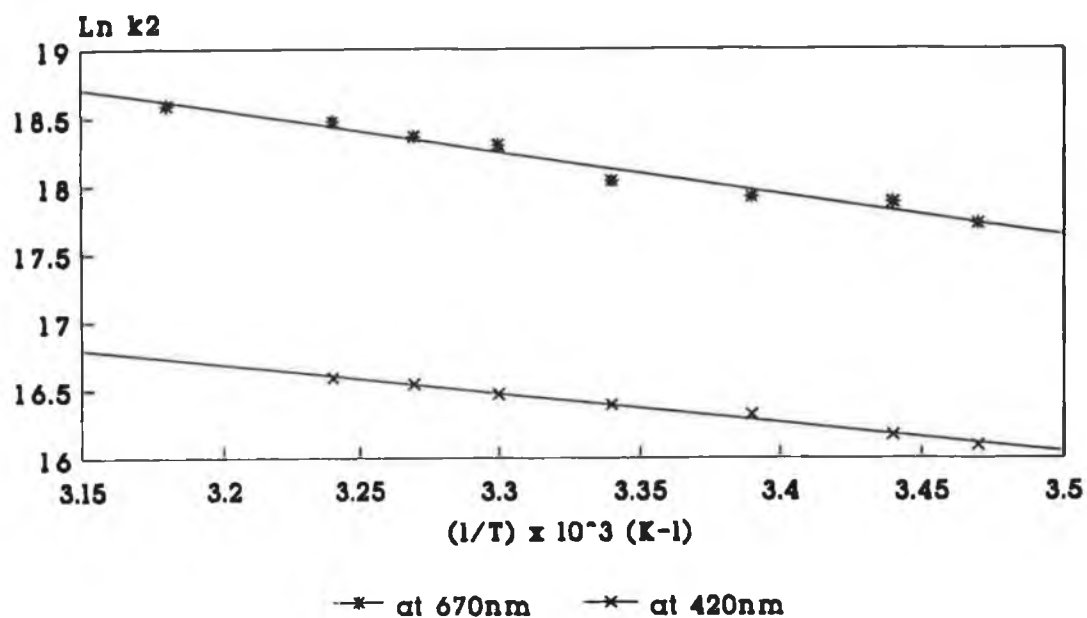


Figure 4.5.3.1 (a) Arrhenius and (b) Eyring plots for the decay monitored at 420nm, in argon saturated solution.

(a)



(b)

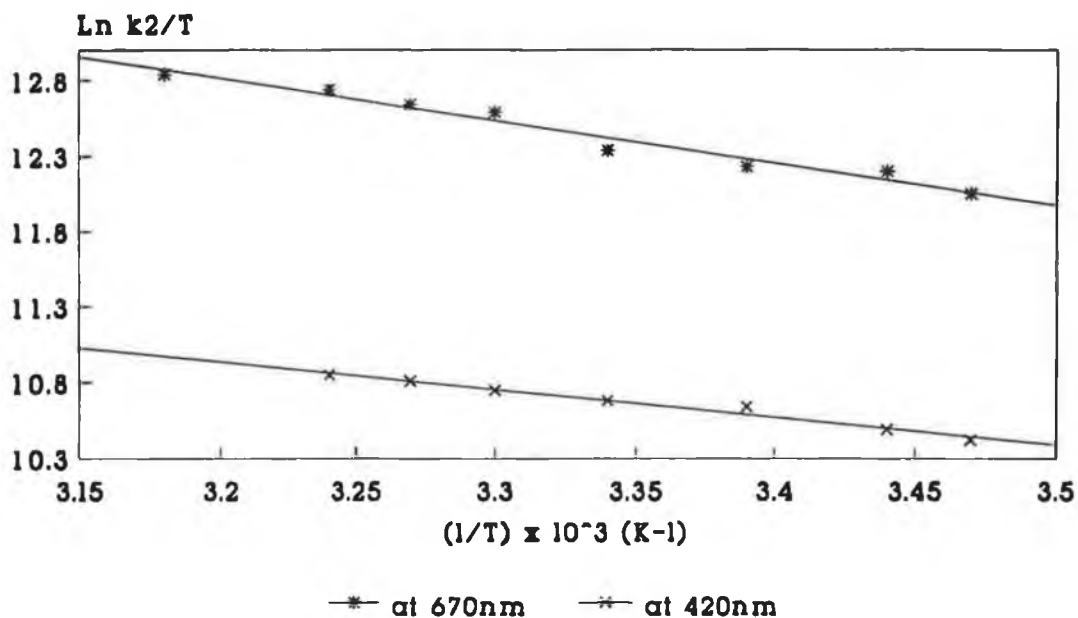


Figure 4.5.3.2 (a) Arrhenius and (b) Eyring plots for the decay monitored at 420nm and the "grow-in" at 670nm, in CO saturated solution.

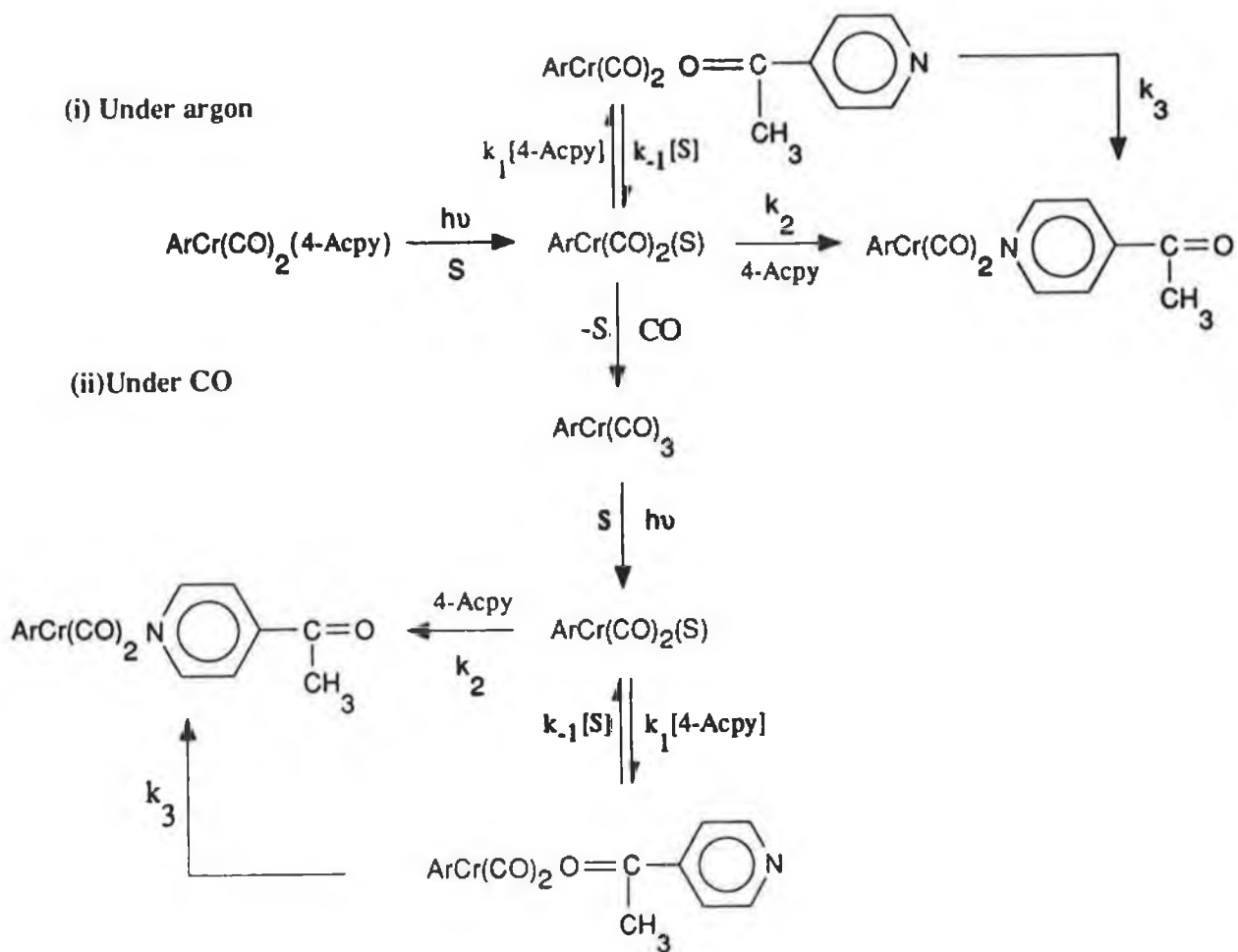
ArCr(CO) ₂ (L) + 4-Acpy (λ (nm))	E _a [‡] (kJmol ⁻¹)	ΔH [‡] (kJmol ⁻¹)	ΔS [‡] (JK ⁻¹ mol ⁻¹)	ΔG _{298K} [‡] (kJmol ⁻¹)
L = 4-Acpy (420) ^a	25	23	-27	31
= 4-Acpy (420) ^b	18	15	-58	32
= 4-Acpy (670) ^b	26	23	-16	28
= CO (670) ^c	25	23	-11	26

^a argon saturated solution, ^b CO saturated solution, ^c Section 4.3.3

Table 4.5.3.4 Summary of the activation parameters obtained for the reaction of ArCr(CO)₂(4-Acpy) in CO and argon saturated cyclohexane solutions containing 4-acetylpyridine.

The activation energy (E_a[‡]) and enthalpy (ΔH[‡]) values obtained for the species formed at 670nm correlate well with those determined for the formation of the same species in the reaction of ArCr(CO)₃ with 4-acetylpyridine (Table 4.5.3.4). This suggests that a similar species is being formed in both reactions. The "grow-in" corresponds with the absorption observed in the UV/visible electronic spectrum of the pure complex, Figure 4.5.1.1. Thus, in the presence of excess ligand and CO saturated cyclohexane, the species forming at 670nm is from the reaction of the photoproduct, ArCr(CO)₃ with 4-acetylpyridine. The ΔH[‡] values are similar to those obtained for the displacement of cyclohexane from ArCr(CO)₂(cyclohexane) by CO (ΔH[‡] = 22 kJmol⁻¹) [33]. The activation entropy values (ΔS[‡] = -16 ± 10 JK⁻¹mol⁻¹) for the species monitored at 670nm suggest the presence of an interchange mechanism in the transition state.

A possible reaction scheme for the reactions observed under both (i) argon and (ii) CO saturated conditions is detailed in Scheme 4.5.3.1.



S = cyclohexane

Scheme 4.5.3.1

4.6 Conclusion

The reaction of ArCr(CO)_3 with pyridine and 4-acetylpyridine produced $\text{ArCr(CO)}_2(\text{py})$ and $\text{ArCr(CO)}_2(4\text{-Acpy})$ respectively. The photochemistry was consistent with dissociative loss of CO as the principal result of electronic excitation. The substituted dicarbonyl complexes were isolated and their photochemistry investigated. However, unlike the tricarbonyls, the dominant photoreaction was dissociative loss of the ligand, i.e. pyridine and 4-acetylpyridine. This feature has also been observed in the isoelectronic $(\eta^5\text{-C}_5\text{H}_5)\text{Mn(CO)}_2(\text{L})$ complexes, L = pyridine or substituted pyridine [25]. As a result of the reactivity of the complexes in solution, the photochemistry in argon and CO saturated cyclohexane was studied in the presence of excess ligand.

Excitation of $\text{ArCr(CO)}_2(\text{py})$ in the presence of pyridine regenerated $\text{ArCr(CO)}_2(\text{py})$ under both argon and carbon monoxide. However, two pathways were operative. Under argon, regeneration of the parent was observed, while under CO, ArCr(CO)_3 was formed which then reacted photochemically with pyridine yielding the final product.

The photochemistry of $\text{ArCr(CO)}_2(4\text{-Acpy})$ was very similar to that observed for the pyridine analogue, however it possessed an additional step. 4-Acetylpyridine has two potential sites accessible for binding to the metal (i) *via* the oxygen lone pair and (ii) *via* the nitrogen lone pair. Thus reaction of this ligand with the primary photoproduct ($\text{ArCr(CO)}_2(\text{cyclohexane})$) and ArCr(CO)_3 (produced from the former) resulted in the formation of both oxygen and nitrogen bound complexes. The O-linked complex is short-lived, and most probably decays to form the solvated complex again. Another possible explanation for the decay is the rearrangement of the O-linked complex to the more stable N-linked isomer. Such a rearrangement was observed by Dobson

and Spradling in the formation of $W(CO)_5(4\text{-Acpy})$ [32]. However, in this study, no evidence was found to support such a rearrangement.

Proposed reaction schemes of the photochemical reactions of both $ArCr(CO)_2(py)$ and $ArCr(CO)_2(4\text{-Acpy})$ observed are detailed in Schemes 4.4.3.4 and 4.5.3.1 respectively. However, it must be stated that these conclusions are only postulations, and that much more detailed work would have to be undertaken to permit elucidation of the intimate photochemistry of these systems.

4.7 References

- 1 Strohmeier, W.; von Hobe, D.; *Z Naturforsch B*, 1963, **18**, 981.
- 2 Rest, A. J.; Sodeau, J. R.; Taylor, D. J.; *J. Chem. Soc., Dalton Trans.*, 1978, 651.
- 3 Hill, R. H.; Wrighton, M. S.; *Organometallics*, 1987, **6**, 632.
- 4 Glavee, G. N.; Jagirdar, B. R.; Schneider, J. J.; Klabunde, K. J.; Radonovich, L. J.; Dodd, K.; *Organometallics*, 1992, **11**, 1043.
- 5 Trembovler, V. N.; Yavorskii, B. M.; Setkina, V. N.; Baranetskaya, N. K.; Zaslavskaya, G. B.; Evdokimova, M. G.; *Russ. J. Phys. Chem.*, 1974, **48**, 1231.
- 6 Trembovler, V. N.; Baranetskaya, N. K.; Fok, N. V.; Zaslavskaya, G. B.; Yavorskii, B. M.; Setkina, V. N.; *J. Organomet. Chem.*, 1976, **117**, 339.
- 7 (a) Strohmeier, W.; Starrico, E. H.; *Z. Phys. Chem.*, 1963, **38**, 315. (b) Mahaffy, C. A.; Pauson, P. L.; *J. Chem. Research (S)*, 1979, 126. (c) Butler, I. S.; Uhm, H. L.; *Comments Inorg. Chem.*, 1988, **7**, 1.
- 8 Traylor, T. G.; Stewart, K. J.; *Organometallics*, 1984, **3**, 325.
- 9 (a) Traylor, T. G.; Stewart, K. J.; Goldberg, M. J.; *J. Am. Chem. Soc.*, 1984, **106**, 4445. (b) Traylor, T. G.; Stewart, K. J.; *J. Am. Chem. Soc.*, 1986, **108**, 6977.
- 10 Cais, M.; Kaftory, M.; Kohn, D. H.; Tatarsky, D.; *J. Organomet. Chem.*, 1979, **184**, 103.
- 11 Strohmeier, W.; Hellmann, H.; *Chem. Ber.*, 1963, **96**, 2859.
- 12 Wrighton, M. S.; Ginley, D. S.; *J. Am. Chem. Soc.*, 1975, **97**, 4246.
- 13 Nasielski, J.; Denisoff, O.; *J. Organomet. Chem.*, 1975, **102**, 65.
- 14 Wrighton, M. S.; *Chem. Revs.*, 1974, **74**, 401.

- 15 Wrighton, M. S.; Haverty, J. L.; *Z. Naturforsch.*, 1975, **30b**, 254.
- 16 Gilbert, A.; Kelly, J. M.; Budzwait, M.; Koerner von Gustorf, E.; *Z. Naturforsch.*, 1976, **31b**, 1091.
- 17 Bamford, C.H.; Al-Lamee, K. G.; Konstantinov, C. J.; *J. Chem. Soc., Faraday Trans.*; 1977, **73**, 1406.
- 18 Kelly, J. M.; Bent, D. V.; Hermann, H.; Schulte-Frohlinde, D.; Koerner von Gustorf, E.; *J. Organomet. Chem.*, 1974, **69**, 259.
- 19 (a) Seder, T. A.; Ouderkirk, A. J.; Weitz, E.; *J. Chem. Phys.*, 1986, **85**, 1977. (b) Seder, T. A.; Church, S. P.; Weitz, E.; *J. Am. Chem. Soc.*, 1986, **108**, 4721. (c) Seder, T. A.; Church, S. P.; Weitz, E.; *J. Am. Chem. Soc.*, 1986, **108**, 7518. (d) Weitz, E.; *J. Phys. Chem.*, 1987, **91**, 3945.
- 20 Fletcher, T. R.; Rosenfeld, R. N.; *J. Am. Chem. Soc.*, 1985, **107**, 2203.
- 21 (a) Ishikawa, Y.; Hackett, P. A.; Rayner, D. M.; *J. Am. Chem. Soc.*, 1987, **109**, 6644. (b) Ishikawa, Y.; Hackett, P. A.; Rayner, D. M.; *J. Phys. Chem.*, 1988, **92**, 3863. (c) Ishikawa, Y.; Brown, C. E.; Hackett, P. A.; Rayner, D. M.; *J. Phys. Chem.*, 1990, **94**, 2404. (d) Brown, C. E.; Ishikawa, Y.; Hackett, P. A.; Rayner, D. M.; *J. Am. Chem. Soc.*, 1990, **112**, 2530.
- 22 (a) Wang, W.; Jin, P.; Liu, Y.; She, Y.; Fu, K.; *Chinese Phys. Letters*, 1991, **8**, 491. (b) Wang, W.; Jin, P.; Liu, Y.; She, Y.; Fu, K.; *J. Phys. Chem.*, 1992, **96**, 1278.
- 23 Bitterwolf, T. E.; Lott, K. A.; Rest, A. J.; Mascetti, J.; *J. Organomet. Chem.*, 1991, **419**, 113.
- 24 McGrath, I. M.; Ph. D. Thesis, Dublin City University, 1993.
- 25 Giordano, P. J.; Wrighton, M. S.; *Inorg. Chem.*, 1977, **16**, 160.

- 26 (a) Wrighton, M. S.; Abrahamson, H. B.; Morse, D. L.; *J. Am. Chem. Soc.*, 1976, **98**, 4105. (b) Wrighton, M. S.; Abrahamson, H. B.; Gray, H. D.; *J. Am. Chem. Soc.*, 1971, **93**, 4336.
- 27 Geoffroy, G. L.; Wrighton, M. S.; *Organometallic Photochemistry*, Academic Press, New York, 1979.
- 28 Gray, H. B.; Beach, N. A.; *J. Am. Chem. Soc.*, 1963, **85**, 2922.
- 29 Carroll, D. G.; McGlynn, S. P.; *Inorg. Chem.*, 1968, **7**, 1285.
- 30 (a) Simon, J. D.; Peters, K. S.; *Chem. Phys. Letters*, 1983, **98**, 53. (b) Welch, J. A.; Peters, K. S.; Vaida, V.; *J. Phys. Chem.*, 1982, **86**, 1941.
- 31 (a) Simon, J. D.; Xie, X.; *J. Phys. Chem.*, 1986, **90**, 6751. (b) Simon, J. D.; Xie, X.; *J. Phys. Chem.*, 1989, **93**, 291. (c) Xie, X.; Simon, J. D.; *J. Am. Chem. Soc.*, 1990, **112**, 1130. (d) Joly, A. G.; Nelson, K. A.; *J. Phys. Chem.*, 1989, **93**, 2876.
- 32 Dobson, G. R.; Spradling, M. D.; *Inorg. Chem.*, 1990, **29**, 880.
- 33 Creaven, B. S.; George, M. W.; Ginzburg, A. G.; Hughes, C.; Kelly, J. M.; Long, C.; McGrath, I. M.; Pryce, M. T.; *Organometallics*, 1993, **12**, 3127.
- 34 (a) Zhang, S.; Zang, V.; Bajaj, H. C.; Dobson, G. R.; van Eldik, R.; *J. Organomet. Chem.*, 1990, **397**, 279. (b) Zhang, S.; Dobson, G. R.; Zang, V.; Bajaj, H. C.; van Eldik, R.; *Inorg. Chem.*, 1990, **29**, 3477. (c) Zhang, S.; Dobson, G. R.; *Organometallics*, 1992, **11**, 2447. (d) Yang, G. K.; Vaida, V.; Peters, K. S.; *Polyhedron*, 1988, **7**, 1619.
- 35 Strohmeier, W.; *Angew. Chem. Int. Ed.*, 1964, **3**, 730.
- 36 Koerner von Gustorf, E.; Grevels, F.-W.; *Fortschr. Chem. Forsch.*, 1969, **13**, 366.
- 37 Balzani, V.; Carassiti, V.; *Photochemistry of Coordination Compounds*, Academic Press, New York, 1970.

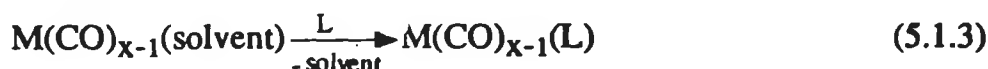
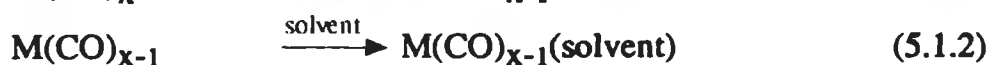
- 38 Farrell, G. A.; Ph. D. Thesis, Dublin City University, 1992.
- 39 Creaven, B. S.; Ph. D. Thesis, Dublin City University, 1989.
- 40 Crocock, B.; Ph. D. Thesis, Dublin City University, 1992.

CHAPTER 5

EXPERIMENTAL

5.1 Photolysis of metal carbonyl complexes

Photosubstitution reactions of metal carbonyl complexes are well known. The reactions usually involve photolysis of the metal carbonyl compound in a solvent medium. The solvent can range from being a donor solvent, for example, alcohol, ether, or cycloalkane to an inert solvent such as an alkane. The function of the solvent is to occupy the vacant site created by ejection of a CO molecule(s) upon photolysis. In the presence of a stronger σ -donor ligand, for example, pyridine the coordinated solvent is easily displaced, yielding $M(CO)_5(L)$ complex, (M = Cr, Mo or W) (equations 5.1.1 - 5.1.3).



Removal of the solvent ensures complete conversion of $M(CO)_{x-1}$ to $M(CO)_{x-1}(L)$.

Photolysis reactions are usually carried out under argon or nitrogen to remove any oxygen present in the system which may react with the reactive intermediate forming the corresponding metal oxides, resulting in decomposition. Also, by maintaining a constant stream of argon or nitrogen throughout the reaction process, ensures that any liberated CO is expelled, thus preventing back reaction and lengthening the photolysis time.

Photochemical substitution reactions have many advantages over thermal substitution reactions. Reactions of the former may be performed at temperatures at or below room temperature, thus permitting the isolation of relatively unstable substitution products. Also, mono- and disubstituted

products may be isolated which is very difficult to achieve in thermal substitution.

5.1.1 Photolysis apparatus

The apparatus employed in the preparation of the substitution complexes is depicted in Figure 5.1.1.1. It consists of a doubled-walled pyrex glass vessel, containing a medium pressure mercury lamp (400 watt), which is water cooled. The solutions to be photolysed are placed in the external vessel and are left stirring throughout the photolysis. Air and carbon monoxide (liberated during the reactions) are expelled by bubbling argon or nitrogen through the solution. The products were isolated by removing the solvent under reduced pressure and purified by recrystallisation and/or classical chromatography, depending on the air sensitivity of the compounds. Identification was obtained by IR, UV/visible and NMR spectroscopy.

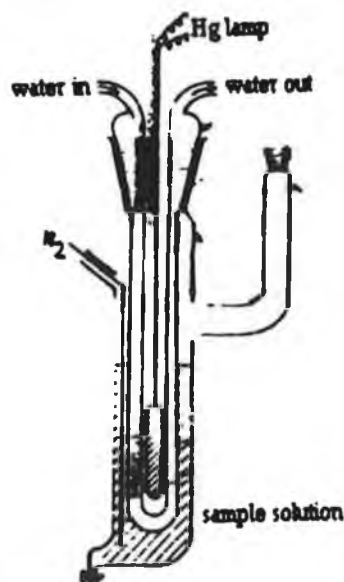


Figure 5.1.1.1 Photolysis apparatus used for the preparation of substituted metal carbonyl complexes.

5.1.2 Materials

$\text{Cr}(\text{CO})_6$ (Strem Chemicals Inc.), 2-methylpyridine, 3-methylpyridine, 4-methylpyridine (BDH), 2-phenylpyridine, 4-phenylpyridine, 2-chloropyridine, 3-chloropyridine, 3-methyl-2-phenylpyridine, and pyridine (Aldrich Chemicals Co.) were used without further purification. 4-Acetylpyridine (Reilly Chemicals) was distilled before use while $\text{ArCr}(\text{CO})_3$ was synthesised (Section 5.1.4.2). The following solvents were all of spectroscopic grade and were used without further purification: cyclohexane, methylcyclohexane, pentane, hexanes, and n-heptane (Aldrich Chemicals Co.). Toluene was distilled from LiAlH_4 and stored over sodium wire under argon, THF was distilled from LiAlH_4 and stored over calcium hydride (CaH_2) under argon, while ethanol was purified by distillation. Argon (IIG) and carbon monoxide (IIG) were used without further purification.

5.1.3 Equipment

UV/visible spectra were recorded on a Hewlett Packard 8425a spectrophotometer using quartz cells, of pathlength, 1cm. Infrared spectra were obtained from either a Perkin Elmer 983-G IR or a Nicolet 205 FT-IR spectrometer, using sodium chloride solution cells (pathlength = 0.1mm) or as KBr pellets. NMR measurements were performed on a Bruker AC-400 MHz spectrometer.

5.1.4 Syntheses of $\text{Cr}(\text{CO})_5(\text{L})$ and $(\eta^6\text{-C}_6\text{H}_6)\text{Cr}(\text{CO})_2(\text{L})$ complexes, where L = pyridine (py) or 4-acetylpyridine (4-Acpy)

5.1.4.1 Preparation of $\text{Cr}(\text{CO})_5(\text{py})$

The yellow complex $\text{Cr}(\text{CO})_5(\text{py})$ was prepared via the tetrahydrofuran complex, $\text{Cr}(\text{CO})_5(\text{THF})$. A THF solution (250ml) containing $\text{Cr}(\text{CO})_6$ (0.5g, 2.3mmol) and a 10-fold molar excess of pyridine was deoxygenated by purging with argon for 15 minutes prior to irradiation and then irradiated with a 400 watt medium pressure mercury lamp (Applied Photophysics) for 3.5hrs. The solution was continuously purged with argon throughout irradiation to avoid any oxidation effects, and the reaction process was monitored by IR spectroscopy. The solvent was removed under reduced pressure and the residue redissolved in purged THF and filtered through silica, to remove unreacted hexacarbonyl. Recrystallisation at -50°C in a 1:2 diethyl ether/pet. ether solution yielded 0.3g (49%) of the yellow crystalline product, $\text{Cr}(\text{CO})_5(\text{pyridine})$.

IR: ν_{CO} , cyclohexane, 2067.7(w), 1919(m), 1938(s) cm^{-1} .

UV: λ_{max} , cyclohexane, 390nm.

$^1\text{H NMR}$ (CDCl_3): δ 7.3 (m, 2H), 7.7 (t, 1H), 8.5 (d, 2H).

5.1.4.2 Preparation of $(\eta^6\text{-C}_6\text{H}_6)\text{Cr}(\text{CO})_3$

Benzene chromium tricarbonyl $\{(\eta^6\text{-C}_6\text{H}_6)\text{Cr}(\text{CO})_3\}$ was synthesised according to a method described by Mahaffy *et al.* [1]. $\text{Cr}(\text{CO})_6$ (4g, 18mmol), benzene (20ml, 0.2mol), butyl ether (125ml) and THF (10ml) in a 250ml round bottom flask, fitted with a gas inlet and a simple reflux condenser were purged with argon for 30 minutes and then heated to reflux for 44hrs. The yellow

solution was then filtered through silica using a sintered-glass crucible and the filtrate removed under vacuum. The remaining residue was washed with light pet. ether (20ml) and recrystallisation from diethyl ether/pet. ether yielded 1.5g (40%) of yellow crystalline $(\eta^6\text{-C}_6\text{H}_6)\text{Cr}(\text{CO})_3$.

IR: ν_{CO} , ether, 1981(s), 1913(s) cm^{-1} .

M.P.: 159 - 160°C.

^1H NMR (CDCl_3): δ 5.33 (s, 6H).

5.1.4.3 Preparation of $(\eta^6\text{-C}_6\text{H}_6)\text{Cr}(\text{CO})_2(\text{py})$

Benzene chromium dicarbonyl pyridine $\{(\eta^6\text{-C}_6\text{H}_6)\text{Cr}(\text{CO})_2(\text{py})\}$ was synthesised according to the method described by Kaim *et al.* [2]. $(\eta^6\text{-C}_6\text{H}_6)\text{Cr}(\text{CO})_3$ (0.2g, 0.9mmol) and pyridine (75 μl , 0.9mmol) were dissolved in 200ml of toluene and irradiated with a 400 watt medium pressure Hg lamp (Applied Photophysics) at 0°C for 3hrs under argon. This resulted in a change in solution colour from yellow to red. After a further 3hrs of continued stirring in the dark, the solvent and unreacted pyridine were removed under vacuum. Recrystallisation of the solid residue in toluene/n-hexane (1/2) at -30°C yielded 0.12g (50%) of red crystalline $(\eta^6\text{-C}_6\text{H}_6)\text{Cr}(\text{CO})_2(\text{py})$. This complex is very air and light sensitive.

IR: ν_{CO} , KBr pellet, 1799(s), 1820(s) cm^{-1} .

UV: λ_{max} , toluene, 476nm.

^1H NMR (CDCl_3): δ 4.68 (br, s, 6H), 6.84 (br, m, 2H), 7.27 (br, t, 1H), 8.99 (br, d, 2H).

5.1.4.4 Preparation of $(\eta^6\text{-C}_6\text{H}_6)\text{Cr}(\text{CO})_2(4\text{-Acpy})$

$(\eta^6\text{-C}_6\text{H}_6)\text{Cr}(\text{CO})_3$ (0.15g, 0.7mmol) and *cis*-cyclooctene (2ml, 15mmol) were dissolved in 180ml n-hexane. The solution was purged with argon for 30 minutes prior to irradiation at 0°C for 1.5hrs under argon with a 400 watt medium pressure Hg lamp (Applied Photophysics). 4-Acetylpyridine (150 μ l, 1.4mmol) upon addition to the orange solution, reacted instantaneously producing a dark blue solution. After 2hrs of continued stirring in the dark, the dark blue product precipitated out and was washed with cyclohexane. Recrystallisation was very difficult because of the extreme sensitivity of the compound to both light and air. Accurate NMR measurements could not be obtained because of the instability of the complex in solution.

IR: ν_{CO} , KBr pellet, 1886.3(s), 1798(m) cm^{-1} , $\nu_{\text{C=O}}$, 1686 cm^{-1} .

UV: λ_{max} , cyclohexane, 666nm.

5.2 Laser flash photolysis

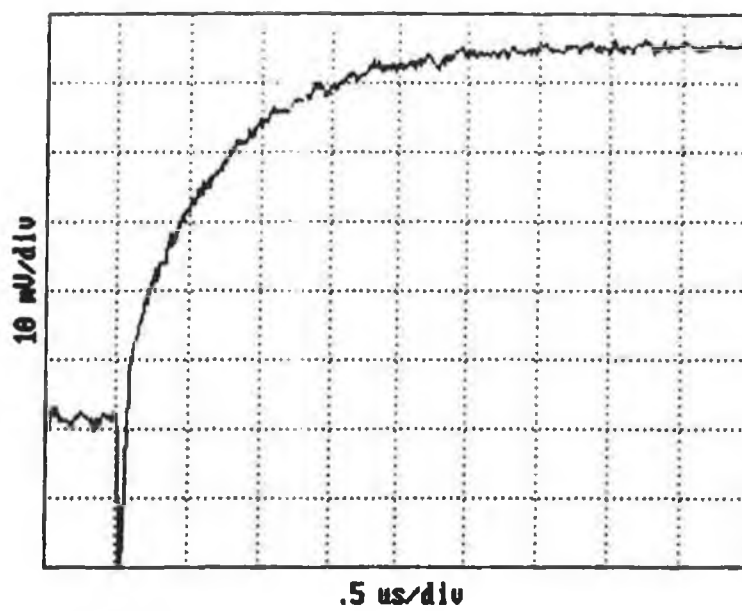
This technique has become very important in the initiation and study of primary photochemical processes. The principle of flash photolysis is the generation of a high concentration of a short-lived intermediate using a very high intensity pulse of radiation of very short duration. The transient species whose lifetime may vary from picoseconds (for vibrational relaxation in solution) to seconds (for some radicals and long-lived chemical species) can be observed by optical absorption or emission spectroscopy. The process can be followed by photographing the emission spectrum using a spectrograph or by the absorption spectrum by triggering an analytical beam passing through the reaction cell to flash at a predetermined time interval after the initial flash.

Alternatively, the process may be followed kinetically by monitoring the emission or absorption at a particular wavelength using a detector coupled to an oscilloscope with a time-based sweep. The latter process was used in this study. Typical traces for the transient absorption and decay are displayed in Figure 5.2.1. The polychromatic nature of the radiation from conventional discharge tubes increases the possibility of generating more than one emitting or absorbing species. The problem is alleviated with lasers because of the monochromatic nature of their irradiation. Other advantages of lasers are that the laser pulse is of very short duration (Q-switching) and is highly reproducible. The range of the laser source can be increased from its fundamental harmonic by employing frequency doubling. Background noise on the oscilloscope trace produced by low intensity sources can be overcome by using a high intensity monitoring beam. This interference can be reduced further by repeating the measurement many times and averaging the results. Spectra of the decay of an intermediate can be obtained point by point by changing the wavelength on the monitoring monochromator and recording a series of readings at a fixed time interval after the flash.

5.2.1 Laser flash photolysis system with UV/visible monitoring

The excitation source used was a Q-switched Nd-YAG (Nd^{3+} doped yttrium aluminium garnet) laser (Spectron Laser Systems) with a fundamental frequency at 1064nm. By employing frequency doubling a second, third or fourth harmonic frequency can be generated at 532, 355 or 266nm respectively. The energy of the pulse can be varied by altering the voltage across the amplifier flash tube. At the frequency employed, 355nm, the energy output was typically 30 - 40 mJ per pulse with a pulse duration of 11ns. The circular laser

(a)



(b)

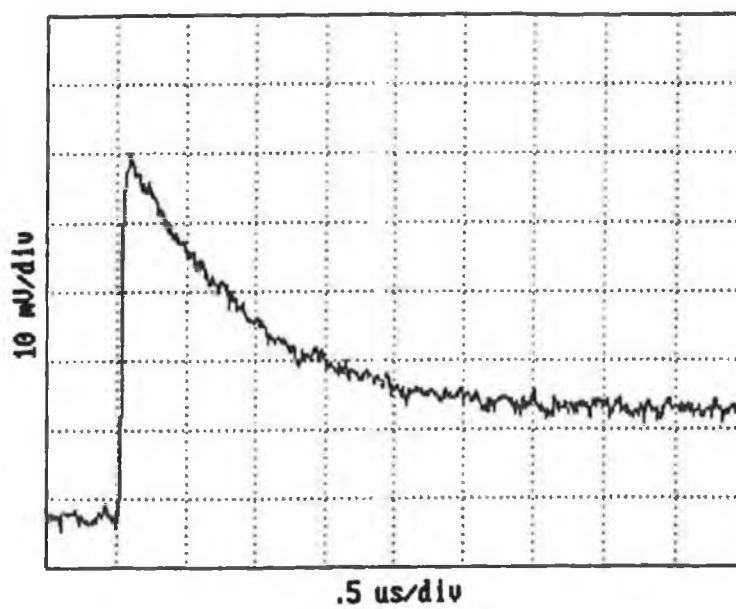


Figure 5.2.1 Typical traces obtained for (a) the absorption and (b) the decay of a transient species.

pulse (ca. 4mm in diameter) is directed *via* two Pellin-Broca prisms onto the sample cuvette. As the pulse passes through the power meter, situated between the second Pellin-Broca prism and the sample holder, the oscilloscope is triggered.

The UV/visible monitoring source was an air cooled 250 watt Xenon arc lamp (Applied Photophysics 40804). The laser beam and the UV light source were arranged so that a crossbeam was formed at the sample holder. A UV filter (cut-off 400 or 345nm) was placed between the Xenon arc lamp and the sample holder to minimise unnecessary photolysis of the sample by the monitoring beam. The output of the lamp was focussed on the front of the sample cuvette and the emerging beam was directed onto the slit of an f/3.4 monochromator (Applied Photophysics) *via* a circular lens. The monochromator contained a grating blazed at 300 or 500nm depending on the wavelength range being monitored. The exit slit of the monochromator possessed a five stage photomultiplier operating at 850 volts which detected absorbance changes and relayed the output to a transient digitiser *via* a variable load resistor. The digitiser, a Phillips PM 3311 storage oscilloscope (later replaced by a Hewlett Packard 54510A model) was connected to an Olivetti PCS 286/287 microcomputer *via* an IEEE-488 interface. The resultant data were stored on floppy disk. A schematic diagram of the layout of the flash photolysis system is shown in Figure 5.2.1.1. In house programs were used to analyse the data. The resultant transients were analysed by first-order kinetics. Each transient signal was an average of at least three shots. A basic outline of the program, allowing transients to be recorded, stored and analysed is described in the following section.

Initially, I_0 , the amount of light passing through the solution before the laser flash, is recorded. This is obtained by recording the voltage corresponding

to that light detected by the photomultiplier tube when the shutter is open less the voltage generated by stray light. I is directly proportional to this voltage. The laser is fired with the shutter open and this firing of the laser triggers the oscilloscope. Thus, the resulting trace shows the change in voltage with time which corresponds to the change in optical density and ultimately, the concentration of the sample as species form or decay away. Typical traces are shown in Figure 5.2.1. The trace obtained is then stored, together with the time-base and the voltage settings of the oscilloscope. The stored data can be used to calculate I_t , the amount of light being transmitted at any time t . An absorbance spectrum of the transient species is obtained by recording transient signals at different monitoring wavelengths. The absorbance readings can then be calculated at any time after the flash. The oscilloscope is set at a delay to enable the absorbance (corresponding to the absorbance of the parent material at that wavelength) to be recorded before the laser pulse. A transient difference spectrum is then obtained from a plot of absorbance *versus* wavelength.

For the determination of activation parameters, the sample cell was immersed in a thermostated water bath and allowed to be equilibrated for 15 minutes. I_0 was measured at the monitoring wavelength and the system readied for analysis prior to the sample being heated so that the transient data could be recorded immediately on removing the cell from the water bath. The sample was heated incrementally from 15 - 40°C, with a transient being recorded for analysis every 5°C. In the case of pentane as solvent, because of its low boiling point, the temperature range used was 0 - 30°C. It was assumed that the concentration of CO remained constant over the temperature ranges studied.

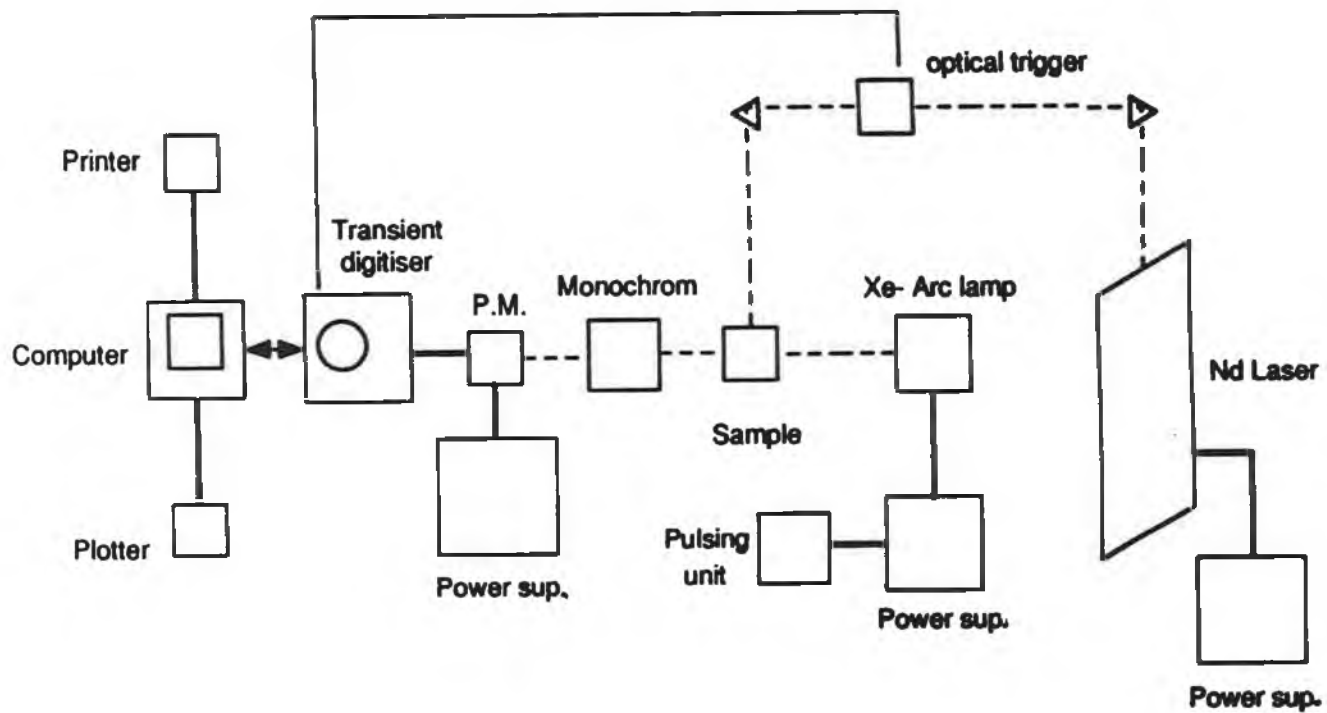


Figure 5.2.1.1 A schematic layout of the laser flash photolysis system.

5.2.2 Sample preparation for flash photolysis

5.2.2.1 Preparation of $\text{Cr}(\text{CO})_6$ in various solvents

Solutions of the metal carbonyl complex in the various solvents, S, (S = cyclohexane, methylcyclohexane, pentane, hexanes and heptane) were adjusted until an absorbance reading of between 0.6 and 2.0 absorbance units (AU) was obtained at the excitation wavelength (355nm). The concentration of the carbonyl compound in solution was then determined from its UV/visible absorption by utilising its previously determined molar extinction coefficient (ϵ) and the Beer-Lambert law (Section 5.7). Absorbance measurements were recorded on a Hewlett-Packard 8452a UV/visible spectrophotometer. The solutions were degassed by three cycles of a freeze-pump-thaw procedure followed by a liquid pumping stage (to remove undesired contaminants, for example, water) in a specially designed degassing bulb with a fluorescence cell attached. Argon or carbon monoxide was added to prevent boiling of the solutions at above ambient temperatures and to check the reversibility of the photochemical reactions observed. The concentration of carbon monoxide was calculated to be 0.9, 0.9*, 1.6, 1.3 and 1.2×10^{-2} mol dm⁻³ in cyclohexane, methylcyclohexane, pentane, hexanes and heptane respectively under 1.0 atmosphere of CO at 298K (see Section 5.5). *The solubility of CO in methylcyclohexane is taken to be the same as that in cyclohexane. The concentration of CO was assumed to remain constant for the experiments in which the temperature was varied.

5.2.2.2 Preparation of $\text{Cr}(\text{CO})_6$ in the presence of excess ligand L, (L = pyridine or substituted pyridine)

The photolysis studies involving excess ligand were performed in both cyclohexane and toluene. Solutions of the metal carbonyl complex were prepared such that an optical density (O.D.) of between 0.6 and 2.0AU was obtained at 354nm. The concentration of the carbonyl complex was calculated from the previously determined molar extinction coefficients (Section 5.7). Pseudo-first-order conditions were maintained by the presence of a minimum 10-fold excess of ligand over the metal carbonyl complex concentration. All the solutions, in 1x1 cm quartz cuvettes were purged with argon for 15 minutes prior to being sealed.

5.2.2.3 Preparation of $\text{ArCr}(\text{CO})_2(\text{L})$ complexes, (L = py, 4-Acpy)

The same procedure as that described in 5.2.2.1 was used with cyclohexane as solvent. As these complexes are unstable in solution, a known concentration of excess ligand was added to prolong their lifetimes.

5.3 Stopped-Flow technique

The stopped-flow technique is the most popular of all the flow methods, which also includes continuous flow and quenched flow techniques. The flow method, invented by Hartridge and Roughton in 1923 was the first technique used in the investigation of fast reactions [3]. The principle of the method is that the concentration of the reactant is measured as a function of distance along the flow tube, by measuring the absorption or some other physical property such

as conductivity at different distances down the tube. The rate of change of concentration of reactant with distance is related to the rate of reaction. A major problem with this method was the large volume of fluid consumed. This obstacle was overcome by modification of the system and development of the stopped-flow apparatus. In this case a steady flow is established and is then brought to a sudden halt, after which the subsequent concentration changes are monitored in real-time. This technique has been embodied in a commercial instrument and as only a small amount of reagents are required, the system is applicable for biological as well as chemical kinetic studies.

5.3.1 Stopped-Flow apparatus

A schematic diagram of the stopped-flow apparatus (SFA-11, Rapid Kinetic Accessory) employed in the kinetic studies is illustrated in Figure 5.3.1.1. The reagent solutions, stored in a pair of 5ml reservoirs were admitted to the 2ml drive syringes through the 3-port valves. The valves were then turned to connect the drive syringes to the flow circuit and by manual pressure on the drive plate, 0.2ml of solution was rapidly expelled from each syringe. As these solutions mixed in the black fused silica cell incorporated into the spectrophotometer thermostated cell holder, the contents remaining from the previous run were displaced. The solution expelled from the cell passed through a third tube back to the drive unit, filling a 2ml stopping syringe. Filling of this syringe stops the flow and activates a microswitch, which triggers the spectrophotometer to measure the absorbance of the freshly mixed solution in the observation cell. The pathlength of the cell used was 10mm.

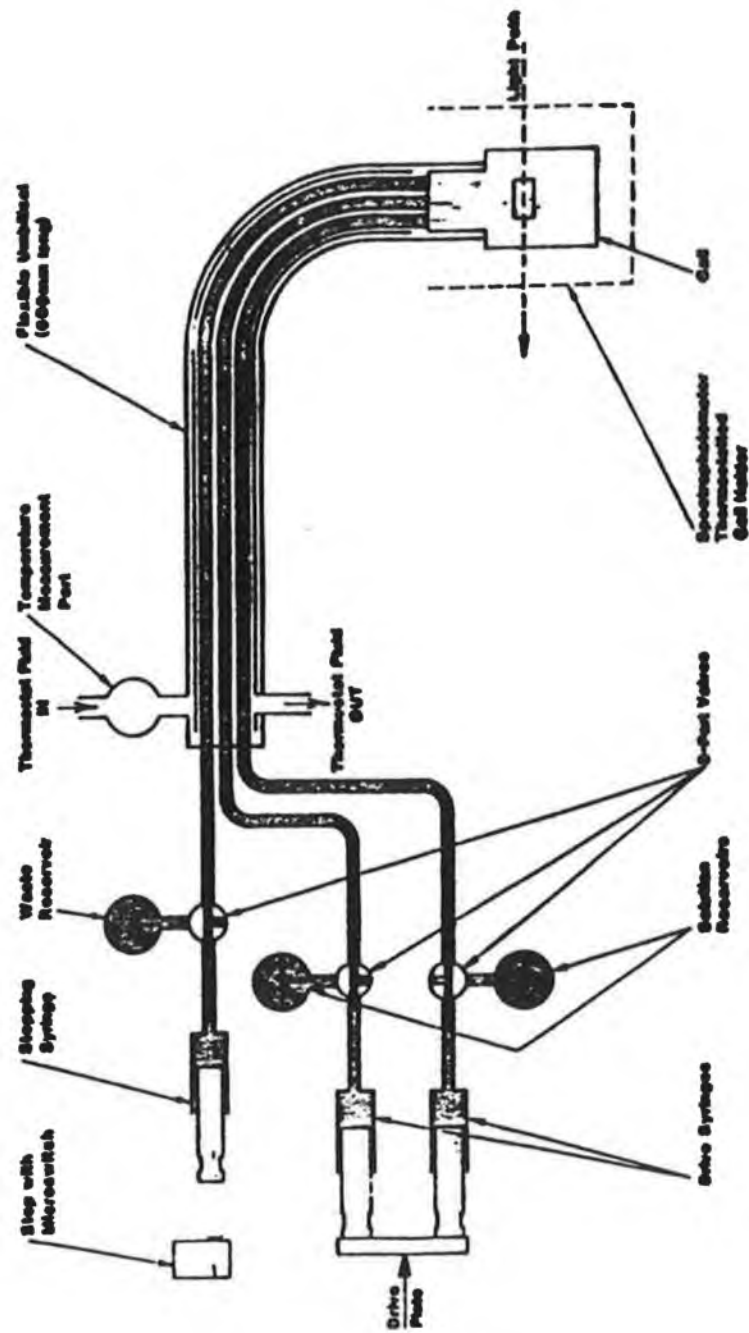


Figure 5.3.1.1 A schematic diagram of the stopped-flow apparatus.

5.3.2 Sample preparation

5.3.2.1 Preparation of $\text{Cr}(\text{CO})_6$ with a range of ligand concentrations

Using THF as solvent, a range of concentrations (10^{-2}M - 2.0M) were prepared for each ligand. A metal complex concentration (10^{-3}M) was used, ensuring pseudo-first-order conditions were maintained. All the solutions, in quartz cuvettes were purged with argon for 10 minutes before use and then sealed with serum caps. The degassed chromium hexacarbonyl solution was converted to the pentacarbonyl solvent adduct upon irradiation for 2 minutes by a 100 watt UV lamp. This process was accompanied by a simultaneous change in solution colour from colourless to yellow. The solvated pentacarbonyl species and the ligand solutions were extracted from the cuvettes *via* the serum caps by disposable syringes which were then installed in the stopped-flow apparatus as solution reservoirs (Figure 5.3.1.1). The same procedure was used for ethanol as solvent.

5.3.2.2 Preparation of solutions for activation studies

The procedure used is that described in 5.3.2.1. The activation parameters were determined at high and low ligand concentrations (1.0M and $5 \times 10^{-2}\text{M}$ respectively). The observation cell, positioned in the spectrophotometer thermostated cell holder was equilibrated for 15 minutes prior to measurements being recorded. The reactions were monitored over a $15 - 50^\circ\text{C}$ range at increments of 5°C . Experiments were conducted in both THF and ethanol, and the activation parameters were calculated according to equations 5.4.1 and 5.4.2.

5.3.3 Determination of kinetic parameters

Repetitive scans at fixed time intervals were obtained for each reaction. Employing a Hewlett-Packard kinetics package which utilises a curve-fitting routine for first-order kinetics, the best first-order fit at a selected monitoring wavelength (380 or 460nm for the formation of $\text{Cr}(\text{CO})_5(\text{L})$ or the decay of $\text{Cr}(\text{CO})_5(\text{S})$, (S = solvent) respectively) for each reaction was obtained and k_{obs} (the pseudo-first-order rate constant) calculated. The observed data were fitted to the expression $A = a_1 + a_2 e^{-kt}$, where A is the absorbance at time t, a_1 and a_2 are constants related to the initial and final absorbances at the monitoring wavelength, and k is the observed first-order rate constant (k_{obs}). Data obtained at 380 and 460nm, and fitted with single exponential curves are presented in Figure 5.3.3.1. The data used in the construction of the plots is an average of three measurements.

5.4 Determination of activation parameters

Activation parameters for the metal carbonyl complexes were calculated from the Arrhenius and Eyring equations [4, 5] (equations 5.4.1 and 5.4.2 respectively).

The Arrhenius equation is given by:

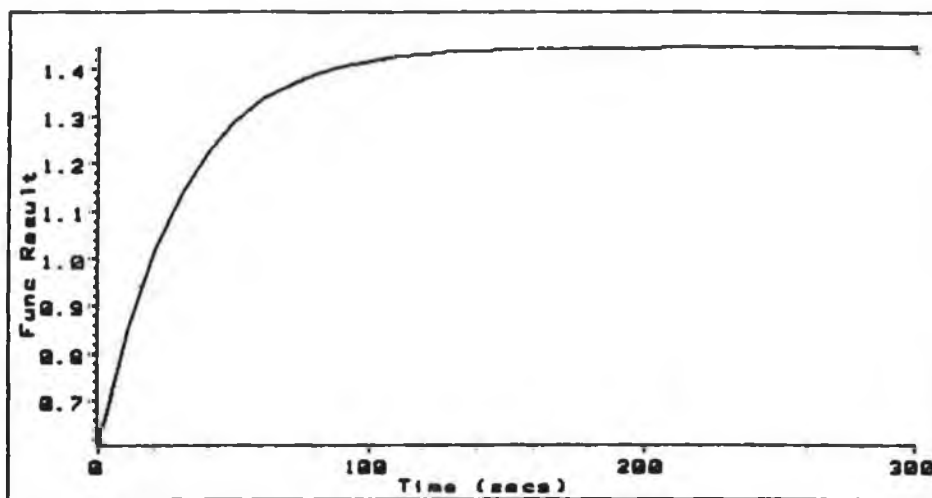
$$\ln k = \ln A - E_a^\ddagger/RT \quad (5.4.1)$$

where A = Frequency factor

E_a^\ddagger = activation energy of the activated complex (kJmol^{-1})

R = Universal gas constant

(a)



(b)

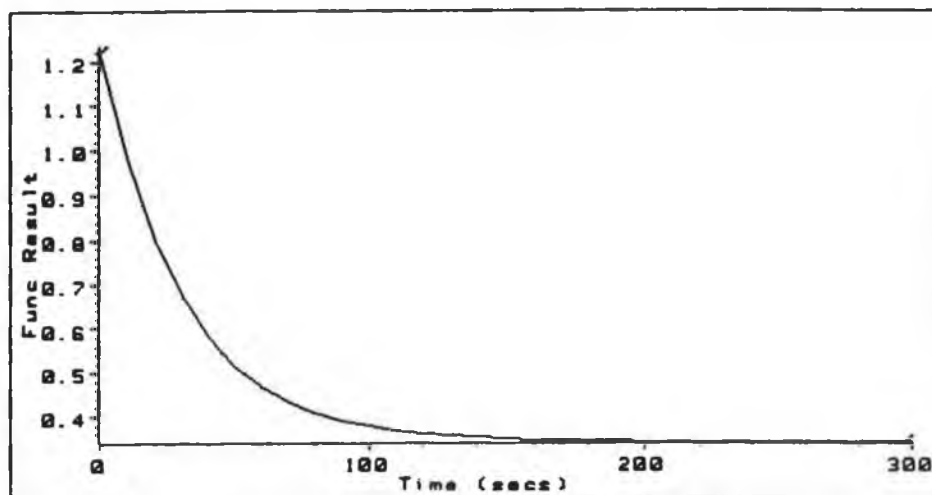


Figure 5.3.3.1 Plots of variation in absorbance *versus* time for (a) the formation of $\text{Cr}(\text{CO})_5(\text{py})$ (380nm) and (b) the decay of $\text{Cr}(\text{CO})_5(\text{THF})$ (460nm), fitted with single exponential curves.

T = absolute temperature (°K)

The rate constant is dependent on the energy of activation. A plot of $\ln k_{\text{obs}}$ versus $1/T$ should yield a straight line of intercept $\ln A$ and slope = $-E_a^\ddagger/R$, from which the activation energy can be determined.

From transition-state theory in thermodynamics the Eyring equation is obtained.

$$k_{\text{obs}} = (kT/h) e^{-\Delta G^\ddagger/RT}$$

if $\Delta G^\ddagger = \Delta H^\ddagger - T\Delta S^\ddagger$

then

$$k_{\text{obs}} = (kT/h) e^{\Delta S^\ddagger/R} e^{-\Delta H^\ddagger/RT}$$

and

$$\ln k_{\text{obs}}/T = \ln k/h + \Delta S^\ddagger/R - \Delta H^\ddagger/RT \quad (5.4.2)$$

where ΔG^\ddagger = Gibbs free energy change of activation

ΔH^\ddagger = enthalpy change of activation (kJ mol^{-1})

ΔS^\ddagger = entropy change of activation ($\text{JK}^{-1}\text{mol}^{-1}$)

k = Boltzmann's constant

h = Planck's constant

T = absolute temperature (°K)

k_{obs} = observed rate constant

A plot of $\ln (k_{\text{obs}}/T)$ versus $1/T$ should yield a straight line of slope = $-\Delta H^\ddagger/R$ and intercept = $\ln k/h + \Delta S^\ddagger/R$.

Therefore ΔH^\ddagger and ΔS^\ddagger can be obtained from the slope and the intercept respectively.

5.5 Determination of solubility of CO in alkane solvents

The solubilities of CO in the alkane solvents were determined using the Ostwald coefficients, reported by Makranczy *et al.* [6]. The calculations for pentane as solvent at 25°C, are given below, as a representative example.

$$\begin{aligned}\text{Molar volume of gas} &= 22.4/273(^{\circ}\text{K}) \times \text{temp. at which solubility is required} \\ &= 22.4/273 \times 298 \\ &= 24.4\end{aligned}$$

Ostwald coefficient for pentane (C_5) = 0.395ml CO/ml pentane/atmosphere

Therefore,

$$\begin{aligned}\text{Solubility of CO in pentane at } 25^{\circ}\text{C} &= 0.395/24.4 \\ &= 1.6 \times 10^{-2} \text{ M at 1 atmosphere.}\end{aligned}$$

5.6 Determination of quantum yields for $\text{Cr}(\text{CO})_6$ in alkane solvents

The concentration of $\text{Cr}(\text{CO})_6$ solution was adjusted until approximately the same in all the solvents. An excess, but constant concentration of pyridine was used throughout, in all the solvents. Samples were purged with argon for 10 minutes and then sealed. Irradiation at 313nm was obtained by using a 200 watt mercury lamp (Applied Photophysics), coupled with an interference Corning 7-54 filter and a solution filter of an aqueous solution of potassium

chromate (K_2CrO_4 , 0.2g\text{L} in 1% NaOH). The samples were arranged in a merry-go round apparatus (Applied Photophysics Ltd.), and irradiated for a fixed period of time. UV/visible absorption spectra of each sample were obtained after fixed periods of irradiation. The rate of formation of $Cr(CO)_5(py)$ in each solvent was compared to that in cyclohexane, for which the quantum yield had previously been determined [7]. The extinction coefficients for the product, $Cr(CO)_5(py)$ are known to be solvent dependent, and therefore had to be accurately determined. However, within the same group of solvents, for example, alkanes, the differences between solvents is very small and therefore all the product yields were measured at 390nm.

5.7 Determination of extinction coefficients

In order to calculate the concentration of the metal carbonyl complex in solution, knowing the absorbance at a particular wavelength, and utilising the Beer-Lambert law (equation 5.7.1), the molar extinction coefficient in that solvent and at that particular wavelength must be known.

The Beer-Lambert law is given by:

$$A = \epsilon cl \quad (5.7.1)$$

where A = Absorbance at a particular wavelength (AU)

ϵ = Molar extinction coefficient ($dm^3mol^{-1}cm^{-1}$)

c = Concentration ($mol\ dm^{-3}$)

l = Pathlength of the cell (cm)

The data used in the determination of the extinction coefficients is given in Appendix C.

5.8 References

- 1 Mahaffy, C. A. L.; Pauson, P. L.; *Inorg. Synth.*, 1979, **19**, 154.
- 2 Kaim, W.; Roth, T.; Olbrich-Deussner, B.; Gross-Lannert, R.; Jordanov, J.; Roth, E. K. H.; *J. Am. Chem. Soc.*, 1992, **114**, 5693.
- 3 Bradley, J. N.; *Fast Reactions*, Clarendon Press, Oxford, 1975.
- 4 Atkins, P. W.; *Physical Chemistry*, Oxford University Press, 1982.
- 5 Avery, H. E.; *Basic Reaction Kinetics and Mechanisms*, Macmillian, London, 1986.
- 6 (a) Makranczy, J.; Megyery-Balog, K.; Ruzs, L.; Patyi, L.; *Hungarian J. Indust. Chem.*, 1976, **4**, 269. (b) Patyi, L.; Furmer, I. E.; Makranczy, J.; Sadilenko, A. S.; Stepanova, Z. G.; Berengarten, M.G.; *Zh. Prikl. Khim.*, 1978, **51**, 1296.
- 7 (a) Nasielski, J.; Colas, A.; *Inorg. Chem.*, 1978, **17**, 237. (b) Nasielski, J.; Colas, A.; *J. Organomet. Chem.*, 1975, **101**, 215.

APPENDIX A

**DATA FOR THE DETERMINATION OF
ACTIVATION PARAMETERS**

(a) Cyclohexane

$(1/T) \times 10^3 \text{ (K}^{-1}\text{)}$	$\text{Ln } k_{\text{obs}}/[\text{CO}]^a$	$\text{Ln } k_{\text{obs}}/[\text{CO}]^a T$
3.46	14.59	8.93
3.41	14.70	9.02
3.36	14.89	9.19
3.30	15.08	9.37
3.24	15.29	9.56
3.19	15.42	9.67
3.15	15.50	9.74
3.10	15.64	9.86

$a [\text{CO}] = 0.9 \times 10^{-2} \text{ mol dm}^{-3}$

(b) Methylcyclohexane

$(1/T) \times 10^3 \text{ (K}^{-1}\text{)}$	$\text{Ln } k_{\text{obs}}/[\text{CO}]^a$	$\text{Ln } k_{\text{obs}}/[\text{CO}]^a T$
3.45	14.92	9.25
3.41	15.04	9.36
3.38	15.21	9.52
3.34	15.32	9.62
3.31	15.40	9.69
3.28	15.53	9.81
3.25	15.57	9.84
3.21	15.72	9.98
3.17	15.78	10.03

$a [\text{CO}] = 0.9 \times 10^{-2} \text{ mol dm}^{-3}$

(c) Pentane

$(1/T) \times 10^3 \text{ (K}^{-1}\text{)}$	$\text{Ln } k_{\text{obs}}/[\text{CO}]^a$	$\text{Ln } k_{\text{obs}}/[\text{CO}]^a T$
3.66	14.59	8.98
3.58	14.79	9.15
3.53	14.91	9.26
3.50	15.04	9.38
3.46	15.12	9.46
3.41	15.20	9.52
3.38	15.25	9.56
3.35	15.31	9.61

$^a [\text{CO}] = 1.6 \times 10^{-2} \text{ mol dm}^{-3}$

(d) Hexanes

$(1/T) \times 10^3 \text{ (K}^{-1}\text{)}$	$\text{Ln } k_{\text{obs}}/[\text{CO}]^a$	$\text{Ln } k_{\text{obs}}/[\text{CO}]^a T$
3.44	15.33	9.66
3.40	15.44	9.75
3.36	15.55	9.85
3.30	15.74	10.03
3.25	15.86	10.13
3.19	16.03	10.28
3.14	16.22	10.45

$^a [\text{CO}] = 1.3 \times 10^{-2} \text{ mol dm}^{-3}$

(e) Heptane

$(1/T) \times 10^3 \text{ (K}^{-1}\text{)}$	$\text{Ln } k_{\text{obs}}/[\text{CO}]^a$	$\text{Ln } k_{\text{obs}}/[\text{CO}]^a T$
3.46	15.47	9.81
3.41	15.56	9.88
3.35	15.79	10.09
3.29	15.90	10.18
3.24	16.08	10.35
3.19	16.31	10.56
3.15	16.45	10.69
3.10	16.52	10.74

$^a [\text{CO}] = 1.2 \times 10^{-2} \text{ mol dm}^{-3}$

Table A1: Data for the determination of energy, enthalpy and entropy of activation for the decay of $\text{Cr}(\text{CO})_5(\text{S})$, S = cyclohexane (a), methylcyclohexane (b), pentane (c), hexanes (d) and heptane (e), monitored at 500nm.

(a) Pyridine

$(1/T) \times 10^3 \text{ (K}^{-1}\text{)}$	$\text{Ln } k_2^a$	$\text{Ln } k_2^a/T$
3.50	17.71	12.05
3.46	17.73	12.06
3.41	17.84	12.16
3.37	17.92	12.23
3.33	17.95	12.24
3.30	18.00	12.29
3.27	18.10	12.38

$^a k_2 = k_{\text{obs}}/[\text{L}], [\text{L}] = 6 \times 10^{-2} \text{ M}$

(b) 3-Methyl-2-Phenylpyridine

$(1/T) \times 10^3 \text{ (K}^{-1}\text{)}$	$\text{Ln } k_2^a$	$\text{Ln } k_2^a/T$
3.50	17.23	11.57
3.46	17.30	11.63
3.43	17.35	11.68
3.39	17.43	11.74
3.36	17.54	11.84
3.31	17.60	11.89
3.28	17.68	11.96
3.25	17.74	12.01
3.21	17.82	12.08

$^a k_2 = k_{\text{obs}}/[L], [L] = 6 \times 10^{-2}\text{M}$

(c) 2-Phenylpyridine

$(1/T) \times 10^3 \text{ (K}^{-1}\text{)}$	$\text{Ln } k_2^a$	$\text{Ln } k_2^a/T$
3.50	16.36	10.70
3.46	16.49	10.80
3.43	16.52	10.84
3.39	16.59	10.90
3.36	16.67	10.98
3.32	16.83	11.12
3.27	16.98	11.26
3.21	17.11	11.37

$^a k_2 = k_{\text{obs}}/[L], [L] = 6 \times 10^{-2}\text{M}$

(d) 4-Phenylpyridine

$(1/T) \times 10^3$ (K ⁻¹)	$\text{Ln } k_2^a$	$\text{Ln } k_2^a/T$
3.49	17.74	12.08
3.46	17.79	12.12
3.39	17.93	12.25
3.36	17.96	12.26
3.31	18.06	12.35
3.24	18.23	12.50

$$^a k_2 = k_{\text{obs}}/[L], [L] = 6 \times 10^{-2}\text{M}$$

(e) 2-Chloropyridine

$(1/T) \times 10^3$ (K ⁻¹)	$\text{Ln } k_2^a$	$\text{Ln } k_2^a/T$
3.51	17.50	11.85
3.47	17.68	12.02
3.41	17.74	12.06
3.36	17.92	12.23
3.32	18.03	12.33
3.28	18.15	12.43
3.24	18.23	12.50
3.20	18.38	12.64

$$^a k_2 = k_{\text{obs}}/[L], [L] = 6 \times 10^{-2}\text{M}$$

(f) 3-Chloropyridine

$(1/T) \times 10^3 \text{ (K}^{-1}\text{)}$	$\text{Ln } k_2^a$	$\text{Ln } k_2^a/T$
3.51	16.91	11.25
3.46	17.01	11.35
3.41	17.14	11.46
3.39	17.18	11.50
3.34	17.28	11.58
3.31	17.32	11.61
3.26	17.54	11.82
3.22	17.63	11.89

$$^a k_2 = k_{\text{obs}}/[L], [L] = 6 \times 10^{-2}\text{M}$$

(g) 2-Picoline

$(1/T) \times 10^3 \text{ (K}^{-1}\text{)}$	$\text{Ln } k_2^a$	$\text{Ln } k_2^a/T$
3.50	16.98	11.33
3.46	17.03	11.37
3.41	17.14	11.46
3.38	17.24	11.55
3.32	17.34	11.64
3.28	17.40	11.68
3.24	17.53	11.80
3.19	17.65	11.91

$$^a k_2 = k_{\text{obs}}/[L], [L] = 6 \times 10^{-2}\text{M}$$

(h) 3-Picoline

$(1/T) \times 10^3 \text{ (K}^{-1}\text{)}$	$\text{Ln } k_2^a$	$\text{Ln } k_2^a/T$
3.39	17.99	12.30
3.36	18.02	12.33
3.30	18.17	12.45
3.26	18.25	12.53
3.22	18.32	12.58
3.16	18.44	12.68

$$^a k_2 = k_{\text{obs}}/[L], [L] = 6 \times 10^{-2}\text{M}$$

(i) 4-Picoline

$(1/T) \times 10^3 \text{ (K}^{-1}\text{)}$	$\text{Ln } k_2^a$	$\text{Ln } k_2^a/T$
3.48	18.67	13.01
3.44	18.77	13.10
3.40	18.84	13.16
3.36	18.96	13.27
3.30	19.01	13.30
3.27	19.08	13.35
3.24	19.14	13.41
3.20	19.22	13.48

$$^a k_2 = k_{\text{obs}}/[L], [L] = 6 \times 10^{-2}\text{M}$$

Table A2: Data for the determination of energy, enthalpy and entropy of activation for the reaction of $\text{Cr(CO)}_5(\text{cyclohexane})$ with L, forming $\text{Cr(CO)}_5(\text{L})$, L = py (a), 3-Me-2-Phpy (b), 2-Phpy (c), 4-Phpy (d), 2-Clpy (e), 3-Clpy (f), 2-Pic (g), 3-Pic (h) and 4-Pic (i), monitored at 510nm.

(a) Pyridine

$(1/T) \times 10^3 \text{ (K}^{-1}\text{)}$	$\text{Ln } k_2^a$	$\text{Ln } k_2^a/T$
3.50	10.80	5.15
3.45	10.93	5.26
3.38	11.22	5.53
3.32	11.32	5.62
3.28	11.46	5.74
3.25	11.58	5.85
3.19	11.76	6.02

$^a k_2 = k_{\text{obs}}/[L], [L] = 6 \times 10^{-2}\text{M}$

(b) 3-Methyl-2-Phenylpyridine

$(1/T) \times 10^3 \text{ (K}^{-1}\text{)}$	$\text{Ln } k_2^a$	$\text{Ln } k_2^a/T$
3.50	10.05	4.39
3.45	10.34	4.68
3.38	10.58	4.89
3.32	10.75	5.05
3.28	11.04	5.32
3.24	11.16	5.43
3.19	11.29	5.55

$^a k_2 = k_{\text{obs}}/[L], [L] = 6 \times 10^{-2}\text{M}$

(c) 2-Phenylpyridine

$(1/T) \times 10^3 \text{ (K}^{-1}\text{)}$	$\text{Ln } k_2^a$	$\text{Ln } k_2^a/T$
3.48	9.91	4.25
3.41	10.14	4.46
3.37	10.20	4.51
3.32	10.39	4.68
3.28	10.56	4.84

$^a k_2 = k_{\text{obs}}/[L], [L] = 6 \times 10^{-2}\text{M}$

(d) 4-Phenylpyridine

$(1/T) \times 10^3 \text{ (K}^{-1}\text{)}$	$\text{Ln } k_2^a$	$\text{Ln } k_2^a/T$
3.50	10.58	4.93
3.44	10.90	5.23
3.38	11.00	5.31
3.32	11.20	5.50
3.28	11.35	5.63
3.24	11.50	5.77

$^a k_2 = k_{\text{obs}}/[L], [L] = 6 \times 10^{-2}\text{M}$

(e) 2-Chloropyridine

$(1/T) \times 10^3 \text{ (K}^{-1}\text{)}$	$\text{Ln } k_2^a$	$\text{Ln } k_2^a/T$
3.50	10.45	4.80
3.45	10.55	4.88
3.38	10.73	5.04
3.32	10.88	5.17
3.28	11.05	5.33
3.25	11.25	5.52
3.20	11.35	5.60

$^a k_2 = k_{\text{obs}}/[L], [L] = 6 \times 10^{-2}\text{M}$

(f) 3-Chloropyridine

$(1/T) \times 10^3 \text{ (K}^{-1}\text{)}$	$\text{Ln } k_2^a$	$\text{Ln } k_2^a/T$
3.51	9.99	4.34
3.44	10.17	4.50
3.38	10.34	4.66
3.32	10.59	4.89
3.28	10.69	4.97
3.24	10.79	5.06

$^a k_2 = k_{\text{obs}}/[L], [L] = 6 \times 10^{-2}\text{M}$

(g) 2-Picoline

$(1/T) \times 10^3 \text{ (K}^{-1}\text{)}$	$\text{Ln } k_2^a$	$\text{Ln } k_2^a/T$
3.50	10.28	4.63
3.44	10.53	4.86
3.38	10.76	5.07
3.32	10.96	5.26
3.28	11.18	5.46
3.24	11.31	5.58

$^a k_2 = k_{\text{obs}}/[L], [L] = 6 \times 10^{-2}\text{M}$

(h) 3-Picoline

$(1/T) \times 10^3 \text{ (K}^{-1}\text{)}$	$\text{Ln } k_2^a$	$\text{Ln } k_2^a/T$
3.51	10.69	5.04
3.44	10.94	5.27
3.38	11.11	5.42
3.32	11.32	5.62
3.28	11.50	5.78

$^a k_2 = k_{\text{obs}}/[L], [L] = 6 \times 10^{-2}\text{M}$

(i) 4-Picoline

$(1/T) \times 10^3 \text{ (K}^{-1}\text{)}$	$\text{Ln } k_2^a$	$\text{Ln } k_2^a/T$
3.48	11.28	5.62
3.42	11.40	5.72
3.37	11.57	5.88
3.32	11.67	5.97
3.29	11.80	6.09
3.24	11.91	6.18

$$^a k_2 = k_{\text{obs}}/[L], [L] = 6 \times 10^{-2}\text{M}$$

Table A3: Data for the determination of energy, enthalpy and entropy of activation for the reaction of $\text{Cr(CO)}_5(\text{toluene})$ with L, forming $\text{Cr(CO)}_5(\text{L})$, L = py (a), 3-Me-2-Phpy (b), 2-Phpy (c), 4-Phpy (d), 2-Clpy (e), 3-Clpy (f), 2-Pic (g), 3-Pic (h) and 4-Pic (i), monitored at 480nm.

In ethanol, $[L] = 5 \times 10^{-2}\text{M}$

(a) Pyridine

$1/T \times 10^3 \text{ (K}^{-1}\text{)}$	$\text{Ln } k_2^a$	$\text{Ln } k_2^a/T$
3.41	-3.27	-8.95
3.33	-2.67	-8.38
3.29	-2.33	-8.05
3.24	-1.94	-7.67
3.20	-1.44	-7.19

$$^a k_2 = k_{\text{obs}}/[L], [L] = 5 \times 10^{-2}\text{M}$$

(b) 3-Chloropyridine

$1/T \times 10^3 \text{ (K}^{-1}\text{)}$	$\text{Ln } k_2^a$	$\text{Ln } k_2^a/T$
3.41	-3.18	-8.86
3.33	-2.73	-8.45
3.28	-2.31	-8.03
3.24	-1.93	-7.66
3.19	-1.33	-7.08
3.14	-1.19	-6.96

$$^a k_2 = k_{\text{obs}}/[L], [L] = 5 \times 10^{-2}\text{M}$$

(c) 4-Phenylpyridine

$1/T \times 10^3 \text{ (K}^{-1}\text{)}$	$\text{Ln } k_2^a$	$\text{Ln } k_2^a/T$
3.45	-3.14	-8.81
3.37	-2.69	-8.38
3.29	-2.13	-7.85
3.25	-2.03	-7.76
3.19	-1.79	-7.54
3.15	-1.49	-7.25

$$^a k_2 = k_{\text{obs}}/[L], [L] = 5 \times 10^{-2}\text{M}$$

(d) 3-Picoline

$1/T \times 10^3 \text{ (K}^{-1}\text{)}$	$\text{Ln } k_2^a$	$\text{Ln } k_2^a/T$
3.45	-3.29	-8.96
3.39	-2.91	-8.59
3.34	-2.58	-8.28
3.30	-2.40	-8.12
3.25	-1.93	-7.66
3.18	-1.62	-7.37

$^a k_2 = k_{\text{obs}}/[L], [L] = 5 \times 10^{-2}\text{M}$

(e) 4-Picoline

$1/T \times 10^3 \text{ (K}^{-1}\text{)}$	$\text{Ln } k_2^a$	$\text{Ln } k_2^a/T$
3.38	-2.57	-8.26
3.30	-2.18	-7.89
3.26	-1.90	-7.62
3.20	-1.63	-7.37
3.16	-1.47	-7.23

$^a k_2 = k_{\text{obs}}/[L], [L] = 5 \times 10^{-2}\text{M}$

In THF, $[L] = 5 \times 10^{-2}M$

(a) Pyridine

$1/T \times 10^3 \text{ (K}^{-1}\text{)}$	$\text{Ln } k_2^a$	$\text{Ln } k_2^a/T$
3.39	-0.64	-6.33
3.29	-0.09	-5.81
3.24	0.16	-5.57
3.19	0.60	-5.15
3.15	0.89	-4.87
3.06	1.39	-4.40

$^a k_2 = k_{\text{obs}}/[L], [L] = 5 \times 10^{-2}M$

(b) 3-Chloropyridine

$1/T \times 10^3 \text{ (K}^{-1}\text{)}$	$\text{Ln } k_2^a$	$\text{Ln } k_2^a/T$
3.34	-0.96	-6.67
3.28	-0.54	-6.26
3.24	-0.15	-5.88
3.19	0.13	-5.61
3.14	0.49	-5.27
3.09	0.78	-4.99

$^a k_2 = k_{\text{obs}}/[L], [L] = 5 \times 10^{-2}M$

(c) 4-Phenylpyridine

$1/T \times 10^3 \text{ (K}^{-1}\text{)}$	$\text{Ln } k_2^a$	$\text{Ln } k_2^a/T$
3.41	-0.89	-6.57
3.36	-0.44	-6.14
3.30	-0.002	-5.72
3.25	0.43	-5.29
3.15	0.90	-4.86

$$^a k_2 = k_{\text{obs}}/[L], [L] = 5 \times 10^{-2}\text{M}$$

(d) 2-Picoline

$1/T \times 10^3 \text{ (K}^{-1}\text{)}$	$\text{Ln } k_2^a$	$\text{Ln } k_2^a/T$
3.41	-1.78	-7.46
3.34	-1.31	-6.98
3.29	-1.00	-6.72
3.24	-0.83	-6.56
3.19	-0.61	-6.36
3.12	-0.10	-5.87

$$^a k_2 = k_{\text{obs}}/[L], [L] = 5 \times 10^{-2}\text{M}$$

(e) 3-Picoline

$1/T \times 10^3 \text{ (K}^{-1}\text{)}$	$\text{Ln } k_2^a$	$\text{Ln } k_2^a/T$
3.44	-0.66	-6.33
3.39	-0.23	-5.91
3.34	0.06	-5.64
3.30	0.30	-5.41
3.25	0.47	-5.26
3.18	0.77	-4.98

$$^a k_2 = k_{\text{obs}}/[L], [L] = 5 \times 10^{-2}\text{M}$$

(f) 4-Picoline

$1/T \times 10^3 \text{ (K}^{-1}\text{)}$	$\text{Ln } k_2^a$	$\text{Ln } k_2^a/T$
3.41	-0.40	-6.08
3.36	-0.07	-5.76
3.30	0.300	-5.42
3.25	0.93	-4.80

$$^a k_2 = k_{\text{obs}}/[L], [L] = 5 \times 10^{-2}\text{M}$$

Table A4: Data for the determination of energy, enthalpy and entropy of activation for the reaction of $\text{Cr(CO)}_5(\text{S})$, ($\text{S} = \text{THF}$ or ethanol) with the various pyridine ligands, L monitored at 380nm, $[\text{L}] = 5 \times 10^{-2}\text{M}$.

In ethanol, [L] = 1M

(a) Pyridine

$1/T \times 10^3 \text{ (K}^{-1}\text{)}$	$\text{Ln } k_2^a$	$\text{Ln } k_2^a/T$
3.42	-4.36	-10.04
3.34	-3.84	-9.54
3.29	-3.22	-8.94
3.25	-2.80	-8.53
3.19	-2.40	-8.14
3.15	-2.01	-7.77

$^a k_2 = k_{\text{obs}}/[L], [L] = 1.0\text{M}$

(b) 3-Chloropyridine

$1/T \times 10^3 \text{ (K}^{-1}\text{)}$	$\text{Ln } k_2^a$	$\text{Ln } k_2^a/T$
3.34	-3.32	-9.02
3.29	-2.95	-8.82
3.24	-2.77	-8.51
3.19	-2.43	-8.18
3.13	-2.08	-7.85

$^a k_2 = k_{\text{obs}}/[L], [L] = 1.0\text{M}$

(c) 2-Picoline

$1/T \times 10^3 \text{ (K}^{-1}\text{)}$	$\text{Ln } k_2^a$	$\text{Ln } k_2^a/T$
3.38	-4.00	-9.69
3.33	-3.80	-9.50
3.29	-3.71	-9.42
3.24	-3.50	-9.23

$$^a k_2 = k_{\text{obs}}/[L], [L] = 1.0M$$

(d) 3-Picoline

$1/T \times 10^3 \text{ (K}^{-1}\text{)}$	$\text{Ln } k_2^a$	$\text{Ln } k_2^a/T$
3.45	-3.67	-9.34
3.39	-3.33	-9.02
3.34	-3.15	-8.86
3.30	-3.03	-8.75
3.20	-2.20	-7.94

$$^a k_2 = k_{\text{obs}}/[L], [L] = 1.0M$$

(e) 4-Picoline

$1/T \times 10^3 \text{ (K}^{-1}\text{)}$	$\text{Ln } k_2^a$	$\text{Ln } k_2^a/T$
3.47	-4.67	-10.33
3.36	-4.09	-9.78
3.30	-3.69	-9.40
3.25	-3.33	-9.06
3.22	-3.26	-9.00
3.15	-2.84	-8.60

$$^a k_2 = k_{\text{obs}}/[L], [L] = 1.0M$$

In THF, [L] = 1M

(a) Pyridine

$1/T \times 10^3 \text{ (K}^{-1}\text{)}$	$\text{Ln } k_2^a$	$\text{Ln } k_2^a/T$
3.45	-1.78	-7.45
3.41	-1.61	-7.29
3.36	-1.37	-7.06
3.29	-1.10	-6.82
3.24	-0.86	-6.59

$^a k_2 = k_{\text{obs}}/[L], [L] = 1.0\text{M}$

(b) 2-Chloropyridine

$1/T \times 10^3 \text{ (K}^{-1}\text{)}$	$\text{Ln } k_2^a$	$\text{Ln } k_2^a/T$
3.41	-2.07	-7.75
3.36	-1.88	-7.58
3.30	-1.57	-7.29
3.24	-1.13	-6.86
3.20	-0.78	-6.53

$^a k_2 = k_{\text{obs}}/[L], [L] = 1.0\text{M}$

(c) 3-Chloropyridine

$1/T \times 10^3 \text{ (K}^{-1}\text{)}$	$\text{Ln } k_2^a$	$\text{Ln } k_2^a/T$
3.45	-2.06	-7.73
3.40	-1.82	-7.50
3.36	-1.54	-7.24
3.30	-1.26	-6.98
3.24	-0.93	-6.66

$$^a k_2 = k_{\text{obs}}/[L], [L] = 1.0\text{M}$$

(d) 2-Picoline

$1/T \times 10^3 \text{ (K}^{-1}\text{)}$	$\text{Ln } k_2^a$	$\text{Ln } k_2^a/T$
3.40	-2.29	-7.97
3.34	-2.02	-7.72
3.29	-1.64	-7.35
3.25	-1.35	-7.07

$$^a k_2 = k_{\text{obs}}/[L], [L] = 1.0\text{M}$$

(e) 3-Picoline

$1/T \times 10^3 \text{ (K}^{-1}\text{)}$	$\text{Ln } k_2^a$	$\text{Ln } k_2^a/T$
3.47	-1.29	-6.95
3.36	-0.99	-6.69
3.30	-0.77	-6.48
3.25	-0.53	-6.26
3.18	-0.21	-5.96

$$^a k_2 = k_{\text{obs}}/[L], [L] = 1.0\text{M}$$

(f) 4-Picoline

$1/T \times 10^3 \text{ (K}^{-1}\text{)}$	$\text{Ln } k_2^a$	$\text{Ln } k_2^a/T$
3.45	-1.61	-7.28
3.41	-1.19	-6.87
3.36	-0.78	-6.48
3.30	-0.29	-6.00
3.25	-0.05	-5.78

$^a k_2 = k_{\text{obs}}/[L], [L] = 1.0\text{M}$

Table A5: Data for the determination of energy, enthalpy and entropy of activation for the reaction of $\text{Cr(CO)}_5(\text{S})$, ($\text{S} = \text{THF}$ or ethanol) with the various pyridine ligands, L monitored at 380nm, $[L] = 1\text{M}$.

APPENDIX B

**DATA FOR THE DETERMINATION OF SECOND-ORDER
RATE CONSTANTS**

(a) Cyclohexane

$[\text{CO}] \times 10^2 \text{ (mol dm}^{-3}\text{)}$	$k_{\text{obs}} \times 10^{-4} \text{ (s}^{-1}\text{)}$
0.225	1.364
0.450	1.979
0.675	2.431
0.900	2.914

(b) Methylcyclohexane

$[\text{CO}] \times 10^2 \text{ (mol dm}^{-3}\text{)}$	$k_{\text{obs}} \times 10^{-4} \text{ (s}^{-1}\text{)}$
0.225	1.794
0.450	2.529
0.675	3.498
0.900	4.116

(c) Pentane

$[\text{CO}] \times 10^2 \text{ (mol dm}^{-3}\text{)}$	$k_{\text{obs}} \times 10^{-4} \text{ (s}^{-1}\text{)}$
0.40	1.146
0.80	2.877
1.20	5.132
1.60	7.438

(d) Hexanes

[CO] x 10 ² (mol dm ⁻³)	k _{obs} x 10 ⁻⁴ (s ⁻¹)
0.33	1.300
0.65	2.877
0.98	4.550
1.30	7.086

(e) Heptane

[CO] x 10 ² (mol dm ⁻³)	k _{obs} x 10 ⁻⁴ (s ⁻¹)
0.30	1.775
0.60	3.399
0.90	5.938
1.20	8.558

Table B1: Data for the plot of k_{obs} (s⁻¹) versus CO concentration (mol dm⁻³) for the reaction of Cr(CO)₅(S) with CO, S = cyclohexane (a), methylcyclohexane (b), pentane (c), hexanes (d) and heptane (e), monitored at 500nm at 25°C.

(a) Pyridine

[L] x 10² (mol dm⁻³)	k_{obs} x 10⁻⁶ (s⁻¹) at 510nm	k_{obs} x 10⁻⁶ (s⁻¹) at 420nm
2.0	1.06	1.13
4.0	2.36	2.42
6.0	3.45	3.47
8.0	4.70	4.64
10.0	6.19	6.50

(b) 3-Methyl-2-Phenylpyridine

[L] x 10² (mol dm⁻³)	k_{obs} x 10⁻⁶ (s⁻¹) at 510nm	k_{obs} x 10⁻⁶ (s⁻¹) at 420nm
2.0	0.60	0.61
4.0	1.26	1.32
6.0	1.78	1.82
8.0	2.16	2.24
10.0	2.48	2.65

(c) 2-Phenylpyridine

[L] x 10² (mol dm⁻³)	k_{obs} x 10⁻⁶ (s⁻¹) at 510nm	k_{obs} x 10⁻⁶ (s⁻¹) at 420nm
2.0	0.35	0.35
4.0	0.61	0.60
6.0	1.18	1.15
8.0	1.67	1.63
10.0	2.22	2.28

(d) 4-Phenylpyridine

$[L] \times 10^2$ (mol dm ⁻³)	$k_{\text{obs}} \times 10^{-6}$ (s ⁻¹) at 510nm	$k_{\text{obs}} \times 10^{-6}$ (s ⁻¹) at 420nm
2.0	1.20	1.11
4.0	2.26	2.30
6.0	2.99	3.09
8.0	4.40	4.41
10.0	4.99	5.02

(e) 2-Chloropyridine

$[L] \times 10^2$ (mol dm ⁻³)	$k_{\text{obs}} \times 10^{-6}$ (s ⁻¹) at 510nm	$k_{\text{obs}} \times 10^{-6}$ (s ⁻¹) at 420nm
2.0	0.75	0.74
4.0	1.14	1.24
6.0	1.77	1.80
8.0	2.44	2.50
10.0	3.00	3.20

(f) 3-Chloropyridine

$[L] \times 10^2$ (mol dm ⁻³)	$k_{\text{obs}} \times 10^{-6}$ (s ⁻¹) at 510nm	$k_{\text{obs}} \times 10^{-6}$ (s ⁻¹) at 420nm
2.0	0.69	0.72
4.0	1.17	1.17
6.0	1.61	1.68
8.0	2.32	2.30
10.0	2.58	2.51

(g) 2-Picoline

$[L] \times 10^2$ (mol dm ⁻³)	$k_{\text{obs}} \times 10^{-6}$ (s ⁻¹) at 510nm	$k_{\text{obs}} \times 10^{-6}$ (s ⁻¹) at 420nm
2.0	0.77	0.77
4.0	1.03	1.11
6.0	1.83	1.86
8.0	2.41	2.46
10.0	2.93	3.05

(h) 3-Picoline

$[L] \times 10^2$ (mol dm ⁻³)	$k_{\text{obs}} \times 10^{-6}$ (s ⁻¹) at 510nm	$k_{\text{obs}} \times 10^{-6}$ (s ⁻¹) at 420nm
2.0	1.44	1.71
4.0	2.96	3.17
6.0	4.15	4.78
8.0	5.72	6.02
10.0	6.95	6.83

(i) 4-Picoline

$[L] \times 10^2$ (mol dm ⁻³)	$k_{\text{obs}} \times 10^{-6}$ (s ⁻¹) at 510nm	$k_{\text{obs}} \times 10^{-6}$ (s ⁻¹) at 420nm
2.0	1.65	1.68
4.0	3.70	3.82
6.0	6.35	7.18
8.0	8.16	8.96
10.0	10.19	11.14

Table B2: Data for the plot of k_{obs} (s⁻¹) versus ligand (L) concentration (mol dm⁻³) for the reaction of Cr(CO)₅(cyclohexane) with L, L = pyridine (a), 3-methyl-2-phenylpyridine (b), 2-phenylpyridine (c), 4-phenylpyridine (d), 2-chloropyridine (e), 3-chloropyridine (f), 2-picoline (g), 3-picoline (h) and 4-picoline (i) at 22°C.

(a) Pyridine

$[L] \times 10^2$ (mol dm ⁻³)	$k_{\text{obs}} \times 10^{-3}$ (s ⁻¹) at 480nm	$k_{\text{obs}} \times 10^{-3}$ (s ⁻¹) at 410nm
2.0	1.05	1.19
4.0	5.84	2.83
6.0	4.08	4.08
8.0	6.00	5.94
10.0	7.91	7.79

(b) 3 Methyl-2-Phenylpyridine

$[L] \times 10^2$ (mol dm ⁻³)	$k_{\text{obs}} \times 10^{-3}$ (s ⁻¹) at 480nm	$k_{\text{obs}} \times 10^{-3}$ (s ⁻¹) at 410nm
2.0	0.65	0.77
4.0	1.64	1.67
6.0	2.33	2.40
8.0	3.09	3.16
10.0	3.83	3.91

(c) 2-Phenylpyridine

$[L] \times 10^2$ (mol dm ⁻³)	$k_{\text{obs}} \times 10^{-3}$ (s ⁻¹) at 480nm	$k_{\text{obs}} \times 10^{-3}$ (s ⁻¹) at 410nm
2.0	1.06	1.16
4.0	1.45	1.48
6.0	1.74	1.57
8.0	2.06	1.78
10.0	2.39	2.55

(d) 4-Phenylpyridine

$[L] \times 10^2$ (mol dm ⁻³)	$k_{\text{obs}} \times 10^{-3}$ (s ⁻¹) at 480nm	$k_{\text{obs}} \times 10^{-3}$ (s ⁻¹) at 410nm
2.0	1.25	1.93
4.0	3.11	3.57
6.0	5.56	5.53
8.0	6.54	6.75
10.0	9.35	9.48

(e) 2-Chloropyridine

$[L] \times 10^2$ (mol dm ⁻³)	$k_{\text{obs}} \times 10^{-3}$ (s ⁻¹) at 480nm	$k_{\text{obs}} \times 10^{-3}$ (s ⁻¹) at 410nm
2.0	1.37	1.41
4.0	1.98	2.29
6.0	3.22	3.40
8.0	4.32	9.41
10.0	5.53	5.91

(f) 3-Chloropyridine

$[L] \times 10^2$ (mol dm ⁻³)	$k_{\text{obs}} \times 10^{-3}$ (s ⁻¹) at 480nm	$k_{\text{obs}} \times 10^{-3}$ (s ⁻¹) at 410nm
2.0	0.52	0.66
4.0	1.04	1.33
6.0	1.65	1.95
8.0	2.43	2.48
10.0	2.76	3.33

(g) 2-Picoline

$[L] \times 10^2$ (mol dm ⁻³)	$k_{\text{obs}} \times 10^{-3}$ (s ⁻¹) at 480nm	$k_{\text{obs}} \times 10^{-3}$ (s ⁻¹) at 410nm
2.0	0.89	0.86
4.0	2.05	2.14
6.0	2.92	2.93
8.0	3.97	3.84
10.0	4.99	4.87

(h) 3-Picoline

$[L] \times 10^2$ (mol dm ⁻³)	$k_{\text{obs}} \times 10^{-3}$ (s ⁻¹) at 480nm	$k_{\text{obs}} \times 10^{-3}$ (s ⁻¹) at 410nm
2.0	2.82	2.76
4.0	3.80	4.03
6.0	5.67	5.66
8.0	7.15	7.33
10.0	8.68	8.83

(i) 4-Picoline

$[L] \times 10^2$ (mol dm ⁻³)	$k_{\text{obs}} \times 10^{-3}$ (s ⁻¹) at 480nm	$k_{\text{obs}} \times 10^{-3}$ (s ⁻¹) at 410nm
2.0	2.33	2.45
4.0	4.60	4.64
6.0	5.75	7.03
8.0	7.89	9.13
10.0	10.56	10.92

Table B3: Data for the plot of k_{obs} (s⁻¹) versus ligand (L) concentration (mol dm⁻³) for the reaction Cr(CO)₅(toluene) with L, L = pyridine (a), 3-methyl-2-phenylpyridine (b), 2-phenylpyridine (c), 3-phenylpyridine (d), 2-chloropyridine (e), 3-chloropyridine (f), 2-picoline (g), 3-picoline (h) and 4-picoline (i) at 22°C.

In THE

[L] (mol dm ⁻³)	$k_{\text{obs}} \times 10^2$ (s ⁻¹) ^a			
	Pyridine	3-Clpy	2-Clpy	4-Phpy
0.01	0.49	0.50	0.16	0.57
0.05	1.64			3.16
0.10	3.46	3.01	1.13	6.45
0.25	6.23	7.17	8.90	
0.50	16.98	14.20	7.13	
0.75	22.30	19.40	12.40	
1.00	28.10	27.90	13.50	
2.00	35.80	39.70	14.20	

^a monitored at 380nm

[L] (mol dm ⁻³)	$k_{\text{obs}} \times 10^2$ (s ⁻¹) ^a		
	2-Picoline	3-Picoline	4-Picoline
0.01	0.39	0.50	0.64
0.05			
0.10	1.82	3.01	4.96
0.25	5.59	7.17	
0.50	8.13	14.20	16.34
0.75	9.60	19.40	
1.00	8.10	27.90	36.40
2.00	10.46	39.70	55.80

^a monitored at 380nm

Table B4: Data for the plot of k_{obs} (s⁻¹) versus ligand (L) concentration (mol dm⁻³) for the reaction of Cr(CO)₅(THF) with L, at 25°C.

In ethanol

[L] (mol dm ⁻³)	$k_{\text{obs}} \times 10^2$ (s ⁻¹) ^a		
	Pyridine	3-Clpy	4-Phpy
0.01	0.25	0.20	0.14
0.05		0.51	0.59
0.10	0.66	0.58	1.03
0.25	1.39	1.16	
0.50	2.86	1.90	
0.75			
1.00	4.68	3.92	
2.00	7.53	5.59	

^a monitored at 380nm

[L] (mol dm ⁻³)	$k_{\text{obs}} \times 10^2$ (s ⁻¹) ^a		
	2-Picoline	3-Picoline	4-Picoline
0.01	0.01	0.07	0.17
0.05			0.48
0.10	0.56	0.39	1.13
0.25	1.40		
0.50	1.60	2.03	2.64
0.75	2.40		
1.00	3.52		4.07
2.00	3.72		6.42

^a monitored at 380nm

Table B5: Data for the plot of k_{obs} (s⁻¹) versus ligand (L) concentration (mol dm⁻³) for the reaction of Cr(CO)₅(ethanol) with L, at 25°C.

APPENDIX C

**DATA FOR THE DETERMINATION OF
EXTINCTION COEFFICIENTS**

(a) Data for extinction coefficient of $\text{Cr}(\text{CO})_6$ in cyclohexane at 354nm

$[\text{Cr}(\text{CO})_6] \times 10^3$ (mol dm^{-3})	O.D. at 354nm (AU)
0.0	0.000
1.0	0.212
1.5	0.296
2.0	0.399
2.5	0.505
3.0	0.615

(b) Data for extinction coefficient of $\text{Cr}(\text{CO})_6$ in methylcyclohexane at 354nm

$[\text{Cr}(\text{CO})_6] \times 10^3$ (mol dm^{-3})	O.D. at 354nm (AU)
0.0	0.000
1.0	0.232
1.5	0.341
2.0	0.469
2.5	0.575
3.0	0.693

(c) Data for extinction coefficient of $\text{Cr}(\text{CO})_6$ in heptane at 354nm

$[\text{Cr}(\text{CO})_6] \times 10^3$ (mol dm ⁻³)	O.D. at 354nm (AU)
0.0	0.000
1.0	0.235
1.5	0.352
2.0	0.468
2.5	0.580
3.0	0.682

(d) Data for extinction coefficient of $\text{Cr}(\text{CO})_6$ in hexanes at 354nm

$[\text{Cr}(\text{CO})_6] \times 10^3$ (mol dm ⁻³)	O.D. at 354nm (AU)
0.0	0.000
0.5	0.111
1.0	0.212
1.5	0.314
2.0	0.414
2.5	0.524

(e) Data for extinction coefficient of $\text{Cr}(\text{CO})_6$ in pentane at 354nm

$[\text{Cr}(\text{CO})_6] \times 10^3$ (mol dm ⁻³)	O.D. at 354nm (AU)
0.0	0.000
0.5	0.141
1.0	0.260
1.5	0.386
2.0	0.469

(f) Data for extinction coefficient of $\text{Cr}(\text{CO})_5(\text{py})$ in cyclohexane at 390nm

$[\text{Cr}(\text{CO})_5(\text{py})]$ $\times 10^4$ (mol dm ⁻³)	O.D. at 390nm (AU)
0.0	0.000
0.2	0.173
0.4	0.199
0.8	0.359
2.0	0.845
4.0	1.740

(g) Data for extinction coefficient of Cr(CO)₆ in toluene at 354nm

[Cr(CO)₆] x 10³ (mol dm⁻³)	O.D. at 354nm (AU)
0.0	0.000
0.9	0.319
1.8	0.508
3.7	0.997
5.5	1.521
7.3	1.888

(h) Data for extinction coefficient of Cr(CO)₆ in THF at 354nm

[Cr(CO)₆] x 10³ (mol dm⁻³)	O.D. at 354nm (AU)
0.0	0.000
0.5	0.087
1.0	0.229
1.5	0.333
2.0	0.465
2.5	0.594
3.0	0.758

(i) Data for extinction coefficient of $\text{Cr}(\text{CO})_6$ in ethanol at 354nm

$[\text{Cr}(\text{CO})_6] \times 10^3$ (mol dm⁻³)	O.D. at 354nm (AU)
0.0	0.000
0.5	0.121
1.0	0.248
1.5	0.364
2.0	0.495
2.5	0.618
3.0	0.724

(j) Data for extinction coefficient of $\text{ArCr}(\text{CO})_3$ in cyclohexane at 354nm

$[\text{ArCr}(\text{CO})_3]$ $\times 10^4$ (mol dm⁻³)	O.D. at 354nm (AU)
0.0	0.000
0.32	0.125
0.64	0.226
0.80	0.299
1.60	0.607
3.20	1.170

(k) Data for extinction coefficient of $\text{ArCr}(\text{CO})_2(\text{py})$ in cyclohexane at 354 and 500nm

$[\text{ArCr}(\text{CO})_2(\text{py})]$ $\times 10^4 \text{ (mol dm}^{-3}\text{)}$	O.D. at 354nm (AU)	O.D. at 500nm (AU)
0.00	0.000	0.000
0.60	0.093	0.137
1.21	0.168	0.261
1.81	0.246	0.385
2.05	0.397	0.543
6.04	1.010	1.513

(l) Data for extinction coefficient of $\text{ArCr}(\text{CO})_2(4\text{-Acpy})$ in cyclohexane at 354 and 670nm

$[\text{ArCr}(\text{CO})_2(4\text{-Acpy})]$ $\times 10^3 \text{ (mol dm}^{-3}\text{)}$	O.D. at 354nm (AU)	O.D. at 670nm (AU)
0.00	0.000	0.000
0.39	0.264	0.280
0.59	0.343	0.363
1.95	1.377	1.853